



*Midwest States Pooled Fund Research Program
Fiscal Years 2014-2015 (Years 24 and 25)
Research Project Number TPF-5(193) Supplement #64 and #79
NDOR Sponsoring Agency Code RFPF-14-CABLE-1 and RFPF-15-CABLE-1*

EVALUATION OF FLOORPAN TEARING AND CABLE SPICES FOR CABLE BARRIER SYSTEMS

Submitted by

Scott K. Rosenbaugh, M.S.C.E., E.I.T.
Research Associate Engineer

Jason A. Hartwell
Former Undergraduate Research Assistant

Robert W. Bielenberg, M.S.M.E., E.I.T.
Research Associate Engineer

Ronald K. Faller, Ph.D., P.E.
Research Associate Professor
MwRSF Director

James C. Holloway, M.S.C.E., E.I.T.
Test Site Manager

Karla A. Lechtenberg, M.S.M.E., E.I.T.
Research Associate Engineer

MIDWEST ROADSIDE SAFETY FACILITY

Nebraska Transportation Center
University of Nebraska-Lincoln
130 Whittier Research Center
2200 Vine Street
Lincoln, Nebraska 68583-0853
(402) 472-0965

Submitted to

MIDWEST STATES POOLED FUND PROGRAM

Nebraska Department of Roads
1500 Nebraska Highway 2
Lincoln, Nebraska 68502

MwRSF Research Report No. TRP-03-324-17

May 16, 2017

TECHNICAL REPORT DOCUMENTATION PAGE

1. Report No. TRP-03-324-17	2.	3. Recipient's Accession No.	
4. Title and Subtitle Evaluation of Floorpan Tearing and Cable Splices for Cable Barrier Systems		5. Report Date May 16, 2017	
		6.	
7. Author(s) Rosenbaugh, S.K., Hartwell, J.H., Bielenberg, R.W., Faller, R.K., Holloway, J.C., and Lechtenberg, K.A.		8. Performing Organization Report No. TRP-03-324-17	
9. Performing Organization Name and Address Midwest Roadside Safety Facility (MwRSF) Nebraska Transportation Center University of Nebraska-Lincoln 130 Whittier Research Center 2200 Vine Street Lincoln, Nebraska 68583-0853		10. Project/Task/Work Unit No.	
		11. Contract © or Grant (G) No. TFP-5(193) Supplement #64 TFP-5(193) Supplement #79	
12. Sponsoring Organization Name and Address Midwest States Pooled Fund Program Nebraska Department of Roads 1500 Nebraska Highway 2 Lincoln, Nebraska 68502		13. Type of Report and Period Covered Final Report: 2014-2017	
		14. Sponsoring Agency Code RPFP-14-CABLE-1 RPFP-15-CABLE-1	
15. Supplementary Notes Prepared in cooperation with U.S. Department of Transportation, Federal Highway Administration.			
16. Abstract <p>This research effort consisted of two objectives related to components of a prototype cable barrier system. The first objective was to mitigate the potential for vehicle floorpan tearing by modifying the cable guardrail posts. A bogie vehicle was equipped with a simulated floorpan designed to replicate the height, thickness, and strength of the floorpan of a Kia Rio vehicle. Baseline testing demonstrated that the top of the Midwest Weak Post (MWP) would contact, and crease the simulated floorpan, which matched the damage observed in actual full-scale vehicle crash tests. Once the test setup provided the desired results, various post configurations were tested including S3x5.7 (S76x8.4) posts, MWPs with edge rounding, MWPs with steel plate edge protectors, and MWPs with weakening holes/slots. Three different weakening patterns were evaluated: ¾-in. (19-mm) diameter hole; three ⅜-in. (10-mm) diameter holes; and ⅜-in. x 1½-in. (10-mm x 29-mm) slots. All three weakening patterns showed the ability to reduce the propensity for floorpan tearing. However, additional bogie testing of the posts resulted in significant reductions in strong-axis strength for the latter two weakening patterns. The ¾-in. (19-mm) diameter hole resulted in a 10 percent reduction in strong-axis bending strength, and thus, was recommended for further evaluation through full-scale vehicle crash testing.</p> <p>The second objective was to investigate the structural capacity of other cable splice hardware that would reduce the propensity for vehicle snag and sheet metal tearing. A review of existing hardware was conducted to identify possible couplers. Next, three component tests were conducted to evaluate two models of Bennett Bolt Works mechanical couplers. Test results for the new coupler, model no. CGBBWTH, showed promise, however the targeted failure strength of 39 kips (174 kN) was not satisfied for either the new coupler, model no. CGBBWTH, or current coupler, model no. CGBBHT. There is potential that the couplers used in test no. BBNC-3 sustained damage in previous testing which would make them susceptible to premature failure, therefore further testing and evaluation of both coupler models will be necessary to gain a better understanding of their strengths and durability.</p>			
17. Document Analysis/Descriptors Cable Barrier, MWP, S3x5.7, Floorpan Testing, Floorpan Tearing, Cable Splice, Dynamic Testing, Bogie Testing		18. Availability Statement No restrictions. Document available from: National Technical Information Services, Springfield, Virginia 22161	
19. Security Class (this report) Unclassified	20. Security Class (this page) Unclassified	21. No. of Pages 213	22. Price

DISCLAIMER STATEMENT

This report was completed with funding from the Federal Highway Administration, U.S. Department of Transportation and the Midwest States Pooled Fund Program. The contents of this report reflect the views and opinions of the authors who are responsible for the facts and the accuracy of the data presented herein. The contents do not necessarily reflect the official views or policies of the state highway departments participating in the Midwest States Pooled Fund Program nor the Federal Highway Administration, U.S. Department of Transportation. This report does not constitute a standard, specification, regulation, product endorsement, or an endorsement of manufacturers.

UNCERTAINTY OF MEASUREMENT STATEMENT

The Midwest Roadside Safety Facility (MwRSF) has determined the uncertainty of measurements for several parameters involved in standard full-scale crash testing and non-standard testing of roadside safety features. Information regarding the uncertainty of measurements for critical parameters is available upon request by the sponsor and the Federal Highway Administration. Test nos. MWFPF-1 through MWFPF-21 and BBNC-1 through BBNC-3 were non-certified component tests conducted for research and development purposes only and are outside the scope of the MwRSF's A2LA Accreditation.

ACKNOWLEDGEMENTS

The authors wish to acknowledge several sources that made a contribution to this project: (1) The Midwest States Pooled Fund Program funded by the Illinois Department of Transportation, Indiana Department of Transportation, Iowa Department of Transportation, Kansas Department of Transportation, Minnesota Department of Transportation, Missouri Department of Transportation, Nebraska Department of Roads, New Jersey Department of Transportation, Ohio Department of Transportation, South Dakota Department of Transportation, Wisconsin Department of Transportation, and Wyoming Department of Transportation for sponsoring this project; and (2) MwRSF personnel for constructing the barriers and conducting the crash tests.

Acknowledgement is also given to the following individuals who made a contribution to the completion of this research project.

Midwest Roadside Safety Facility

J.D. Reid, Ph.D., Professor
J.D. Schmidt, Ph.D., P.E., Research Associate Professor
C.S. Stolle, Ph.D., E.I.T., Research Associate Professor
A.T. Russell, B.S.B.A., Shop Manager
S.M. Tighe, Laboratory Mechanic
D.S. Charroin, Laboratory Mechanic
M.A. Rasmussen, Laboratory Mechanic
E.W. Krier, Laboratory Mechanic
Undergraduate and Graduate Research Assistants

Illinois Department of Transportation

Priscilla A. Tobias, P.E., State Safety Engineer/Bureau Chief
Tim Sheehan, P.E., Safety Design Engineer
Paul L. Lorton, P.E., Safety Programs Unit Chief

Indiana Department of Transportation

Todd Shields, P.E., Maintenance Field Support Manager

Iowa Department of Transportation

Chris Poole, P.E., Roadside Safety Engineer
Brian Smith, P.E., Methods Engineer
Khyle Clute, P.E., Methods Transportation Engineer

Kansas Department of Transportation

Ron Seitz, P.E., Bureau Chief
Scott King, P.E., Road Design Bureau Chief

Kelly Keele, P.E., Road Design Leader
Thomas Rhoads, P.E., Engineering Associate III, Bureau of Road Design

Minnesota Department of Transportation

Michael Elle, P.E., Design Standards Engineer

Missouri Department of Transportation

Ronald Effland, P.E., ACTAR, LCI, Non-Motorized Transportation Engineer
Joseph G. Jones, P.E., former Engineering Policy Administrator

Nebraska Department of Roads

Phil TenHulzen, P.E., Design Standards Engineer
Jim Knott, P.E., State Roadway Design Engineer
Jodi Gibson, Research Coordinator

New Jersey Department of Transportation

Dave Bizuga, Senior Executive Manager, Roadway Design Group 1

Ohio Department of Transportation

Don Fisher, P.E., Roadway Standards Engineer
Maria E. Ruppe, P.E., former Roadway Standards Engineer

South Dakota Department of Transportation

David Huft, P.E., Research Engineer
Bernie Clocksin, P.E., Lead Project Engineer

Wisconsin Department of Transportation

Jerry Zogg, P.E., Chief Roadway Standards Engineer
Erik Emerson, P.E., Standards Development Engineer
Rodney Taylor, P.E., Roadway Design Standards Unit Supervisor

Wyoming Department of Transportation

William Wilson, P.E., Architectural and Highway Standards Engineer

Federal Highway Administration

John Perry, P.E., Nebraska Division Office
Danny Briggs, Nebraska Division Office

TABLE OF CONTENTS

TECHNICAL REPORT DOCUMENTATION PAGE	i
DISCLAIMER STATEMENT	ii
UNCERTAINTY OF MEASUREMENT STATEMENT	ii
ACKNOWLEDGEMENTS	iii
TABLE OF CONTENTS	v
LIST OF FIGURES	viii
LIST OF TABLES	xii
1 INTRODUCTION	1
1.1 Background	1
1.2 Research Objectives	2
1.3 Scope	2
2 MITIGATION OF FLOORPAN TEARING	3
2.1 Exploration of Floorpan Tearing	3
2.2 Post Modifications to Mitigate Tearing	5
2.2.1 Breakaway Posts	5
2.2.2 Hinged Posts	5
2.2.3 Post Weakening	5
2.2.4 Edge Rounding	6
2.2.5 Edge Hemming	6
2.2.6 Edge Protectors	7
2.2.7 Closed Cross-Section Post	7
3 STATIC COUPON TESTING	8
3.1 Purpose	8
3.2 Scope	8
3.3 Static Testing Results	8
3.4 Discussion	13
4 COMPONENT TESTING CONDITIONS – FLOORPAN TEARING	14
4.1 Purpose	14
4.2 Scope	14
4.3 Equipment and Instrumentation	25
4.3.1 Bogie Vehicle	25
4.3.2 Accelerometers	34
4.3.3 Retroreflective Optic Speed Trap	34
4.3.4 Digital Photography	34
4.4 Data Processing	34
5 TESTING RESULTS - FLOORPAN TEARING	36

5.1 Results.....	36
5.1.1 Test No. MWFPF-1	36
5.1.2 Test No. MWFPF-2	40
5.1.3 Test No. MWFPF-3	46
5.1.4 Test No. MWFPF-4	51
5.1.5 Test No. MWFPF-5	55
5.1.6 Test No. MWFPF-6	60
5.1.7 Test No. MWFPF-7	65
5.1.8 Test No. MWFPF-8	69
5.1.9 Test No. MWFPF-11	74
5.1.10 Test No. MWFPF-12	78
5.1.11 Test No. MWFPF-13	81
5.1.12 Test No. MWFPF-14	87
5.1.13 Test No. MWFPF-15	90
5.1.14 Test No. MWFPF-18	93
5.1.15 Test No. MWFPF-21	97
5.2 Discussion	101
6 COMPONENT TESTING CONDITIONS – POST STRENGTH.....	106
6.1 Purpose.....	106
6.2 Scope.....	106
6.3 Equipment and Instrumentation.....	114
6.3.1 Bogie Vehicle.....	114
6.3.2 Accelerometers	115
6.3.3 Retroreflective Optic Speed Trap	115
6.3.4 Digital Photography	115
6.4 Data Processing.....	115
7 TESTING RESULTS – POST STRENGTH EVALUATION.....	116
7.1 Results.....	116
7.1.1 Test No. MWFPF-9	116
7.1.2 Test No. MWFPF-10	119
7.1.3 Test No. MWFPF-16 Post 1.....	121
7.1.1 Test No. MWFPF-16 Post 2.....	123
7.1.2 Test No. MWFPF-17 Post 1.....	125
7.1.1 Test No. MWFPF-17 Post 2.....	127
7.1.2 Test No. MWFPF-19	129
7.1.3 Test No. MWFPF-20	131
7.2 Discussion	133
8 EVALUATION OF SPLICE HARDWARE.....	135
8.1 Purpose.....	135
8.2 Review of Wire Rope Coupler Options	136
8.3 Component Testing Scope and Instrumentation	138
8.4 Testing Results.....	145
8.4.1 Test No. BBNC-1.....	145
8.4.1 Test No. BBNC-2.....	147

8.4.2 Test No. BBNC-3..... 149

8.4.3 Discussion 151

9 SUMMARY, CONCLUSIONS, AND RECOMMENDATIONS 153

10 REFERENCES 156

11 APPENDICES 158

 Appendix A. Static Tension Testing Results 159

 Appendix B. Bogie Test Results 167

 Appendix C. Evaluation Of Splice Hardware Drawing Set 191

 Appendix D. Material Specifications 199

 Appendix E. Coupler Testing – Load Cell Results 207

LIST OF FIGURES

Figure 1. Current Cable Median Barrier Prototype	1
Figure 2. Post Shape Free Edges.....	3
Figure 3. Sheet Steel Edge Rounding Process and Types	6
Figure 4. Sheet Steel Edge Hemming	6
Figure 5. Static Testing Coupon Dimensions	8
Figure 6. Engineering Stress vs. Strain for Static Coupon Tests	11
Figure 7. True Stress vs. True Strain for Static Coupon Tests	12
Figure 8. Dynamic Component Test Setup, Floorpan Tearing Evaluation.....	17
Figure 9. MWP with Rounded Corners, Test Nos. MWPFP-1 and MWPFP-2.....	18
Figure 10. MWP with ¾-in. (19-mm) Diameter Holes, Test Nos. MWPFP-3, MWPFP-7 Through MWPFP-8, MWPFP-18, and MWPFP-21	19
Figure 11. S3x5.7 (S76x8.5) Posts, Test Nos. MWPFP-4 and MWPFP-5.....	20
Figure 12. MWP with Simulated #1 Edge Rounding, Test No. MWPFP-6	21
Figure 13. MWP with Three ¾-in. (10-mm) Diameter Holes, Test Nos. MWPFP-11 and MWPFP-14	22
Figure 14. MWP with ¾-in. x 1 ½-in. (10-mm x 29-mm) Slots, Test Nos. MWPFP-12 and MWPFP-15	23
Figure 15. MWP with Steel Plate Edge Protector, Test No. MWPFP-13	24
Figure 16. Bogie Vehicle and Guidance Track - Floorpan Testing.....	26
Figure 17. Bogie Details for Floorpan Evaluation.....	27
Figure 18. Bogie Details, Undercarriage Assembly	28
Figure 19. Bogie Details, Undercarriage Welds	29
Figure 20. Bogie Details, Floorpan Connections.....	30
Figure 21. Bogie Details, Floorpan and Undercarriage Components.....	31
Figure 22. Bogie Details, Undercarriage Components	32
Figure 23. Bogie Details, Fasteners	33
Figure 24. Time-Sequential and Post Damage Photographs, Test No. MWPFP-1	37
Figure 25. Simulated Floorpan Damage, Test No. MWPFP-1	38
Figure 26. Force vs. Deflection and Energy vs. Deflection, Test No. MWPFP-1	39
Figure 27. Time-Sequential Photographs Underneath Bogie, Test No. MWPFP-2	42
Figure 28. Time-Sequential and Post Damage Photographs, Test No. MWPFP-2	43
Figure 29. Simulated Floorpan Damage, Test No. MWPFP-2	44
Figure 30. Force vs. Deflection and Energy vs. Deflection, Test No. MWPFP-2.....	45
Figure 31. MWP with ¾-in. (19-mm) Diameter Weakening Holes	46
Figure 32. Time-Sequential and Post Damage Photographs, Test No. MWPFP-3	48
Figure 33. Simulated Floorpan Damage, Test No. MWPFP-3	49
Figure 34. Force vs. Deflection and Energy vs. Deflection, Test No. MWPFP-3.....	50
Figure 35. Time-Sequential and Post Damage Photographs, Test No. MWPFP-4	52
Figure 36. Simulated Floorpan Damage, Test No. MWPFP-4	53
Figure 37. Force vs. Deflection and Energy vs. Deflection, Test No. MWPFP-4.....	54
Figure 38. Time-Sequential and Post Damage Photographs, Test No. MWPFP-5	57
Figure 39. Simulated Floorpan Damage, Test No. MWPFP-5	58
Figure 40. Force vs. Deflection and Energy vs. Deflection, Test No. MWPFP-5.....	59
Figure 41. MWP with Simulated No. 1 Edge Rounding, Test No. MWPFP-6	61
Figure 42. Time-Sequential and Post Damage Photographs, Test No. MWPFP-6	62

Figure 43. Simulated Floorpan Damage, Test No. MWPF-6	63
Figure 44. Force vs. Deflection and Energy vs. Deflection, Test No. MWPF-6	64
Figure 45. Time-Sequential and Post Damage Photographs, Test No. MWPF-7	66
Figure 46. Simulated Floorpan Damage, Test No. MWPF-7	67
Figure 47. Force vs. Deflection and Energy vs. Deflection, Test No. MWPF-7	68
Figure 48. Time-Sequential and Post Damage Photographs, Test No. MWPF-8	71
Figure 49. Simulated Floorpan Damage, Test No. MWPF-8	72
Figure 50. Force vs. Deflection and Energy vs. Deflection, Test No. MWPF-8	73
Figure 51. MWP with Three 3/8-in. (10-mm) Diameter Weakening Holes	74
Figure 52. Time-Sequential and Post Damage Photographs, Test No. MWPF-11	76
Figure 53. Force vs. Deflection and Energy vs. Deflection, Test No. MWPF-11	77
Figure 54. MWP with 3/8-in. x 1 1/8-in. (10-mm x 29-mm) Weakening Slots	78
Figure 55. Time-Sequential and Post Damage Photographs, Test No. MWPF-12	79
Figure 56. Force vs. Deflection and Energy vs. Deflection, Test No. MWPF-12	80
Figure 57. MWPs with Steel Plate Edge Protectors	81
Figure 58. Time-Sequential and Post Damage Photographs, Test No. MWPF-13	83
Figure 59. Simulated Floorpan Damage, Test No. MWPF-13	84
Figure 60. Post Damage, Test No. MWPF-13	85
Figure 61. Force vs. Deflection and Energy vs. Deflection, Test No. MWPF-13	86
Figure 62. Time-Sequential and Post Damage Photographs, Test No. MWPF-14	88
Figure 63. Force vs. Deflection and Energy vs. Deflection, Test No. MWPF-14	89
Figure 64. Time-Sequential and Post Damage Photographs, Test No. MWPF-15	91
Figure 65. Force vs. Deflection and Energy vs. Deflection, Test No. MWPF-15	92
Figure 66. Time-Sequential and Post Damage Photographs, Test No. MWPF-18	94
Figure 67. Simulated Floorpan Damage, Test No. MWPF-18	95
Figure 68. Force vs. Deflection and Energy vs. Deflection, Test No. MWPF-18	96
Figure 69. Time-Sequential and Post Damage Photographs, Test No. MWPF-21	98
Figure 70. Simulated Floorpan Damage, Test No. MWPF-21	99
Figure 71. Force vs. Deflection and Energy vs. Deflection, Test No. MWPF-21	100
Figure 72. Single Post Dynamic Component Test Setup, Test Nos. MWPF-9, MWPF-10, MWPF-19, and MWPF-20	108
Figure 73. Double Post Dynamic Component Test Setup, Test Nos. MWPF-16 and MWPF-17	109
Figure 74. Unmodified MWP, Test Nos. MWPF-10 and MWPF-19	110
Figure 75. MWP with 3/4-in. (19-mm) Holes, Test Nos. MWPF-9 and MWPF-20	111
Figure 76. MWP with three 3/8-in. (10-mm) Holes, Test No. MWPF-16	112
Figure 77. MWP with 3/8-in. x 1 1/8-in. (10-mm x 29-mm) Slots, Test No. MWPF-17	113
Figure 78. Second Rigid-Frame Bogie and Guidance Track	114
Figure 79. Force vs. Deflection and Energy vs. Deflection, Test No. MWPF-9	117
Figure 80. Time-Sequential and Post-Impact Photographs, Test No. MWPF-9	118
Figure 81. Force vs. Deflection and Energy vs. Deflection, Test No. MWPF-10	119
Figure 82. Time-Sequential and Post-Impact Photographs, Test No. MWPF-10	120
Figure 83. Force vs. Deflection and Energy vs. Deflection, Test No. MWPF-16 Post 1	121
Figure 84. Time-Sequential and Post-Impact Photographs, Test No. MWPF-16 Post 1	122
Figure 85. Force vs. Deflection and Energy vs. Deflection, Test No. MWPF-16 Post 2	123
Figure 86. Time-Sequential and Post-Impact Photographs, Test No. MWPF-16 Post 2	124
Figure 87. Force vs. Deflection and Energy vs. Deflection, Test No. MWPF-17 Post 1	125

Figure 88. Time-Sequential and Post-Impact Photographs, Test No. MWFPF-17 Post 1	126
Figure 89. Force vs. Deflection and Energy vs. Deflection, Test No. MWFPF-17 Post 2	127
Figure 90. Time-Sequential and Post-Impact Photographs, Test No. MWFPF-17 Post 2	128
Figure 91. Force vs. Deflection and Energy vs. Deflection, Test No. MWFPF-19	129
Figure 92. Time-Sequential and Post-Impact Photographs, Test No. MWFPF-19	130
Figure 93. Force vs. Deflection and Energy vs. Deflection, Test No. MWFPF-20	131
Figure 94. Time-Sequential and Post-Impact Photographs, Test No. MWFPF-20	132
Figure 95. Bennett Bolt Works, Inc. Cable Coupler – Model No. CGBBHT	135
Figure 96. Vehicle Door and A-Pillar Damage from Splice Snagging	136
Figure 97. Bennett Bolt Coupler Dimensions, Model No. CGBBHT	137
Figure 98. Bennett Bolt Works Coupler Model Nos. CGBBHT (Left) and CGBBWTH (Right)	138
Figure 99. Coupler Testing Layout, Test Nos. BBNC-1 through BBNC-3	140
Figure 100. Bennett Bolt Works Coupler Model No. CGBBWTH, Test Nos. BBNC-1 and BBNC-2	141
Figure 101. Coupler Model No. CGBBHT and Associated Splice Hardware, Test No. BBNC-3	142
Figure 102. Test Installation Photographs, Test Nos. BBNC-1 through BBNC-3	143
Figure 103. Test Installation Photographs, Test No. BBNC-1	144
Figure 104. Test Installation Photographs, Test No. BBNC-2	144
Figure 105. Test Installation Photographs, Test No. BBNC-3	144
Figure 106. Time-Sequential and Post-Test Photographs, Test No. BBNC-1	146
Figure 107. Time-Sequential and Post-Test Photographs, Test No. BBNC-2	148
Figure 108. Time-Sequential and Post-Test Photographs, Test No. BBNC-3	150
Figure A-1. Test No. BFPC-1 Results	160
Figure A-2. Test No. BFPC-2 Results	161
Figure A-3. Test No. BFPC-3 Results	162
Figure A-4. Test No. BFPC-4 Results	163
Figure A-5. Test No. KFPC-1 Results	164
Figure A-6. Test No. KFPC-2 Results	165
Figure A-7. Test No. KFPC-3 Results	166
Figure B-1. Test No. MWFPF-1 Results (SLICE-2)	168
Figure B-2. Test No. MWFPF-2 Results (SLICE-2)	169
Figure B-3. Test No. MWFPF-3 Results (SLICE-2)	170
Figure B-4. Test No. MWFPF-4 Results (SLICE-2)	171
Figure B-5. Test No. MWFPF-5 Results (SLICE-2)	172
Figure B-6. Test No. MWFPF-6 Results (SLICE-2)	173
Figure B-7. Test No. MWFPF-7 Results (SLICE-2)	174
Figure B-8. Test No. MWFPF-8 Results (SLICE-2)	175
Figure B-9. Test No. MWFPF-9 Results (SLICE-2)	176
Figure B-10. Test No. MWFPF-10 Results (SLICE-2)	177
Figure B-11. Test No. MWFPF-11 Results (SLICE-2)	178
Figure B-12. Test No. MWFPF-12 Results (SLICE-2)	179
Figure B-13. Test No. MWFPF-13 Results (SLICE-2)	180
Figure B-14. Test No. MWFPF-14 Results (SLICE-2)	181
Figure B-15. Test No. MWFPF-15 Results (SLICE-2)	182
Figure B-16. Test No. MWFPF-16 P1 Results (SLICE-2)	183

Figure B-17. Test No. MWPFP-16 P2 Results (SLICE-2).....	184
Figure B-18. Test No. MWPFP-17 P1 Results (SLICE-2).....	185
Figure B-19. Test No. MWPFP-17 P2 Results (SLICE-2).....	186
Figure B-20. Test No. MWPFP-18 Results (SLICE-2).....	187
Figure B-21. Test No. MWPFP-19 Results (SLICE-2).....	188
Figure B-22. Test No. MWPFP-20 Results (SLICE-2).....	189
Figure B-23. Test No. MWPFP-21 Results (SLICE-2).....	190
Figure C-1. System Layout, Test Nos. BBNC-1 through BBNC-3.....	192
Figure C-2. System Details, Test Nos. BBNC-1 through BBNC-3.....	193
Figure C-3. Cable Router Assembly, Test Nos. BBNC-1 through BBNC-3.....	194
Figure C-4. Cable Router Weld Detail, Test Nos. BBNC-1 through BBNC-3.....	195
Figure C-5. Cable Router Components, Test Nos. BBNC-1 through BBNC-3.....	196
Figure C-6. End Cable Connector Detail, Test Nos. BBNC-1 through BBNC-3.....	197
Figure C-7. Bill of Materials, Test Nos. BBNC-1 through BBNC-3.....	198
Figure D-1. Simulated Floorpan Sheet Steel.....	200
Figure D-2. S3x5.7 (S76x8.5) Posts, Test Nos. MWPFP-4 and MWPFP-5.....	201
Figure D-3. Midwest Weak Posts (MWP).....	202
Figure D-4. Midwest Weak Posts (MWP), Continued.....	203
Figure D-5. New Bennett Bolt Works Coupler, Model No. CGBBWTH.....	204
Figure D-6. Malleable Iron Wedge for Bennett Couplers.....	205
Figure D-7. Current Bennett Bolt Works Coupler, Model No. CGBBHT.....	206
Figure E-1. Test No. BBNC-1 Results, Tension Load Cell.....	208
Figure E-2. Test No. BBNC-2 Results, Tension Load Cell.....	209
Figure E-3. Test No. BBNC-2 Results, Compression Load Cell.....	210
Figure E-4. Test No. BBNC-3 Results, Tension Load Cell.....	211
Figure E-5. Test No. BBNC-3 Results, Compression Load Cell.....	212

LIST OF TABLES

Table 1. Previous Full-Scale Tests Exhibiting Undercarriage Tearing	4
Table 2. Summary of Static Tensile Testing.....	10
Table 3. Dynamic Component Testing Matrix, Floorpan Tearing Evaluation	16
Table 4. Floorpan Damage Measurements, Test No. MWPFP-1	40
Table 5. Floorpan Damage Measurements, Test No. MWPFP-2	46
Table 6. Floorpan Damage Measurements, Test No. MWPFP-3	51
Table 7. Floorpan Damage Measurements, Test No. MWPFP-4	55
Table 8. Floorpan Damage, Test No. MWPFP-5.....	60
Table 9. Floorpan Damage Measurements, Test No. MWPFP-6	65
Table 10. Floorpan Damage Measurements, Test No. MWPFP-7	69
Table 11. Floorpan Damage Measurements, Test No. MWPFP-8	74
Table 12. Floorpan Damage Measurements, Test No. MWPFP-13	87
Table 13. Floorpan Damage Measurements, Test No. MWPFP-18	97
Table 14. Floorpan Damage Measurements, Test No. MWPFP-21	101
Table 15. Component Testing Summary, Floorpan Tearing Evaluation	104
Table 16. Component Testing Summary of Forces and Energies	105
Table 17. Dynamic Component Testing Matrix, Post Strength Evaluation	107
Table 18. Component Testing Summary, Strong-Axis Bending Impacts	134
Table 19. Test Results for Test Nos. BBNC-1 through BBNC-3	151

1 INTRODUCTION

1.1 Background

In recent years, the Midwest States Pooled Fund has been developing a non-proprietary, high-tension, cable median barrier in conjunction with the Midwest Roadside Safety Facility (MwRSF). The barrier was to be developed for placement anywhere within a 6H:1V V-ditch as well as to satisfy the Test Level 3 (TL-3) evaluation criteria published in the *Manual for Assessing Safety Hardware (MASH)* [1]. The most recent design prototype was a four cable system supported by Midwest Weak Posts (MWP) [2], as shown in Figure 1.



Figure 1. Current Cable Median Barrier Prototype

Development of the cable median barrier has progressed through multiple crash tests in accordance with MASH TL-3. Full-scale testing and evaluation with a 1500A sedan and 2270P pickup trucks resulted in satisfactory system performance [3]. However, full-scale crash testing with the 1100C small car resulted in the top of the post tearing the vehicle's floorpan and penetrating into the occupant compartment as the vehicle overrode the system posts [4].

Review of the test vehicles and high-speed videos revealed that the tears were caused by a combination of the post's weak-axis bending strength and cross-sectional geometry. The strength of the post, specifically the elastic restoration force of the MWP, caused the top of each overridden post to press up on the undercarriage of the vehicle. The cross-sectional geometry of the MWP contained free, or exposed, edges that transmitted the post contact forces into the floorpan over a very narrow area. Thus, the free edge created high stress concentrations in the floorpan and ultimately resulted in scraping, gouging, and tearing. These tears were deemed penetrations into the vehicle's occupant compartment and prevented the full-scale crash tests

from satisfying the MASH safety criteria. Therefore, modifications to the MWP were needed to prevent tearing of the vehicle's floorpan.

During the full-scale crash testing of the cable median barrier prototype, observations were made concerning tears in the vehicle's exterior sheet metal due to contact with the cable splices during redirection [3-4]. Sheet metal tearing had been observed on all three vehicle types (1100C, 1500A, and 2270P) and was common along vehicle fenders, front doors, and A-pillars. These tears were only to the exterior sheet metal layer and did not result in penetration of the occupant compartment. Thus, they did not affect the MASH evaluation of the cable barrier. However, they do illustrate the ability of the current cable splice to act as a potential snag hazard and could potentially cause significant damage to the vehicle. Utilization of different cable splice hardware may reduce the propensity for snag and/or sheet metal tearing. Therefore, an evaluation was desired into the strength and geometry of all available cable splice hardware.

1.2 Research Objectives

The research and development effort described herein contained two independent objectives. The first objective was to mitigate the potential for vehicle floorpan tearing by modifying the MWP utilized in the current cable median barrier prototype. The second objective was to investigate other cable splice hardware for the use in the cable median barrier that would reduce the propensity for snag and sheet metal tearing.

1.3 Scope

Exploration into the mitigation of floorpan tearing began with an analysis into the mechanisms forming the tears. Next, various modifications to the MWP were identified that could reduce the propensity for floorpan tearing. The modifications thought to be the most effective were then evaluated through dynamic component testing with a bogie vehicle equipped with a simulated small car floorpan. Additional dynamic tests were conducted with a separate bogie vehicle to evaluate the strong-axis bending strength of the modified MWP. Finally, conclusions and recommendations were made concerning potential post modifications to alleviate floorpan tearing.

Investigation into alternative splice hardware began with a literature review of currently available splice connections for ¾-in. (19-mm) diameter, 3x7 wire rope. After reviewing the splice options with the project sponsors, a total of three dynamic component tests were conducted on the current cable splice and the selected alternative splice. Finally, conclusions and recommendations were formulated based on the component tests.

2 MITIGATION OF FLOORPAN TEARING

2.1 Exploration of Floorpan Tearing

Prior to the development of system modifications to prevent tearing of the vehicle's floorpan, the physical mechanisms causing these tears to form had to be identified. Thus, the high-speed videos, system posts, and the vehicles from test nos. MWP-6 and MWP-7 [4] were analyzed and inspected. Through this effort, two post characteristics were identified as factors resulting in the tearing of vehicle floorpans: (1) the weak-axis bending strength of the post and (2) the presence of free edges.

The weak-axis bending strength of the post, and specifically the elastic response, is critical for the top of the post to contact, crease, and tear the vehicle's floorpan. When a vehicle runs over a post, a plastic hinge forms in the post, and the post is bent over such that the top of the post passes underneath the vehicle's bumper and undercarriage. However, an elastic response in the post causes it to spring back and push up against the vehicle's floorpan. The top of the post then applies a vertical force to the vehicle floorpan proportional to the elastic restoration strength remaining in the hinged post. Since material failure is associated with the magnitude of the applied force, the propensity for floorpan tearing is directly related to the elastic bending strength of the posts utilized in the barrier system.

The presence of free edges within the post's cross-section amplifies the effect of this restoration force. Free edges are characterized as areas of the post's cross section where an end of a flange, or another thin element, is exposed within the cross section. The location of free edges on common post shapes are shown in Figure 2. The thin elements and small contact areas of these free edges result in higher stress concentrations during impact events. Thus, under equivalent restoration forces, posts with free edges will impart higher stresses to the vehicle's floorpan than posts with continuous faces or closed cross sections.

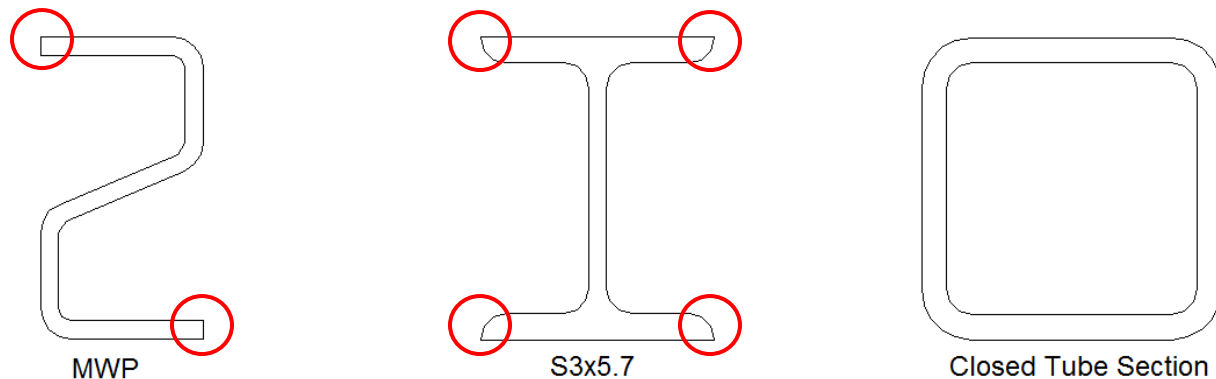


Figure 2. Post Shape Free Edges

A review of previous full-scale tests conducted on barrier systems utilizing posts with free edges was undertaken as part of the investigation into the mechanics of floorpan tearing. This review included tests conducted according to the *MASH* or the *National Cooperative Research Program (NCHRP) Report No. 350* criteria [1, 5]. An additional three full-scale crash

tests encountered tearing of the vehicle floorpan, while two other crash tests had tearing of the gas tank or the underside of the trunk. Although the tearing of the gas tank or the underside of the trunk did not penetrate into the occupant compartment, the sheet metal forming the gas tank and underside of the trunk was similar to that of the floorpan. Thus, these tests demonstrated a propensity for floorpan tearing. All seven crash tests with tearing of the vehicle undercarriage are summarized in Table 1. Numerous full-scale tests also contained scraping and gouging of the vehicle undercarriage (damage typically accompanying tears), but only the tests which exhibited tearing were included in the table.

The review of previous full-scale tests revealed that tearing of the pickup truck floorpans was not found. This is due to the floorpan of a pickup truck being located above the frame elements of the truck. Thus, the elastic spring back of a steel post would not be enough for the top of post to impact the floorpan. In contrast, the floorpans of small cars and sedans are located flush with the rest of the vehicle undercarriage leaving these floorpans susceptible to contact with barrier components.

Table 1. Previous Full-Scale Tests Exhibiting Undercarriage Tearing

Test	Ref.	System	Post	Vehicle	Tearing Location
MWP-6	[4]	Cable Barrier	MWP	2009 Kia Rio	Floorpan
MWP-7	[4]	Cable Barrier	MWP	2009 Kia Rio	Floorpan
4CMBLT-1	[6]	Cable Barrier	S3x5.7	2006 Ford Taurus	Floorpan
CT-2	[7]	Cable End Terminal	S3x5.7	1995 Geo Metro	Floorpan
NYBBT-3	[8]	Box Beam End Terminal	S3x5.7	2002 Kia Rio	Floorpan & Gas Tank
4CMB-4	[9]	Cable Barrier	S3x5.7	2002 Kia Rio	*Trunk
473750-4	[10]	Weak-Post W-Beam	S3x5.7	1997 Geo Metro	*Gas Tank

* Tears in vehicle undercarriage, but not into occupant compartment. Test passed.

All floorpan tearing was associated with impacts into weak-post barrier systems. Tests with strong-post systems, such as the Midwest Guardrail System or the G4(1S), did not show evidence of floorpan tearing. Further investigation of these crash tests revealed that reduced system deflections associated with small car tests into strong-post guardrail systems as compared to weak-post guardrail systems may reduce the propensity for the undercarriage of small cars to significantly pass over the top of posts during oblique impacts. The front of small cars and the front impact-side tires often contact and/or override the strong posts, but the vehicles are often redirected prior to the floorpan being contacted by the posts. This behavior may only apply to oblique impacts as end-on impacts would allow the center of the vehicle to override several posts where the floorpan may be contacted by bent or hinged, steel posts.

Finally, the numerous post sections and barrier types listed in Table 1 demonstrate that floorpan tearing may not be exclusive to one specific barrier system. Rather, this list supports the theory that these tears are the result of the combination of (1) the elastic response and upward contact between the undercarriage and the overridden posts and (2) the presence of free edges

within the post's cross-section. Further, the review of previous crash testing suggests that floorpan tearing may be alleviated by eliminating one or both of the noted characteristics.

2.2 Post Modifications to Mitigate Tearing

After the investigation into the history and mechanisms behind vehicle floorpan tearing, multiple design modifications were considered for use in the prototype cable median barrier being developed by the Midwest States Pooled Fund Program. The design modifications focused on altering the MWP in order to minimize either the elastic spring-back in the post or the exposure of the free edges. A brief discussion on each of these potential design retrofits is provided in the following sections.

2.2.1 Breakaway Posts

One proposed method to eliminate the elastic spring-back of a guardrail post was to add a breakaway mechanism to the MWP. Modifying the post such that the top of the post releases from the base at designated loads and/or displacements. The posts could still provide lateral resistance to the cables during impact events, but it would breakaway when directly impacted by the vehicle. A breakaway post could potentially eliminate the elastic response of the post and prevent the top of the posts from contacting the bottom of the vehicle's floorpan. However, after the post released from its base, the top of the post could become debris with potential for interaction with the redirecting vehicle, causing vehicle instabilities or spearing of the undercarriage of an overriding vehicle. Additionally, the top of the post may remain attached to the system cables and affect the capture/interlock of the cables with the vehicle. Due to these possible negative outcomes associated with post debris, the concept of adding a breakaway mechanism to the system posts was not selected for further development at this time.

2.2.2 Hinged Posts

Hinged posts function similar to breakaway posts in that the hinging mechanism activates at a prescribed load or displacement. However, the top of a hinged post remains attached to the base so the risks associated with post debris are mitigated. The development of a hinged version of the MWP would require significant time and resources. Additionally, existing hinged-post patents would need to be reviewed to prevent infringing upon any proprietary technology. Consequently, a hinged post for the cable system was not selected for further development.

2.2.3 Post Weakening

The elastic spring-back of a deformed guardrail post can be reduced by weakening it. Punching holes or cutting the post near the plastic hinge location reduces the weak-axis bending strength of the post without using a different post section. A reduction in weak-axis bending strength would decrease the elastic spring-back force of a post. Further, discontinuities, such as holes and notches, create stress concentrations when loaded, which could lead to tearing in the post cross section and further reductions to the elastic response of a deformed post. Properly designed holes and/or notches would reduce a post's weak-axis bending strength without greatly affecting the strong-axis bending strength so that overall system performance is not greatly changed. Finally, weakening mechanisms can be added to the punch pattern of an MWP at

minimal additional cost. Thus, the effectiveness of weakening holes was selected for further evaluation and component testing.

2.2.4 Edge Rounding

One method to mitigate the cutting potential associated with the exposed edges of the MWP is to round the edges. Edge rounding is commonly utilized during the fabrication of sheet steel products to remove the sharp edges. After being cut to the desired shape, the sheet steel is fed through a roller which rounds the sides of the sheet and eliminates the sharp edges, as shown in Figure 3. There are various types of edge rounding, characterized by the resulting shape of the steel edges. No. 4 edge rounding utilizes a small radius for each individual edge, while no. 1 edge rounding creates a continuous semi-circle joining the top and bottom surfaces. Due to the low-cost associated with this common manufacturing practice, edge rounding was selected for further evaluation and component testing.

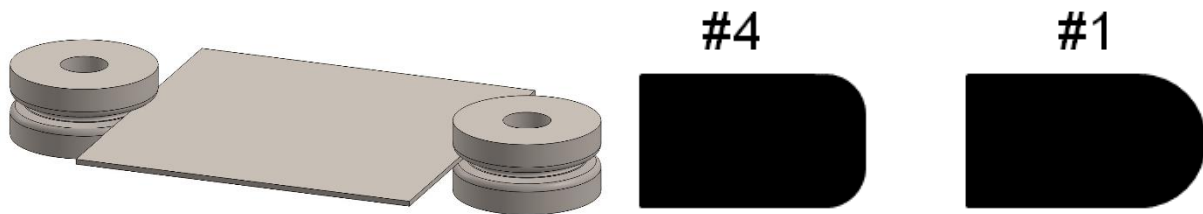


Figure 3. Sheet Steel Edge Rounding Process and Types

2.2.5 Edge Hemming

Edge hemming is another common manufacturing technique utilized to eliminate the sharp edges of sheet steel products. Edge hemming involves folding the exposed edge of the sheet steel 180 degrees so that the sharp edges are facing inward. Because edge hemming is another common practice in sheet steel manufacturing, it can be performed at a relatively low cost. However, the MWP is fabricated from 7-gauge (4.6-mm thick) steel which would be difficult to bend at such a tight radius. Therefore, edge hemming was not selected for further evaluation.



Figure 4. Sheet Steel Edge Hemming

2.2.6 Edge Protectors

Another method of mitigating the cutting potential of the free edges would be to prevent direct contact to the exposed edges. Edge protectors are attached to the post to shield the exposed edges from direct contact with vehicle floorpans. Edge protectors could be made from various materials (e.g., steel, rubber, plastic, fiberglass) and applied along an exposed edge or wrapped over the top of the post. Due to the vast range of possible designs and the benefits associated with preventing direct contact with the floorpan, edge protectors were explored and evaluated through component testing.

2.2.7 Closed Cross-Section Post

The risk of floorpan tearing due to direct contact with a free edge could be completely eliminated if the post had no free edges. Closed-section posts, such as circular and rectangular tubes, provide much larger surface areas in which to distribute the contact load. The stress concentrations from contact with a free edge never forms, and the propensity for sheet metal tearing is reduced. Unfortunately, changing the post section from the current MWP would also require alterations to the cable attachment brackets and top cable keeper rod. Therefore, the use of a closed cross-section post in lieu of the MWP was not initially selected for development and evaluation due to a desire to use the existing MWP and cable-to-post attachments.

3 STATIC COUPON TESTING

3.1 Purpose

Dynamic component testing was desired to evaluate the effectiveness of post modifications to reduce the propensity for tearing of the vehicle's floorpan. However, before testing could begin, a simulated small car vehicle floorpan was required. Measurements taken from the 2009 Kia Rio vehicles used in test nos. MWP-6 and MWP-7 indicated an average floorpan thickness of 0.025 in. (0.64 mm). Thus, 24-gauge (0.61-mm) sheet steel was obtained to simulate the floorpan of an 1100C small car vehicle during the evaluation of floorpan tearing. Unfortunately, the chemical and mechanical properties of the actual floorpan steel were unknown. Therefore, static tensile tests were required to ensure that the 24-gauge (0.61-mm) sheet steel had similar mechanical properties to that of the actual vehicle floorpan.

3.2 Scope

A total of seven static tensile tests were performed on coupon samples. Four coupons were cut from 24-gauge (0.61-mm) ASTM A653 sheet steel and evaluated in test nos. BFPC-1 through BFPC-4. Three coupons were cut from an actual Kia Rio floorpan and evaluated in test nos. KFPC-1 through KFPC-3. All seven coupons were cut according to the ASTM A370 standards [11] with a 0.50-in. (12.7-mm) width and 8-in. (200-mm) total length, as shown in Figure 5.

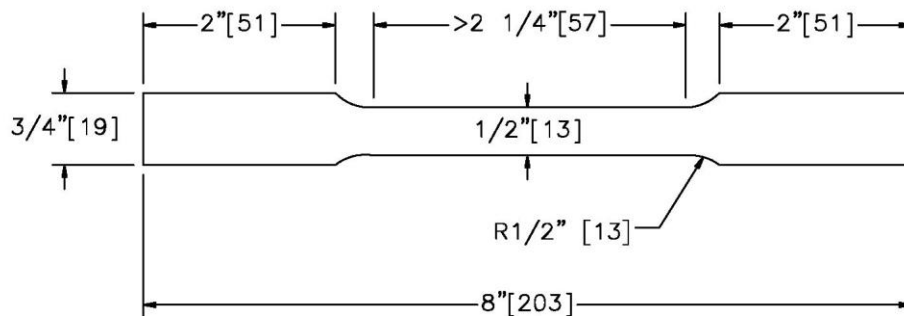


Figure 5. Static Testing Coupon Dimensions

An MTS Landmark Test System equipped with a 22 kip (100 kN) load cell was utilized to conduct the static testing. The samples were clamped on each end with a grip pressure of 1.5 ksi (10 MPa) and subjected to a loading rate of 0.2 in./in./sec until failure. An LX Series 500 Laser extensometer and an MTS Model no. 634.25E-24 mechanical extensometer were used to record displacements in the specimen. A standard-speed digital video and a digital camera were used to document the tests.

3.3 Static Testing Results

All seven of the tensile coupons fractured within the reduced cross-section region of the coupons. Further, the fracture locations were all within the gauge lengths of the laser extensometer, so accurate displacements and strains were recorded until the time of fracture. A

significant amount of necking was observed around the fracture location for all tests, a phenomenon typical of steel tensile failure. Pre-test and post-test measurements were recorded to calculate the reduction in cross-sectional area at fracture.

The extensometer and load cell data for each static test were analyzed to calculate peak loads and displacements at fracture, yield stress, Young's modulus, and ultimate tensile strength. A summary of the analyzed data results is shown in Table 2. Average results for both source materials, the 24-gauge (0.61-mm) sheet steel and the Kia Rio floorpan, were also calculated and included in the highlighted columns of Table 2. Engineering stress vs. strain curves for each test are shown in Figure 6 and true stress vs. strain curves for each test are shown in Figure 7. Detailed results for each test are provided individually in Appendix A. Although the individual extensometers produced similar results, the values described herein were calculated from the laser extensometer data in order to provide results through fracture.

Table 2. Summary of Static Tensile Testing

Test No.	BFPC-1	BFPC-2	BFPC-3	BFPC-4	Average	KFPC-1	KFPC-2	KFPC-3	Average
Source Material	24-gauge A653	24-gauge A653	24-gauge A653	24-gauge A653	24-gauge A653	Kia Rio Floorpan	Kia Rio Floorpan	Kia Rio Floorpan	Kia Rio Floorpan
Thickness in. (mm)	0.025 (0.635)	0.026 (0.660)	0.025 (0.635)	0.026 (0.660)	0.026 (0.660)	0.025 (0.635)	0.026 (0.660)	0.026 (0.660)	0.026 (0.660)
Width in. (mm)	0.501 (12.7)	0.504 (12.8)	0.505 (12.8)	0.507 (12.9)	0.504 (12.8)	0.493 (12.5)	0.492 (12.5)	0.492 (12.5)	0.492 (12.5)
Yield Load lb (kg)	553 (251)	537 (244)	565 (256)	560 (254)	553 (251)	498 (226)	488 (221)	476 (216)	488 (221)
Peak Load lb (kg)	686 (311)	688 (312)	700 (318)	695 (315)	692 (314)	618 (280)	611 (277)	599 (272)	610 (277)
Failure Load lb (kg)	617 (280)	619 (218)	630 (286)	625 (283)	623 (283)	557 (253)	550 (250)	539 (244)	549 (249)
Yield Strength-2% offset ksi (GPa)	43.8 (302)	41.4 (285)	44.1 (304)	42.3 (292)	42.9 (296)	44.3 (305)	42.2 (291)	41.9 (289)	42.8 (295)
Young's Modulus ksi (GPa)	21,934 (151,229)	20,887 (144,010)	22,320 (153,890)	21,358 (147,258)	21,625 (149,099)	22,289 (153,677)	21,247 (146,492)	20,998 (144,776)	21,511 (148,313)
Ultimate Tensile Strength ksi (GPa)	54.4 (375)	53.0 (365)	54.8 (378)	52.5 (362)	53.7 (370)	54.9 (379)	52.9 (365)	52.7 (363)	53.5 (369)
Eng. Stress at Failure ksi (GPa)	48.9 (337)	47.7 (329)	49.3 (340)	47.2 (325)	48.3 (333)	49.4 (341)	47.6 (328)	47.4 (328)	48.2 (332)
True Stress at Failure ksi (GPa)	73.6 (507)	73.2 (505)	72.3 (498)	73.7 (508)	73.2 (505)	90.3 (623)	105.3 (726)	96.6 (666)	97.4 (672)
True Strain at Failure (in./in.)	0.41	0.43	0.38	0.44	0.42	0.60	0.79	0.71	0.70
Reduction in Area	33.6%	34.7%	31.8%	35.9%	34.0%	45.2%	54.8%	50.9%	50.3%
2-in. Elongation at Fracture	24.6%	24.4%	25.8%	26.4%	25.3%	30.8%	32.5%	32.5%	31.9%

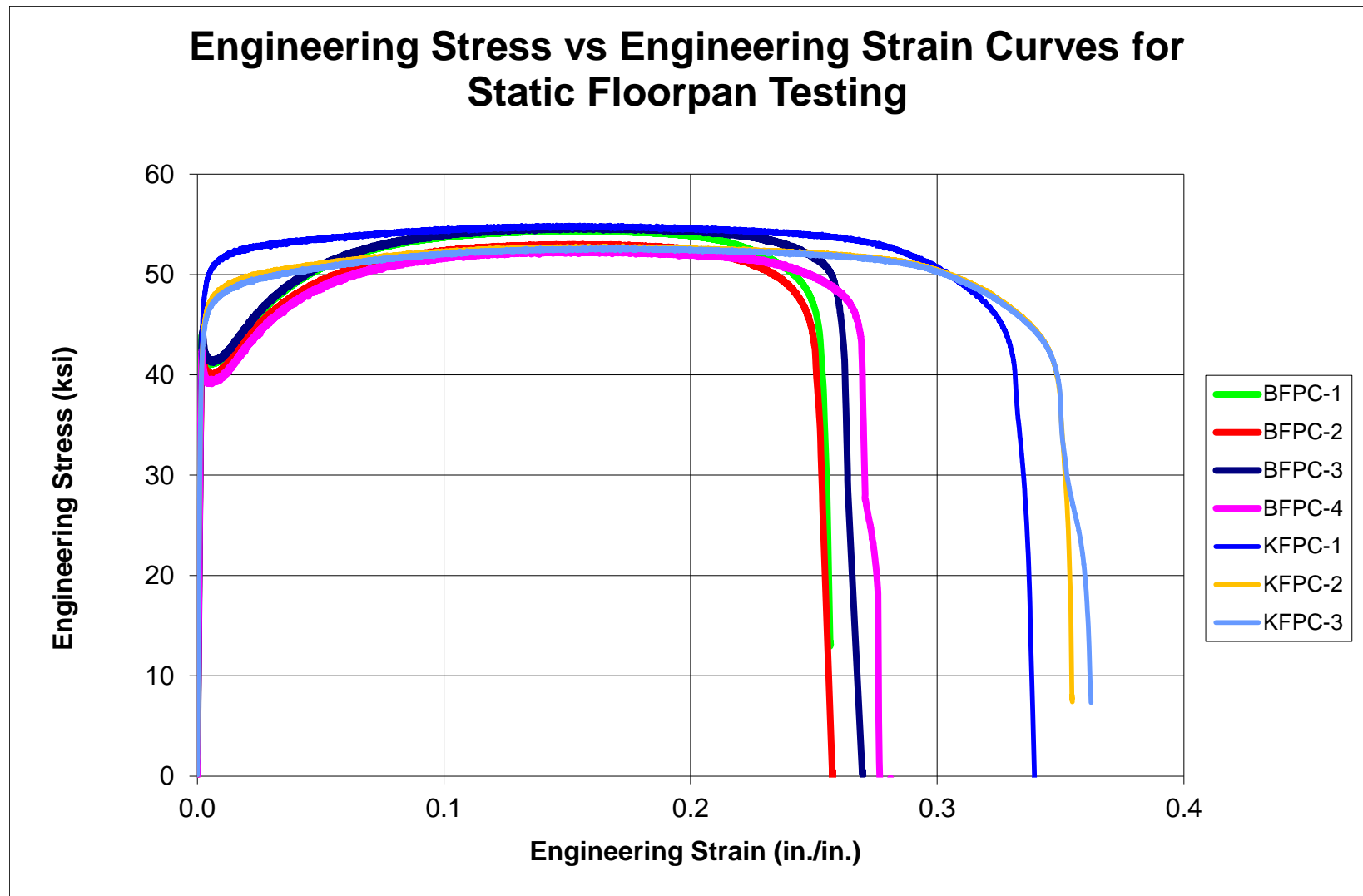


Figure 6. Engineering Stress vs. Strain for Static Coupon Tests

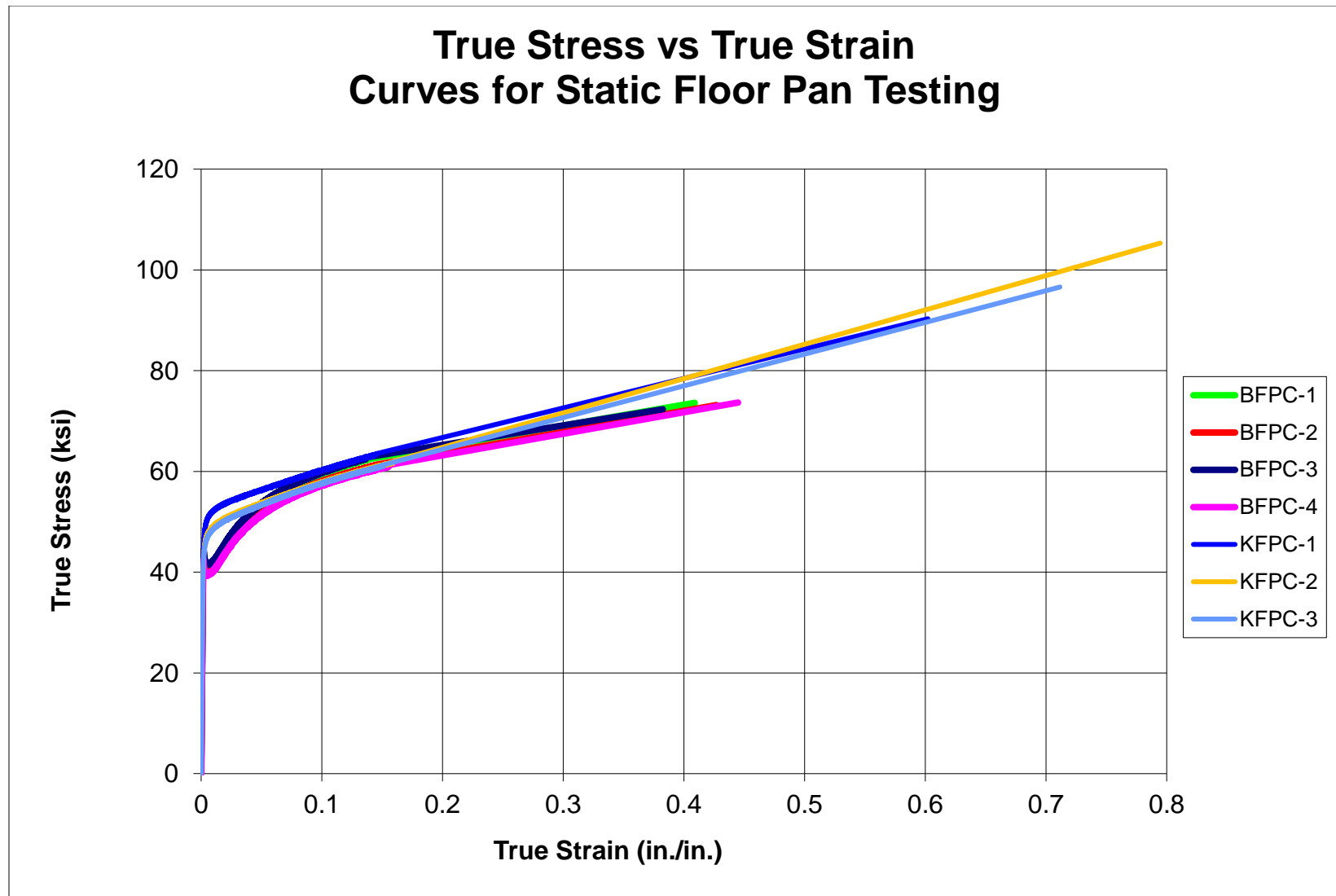


Figure 7. True Stress vs. True Strain for Static Coupon Tests

3.4 Discussion

The tensile strength of the 24-gauge (0.61-mm) ASTM A653 sheet steel was found to be very similar to that of the steel used in the actual Kia Rio floorpan. The 2-percent offset yield strengths, elastic moduli, and ultimate tensile strengths of the two source materials differed by less than 1 percent. The average peak and failure loads of the 24-gauge (0.61-mm) sheet steel were higher, but this can be attributed to the sheet steel coupon samples having a slightly larger width than the Kia Rio floorpan coupon samples.

The two materials differed in ductility and behavior at the onset of yielding. The Kia Rio coupon samples demonstrated greater ductility with a 6.6 percent increase in elongation at fracture and a 66 percent increase in true strain at failure compared to the 24-gauge (0.61-mm) sheet steel. Additionally, the Kia Rio samples exhibited smooth transitions between the elastic and plastic loading portions of the curves and nearly resembled an elastic-perfectly plastic steel, as shown in Figure 6. Alternatively, the 24-gauge (0.61-mm) sheet steel exhibited a stress drop at the onset of yielding, which is characteristic of low-carbon steels. Thus, the steel alloy utilized in the actual Kia Rio floorpan likely has a higher carbon content than the ASTM A653 sheet steel.

Overall, the 24-gauge (0.61-mm) sheet steel compared favorably to the steel utilized in the Kia Rio floorpan. The thickness and ultimate stress of the sheet steel was nearly identical to that of the floorpan steel. Thus, the onset of failure/tearing should occur at similar loads. The reduced ductility of the sheet steel may cause it to rupture or tear easier than the actual floorpan making any results observed from component testing with this sheet steel conservative in relation to actual floorpans. Therefore, the 24-gauge (0.61-mm) ASTM A653 sheet steel was recommended for use as a surrogate floorpan during component tests designed to evaluate the potential for floorpan tearing.

4 COMPONENT TESTING CONDITIONS – FLOORPAN TEARING

4.1 Purpose

Previous full-scale crash tests on a prototype cable median barrier resulted in the top of the MWP tearing through the vehicle floorpan [4]. These tears are classified as penetrations into the occupant compartment, which is a violation of the MASH criteria. Dynamic component testing was desired to analyze floorpan tearing and evaluate the potential of various post retrofits to mitigate the propensity for tearing.

4.2 Scope

A total of fifteen dynamic bogie tests were conducted in order to evaluate the propensity for floorpan tearing associated with cable barrier posts. Each test involved two posts being impacted and overrun by a bogie vehicle equipped with a simulated small car floorpan. The posts were spaced 8 feet (2.4 m) apart longitudinally and were offset 4¼ in. (108 mm) laterally so that the posts contacted the simulated floorpan independently. The posts were installed in either an 8-in (203-mm) diameter hole cored into the tarmac or an 18-in. (457-mm) hole augured into a soil test pit. Both hole types were backfilled with compacted soil to MASH specifications. Post orientation was varied between tests to evaluate the effect of impacting and overriding the posts from multiple angles. Eight different post configurations were evaluated, but the posts within each individual test were identical in both configuration and orientation. The bogie vehicle impacted the posts at a height of 12 in. (305 mm) above groundline at a targeted impact speed of 25 mph (40 km/h). The dynamic testing matrix is summarized in Table 3, while the test setup to evaluate floorpan tearing is shown in Figure 8.

The first two tests were conducted on the MWP in an effort to replicate the tearing observed during full-scale crash testing and validate the test setup. The MWP used within test nos. MWFP-1 and MWFP-2 were identical to the prototype cable median barrier in crash test no. MWP-7. The MWP had keyways and bolt holes cut into its flanges where the cable brackets would be attached. Two top corners of the post were radiused to ⅝ in. (16 mm), as shown in Figure 9. The other two corners were radiused to ¼ in. (6 mm). Once the test setup demonstrated the ability to replicate the tearing observed during full-scale testing, the testing and evaluation efforts focused on modifications to the MWP to mitigate tearing.

A total of nine tests were conducted on the MWP with various weakening holes or slots cut into the upstream and downstream surfaces of the posts at groundline. Five tests were conducted on the MWP with ¾-in. (19-mm) diameter holes cut into both surfaces, two tests were conducted on the MWP with three ⅜-in. (10-mm) holes cut into both surfaces, and two tests were conducted on the MWP with ⅜-in. x 1⅝-in. slots (10-mm x 29-mm) slots cut into both surfaces, as shown in Figures 10 through 14, respectively.

One test, test no. MWFP-6, was conducted to evaluate the effects of edge rounding on the MWP. Edge rounding is typically only performed on flat sheet steel. Since MwRSF already had the MWPs on site, the edge rounding was simulated to save time and minimize cost. Thus, a ⅜-in. (5-mm) steel rod was welded to the free edge of the post to simulate no. 1 edge rounding, as shown in Figure 12. The rod was only welded to the top 11½ in. (292 mm) of the post which may be in contact with the simulated floorpan, so the bending strength of the posts was not

affected. If edge rounding was shown to prevent tearing, a new MWP with actual rounded edges would be fabricated for the next full-scale crash test.

One test, test no. MWPPF-13, was conducted to evaluate the effects of adding an edge protector to the free edges of the posts. Each edge protector was a $\frac{3}{16}$ -in. (5-mm) thick steel plate bent at 90 degrees, as shown in Figure 15. The longer sides of the plates were welded to the strong-axis flanges of the MWP, and the shorter sides were cut to match the geometry of the V-notch cut into the top of the MWP. This edge protector configuration was selected for testing, because it would also represent the effects of extending the flanges at the top of the post and folding them over at 90 degrees, effectively shielding the free edges of the post from direct contact. If this retrofit showed promise, a new MWP could be fabricated with extended flanges that folded over to match the effect of this welded-on edge protector.

Finally, two tests were conducted on S3x5.7 (S76x8.5) posts, which are commonly used as weak posts in other cable barrier systems. As discussed in Chapter 2, floorpan tearing had been observed in multiple crash tests into barrier systems utilizing S3x5.7 (S76x8.5) posts. These more traditional weak posts were evaluated as part of this study to compare the propensity for tearing between S3x5.7 (S76x8.5) posts and the MWP. The S3x5.7 (S76x8.5) posts were evaluated at two different heights, 39¼ in. (997 mm) matching the current MWP cable system posts and 31 in. (787 mm) matching the low-tension cable barrier system posts, as shown in Figure 11.

Material specifications, mill certifications, and certificates of conformity for the posts are shown in Appendix B. A compacted, coarse, crushed limestone material that met AASHTO standard soil designation M147 Grade B, as recommended by MASH, was utilized for all tests [1].

Table 3. Dynamic Component Testing Matrix, Floorpan Tearing Evaluation

Test	Post				Post Installed in Tarmac/Soil	Targeted Impact Conditions		
	Type	Above-Ground Height in. (mm)	Modifications			Speed mph (km/h)	Height in. (mm)	Angle (deg)
			Top Radius in. (mm)	Groundline in. (mm)				
MWPFP-1	MWP	39¼ (997)	⅝ (16)	-	Tarmac	25 (40)	12 (305)	0
MWPFP-2	MWP	39¼ (997)	⅝ (16)	-	Tarmac	25 (40)	12 (305)	0
MWPFP-3	MWP	39¼ (997)	⅝ (16)	Ø¾ (19) holes	Tarmac	25 (40)	12 (305)	0
MWPFP-4	S3x5.7	39¼ (997)	-	-	Tarmac	25 (40)	12 (305)	0
MWPFP-5	S3x5.7	31 (787)	-	-	Tarmac	25 (40)	12 (305)	0
MWPFP-6	MWP	39¼ (997)	⅝ (16) with #1 Edge Protection	-	Tarmac	25 (40)	12 (305)	0
MWPFP-7	MWP	39¼ (997)	⅝ (16)	Ø¾ (19) holes	Soil	25 (40)	12 (305)	0
MWPFP-8	MWP	39¼ (997)	⅝ (16)	Ø¾ (19) holes	Soil	25 (40)	12 (305)	-25
MWPFP-11	MWP	39¼ (997)	⅝ (16)	(3) Ø⅜ (10) holes	Tarmac	25 (40)	12 (305)	0
MWPFP-12	MWP	39¼ (997)	⅝ (16)	Ø⅜ (10) x 1⅝ (29) slots	Tarmac	25 (40)	12 (305)	0
MWPFP-13	MWP	39¼ (997)	Flange Extension	-	Tarmac	25 (40)	12 (305)	0
MWPFP-14	MWP	39¼ (997)	⅝ (16)	(3) Ø⅜ (10) holes	Soil	25 (40)	12 (305)	25
MWPFP-15	MWP	39¼ (997)	⅝ (16)	Ø⅜ (10) x 1⅝ (29) slots	Soil	25 (40)	12 (305)	25
MWPFP-18	MWP	39¼ (997)	⅝ (16)	Ø¾ (19) holes	Soil	25 (40)	12 (305)	25
MWPFP-21	MWP	39¼ (997)	⅝ (16)	Ø¾ (19) holes	Soil	25 (40)	12 (305)	-25

0 degree orientation corresponds to impacts along the longitudinal axis of the post/barrier

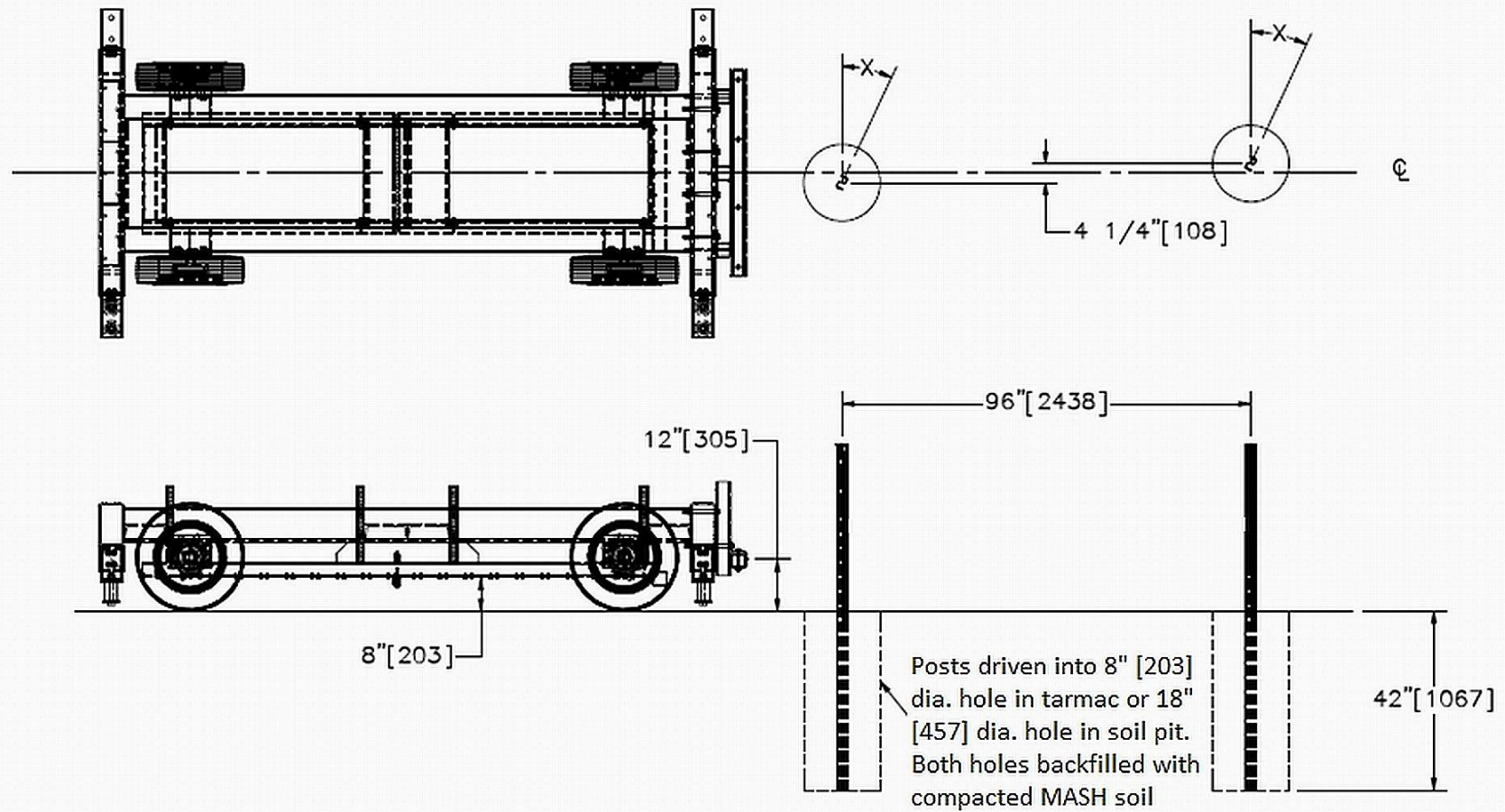


Figure 8. Dynamic Component Test Setup, Floorpan Tearing Evaluation

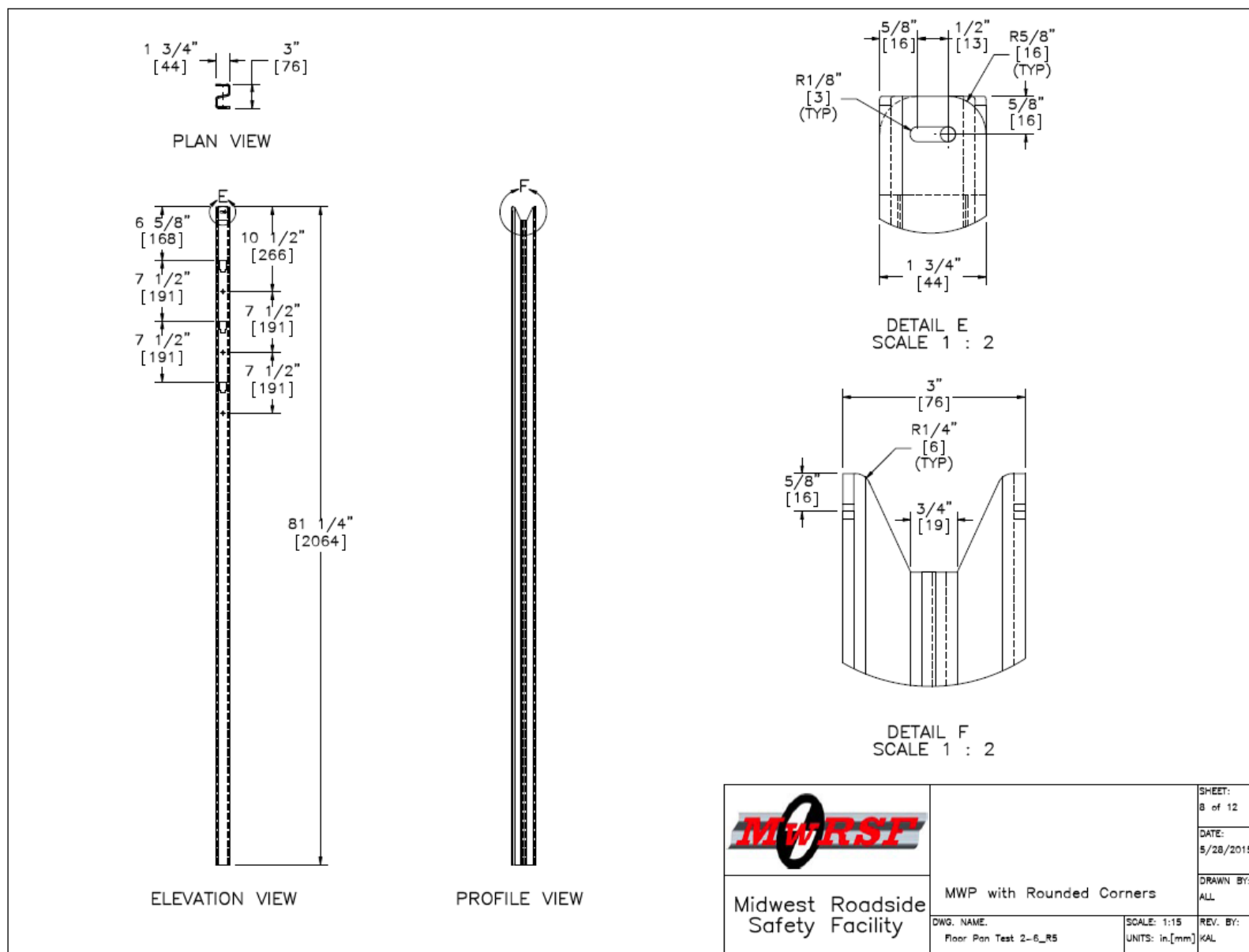


Figure 9. MWP with Rounded Corners, Test Nos. MWFPF-1 and MWFPF-2

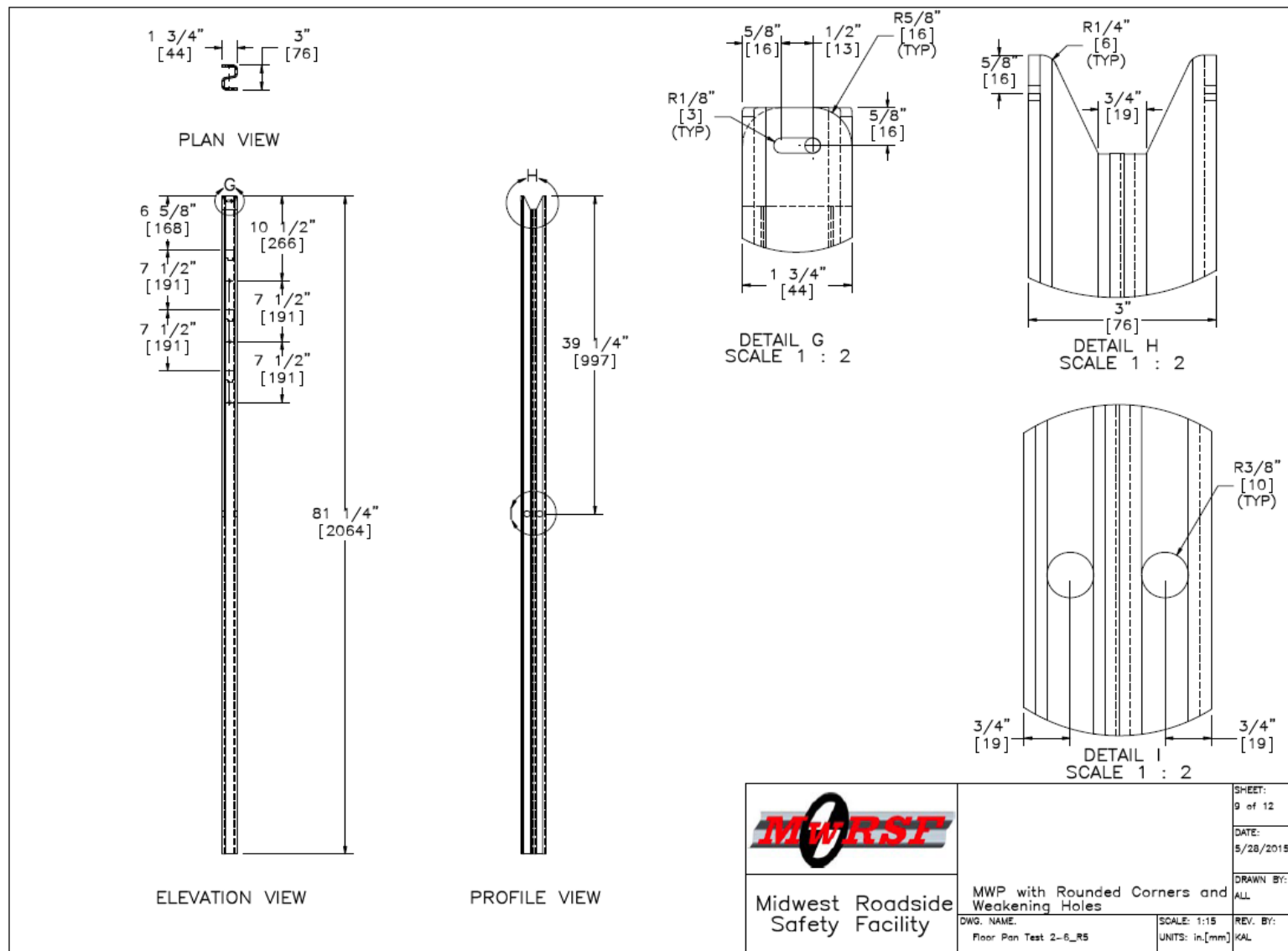


Figure 10. MWP with 3/4-in. (19-mm) Diameter Holes, Test Nos. MWFPF-3, MWFPF-7 Through MWFPF-8, MWFPF-18, and MWFPF-21

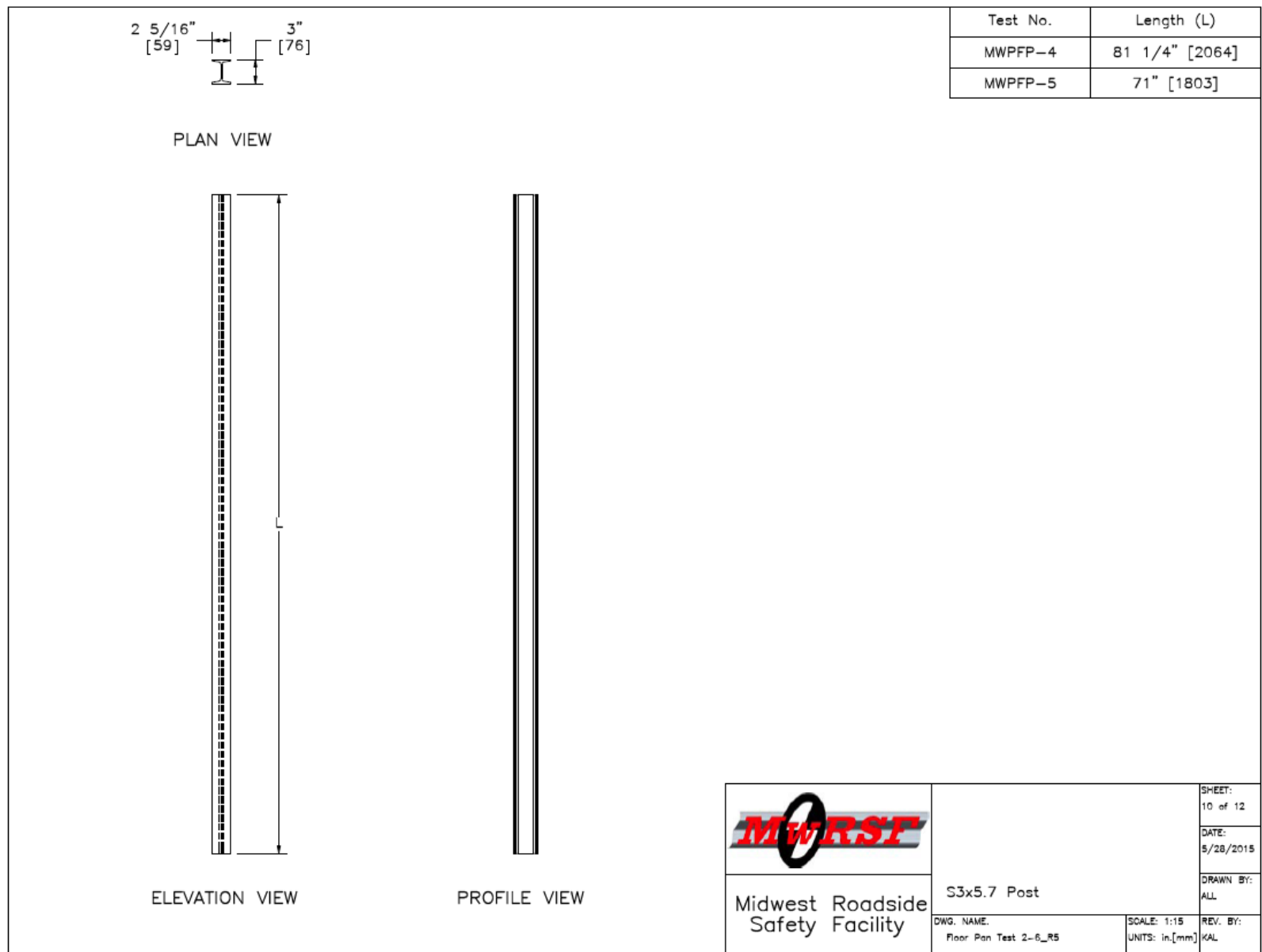


Figure 11. S3x5.7 (S76x8.5) Posts, Test Nos. MWPFP-4 and MWPFP-5

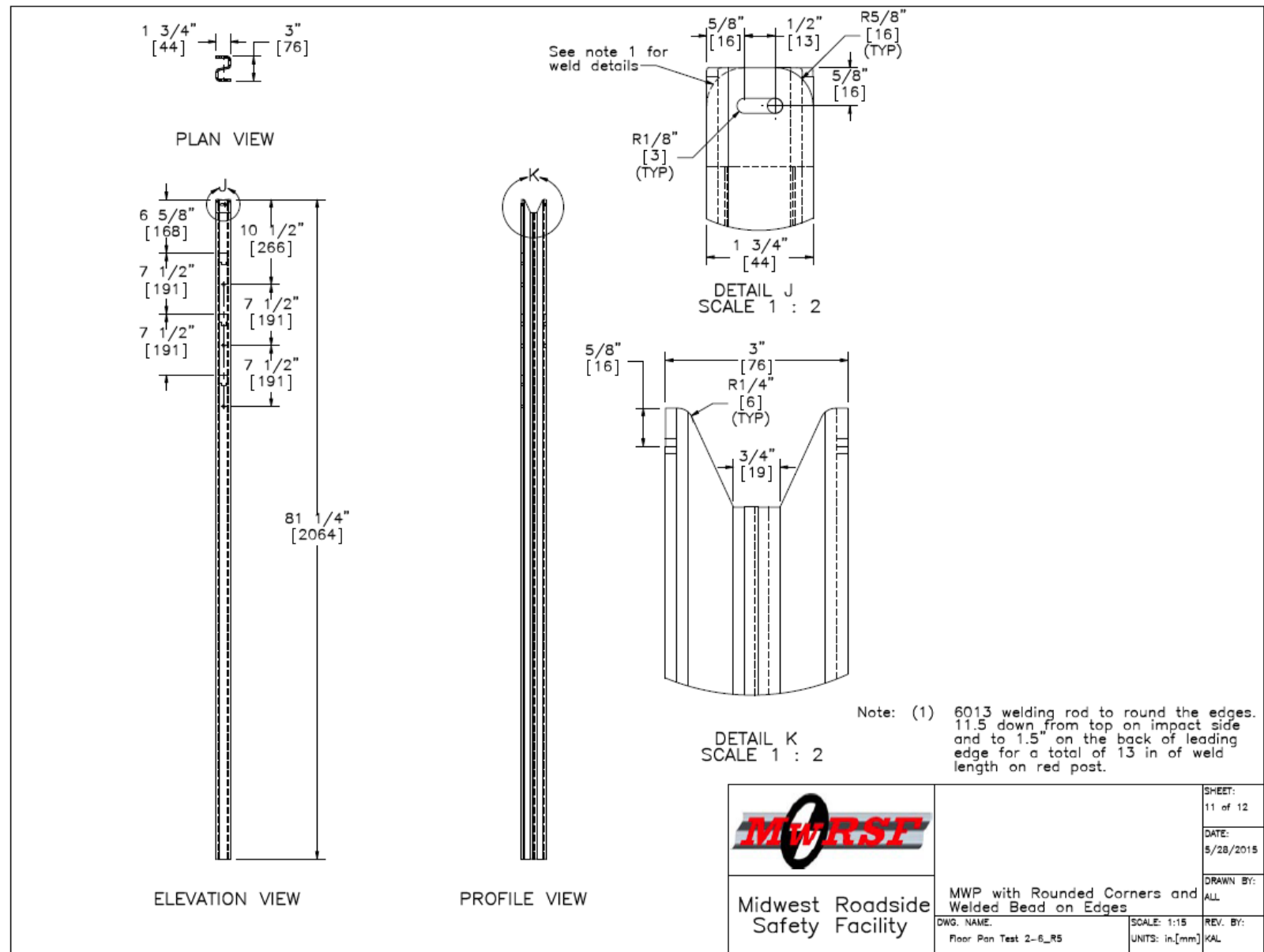


Figure 12. MWP with Simulated #1 Edge Rounding, Test No. MWFPF-6

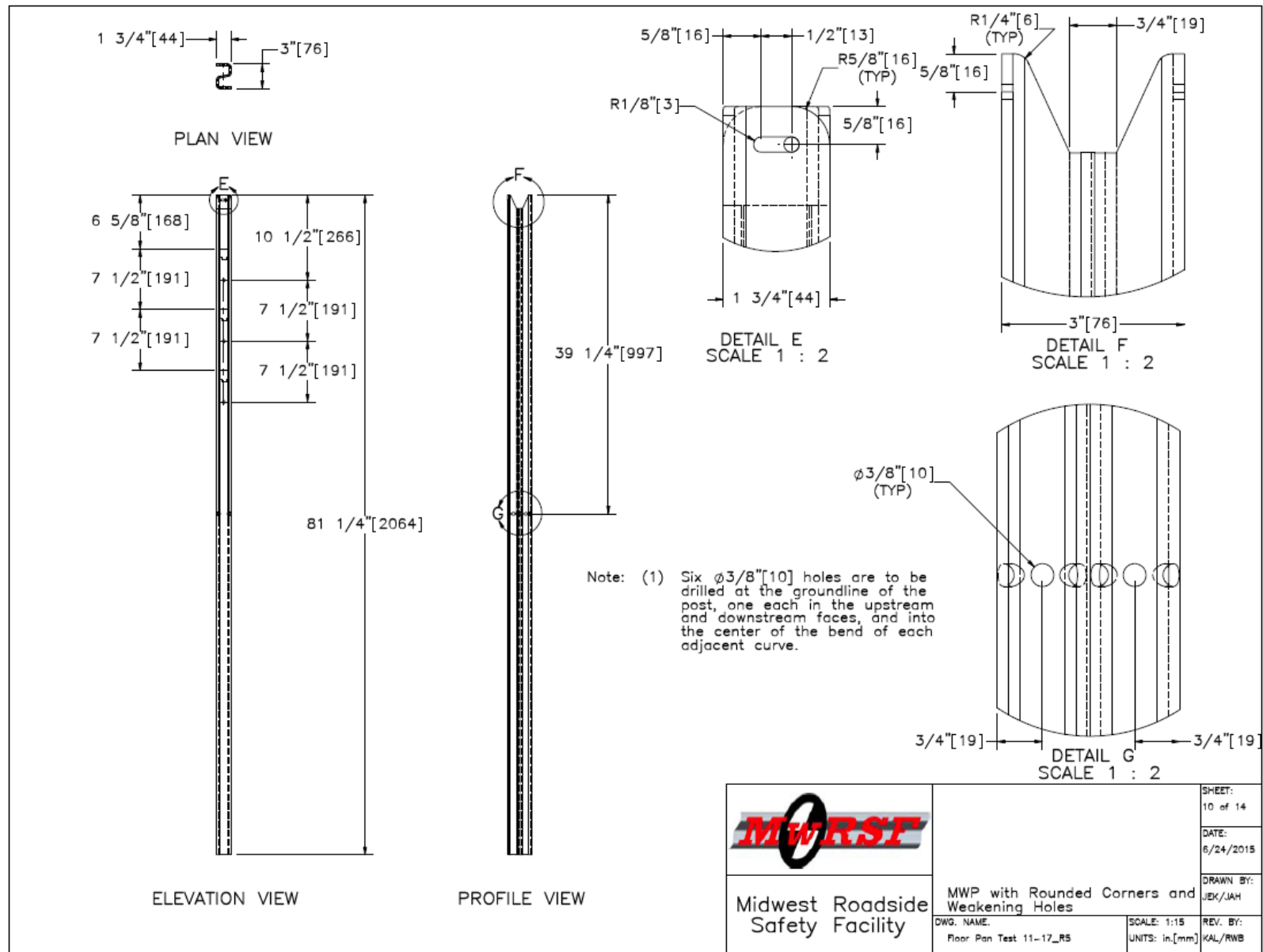


Figure 13. MWP with Three 3/8-in. (10-mm) Diameter Holes, Test Nos. MWFPF-11 and MWFPF-14

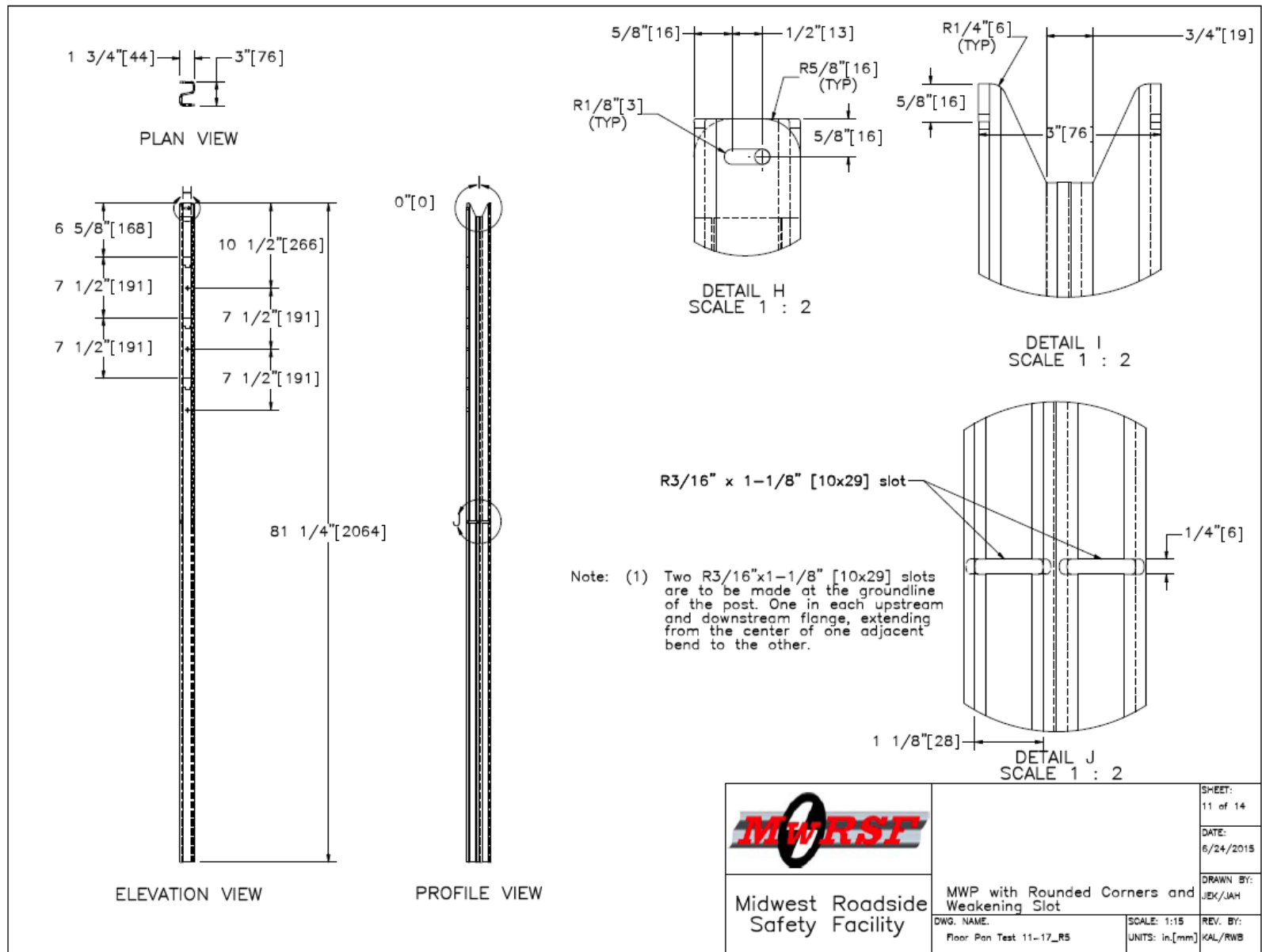


Figure 14. MWP with 3/8-in. x 1 1/8-in. (10-mm x 29-mm) Slots, Test Nos. MWFPF-12 and MWFPF-15

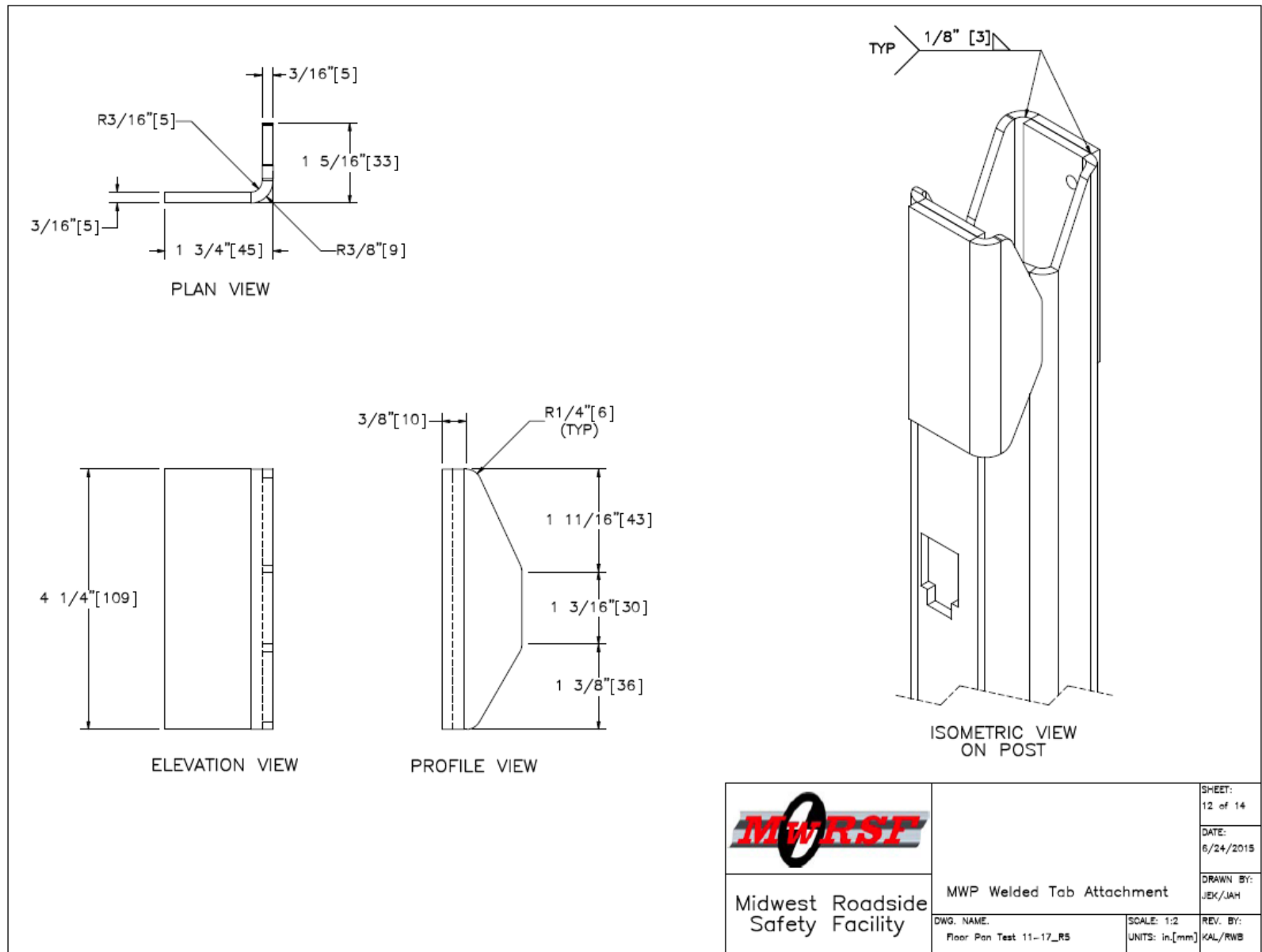


Figure 15. MWP with Steel Plate Edge Protector, Test No. MWFPF-13

4.3 Equipment and Instrumentation

Equipment and instrumentation that was utilized to collect and record data during the dynamic bogie tests included: a bogie vehicle; an accelerometer; a retroreflective speed trap; high-speed and standard-speed digital video; and still cameras.

4.3.1 Bogie Vehicle

A rigid-frame bogie vehicle, equipped with a simulated small car floorpan, was used to impact the posts. The simulated floorpan consisted of a 120-in. x 23¾-in. (3,048-mm x 603-mm) sheet of 24-gauge (0.61-mm) ASTM A653 steel. The sheet steel was mounted to the bottom of an undercarriage frame at a height of 8 in. (203 mm), which matched the height of the Kia Rio floorpans from the previous full-scale crash tests. The undercarriage frame was constructed from 3½-in. x 3½-in. x ⅜-in. (90-mm x 90-mm x 10-mm) steel tubes and was bolted to the inside of the bogie vehicle frame. The front beam of the undercarriage frame was positioned in front of the simulated floorpan and shifted downward 1¾ in. (44 mm). This vertical offset prevented the top of the post from snagging on the front edge of the sheet steel, and acted as a stiff cross member of the vehicle undercarriage (e.g., frame element, axle) that caused the post to bend down and spring back upward toward the floorpan as the bogie overrode the top of the post. A 1¾-in. (44-mm) square tube was bolted underneath and across the middle of the simulated floorpan to create a second location where the post would be pushed down and allowed to spring back upward. Photographs of the bogie vehicle are shown in Figure 16, while details of the simulated vehicle undercarriage are shown in Figures 17 through 23.

The bogie impact head consisted of a 2½-in. x 2½-in. x ¼-in. (64-mm x 64-mm x 6-mm) square tube mounted to the front of the bogie at a height of 12 in. (305 mm), measured to the center of the tube. A ¾-in. (19-mm) thick neoprene pad was wrapped around the tube to prevent local damage to the posts during impact. The weight of the bogie with the addition of the impact head and simulated floorpan was approximately 2,400 lb (1,089 kg).

A pickup truck with a reverse-cable tow system was used to propel the bogie to a target impact speed of 25 mph (40 km/h). When the bogie approached the end of the guidance system, it was released from the tow cable, allowing it to be free rolling when it impacted the post. A remote-controlled, braking system was installed on the bogie, thus allowing it to be brought safely to rest after the test.



Figure 16. Bogie Vehicle and Guidance Track - Floorpan Testing

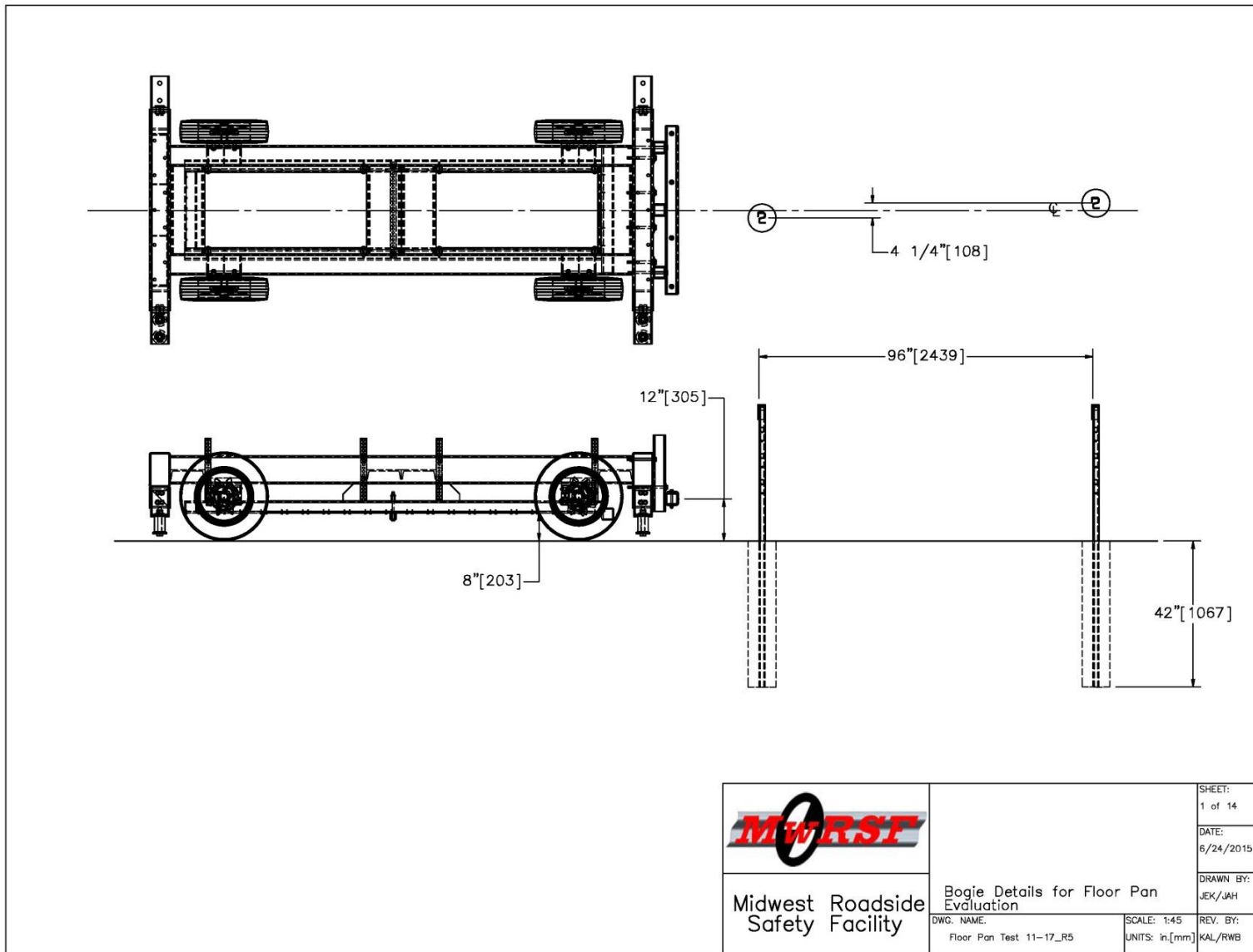


Figure 17. Bogie Details for Floorpan Evaluation

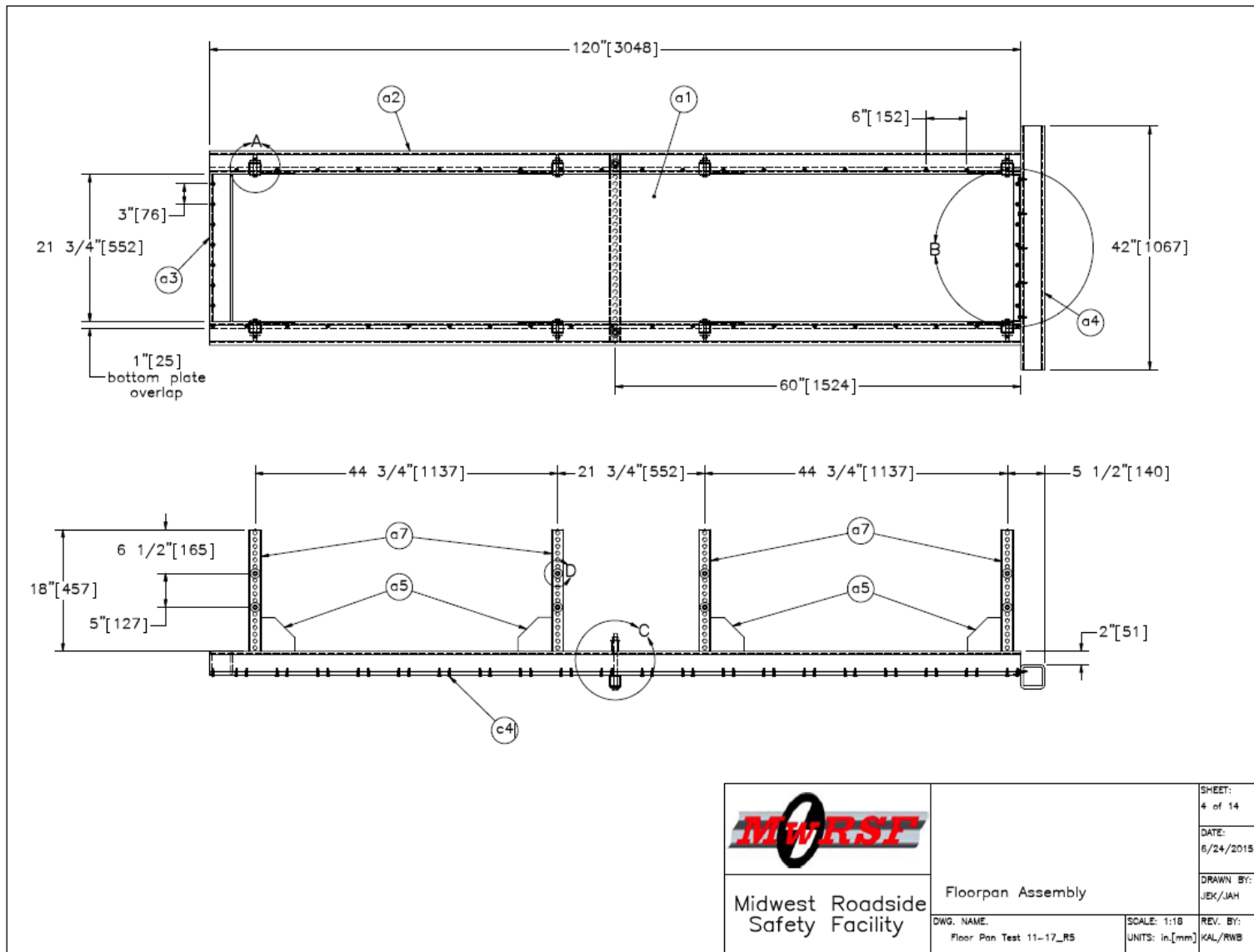


Figure 18. Bogie Details, Undercarriage Assembly

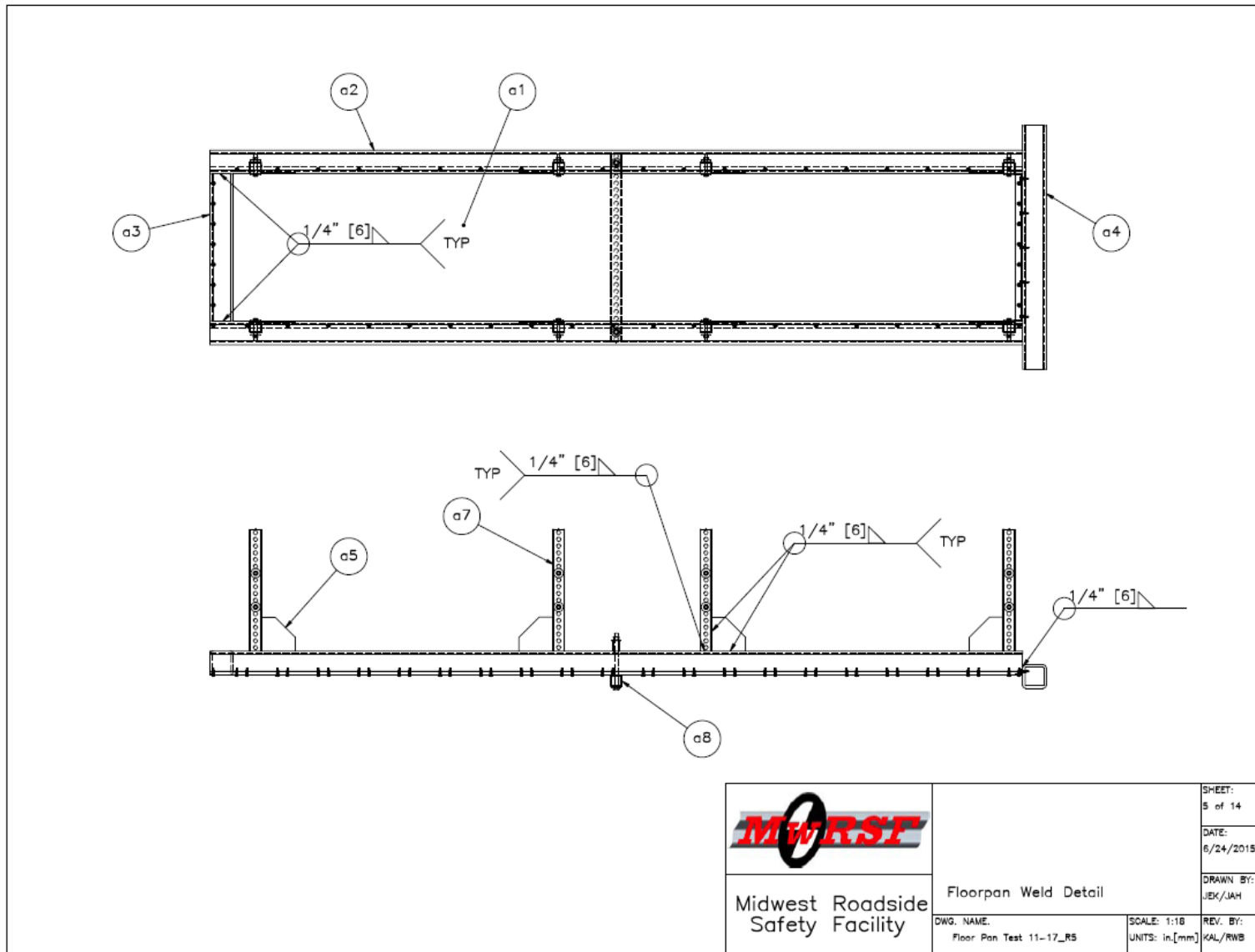


Figure 19. Bogie Details, Undercarriage Welds

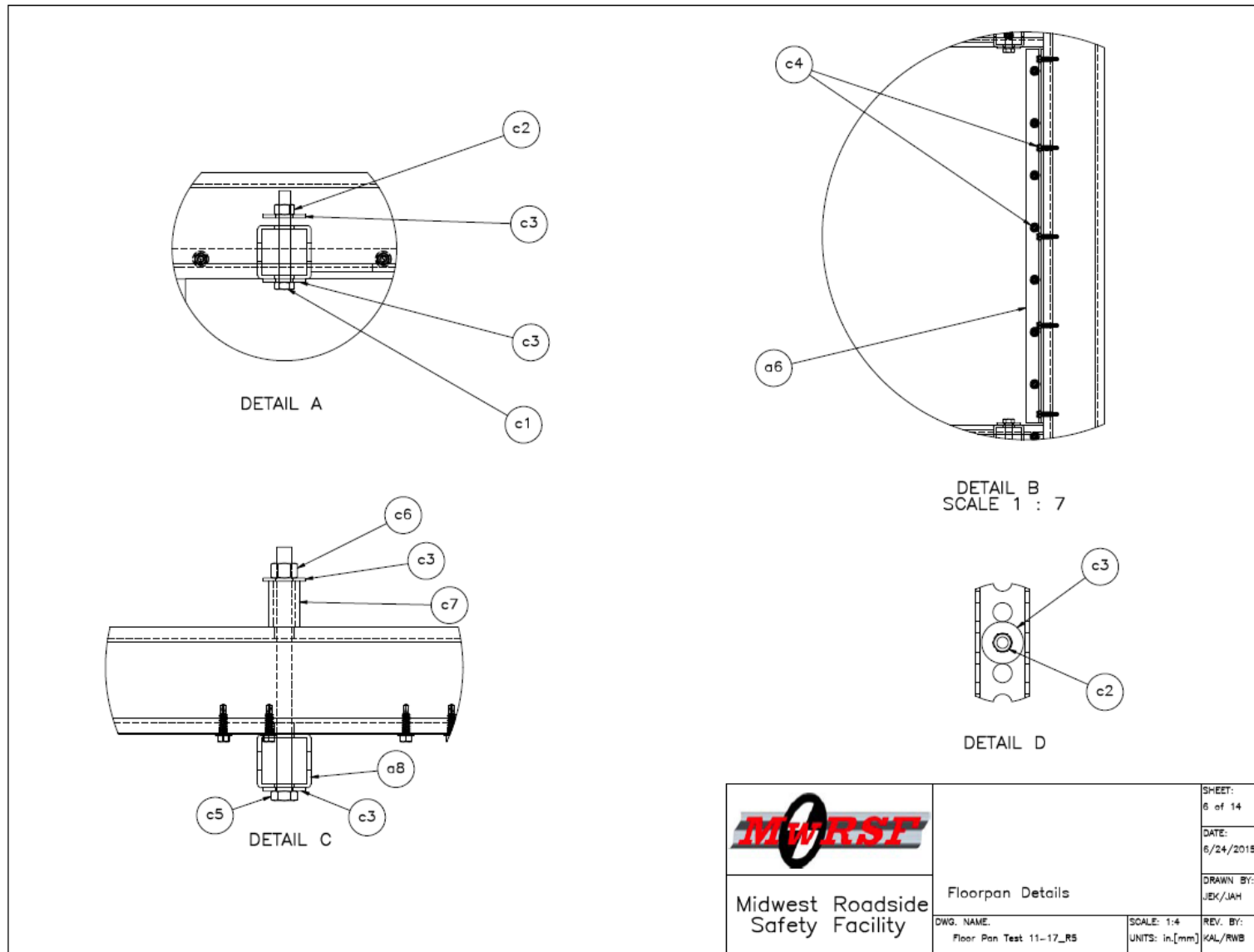


Figure 20. Bogie Details, Floorpan Connections

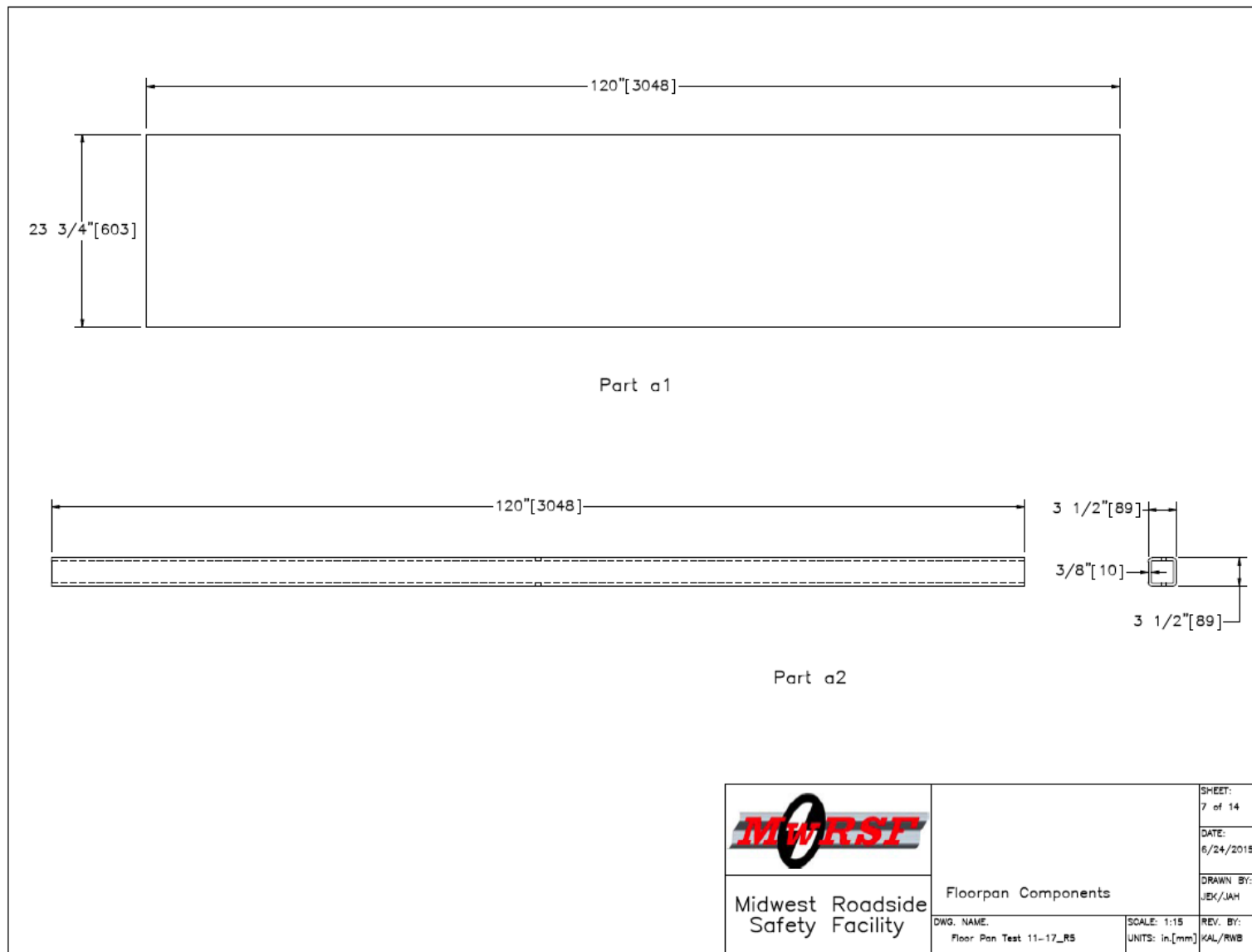


Figure 21. Bogie Details, Floorpan and Undercarriage Components

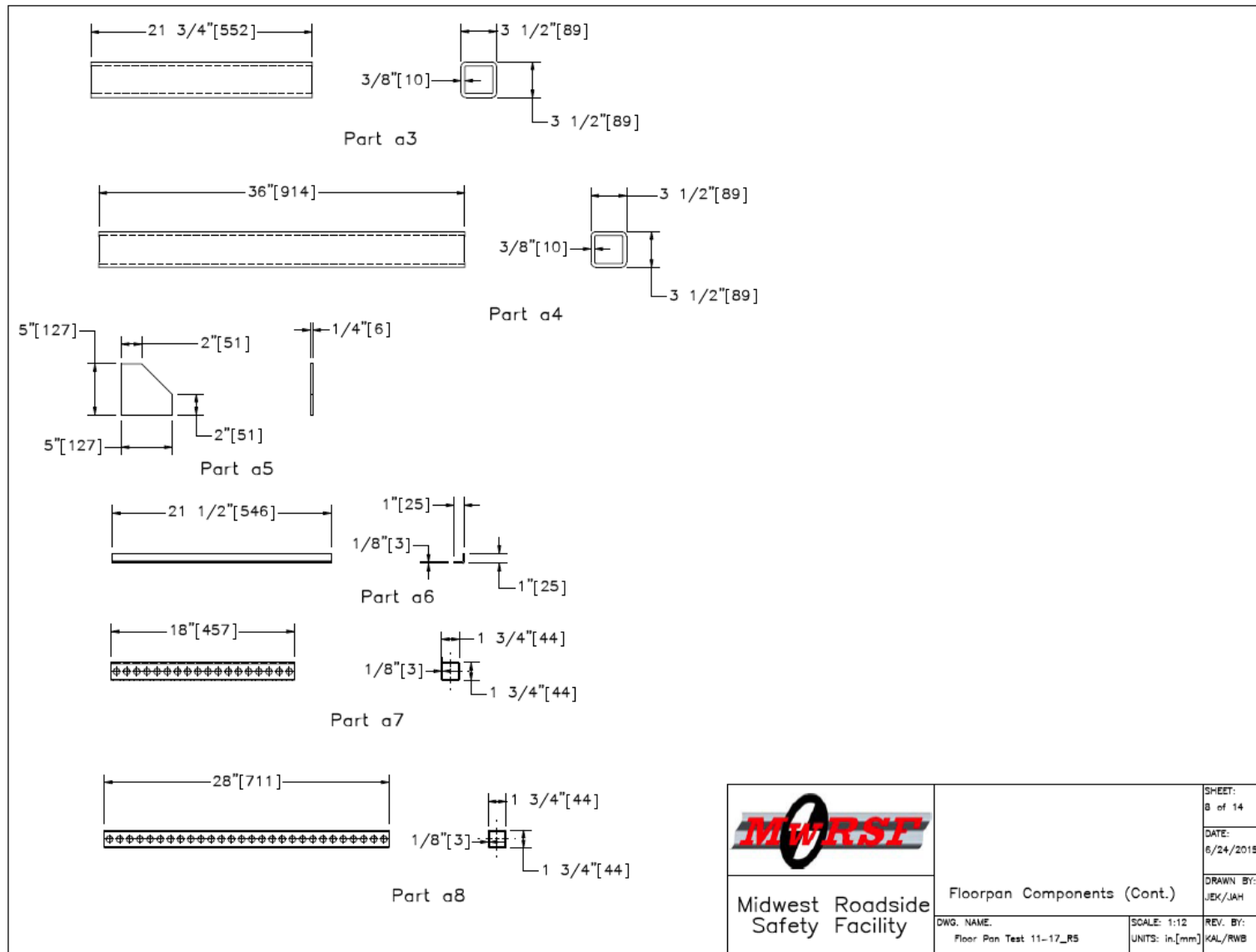


Figure 22. Bogie Details, Undercarriage Components

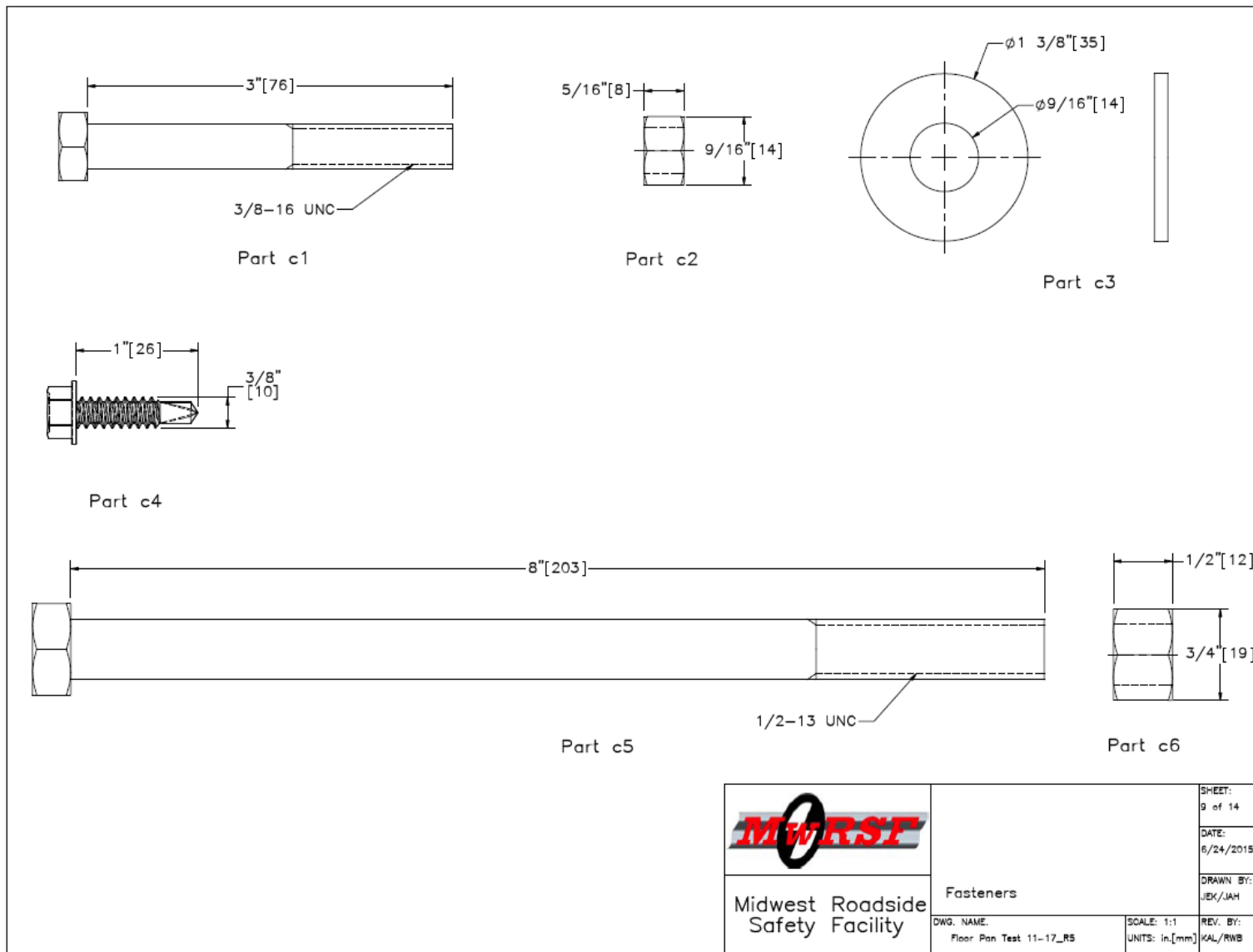


Figure 23. Bogie Details, Fasteners

4.3.2 Accelerometers

One environmental shock and vibration sensor/recorder system was used to measure the accelerations in the longitudinal, lateral, and vertical directions. The accelerometer was mounted near the center of gravity of the bogie vehicle. The electronic accelerometer data obtained in dynamic testing was filtered using the SAE Class 60 and the SAE Class 180 Butterworth filters conforming to the SAE J211/1 specifications [12].

The SLICE-2 accelerometer unit was a modular data acquisition system manufactured by Diversified Technical Systems Inc. of Seal Beach, California. The acceleration sensors were mounted inside the body of a custom built SLICE 6DX event data recorder and recorded data at 10,000 Hz to the onboard microprocessor. The SLICE 6DX was configured with 7 GB of non-volatile flash memory, a range of ± 500 g's, a sample rate of 10,000 Hz, and a 1,650 Hz (CFC 1000) anti-aliasing filter. The "SLICEWare" computer software program and a customized Microsoft Excel worksheet were used to analyze and plot the accelerometer data.

4.3.3 Retroreflective Optic Speed Trap

The retroreflective optic speed trap was used to determine the speed of the bogie vehicle before impact. Five retroreflective targets, spaced at approximately 18-in. (457-mm) intervals, were applied to the side of the vehicle. When the emitted beam of light was reflected by the targets and returned to the Emitter/Receiver, a signal was sent to the data acquisition computer as well as the external LED box activating the LED flashes. The speed was then calculated using the spacing between the retroreflective targets and the time between the signals. LED lights and high-speed digital video analysis are used only as a backup in the event that vehicle speeds cannot be determined from the electronic data.

4.3.4 Digital Photography

A combination of one AOS high-speed digital video camera, five GoPro digital video cameras, and one JVC digital camera were used to document each test. The AOS high-speed camera had a frame rate of 500 frames per second, the GoPro video cameras had a frame rate of 120 frames per second, and the JVC digital video camera had a frame rate of 29.97 frames per second. Three cameras- one AOS, one GoPro, and one JVC video camera- were placed laterally from the post, with a view perpendicular to the bogie's direction of travel. The remaining cameras were placed at various locations on and around the bogie- two cameras with view of the bogie's floorpan and the remainder placed with view of the posts. A Nikon D50 digital still camera was also used to document pre- and post-test conditions for all tests.

4.4 Data Processing

The electronic accelerometer data obtained in dynamic testing was filtered using the SAE Class 60 Butterworth filter conforming to the SAE J211/1 specifications [12]. The pertinent acceleration signal was extracted from the bulk of the data signals. The processed acceleration data was then multiplied by the mass of the bogie to get the impact force using Newton's Second Law. Next, the acceleration trace was integrated to find the change in velocity versus time. Initial velocity of the bogie, calculated from the retroreflective optic speed trap data, was then used to determine the bogie velocity, and the calculated velocity trace was integrated to find the bogie's

displacement. This displacement is also the displacement of the post. Combining the previous results, a force vs. deflection curve was plotted for each test. Finally, integration of the force vs. deflection curve provided the energy vs. deflection curve for each test.

5 TESTING RESULTS - FLOORPAN TEARING

5.1 Results

A total of fifteen dynamic component tests were conducted with the simulated vehicle floorpan bogie. A summary of each bogie test, including sequential and post-test photographs, is provided in the following sections. The accelerometer data for each test was processed in order to obtain force vs. deflection and energy vs. deflection curves. Detailed accelerometer results for each test are provided in Appendix B.

5.1.1 Test No. MWPFP-1

Test no. MWPFP-1 was conducted on two MWPs installed in strong soil with a 0-degree orientation angle, thus creating an impact about the post's weak-axis of bending. This test was an attempt to replicate the floorpan tearing witnessed during full scale test nos. MWP-6 and MWP-7 and to validate the testing setup and procedure. During the test, the bogie impacted the first post at a speed of 25.0 mph (40.2 km/h). The bogie then went on to impact the second post at 0.220 seconds and caused similar deformation and spring-back characteristics as observed in the first post. The bogie overrode both posts. However, the top corners of both posts left distinct creases or gouge marks that began near the front edge of the simulated floorpan and extended the length of the bogie undercarriage. Tearing was also observed within both creases corresponding to the free edges of the posts. These creases and tears were similar to the damage found in test nos. MWP-6 and MWP-7.

Unfortunately, the crossbeams located at the front and mid-span of the simulated floorpan had not been installed for test no. MWPFP-1. Thus, the front edge of the sheet steel was exposed to contact, and the posts snagged on the simulated floorpan. The simulated floorpan was torn from the front of the undercarriage frame, as shown in Figure 25. This result allowed a broader area of the simulated floorpan to deform and reduced the severity of the localized gouging and tearing. Therefore, modifications to the test setup were required to accurately replicate the floorpan of a Kia Rio. Subsequently, crossbeams were added to eliminate this problem for subsequent tests and to simulate undercarriage support members.

Force vs. deflection and energy vs. deflection curves were created from the accelerometer data. Additionally, the high-speed video was analyzed to determine the times when the bogie overrode each post, the posts contacted the simulated floorpan, and the posts lost contact with the bogie vehicle. Results from the data and video analysis are shown in Figure 30. The recorded impact loads were lower for the bogie impact with the second post. This finding was likely due to a combination of a reduced impact velocity and a higher impact point on the second post. The reduced impact velocity resulted from the energy absorbed by the impact with the first post, while the higher impact point was caused by the bogie pitching upward as it overrode the first post.



Figure 24. Time-Sequential and Post Damage Photographs, Test No. MWFPF-1



Figure 25. Simulated Floorpan Damage, Test No. MWFPF-1

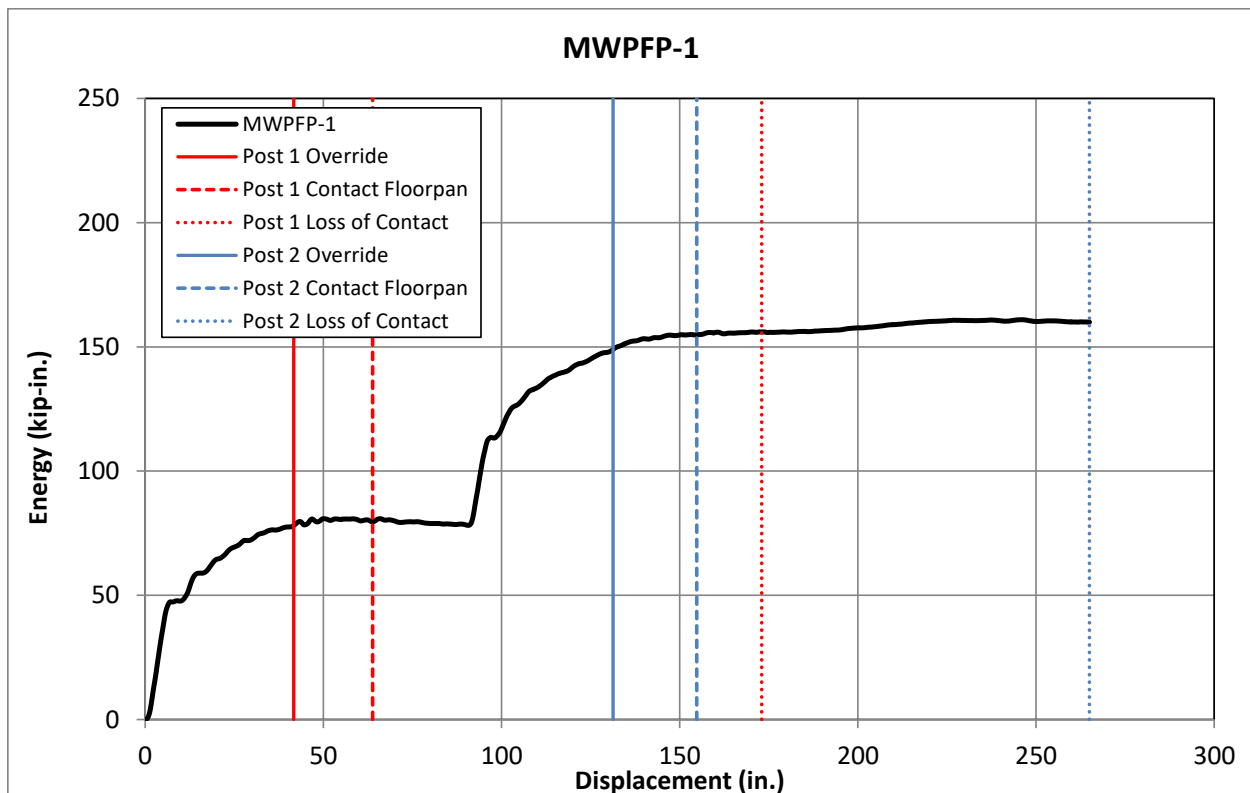
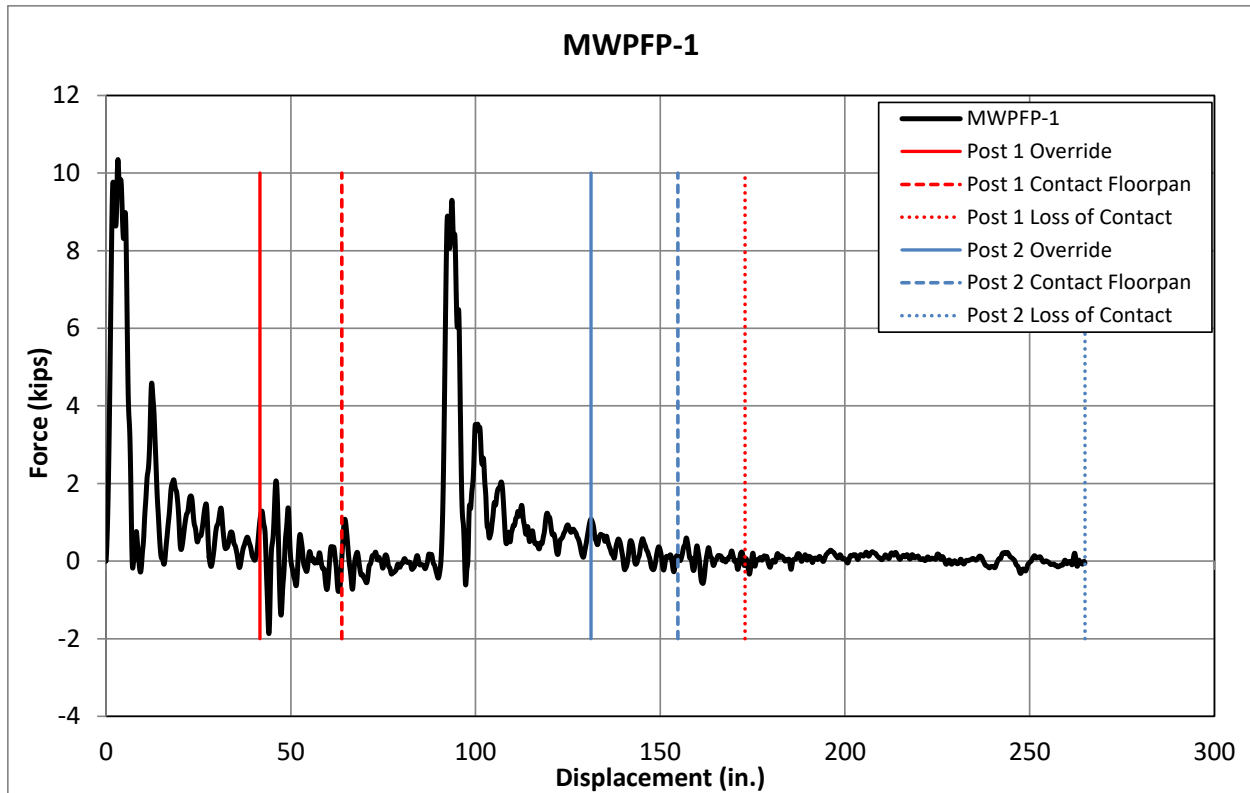


Figure 26. Force vs. Deflection and Energy vs. Deflection, Test No. MWPFP-1

Table 4. Floorpan Damage Measurements, Test No. MWPFP-1

MWPFP-1 Floorpan Damage				
Description	1st Post		2nd Post	
	Free Edge in. (mm)	Continuous Edge in. (mm)	Free Edge in. (mm)	Continuous Edge in. (mm)
Tear Length	3½ (89)	-	2½ (64)	-
Max. Tear Width	⅛ (2)	-	⅛ (2)	-
Crease Length	107¾ (2,737)	106½ (2,705)	106½ (2,705)	-

5.1.2 Test No. MWPFP-2

Test no. MWPFP-2 was conducted on MWPs installed in 8-in. (203-mm) diameter concrete sleeves with a 0-degree orientation angle, thus creating an impact about the post's weak-axis of bending. During the test, the bogie impacted the first post with a speed of 25.8 mph (41.5 km/h). Upon impact, a plastic hinge formed in the post near the groundline, and the post bent over until the bogie overrode it. As the crossbeams passed over the post, elastic restoration caused the top of the post to rebound upward and contact the simulated floorpan. The first post impacted the front and rear bays of the simulated floorpans 0.158 seconds and 0.298 seconds after impact, respectively. The bogie impacted the second post at 0.224 seconds and caused similar deformation and spring-back characteristics as observed in the first post. The second post impacted the front and rear bays of the simulated floorpans at 0.396 seconds and 0.540 seconds, respectively. The elastic spring-back of the posts and the contact with the simulated floorpan were captured via digital video taken underneath the bogie vehicle, as shown in Figure 27.

The posts were bent plastically near the groundline, and contact marks were found on the top half of the post along the free edge and impact side face of the post, as shown in Figure 28. Damage to the simulated floorpan included creasing and tearing due to contact from the top corners of both posts, as shown in Figure 29. Two tears were found in both the front and rear bays of the simulated floorpan. These tears corresponded to the location of initial contact between the free edges of the posts and the floorpan as the posts passed the crossbeams and rebounded upward. The largest tear was 5 in. (127 mm) long and had a maximum width of ½ in. (13 mm). Creases in the simulated floorpan were found extending from the tears toward the rear of the bogie. Approximately 3 in. (76 mm) to the right of the tears and creases caused by the free edges, additional creases caused by the continuous edges of the posts were present on the floorpan. All tears and creases observed on the simulated floorpan were measured and are summarized in Table 5.

Force vs. deflection and energy vs. deflection curves were created from the accelerometer data. Additionally, the high-speed video was analyzed to determine the times when the bogie overrode each post, the posts contacted the simulated floorpan, and the posts lost contact with the bogie vehicle. Results from the data and video analysis are shown in Figure 30. The recorded impact loads were lower for the bogie impact with the second post. This finding was likely due to a combination of a reduced impact velocity and a higher impact point on the second post. The reduced impact velocity resulted from the energy absorbed by the impact with the first post,

while the higher impact point was caused by the bogie pitching upward as it overrode the first post.

Test no. MWFPF-2 provided very similar results as compared to full-scale crash testing. The elastic response of the overridden posts applied a vertical contact force to the simulated floorpan. Tears observed in the simulated floorpan were all caused by the free edges of the posts and were similar in length and opening width to those found in the test vehicles of test nos. MWP-6 and MWP-7. Additionally, creases running the length of the simulated floorpan were formed from contact with both edges the posts. Therefore, the bogie testing setup was thought to accurately replicate the floorpan damage observed in full-scale test nos. MWP-6 and MWP-7. The same test setup was utilized in the remaining bogie tests to evaluate various tearing mitigation methods.



0.151 sec



0.387 sec



0.159 sec



0.403 sec



0.193 sec



0.437 sec



0.294 sec



0.537 sec



0.302 sec



0.546 sec

Figure 27. Time-Sequential Photographs Underneath Bogie, Test No. MWFPF-2



Figure 28. Time-Sequential and Post Damage Photographs, Test No. MWFPF-2



Rear Bay



Front Bay



Figure 29. Simulated Floorpan Damage, Test No. MWFPF-2

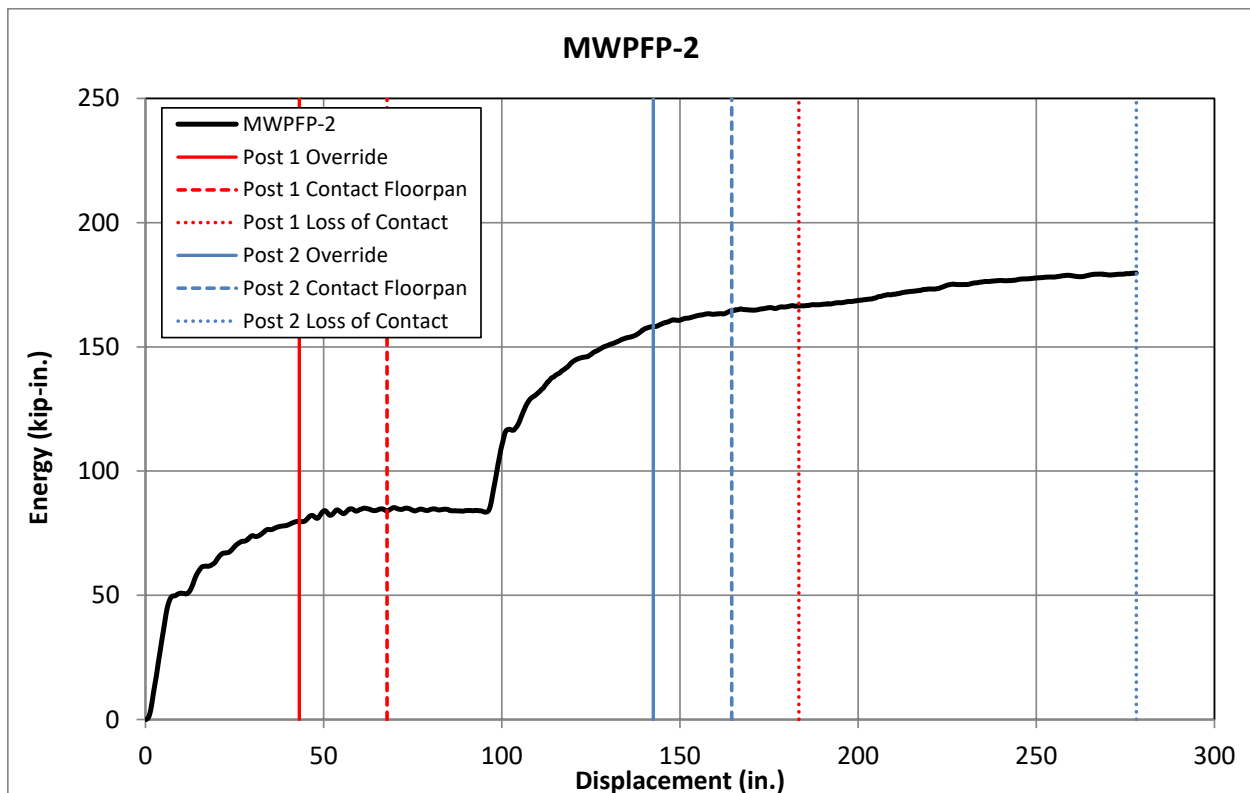
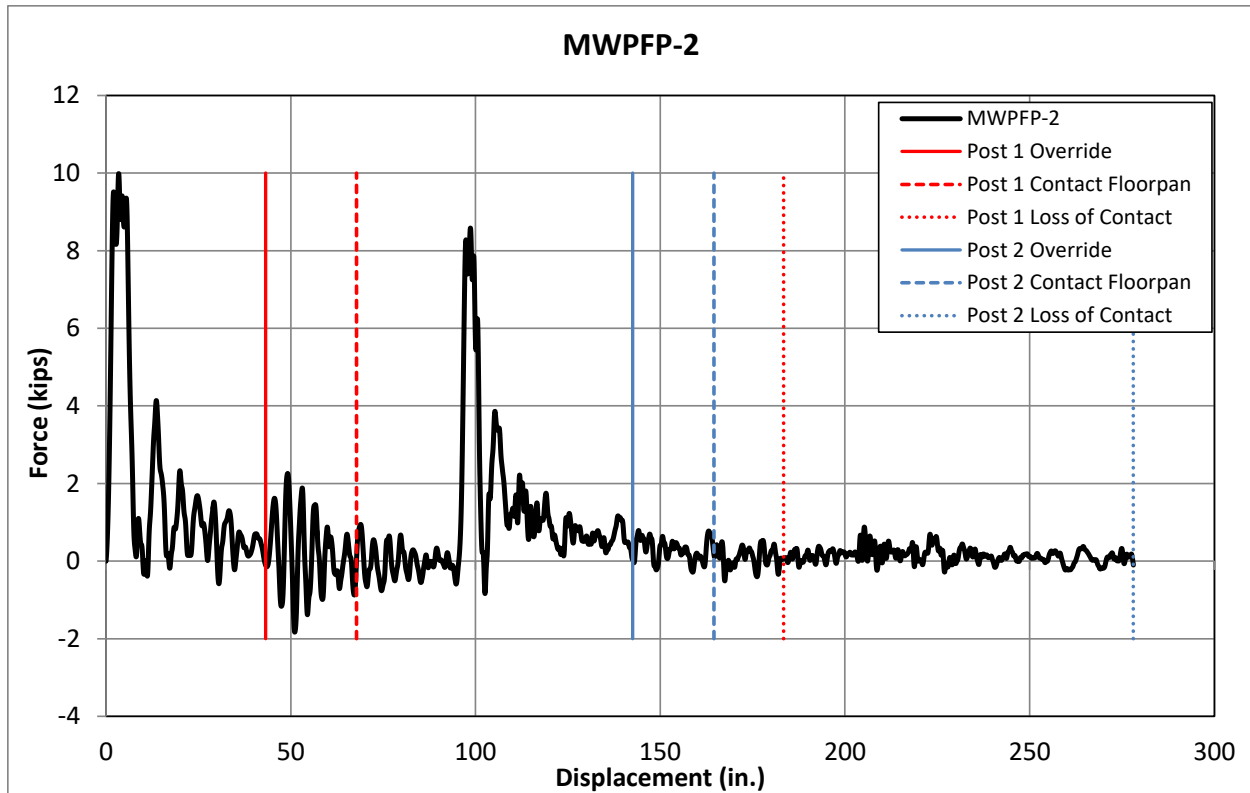


Figure 30. Force vs. Deflection and Energy vs. Deflection, Test No. MWPFP-2

Table 5. Floorpan Damage Measurements, Test No. MWPFP-2

MWPFP-2 Floorpan Damage					
Location	Description	1st Post		2nd Post	
		Free Edge in. (mm)	Continuous Edge in. (mm)	Free Edge in. (mm)	Continuous Edge in. (mm)
Front Bay	Tear Length	5 (127)	-	4¼ (108)	-
	Max. Tear Width	½ (13)	-	¾ (5)	-
	Crease Length	31 (787)	3½ (89)	33½ (851)	37 (940)
Rear Bay	Tear Length	4½ (114)	-	2¾ (70)	-
	Max. Tear Width	½ (13)	-	⅛ (3)	-
	Crease Length	48¼ (1,226)	3 (76)	51 (1,296)	48½ (1,232)

5.1.3 Test No. MWPFP-3

Test no. MWPFP-3 was conducted on the modified MWP with ¾-in. (19-mm) diameter weakening holes in the weak-axis flanges at groundline, as shown in **Error! Reference source not found.** The posts were installed in 8-in. (203-mm) diameter concrete sleeves with a 0-degree orientation angle, thus creating an impact about the post's weak-axis of bending. During the test, the bogie impacted the first post at a speed of 26.8 mph (43.1 km/h). Upon impact, a plastic hinge formed in the post at the groundline, and the post bent over until the bogie overrode it. As the crossbeams passed over the post, elastic restoration caused the top of the post to rebound upward and contact the simulated floorpan. The first post impacted the front and rear bays of the simulated floorpan 0.156 seconds and 0.286 seconds after impact, respectively. The bogie impacted the second post at 0.212 seconds and caused similar deformation and spring-back characteristics as observed in the first post. The second post impacted the front and rear bays of the simulated floorpans at 0.376 seconds and 0.504 seconds, respectively.



Figure 31. MWP with ¾-in. (19-mm) Diameter Weakening Holes

The posts were bent plastically near the groundline, and tearing was found in both posts, as shown in Figure 32. The tears initiated from the weakening holes on the impact side of the posts and extended into the webs and adjacent flanges. Contact marks were found on the top half of the post along the free edge and impact side face of the post. Damage to the simulated floorpan included scrapes and creases but no tearing. Four creases were found in both the front and rear bays of the simulated floorpan, as shown in Figure 33. The creases resulting from contact with the free edges of the posts extended nearly the entire length of the bogie vehicle, while the creases resulting from contact with the continuous edges of the posts were limited in length. All creases observed on the simulated floorpan were measured and are summarized in Table 6.

Force vs. deflection and energy vs. deflection curves were created from the accelerometer data. Additionally, the high-speed video was analyzed to determine the times when the bogie overrode each post, the posts contacted the simulated floorpan, and the posts lost contact with the bogie vehicle. Results from the data and video analysis are shown in Figure 34. The peak impact loads and absorbed energies were relatively constant between the two posts.



Figure 32. Time-Sequential and Post Damage Photographs, Test No. MWFPF-3



Front Bay



Front Bay



Front Bay



Rear Bay

Figure 33. Simulated Floorpan Damage, Test No. MWFPF-3

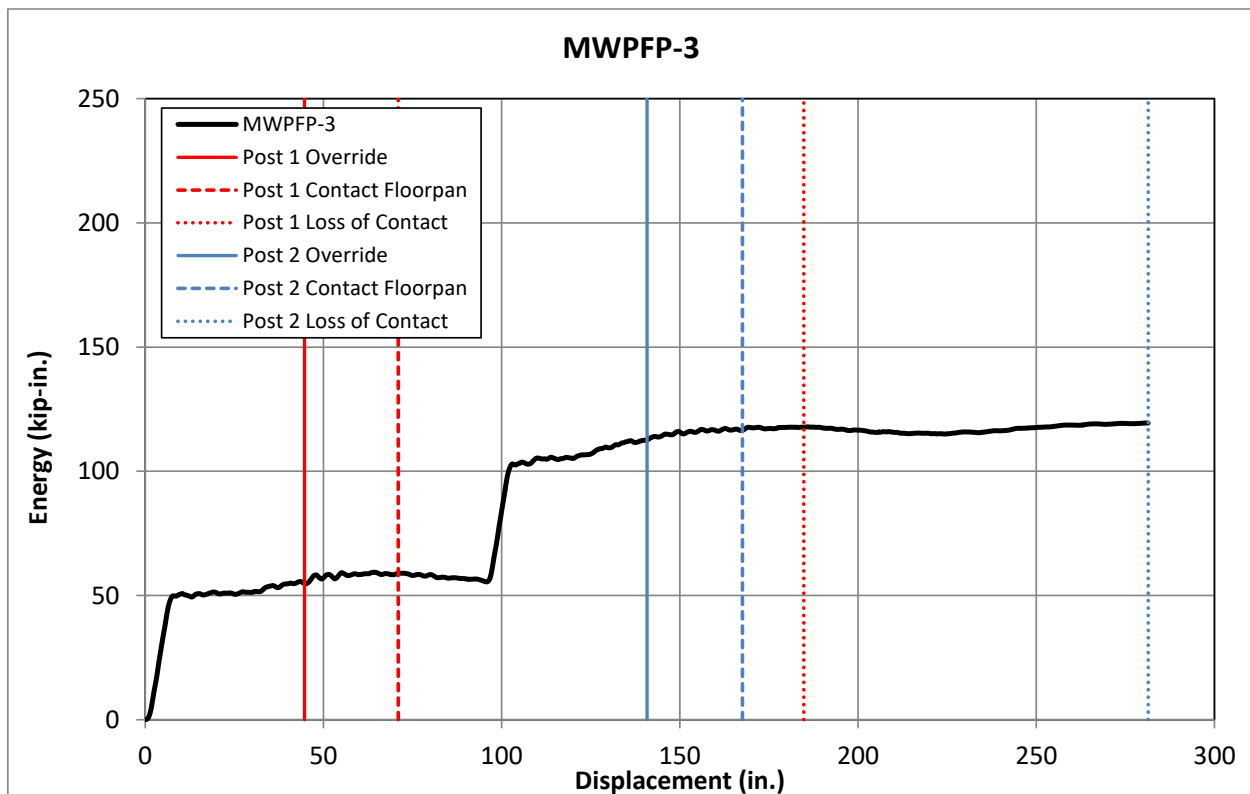
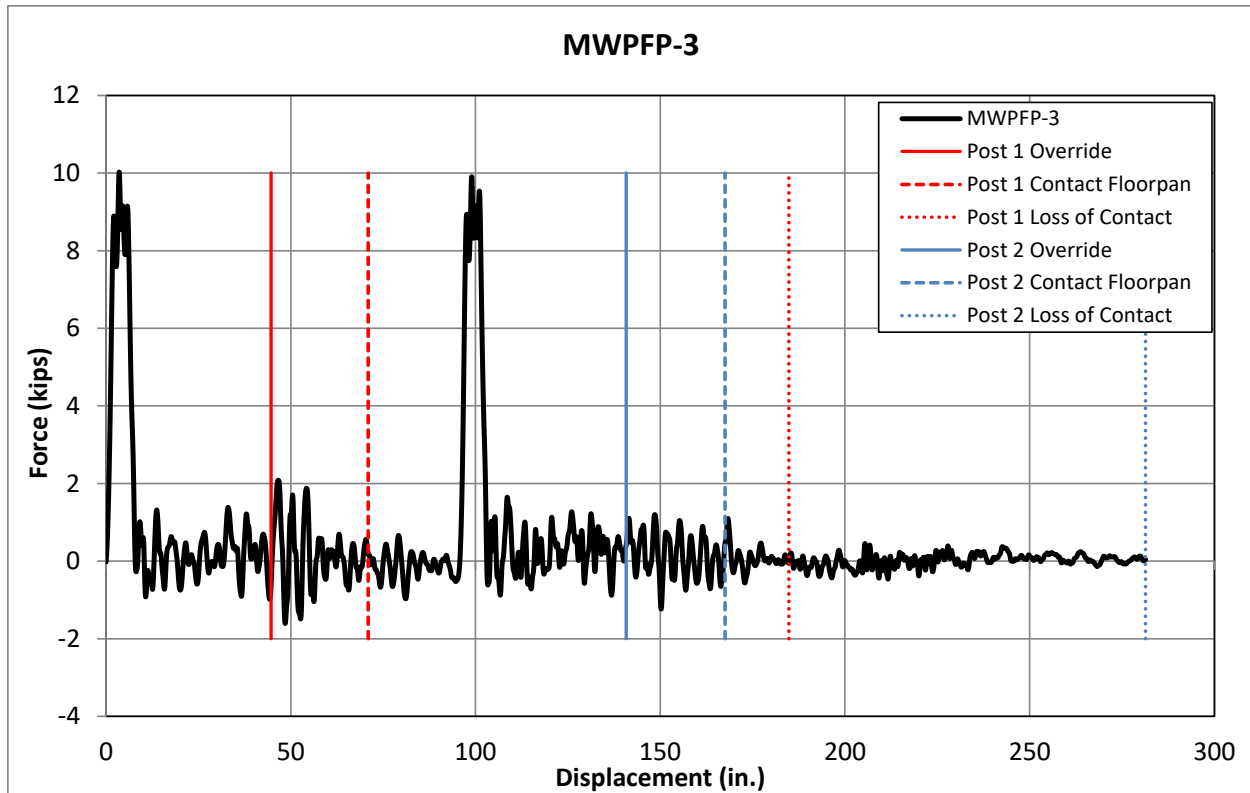


Figure 34. Force vs. Deflection and Energy vs. Deflection, Test No. MWPFP-3

Table 6. Floorpan Damage Measurements, Test No. MWPFP-3

MWPFP-3 Floorpan Damage					
Location	Description	1st Post		2nd Post	
		Free Edge in. (mm)	Continuous Edge in. (mm)	Free Edge in. (mm)	Continuous Edge in. (mm)
Front Bay	Tear Length	-	-	-	-
	Max. Tear Width	-	-	-	-
	Crease Length	35 ³ / ₈ (899)	4 (102)	31 ¹ / ₂ (800)	3 (76)
Rear Bay	Tear Length	-	-	-	-
	Max. Tear Width	-	-	-	-
	Crease Length	51 ¹ / ₂ (1,308)	3 ¹ / ₂ (89)	51 (1,295)	2 ¹ / ₂ (64)

5.1.4 Test No. MWPFP-4

Test no. MWPFP-4 was conducted on S3x5.7 (S76x8.5) posts with a height of 39¹/₄ in. (997 mm) above the groundline, matching that of the MWP in the prototype cable barrier system. The posts were installed in 8-in. (203-mm) diameter concrete sleeves with a 0-degree orientation angle, thus creating an impact about the post's weak-axis of bending. During the test, the bogie impacted the first post at a speed of 27.9 mph (44.9 km/h). Upon impact, a plastic hinge formed in the post near groundline, and the post bent over until the bogie overrode it. As the crossbeams passed over the post, elastic restoration caused the top of the post to rebound upward and contact the simulated floorpan. The first post impacted the front and rear bays of the simulated floorpan 0.152 seconds and 0.280 seconds after impact, respectively. The bogie impacted the second post at 0.210 seconds and caused similar deformation and spring-back characteristics as observed in the first post. The second post impacted the front and rear bays of the simulated floorpans at 0.370 seconds and 0.508 seconds, respectively.

The posts were bent plastically near the groundline, and contact marks were present on both edges of the posts, as shown in Figure 35. Damage to the simulated floorpan included tearing and creasing due to contact with the top corners of both posts, as shown in Figure 36. Four tears were found in both the front and rear bays of the simulated floorpan. These tears corresponded to the location of initial contact between the free edges of the posts and the floorpan as the posts passed the crossbeams and rebounded upward. The largest tear was 6³/₄ in. (171 mm) long and had a maximum width of ⁵/₁₆ in. (8 mm). Creases in the simulated floorpan were found following all four tears and extending toward the rear of the bogie. All of the tears and creases observed on the simulated floorpan were measured and summarized in Table 7.

Force vs. deflection and energy vs. deflection curves were created from the accelerometer data. Additionally, the high-speed video was analyzed to determine when the bogie overrode each post, the posts contacted the simulated floorpan, and the posts lost contact with the bogie vehicle. Results from the data and video analysis are shown in Figure 37. The impact loads were lower for the bogie impact with the second post. This finding was likely due to a combination of a reduced impact velocity and a higher impact point on the second post. The reduced impact velocity resulted from the energy absorbed by the impact with the first post, while the higher impact point was caused by the bogie pitching upward as it overrode the first post.



Figure 35. Time-Sequential and Post Damage Photographs, Test No. MWFPF-4



Front Bay



Rear Bay

Figure 36. Simulated Floorpan Damage, Test No. MWFPF-4

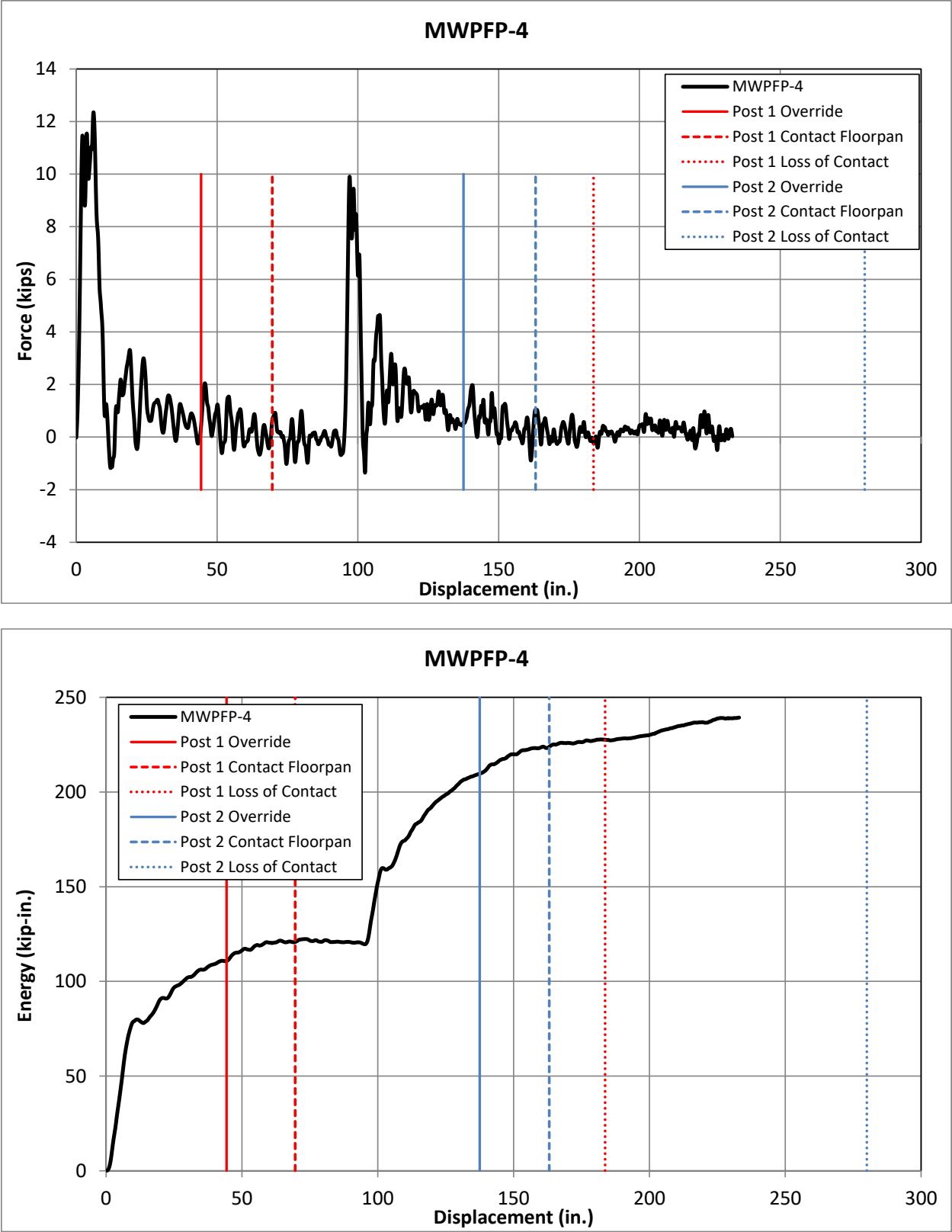


Figure 37. Force vs. Deflection and Energy vs. Deflection, Test No. MWPFP-4

Table 7. Floorpan Damage Measurements, Test No. MWFPF-4

MWFPF-4 Floorpan Damage					
Location	Description	1st Post		2nd Post	
		Left Flange in. (mm)	Right Flange in. (mm)	Left Flange in. (mm)	Right Flange in. (mm)
Front Bay	Tear Length	5¾ (146)	5 (127)	4½ (114)	5 (127)
	Max. Tear Width	⅜ (5)	¼ (6)	⅜ (5)	¼ (6)
	Crease Length	31 (787)	30½ (775)	31 (787)	32 (813)
Rear Bay	Tear Length	6¾ (171)	6¼ (159)	6¼ (159)	6 (152)
	Max. Tear Width	⅝ (8)	¼ (6)	⅛ (3)	⅛ (3)
	Crease Length	51 (1,295)	51 (1,295)	49 (1,244)	49 (1,244)

5.1.5 Test No. MWFPF-5

Test no. MWFPF-5 was conducted on S3x5.7 (S76x8.5) posts with a height of 31 in. (787 mm) above the groundline, matching the height of a typical post in the non-proprietary, low-tension, cable barrier system. The posts were installed in 8-in. (203-mm) diameter concrete sleeves with a 0-degree orientation angle, thus creating an impact about the post's weak-axis of bending. During the test, the bogie impacted the first post at a speed of 30.5 mph (49.1 km/h). Upon impact, a plastic hinge formed in the post near the groundline, and the post bent over until the bogie overrode it. As the crossbeams passed over the post, elastic restoration caused the top of the post to rebound upward and impact the simulated floorpan. The first post impacted the front and rear bays of the simulated floorpan 0.124 seconds and 0.234 seconds after impact, respectively. The bogie impacted the second post at 0.188 seconds and caused similar deformation and spring-back characteristics as observed in the first post. The second post impacted the front and rear bays of the simulated floorpans at 0.312 seconds and 0.434 seconds, respectively.

The posts were bent plastically near the groundline, and contact marks were present on both edges of the posts, as shown in Figure 38. Damage to the simulated floorpan included tearing and creasing due to contact with the top corners of both posts, as shown in Figure 39. Four tears were found in both the front and rear bays of the simulated floorpan corresponding to the location of initial contact between the posts and the floorpan as the posts passed the crossbeams and rebounded upward. The largest of these initial tears was 6½ in. (165 mm) long and had a maximum width of ¼ in. (6 mm). Continued contact with one of the posts resulted in two additional tears in the front bay measuring 16 in. (406 mm) and 13 in. (330 mm) in length. The shorter height of the posts appeared to cause higher restoration forces, which led to these additional tears. Creases were also found in the simulated floorpan extending from the initial tears toward the rear of the bogie. All of the tears and creases observed on the simulated floorpan were measured and are summarized in Table 8.

Force vs. deflection and energy vs. deflection curves were created from the accelerometer data. Additionally, the high-speed video was analyzed to determine the times when the bogie overrode each post, the posts contacted the simulated floorpan, and the posts lost contact with the bogie vehicle. Results from the data and video analysis are shown in Figure 40. The impact loads

were lower for the bogie impact with the second post. This finding was likely due to a combination of a reduced impact velocity and a higher impact point on the second post. The reduced impact velocity resulted from the energy absorbed by the impact with the first post, while the higher impact point was caused by the bogie pitching upward as it overrode the first post.



IMPACT



0.050 sec



0.100 sec



0.150 sec



0.200 sec



0.250 sec



Figure 38. Time-Sequential and Post Damage Photographs, Test No. MWFPF-5



Front Bay



Rear Bay

Figure 39. Simulated Floorpan Damage, Test No. MWFPF-5

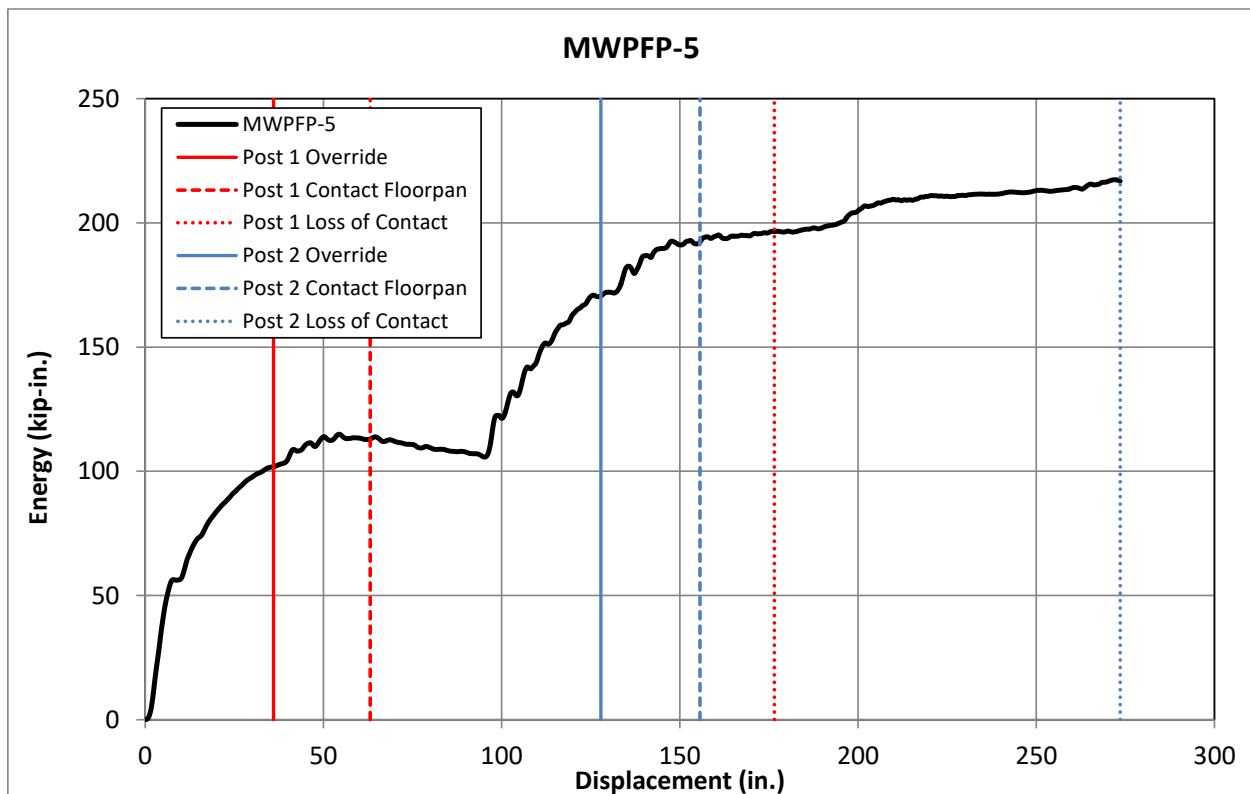
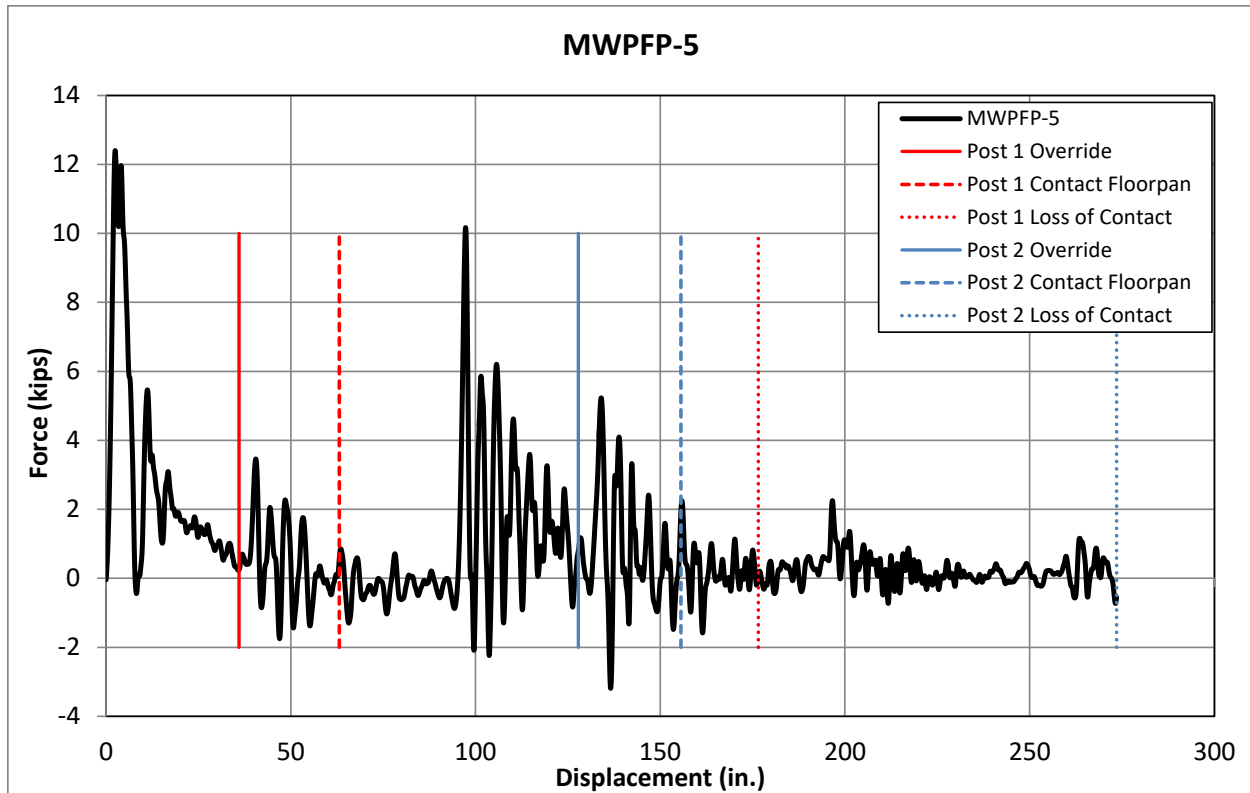


Figure 40. Force vs. Deflection and Energy vs. Deflection, Test No. MWPFP-5

Table 8. Floorpan Damage, Test No. MWFPF-5

MWFPF-5 Floorpan Damage					
Location	Description	1st Post		2nd Post	
		Left Flange in. (mm)	Right Flange in. (mm)	Left Flange in. (mm)	Right Flange in. (mm)
Front Bay	Initial Tear Length	6 (152)	5½ (140)	3¼ (83)	2¾ (70)
	Max. Tear Width	⅛ (3)	¼ (6)	¼ (6)	¼ (6)
	Crease Length	33 (838)	35½ (902)	-	-
	2 nd Tear Length	16 (406)	13 (330)	-	-
	Max. Tear Width	⅟ ₁₆ (2)	¼ (6)	-	-
Rear Bay	Tear Length	6½ (165)	6½ (165)	3½ (89)	2¾ (70)
	Max Tear Width	⅛ (3)	¼ (6)	⅛ (3)	⅜ ₁₆ (5)
	Crease Length	49½ (1,257)	48½ (1,232)	54 (1,372)	54 (1,372)

5.1.6 Test No. MWFPF-6

Test no. MWFPF-6 was conducted on the MWP with simulated no. 1 edge rounding applied along the free edges near the top of each post, as shown in Figure 41. The posts were installed in 8-in. (203-mm) diameter concrete sleeves with a 0-degree orientation angle, thus creating an impact about the post's weak-axis of bending. During the test, the bogie impacted the first post with a speed of 28.1 mph (45.2 km/h). Upon impact, a plastic hinge formed in the post near the groundline, and the post bent over until the bogie overrode it. As the crossbeams passed over the post, elastic restoration caused the top of the post to rebound upward and impact the simulated floorpan. The first post impacted the front and rear bays of the simulated floorpans 0.146 seconds and 0.270 seconds after impact, respectively. The bogie impacted the second post at 0.208 seconds and caused similar deformation and spring-back characteristics as observed in the first post. The second post impacted the front and rear bays of the simulated floorpans at 0.360 seconds and 0.494 seconds, respectively.

The posts were bent plastically near the groundline, and contact marks were found on the top half of the post along the free edge and impact side face of the post, as shown in Figure 42. Damage to the simulated floorpan included creasing and tearing due to contact from the top corners of both posts, as shown in Figure 43. Two tears were found in both the front and rear bays of the simulated floorpan. These tears corresponded to the location of initial contact between the free edges of the posts and the floorpan as the posts passed the crossbeams and rebounded upward. The largest tear was 12¾ in. (324 mm) long and had a maximum width of ½ in. (13 mm). Creases in the simulated floorpan were found extending from the tears toward the rear of the bogie. Additional creases caused by the continuous edges of the posts were present in the floorpan, approximately 3 in. (76 mm) to the right of the tears and creases caused by the free edges of the post. All tears and creases observed on the simulated floorpan were measured and are summarized in Table 9.

Force vs. deflection and energy vs. deflection curves were created from the accelerometer data. Additionally, the high-speed video was analyzed to determine the times when the bogie

overrode each post, the posts contacted the simulated floorpan, and the posts lost contact with the bogie vehicle. Results from the data and video analysis are shown in Figure 44. The recorded impact loads were lower for the bogie impact with the second post. This finding was likely due to a combination of a reduced impact velocity and a higher impact point on the second post. The reduced impact velocity resulted from the energy absorbed by the impact with the first post, while the higher impact point was caused by the bogie pitching upward as it overrode the first post.



Figure 41. MWP with Simulated No. 1 Edge Rounding, Test No. MWPFP-6



Figure 42. Time-Sequential and Post Damage Photographs, Test No. MWFPF-6



Front Bay



Rear Bay

Figure 43. Simulated Floorpan Damage, Test No. MWPF6-6

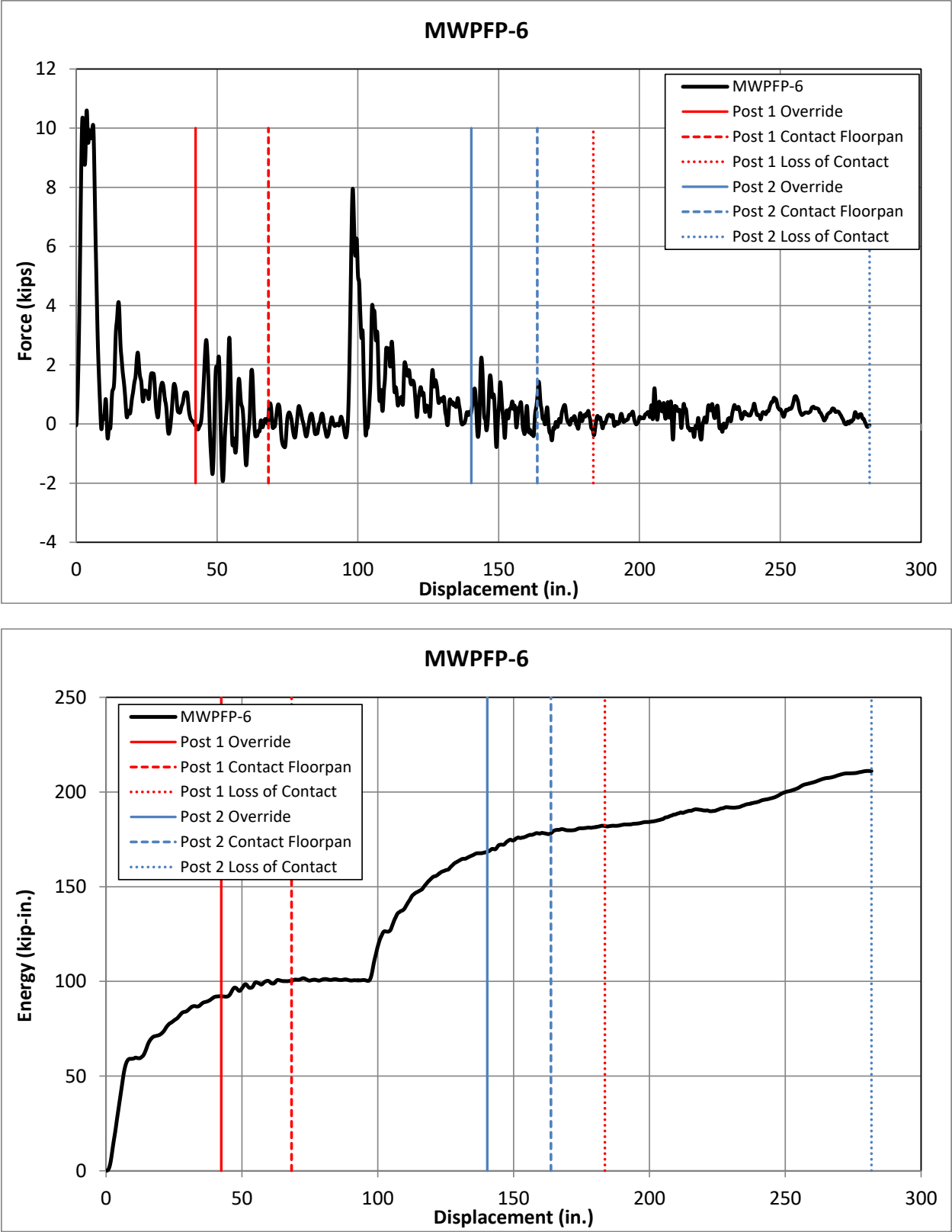


Figure 44. Force vs. Deflection and Energy vs. Deflection, Test No. MWPFP-6

Table 9. Floorpan Damage Measurements, Test No. MWPFP-6

MWPFP-6 Floorpan Damage					
Location	Description	1st Post		2nd Post	
		Free Edge in. (mm)	Continuous Edge in. (mm)	Free Edge in. (mm)	Continuous Edge in. (mm)
Front Bay	Tear Length	12¾ (324)	-	2 (51)	-
	Max. Tear Width	½ (13)	-	¼ (6)	-
	Crease Length	40½ (1,029)	34 (864)	40 (1,016)	44 (1,118)
Rear Bay	Tear Length	7 (178)	-	5 (127)	-
	Max. Tear Width	½ (13)	-	¼ (6)	-
	Crease Length	52 (1,321)	4 (102)	56 (1,422)	58½ (1,486)

5.1.7 Test No. MWPFP-7

Test no. MWPFP-7 was conducted on the MWP with ¾-in. (19-mm) diameter weakening holes in the weak-axis flanges at the groundline. The posts were installed in a strong soil with a 0-degree orientation angle, thus creating an impact about the post's weak-axis of bending. During the test, the bogie impacted the first post at a speed of 29.7 mph (47.8 km/h). Upon impact, a plastic hinge formed in the post at the groundline, and the post bent over until the bogie overrode it. As the crossbeams passed over the post, elastic restoration caused the top of the post to rebound upward and impact the simulated floorpan. The first post impacted the front and rear bays of the simulated floorpan 0.142 seconds and 0.262 seconds after impact, respectively. The bogie impacted the second post at 0.186 seconds and caused similar deformation and spring-back characteristics as observed in the first post. The second post impacted the front and rear bays of the simulated floorpans at 0.338 seconds and 0.458 seconds, respectively.

The posts were bent plastically near the groundline, and tearing was present in both posts, as shown in Figure 45. The tears initiated from the weakening holes on the impact side of the posts and extended into the webs and adjacent flanges. The posts displaced approximately 1 in. (25 mm) through the soil at the groundline. Contact marks were found on the top half of the post along the free edge and impact side face of the post. Damage to the simulated floorpan included scrapes and creases, but no tearing. Four creases were found in both the front and rear bays of the simulated floorpan, as shown in Figure 46. The two creases in each bay resulted from contact with the free edges of the posts and extended nearly the entire length of the bogie vehicle. The creases resulting from contact with the continuous edges of the posts were limited to less than 6 in. (152 mm). All creases observed on the simulated floorpan were measured and summarized in Table 10.

Force vs. deflection and energy vs. deflection curves were created from the accelerometer data. Additionally, the high-speed video was analyzed to determine the times when the bogie overrode each post, the posts contacted the simulated floorpan, and the posts lost contact with the bogie vehicle. Results from the data and video analysis are shown in Figure 47. The peak impact loads and absorbed energies were relatively constant between the two posts.

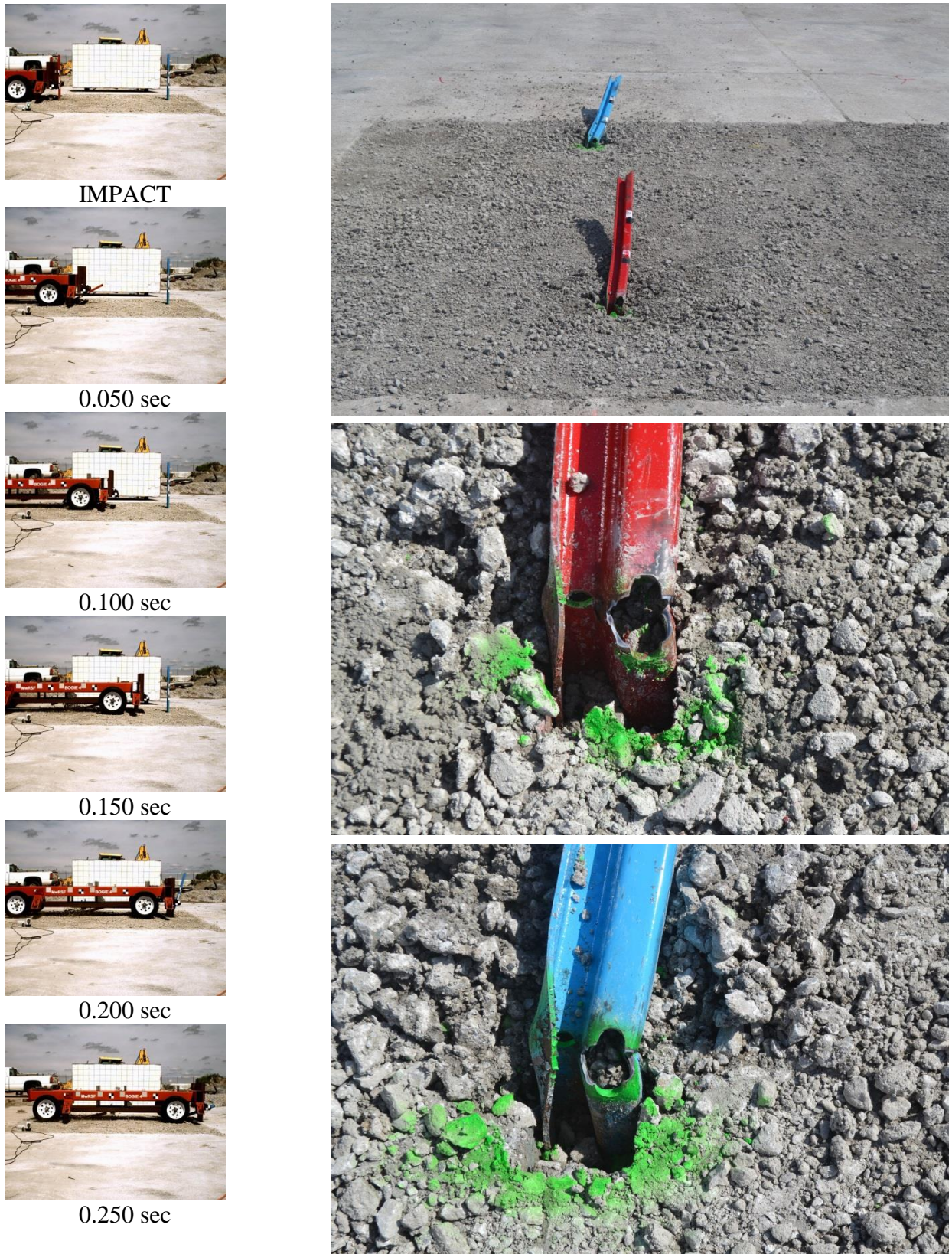


Figure 45. Time-Sequential and Post Damage Photographs, Test No. MWFPF-7



Front Bay

Rear Bay

Figure 46. Simulated Floorpan Damage, Test No. MWPPF-7

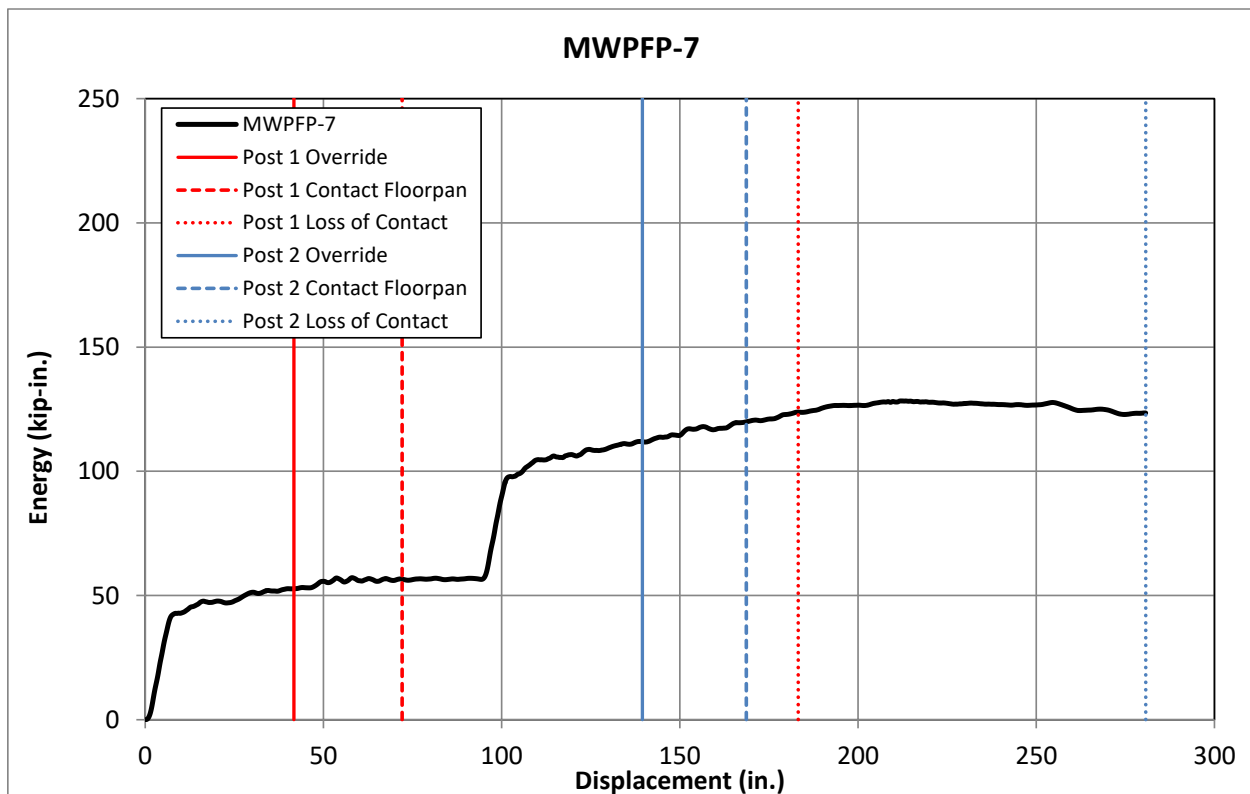
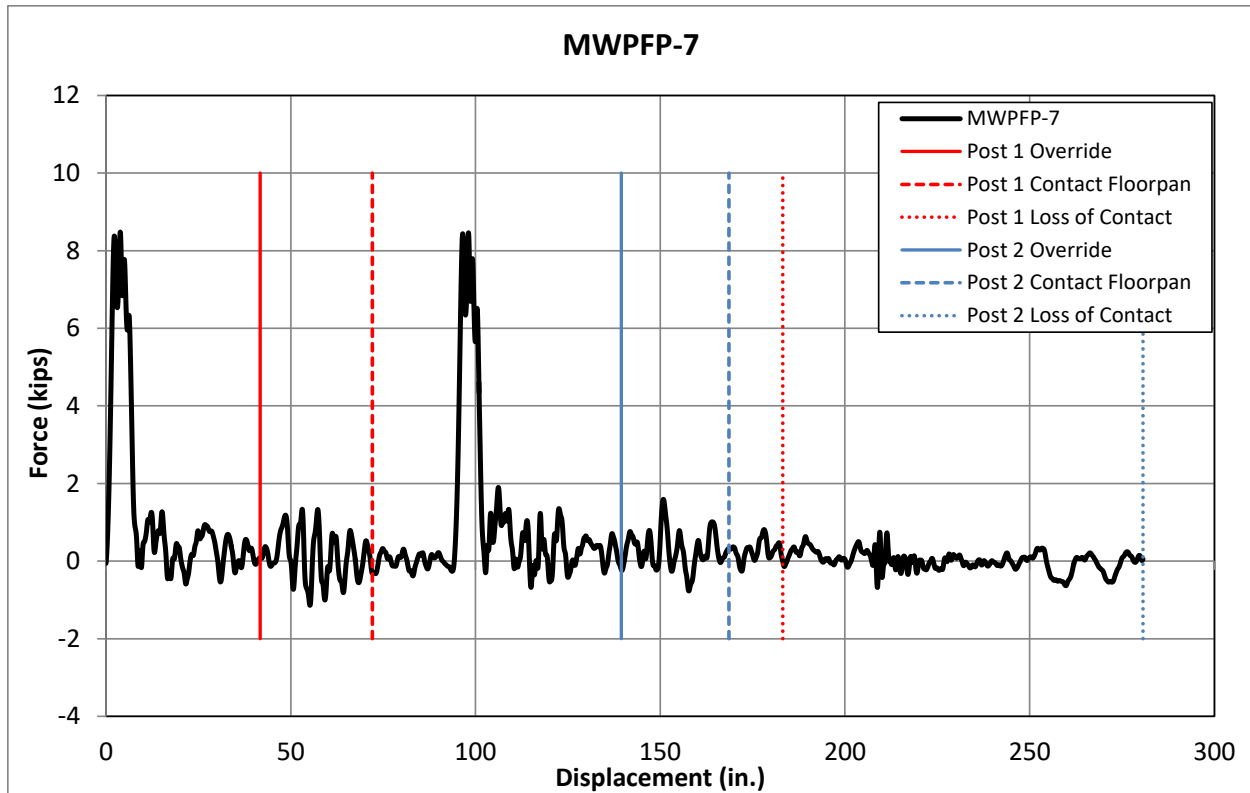


Figure 47. Force vs. Deflection and Energy vs. Deflection, Test No. MWPFP-7

Table 10. Floorpan Damage Measurements, Test No. MWPFP-7

MWPFP-7 Floorpan Damage					
Location	Description	1st Post		2nd Post	
		Free Edge in. (mm)	Continuous Edge in. (mm)	Free Edge in. (mm)	Continuous Edge in. (mm)
Front Bay	Tear Length	-	-	-	-
	Max. Tear Width	-	-	-	-
	Crease Length	34½ (876)	3½ (89)	41½ (1,054)	6 (152)
Rear Bay	Tear Length	-	-	-	-
	Max. Tear Width	-	-	-	-
	Crease Length	55¼ (1,410)	5 (127)	54 (1,372)	2¼ (57)

5.1.8 Test No. MWPFP-8

Test no. MWPFP-8 was conducted on the MWP with ¾-in. (19-mm) diameter weakening holes in the weak-axis flanges at the groundline. The posts were installed in a strong soil with a 65-degree orientation angle as measured from the longitudinal (weak) axis. The posts were targeted for a 25-degree orientation angle, but during installation the angle was measured relative to the strong axis instead of the weak axis. During the test, the bogie impacted the first post at a speed of 26.6 mph (42.8 km/h). Upon impact, a plastic hinge formed in the post at the groundline, and the post bent over until the bogie overrode it. As the crossbeams passed over the post, elastic restoration caused the top of the post to rebound upward and impact the simulated floorpan. The first post impacted the front and rear bays of the simulated floorpan 0.160 seconds and 0.300 seconds after impact, respectively. The bogie impacted the second post at 0.217 seconds and caused similar deformation and spring-back characteristics as observed in the first post. The second post impacted the front and rear bays of the simulated floorpans at 0.386 seconds and 0.544 seconds, respectively.

The posts were bent plastically near groundline, and contact marks were found along the top half of the post, as shown in Figure 48. No tearing was observed in the post around the weakening holes. The posts displaced 2 to 3 in. (51 to 76 mm) through the soil at the groundline. Damage to the simulated floorpan included tears and creases, as shown in Figure 49. Tears were found in the front and rear bays corresponding to contact from the free edge of the first post. Each bay had an initial tear near the crossbeam, the largest of which was 10¾ in. (273 mm) long with a maximum opening width of ⅝ in. (16 mm). Creasing followed these tears and eventually led to secondary tears measuring 25 in. (635 mm) and 18½ in. (470 mm). The free edge of the second post left a prominent crease along the front bay of the simulated floorpan and a short crease on the rear bay before sliding to the side of the bogie and losing contact with the floorpan. Due to the orientation angle of the post, the continuous edges left only minor creases in the floorpan. All tears and creases observed on the simulated floorpan were measured and are summarized in Table 11.

Force vs. deflection and energy vs. deflection curves were created from the accelerometer data. Additionally, the high-speed video was analyzed to determine the times in which the bogie

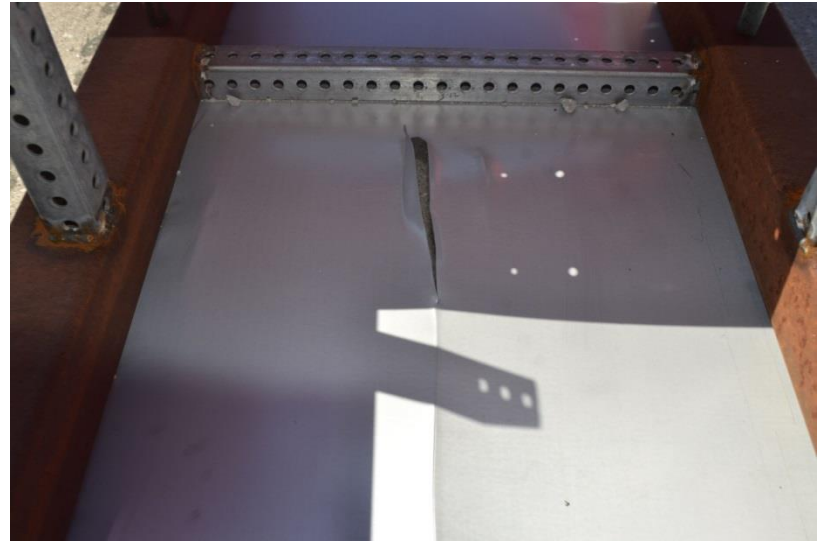
overrode each post, the posts contacted the simulated floorpan, and the posts lost contact with the bogie vehicle. Results from the data and video analysis are shown in Figure 50. The recorded impact loads were lower for the bogie impact with the second post. This finding was likely due to a combination of a reduced impact velocity and a higher impact point on the second post. The reduced impact velocity resulted from the energy absorbed by the impact with the first post, while the higher impact point was caused by the bogie pitching upward as it overrode the first post.



Figure 48. Time-Sequential and Post Damage Photographs, Test No. MWFPF-8



Front Bay



Rear Bay

Figure 49. Simulated Floorpan Damage, Test No. MWPFPP-8

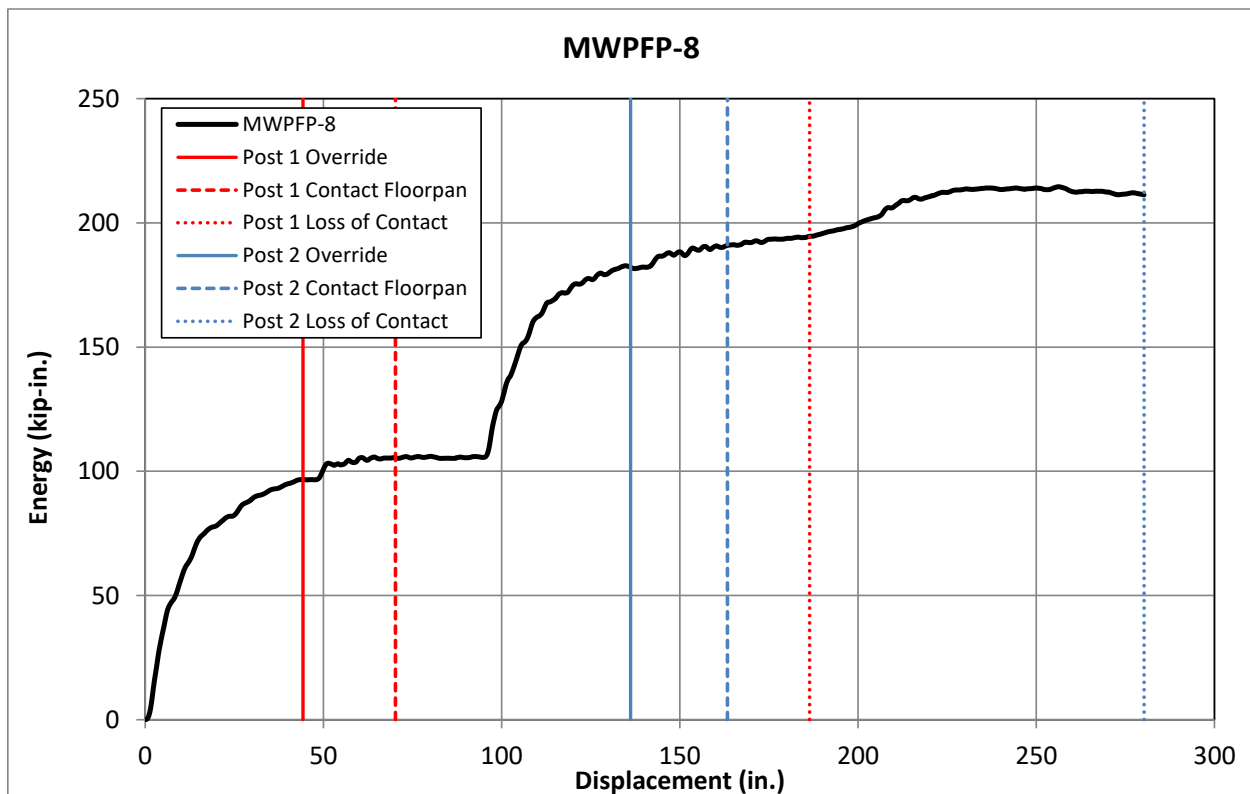
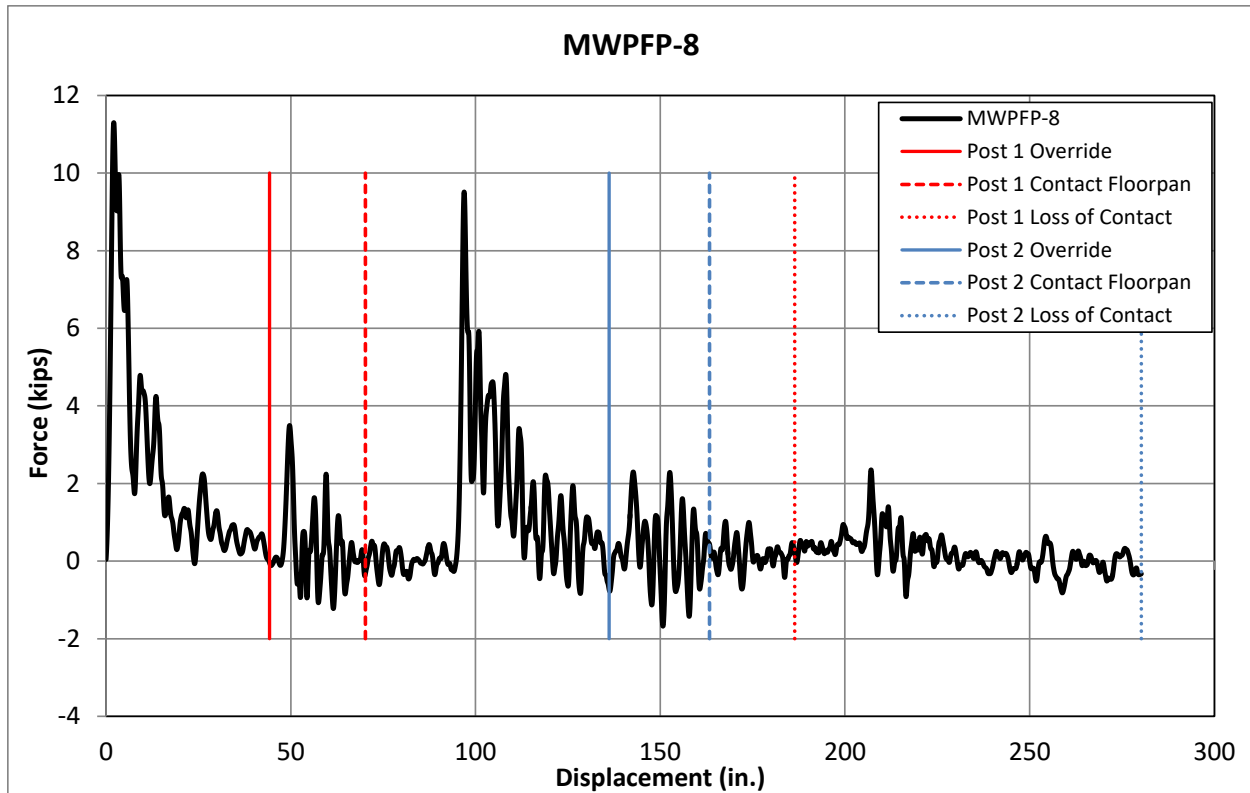


Figure 50. Force vs. Deflection and Energy vs. Deflection, Test No. MWPFP-8

Table 11. Floorpan Damage Measurements, Test No. MWPFP-8

MWPFP-8 Floorpan Damage					
Location	Description	1st Post		2nd Post	
		Free Edge in. (mm)	Continuous Edge in. (mm)	Free Edge in. (mm)	Continuous Edge in. (mm)
Front Bay	Tear Length	10¾ (273)	-	-	-
	Max. Tear Width	⅝ (16)	-	-	-
	Crease Length	9 (229)	5 (127)	31 (787)	-
	2 nd Tear Length	25 (635)	-	-	-
	Max. Tear Width	⅛ (3)	-	-	-
Rear Bay	Tear Length	8¾ (222)	-	-	-
	Max. Tear Width	¾ (19)	-	-	-
	Crease Length	24¾ (629)	5 (127)	6 (152)	-
	2 nd Tear Length	18½ (470)	-	-	-
	Max. Tear Width	⅛ (3)	-	-	-

5.1.9 Test No. MWPFP-11

Test no. MWPFP-11 was conducted on the MWP with three ⅜-in. (10-mm) diameter weakening holes in the weak-axis flanges at the groundline, as shown in Figure 51. The posts were installed in 8-in. (203-mm) diameter concrete sleeves with a 0-degree orientation angle, thus creating an impact about the post's weak-axis of bending. During the test, the bogie impacted the first post at a speed of 25.9 mph (41.7 km/h). Upon impact, the post began to bend and tear near the groundline, and the post bent over until the bogie overrode it. Due to the severity of the tearing, the post bent all the way down to the ground and did not spring back upward. Thus, the post never contacted the simulated floorpan. The bogie impacted the second post at 0.219 seconds and caused similar behavior as observed in the first post.



Figure 51. MWP with Three ⅜-in. (10-mm) Diameter Weakening Holes

The posts were completely bent over, and tearing was present in both posts, as shown in Figure 52. The tears initiated from the weakening holes on the impact side of the posts and extended into the webs and adjacent flanges. Additional tears occurred in the free edges of the posts leaving only the backside face of the posts to hold the posts together. After the tears formed in the posts, the angular momentum of the top of the posts rotated backward and then impacted the ground causing the bottom of the posts to pull out of the ground vertically a few inches. The simulated floorpan was undamaged as the posts never contacted the undercarriage of the bogie vehicle.

Force vs. deflection and energy vs. deflection curves were created from the accelerometer data. Additionally, the high-speed video was analyzed to determine the times in which the bogie overrode each post and the posts lost contact with the bogie vehicle. Results from the data and video analysis are shown in Figure 53. The peak impact loads and absorbed energies were relatively constant between the two posts.

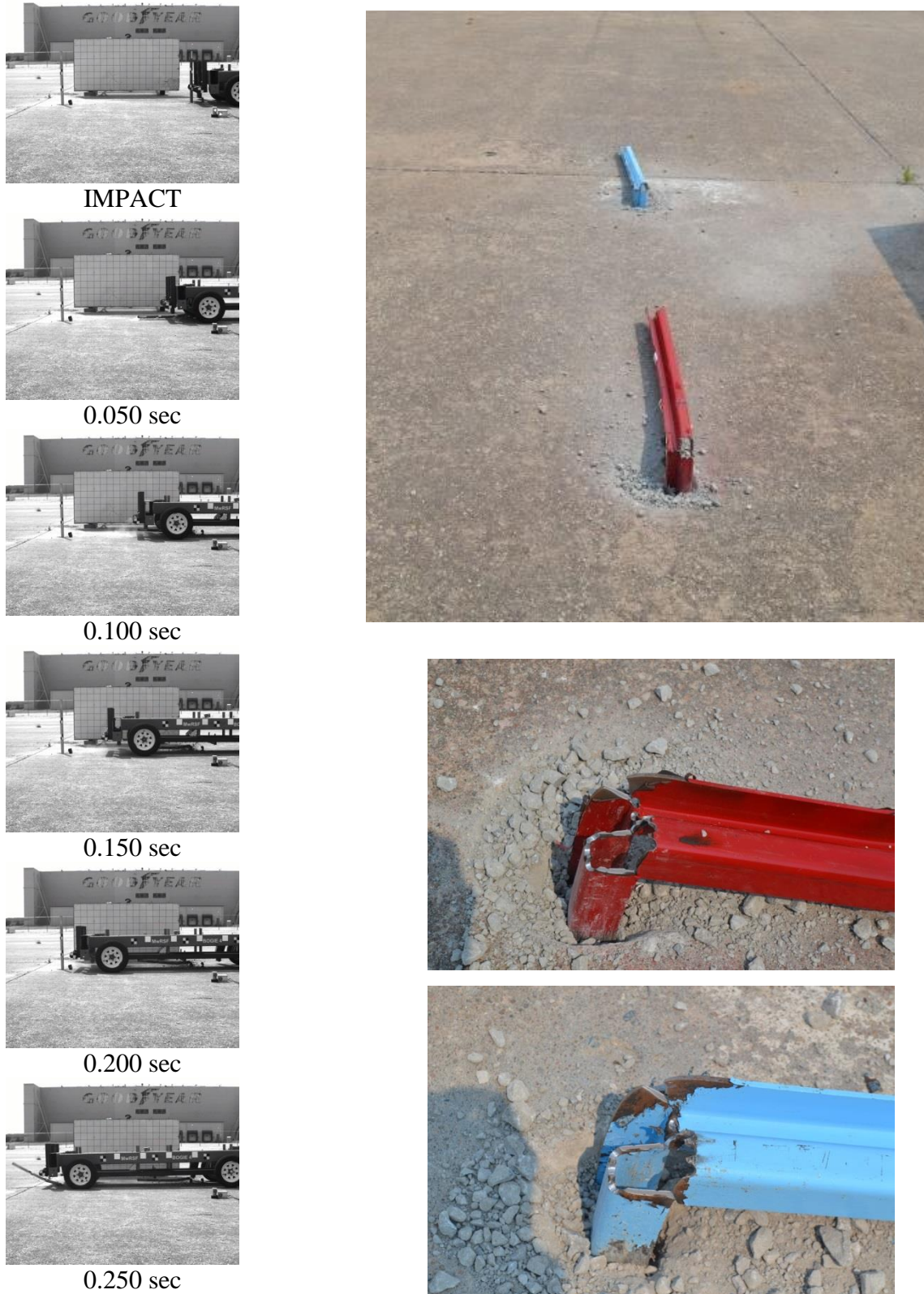


Figure 52. Time-Sequential and Post Damage Photographs, Test No. MWFPF-11

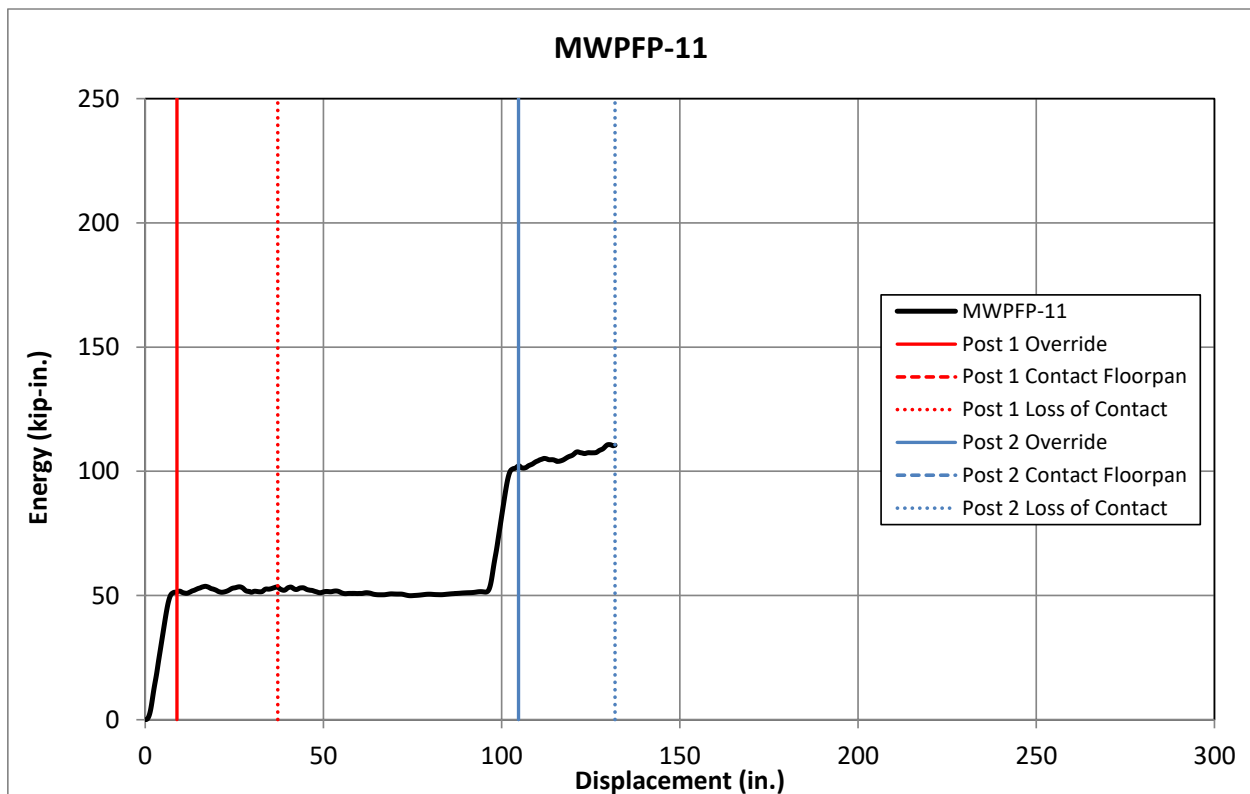
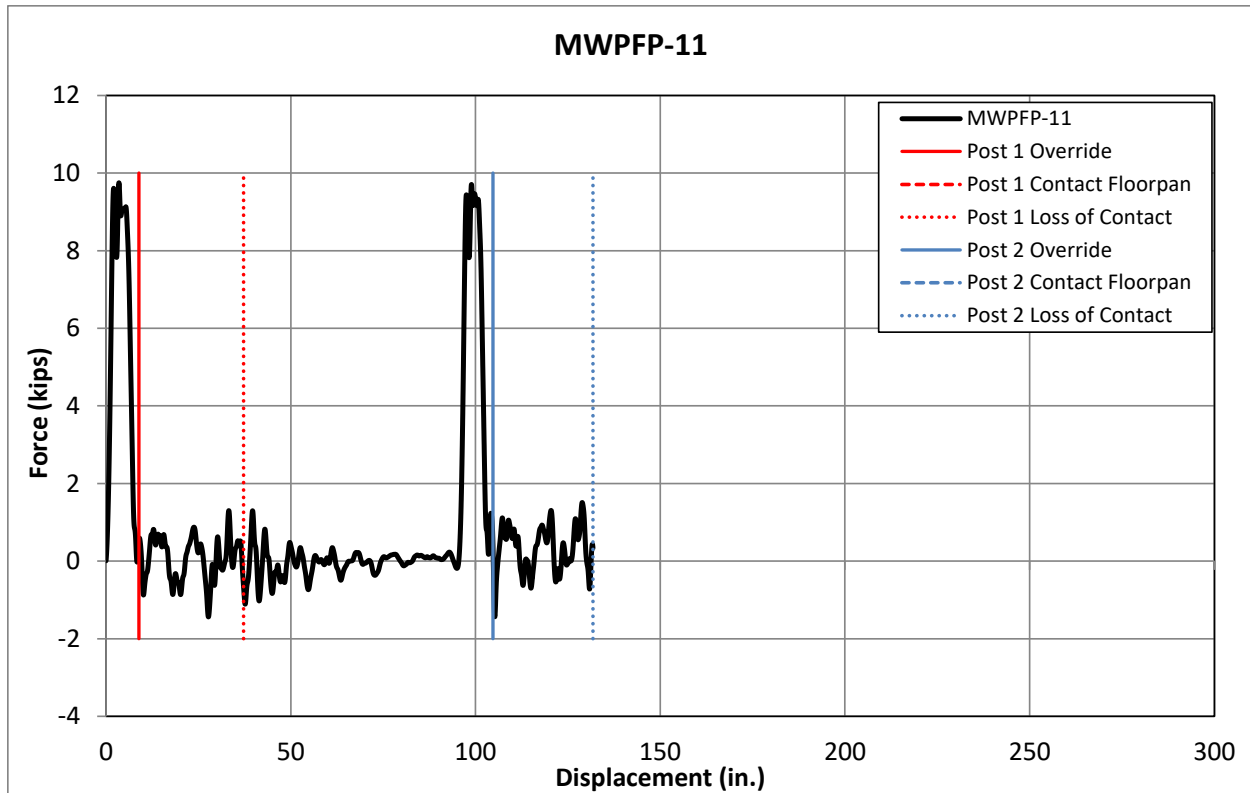


Figure 53. Force vs. Deflection and Energy vs. Deflection, Test No. MWPFP-11

5.1.10 Test No. MWFPF-12

Test no. MWFPF-12 was conducted on the MWP with $\frac{3}{8}$ -in. x $1\frac{1}{8}$ -in. (10-mm x 29-mm) weakening slots in the weak-axis flanges at the groundline, as shown in Figure 54. The posts were installed in 8-in. (203-mm) diameter concrete sleeves with a 0-degree orientation angle, thus creating an impact about the post's weak-axis of bending. During the test, the bogie impacted the first post at a speed of 24.4 mph (39.3 km/h). Upon impact, the post began to bend and tear near groundline, and the post bent over until the bogie overrode it. Eventually, the top of the post tore away from the bottom. Due to rupturing, the post never contacted the simulated floorpan. The bogie impacted the second post at 0.232 seconds and caused similar behavior as observed in the first post.



Figure 54. MWP with $\frac{3}{8}$ -in. x $1\frac{1}{8}$ -in. (10-mm x 29-mm) Weakening Slots

Both posts had ruptured at the groundline, as shown in Figure 55. Tearing was initiated around the weakening slots on the impact side of the posts and continued through the entire cross section. The simulated floorpan was undamaged as the posts never contacted the undercarriage of the bogie vehicle.

Force vs. deflection and energy vs. deflection curves were created from the accelerometer data. Additionally, the high-speed video was analyzed to determine the times in which the bogie overrode each post and the posts lost contact with the bogie vehicle. Results from the data and video analysis are shown in Figure 56. The recorded loads were significantly higher during the impact with the second post due to the crossbeam of the bogie impacting the detached portion of the first post at the same time. The top of the first post was subsequently propelled downstream. Thus, the unusually high force is a combination of the bogie impacting both posts simultaneously.



IMPACT



0.050 sec



0.100 sec



0.150 sec



0.200 sec



0.250 sec

Figure 55. Time-Sequential and Post Damage Photographs, Test No. MWFPF-12

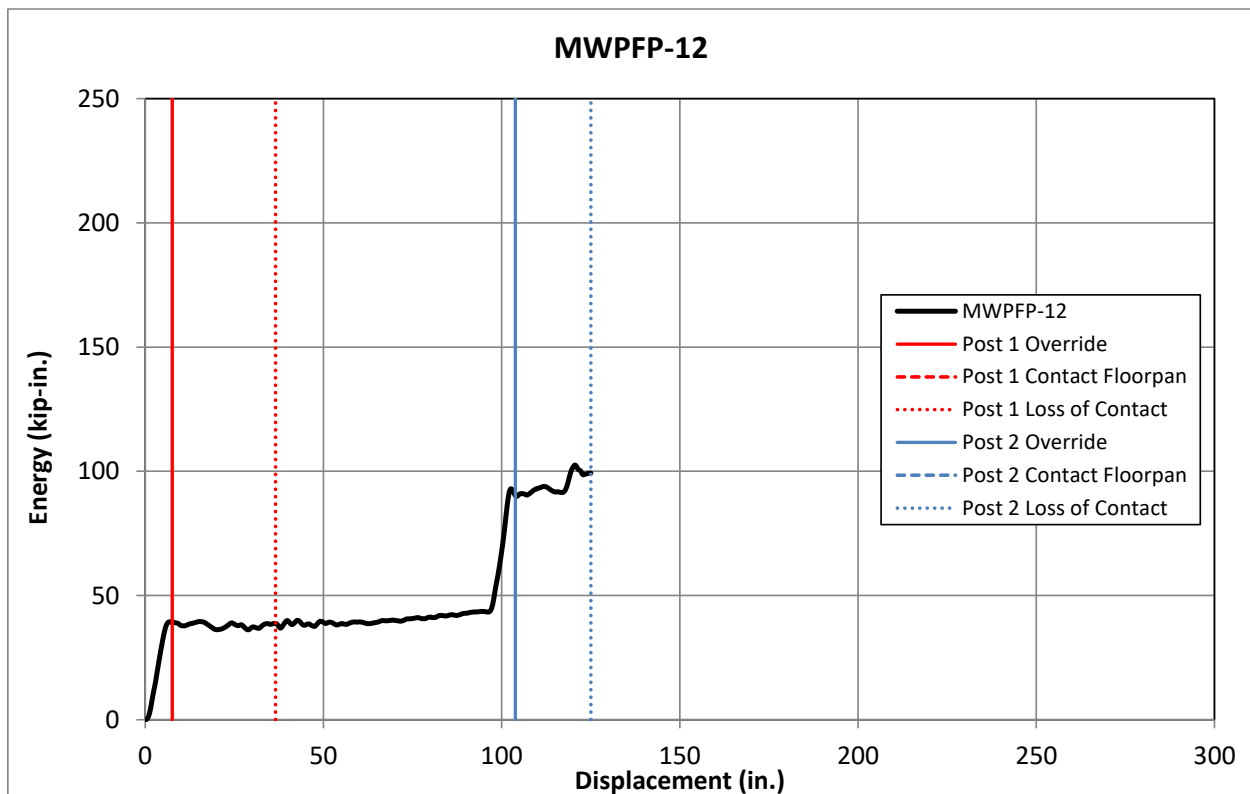
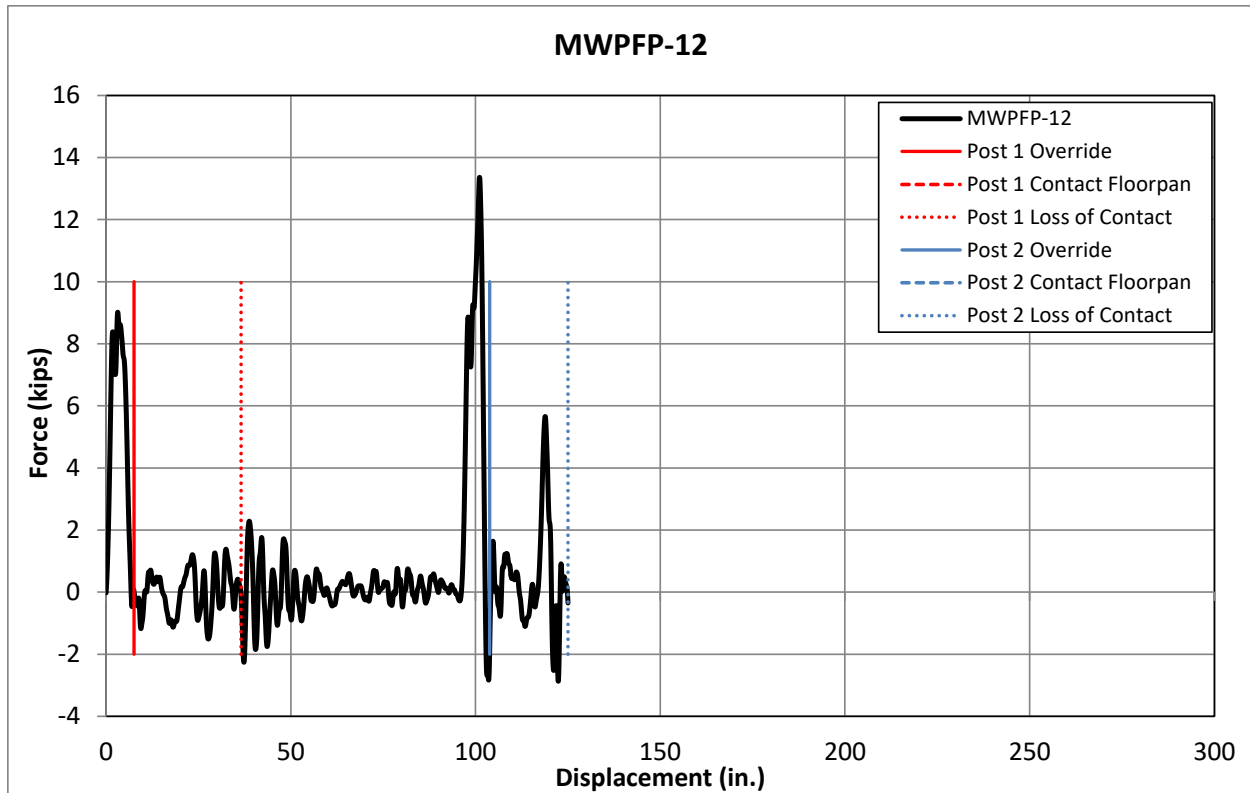


Figure 56. Force vs. Deflection and Energy vs. Deflection, Test No. MWPFP-12

5.1.11 Test No. MWFPF-13

Test no. MWFPF-13 was conducted on the MWP with steel plate edge protectors welded to the top of the posts, as shown in Figure 57. The posts were installed in 8-in. (203-mm) diameter concrete sleeves with a 0-degree orientation angle, thus creating an impact about the post's weak-axis of bending. During the test, the bogie impacted the first post at a speed of 24.2 mph (38.9 km/h). Upon impact, a plastic hinge formed in the post near the groundline, and the post bent over until the bogie overrode it. As the crossbeams passed over the post, elastic restoration caused the top of the post to rebound upward and impact the simulated floorpan. The first post impacted the front and rear bays of the simulated floorpan at 0.170 seconds and 0.322 seconds after impact, respectively. The bogie impacted the second post at 0.238 seconds and caused similar deformation and spring-back characteristics as observed in the first post. The second post impacted the front and rear bays of the simulated floorpan at 0.426 seconds and 0.588 seconds, respectively.



Figure 57. MWPs with Steel Plate Edge Protectors

The posts were bent plastically near the groundline, and contact marks were found along the impact side of the posts, as shown in Figure 58. Damage to the simulated floorpan included tearing and creasing due to contact from the top corners of both posts, as shown in Figure 59. Two tears were found in both the front and rear bays of the simulated floorpan. These tears corresponded to the location of initial contact between the continuous edges of the posts and the floorpan as the posts passed the crossbeams and rebounded upward. The largest tear was 3 in. (76 mm) long and had a maximum width of ¼ in. (6 mm). Creases in the simulated floorpan were found along the entire length of the simulated floorpan. All tears and creases observed on the simulated floorpan were measured and are summarized in Table 12.

Closer inspection of the posts revealed that the continuous edges of the posts did not incorporate a radius as intended. A ¼-in. (6-mm) radius was added to the MWP between the top edge and the V-notch to eliminate sharp edges or corners near the top of the post. As shown in

Figure 60, the lack of a radius at this location resulted in a sharp corner exposed to contact with an impacting vehicle. Further, these sharp corners were responsible for all four tears observed in the simulated floorpan. The protected free-edge sides of the posts caused only creasing in the simulated floorpan. Thus, the steel plate edge protector may have actually prevented tearing if the posts had been fabricated correctly.

Force vs. deflection and energy vs. deflection curves were created from the accelerometer data. Additionally, the high-speed video was analyzed to determine the times in which the bogie overrode each post, the posts contacted the simulated floorpan, and the posts lost contact with the bogie vehicle. Results from the data and video analysis are shown in Figure 61. The recorded loads were lower for the bogie impact with the second post. This finding was likely due to a combination of a reduced impact velocity and a higher impact point on the second post. The reduced impact velocity resulted from the energy absorbed by the impact with the first post, while the higher impact point was caused by the bogie pitching upward as it overrode the first post.

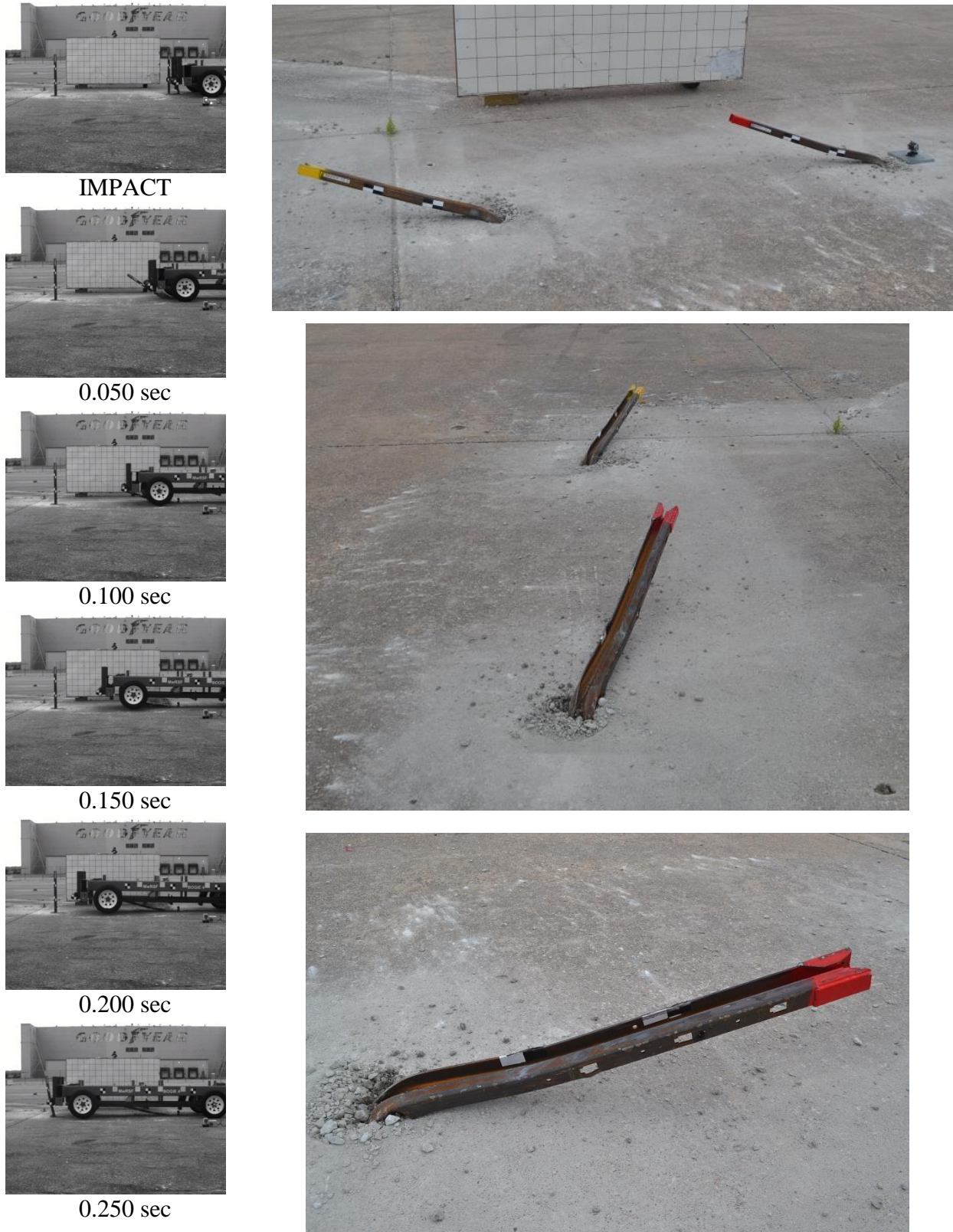


Figure 58. Time-Sequential and Post Damage Photographs, Test No. MWFPF-13



Front Bay

Rear Bay

Figure 59. Simulated Floorpan Damage, Test No. MWPPF-13



Figure 60. Post Damage, Test No. MWFPF-13

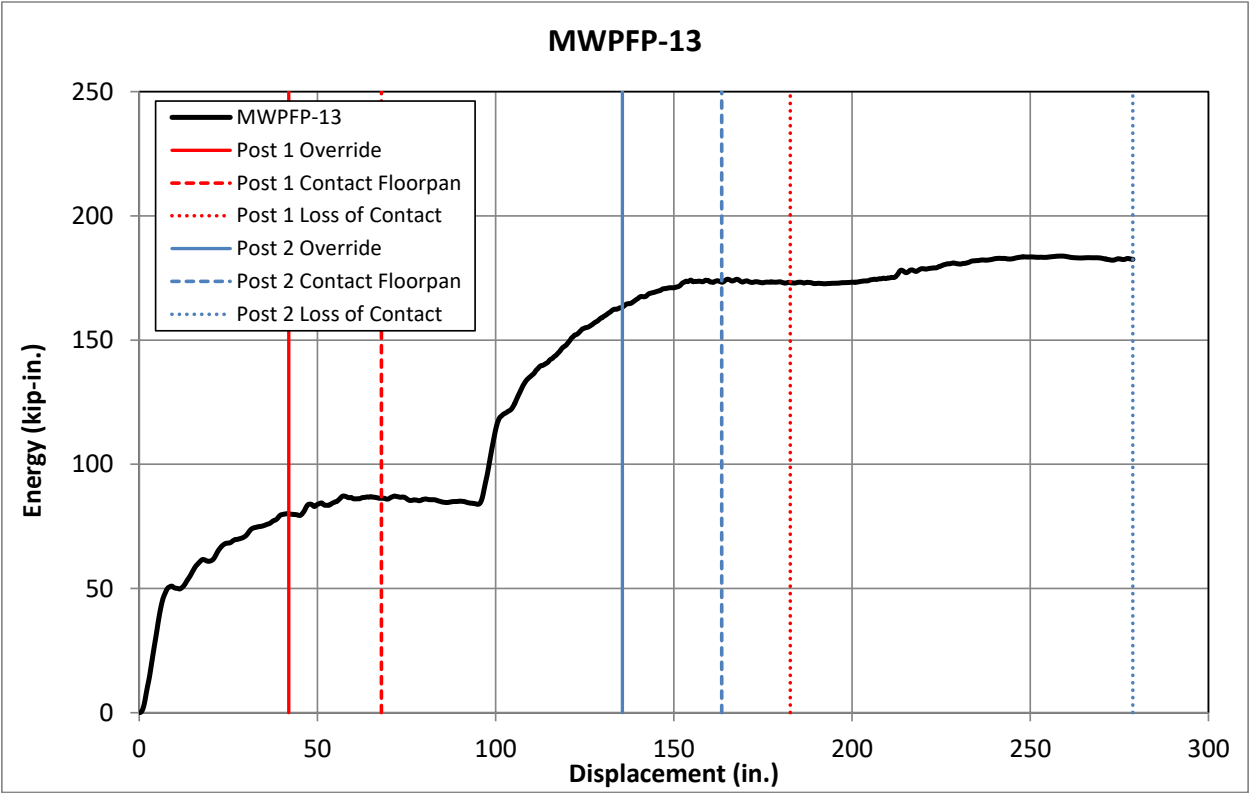
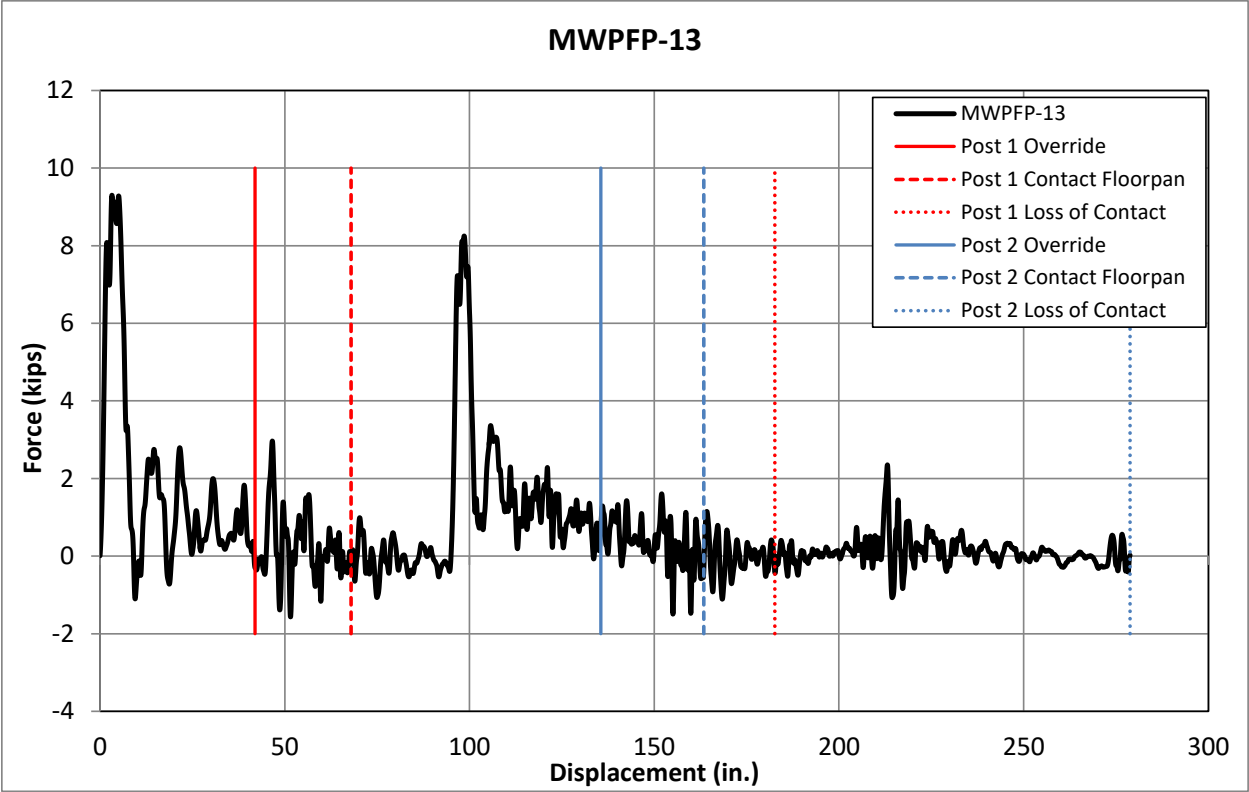


Figure 61. Force vs. Deflection and Energy vs. Deflection, Test No. MWPFP-13

Table 12. Floorpan Damage Measurements, Test No. MWFPF-13

MWFPF-13 Floorpan Damage					
Location	Description	1st Post		2nd Post	
		Free Edge in. (mm)	Continuous Edge in. (mm)	Free Edge in. (mm)	Continuous Edge in. (mm)
Front Bay	Tear Length	-	3 (76)	-	1½ (38)
	Max. Tear Width	-	¼ (6)	-	¼ (6)
	Crease Length	40 (1,016)	31 (787)	33 (838)	-
Rear Bay	Tear Length	-	2 (51)	-	1½ (38)
	Max. Tear Width	-	¼ (6)	-	¼ (6)
	Crease Length	49½ (1,257)	43 (1,092)	53½ (1,359)	4 (102)

5.1.12 Test No. MWFPF-14

Test no. MWFPF-14 was conducted on the MWP with three ⅜-in. (10-mm) diameter weakening holes in the weak-axis flanges at the groundline. The posts were installed in strong soil with a 25-degree orientation angle matching the impact angle of full-scale MASH testing for median barriers. During the test, the bogie impacted the first post at a speed of 26.7 mph (43.0 km/h). Upon impact, the post began to bend and tear near the groundline, and the post bent over until the bogie overrode it. Due to the severity of the tearing, the post bent completely down to the ground and did not spring back upward. Thus, the post never contacted the simulated floorpan. The bogie impacted the second post at 0.212 seconds and caused similar behavior as observed in the first post.

The posts were completely bent over, and tearing was present in both posts, as shown in Figure 62. The tears initiated from the weakening holes on the impact side of the posts and extended through the adjacent flanges and the webs. Only the opposite-side flanges and the backside faces of the posts were still intact and held the posts together. The posts displaced approximately 1½ in. (38 mm) through the soil at the groundline. The simulated floorpan was undamaged as the posts never contacted the undercarriage of the bogie vehicle.

Force vs. deflection and energy vs. deflection curves were created from the accelerometer data. Additionally, the high-speed video was analyzed to determine the times in which the bogie overrode each post and the posts lost contact with the bogie vehicle. Results from the data and video analysis are shown in Figure 63. The peak impact loads and absorbed energies were relatively constant between the two posts.

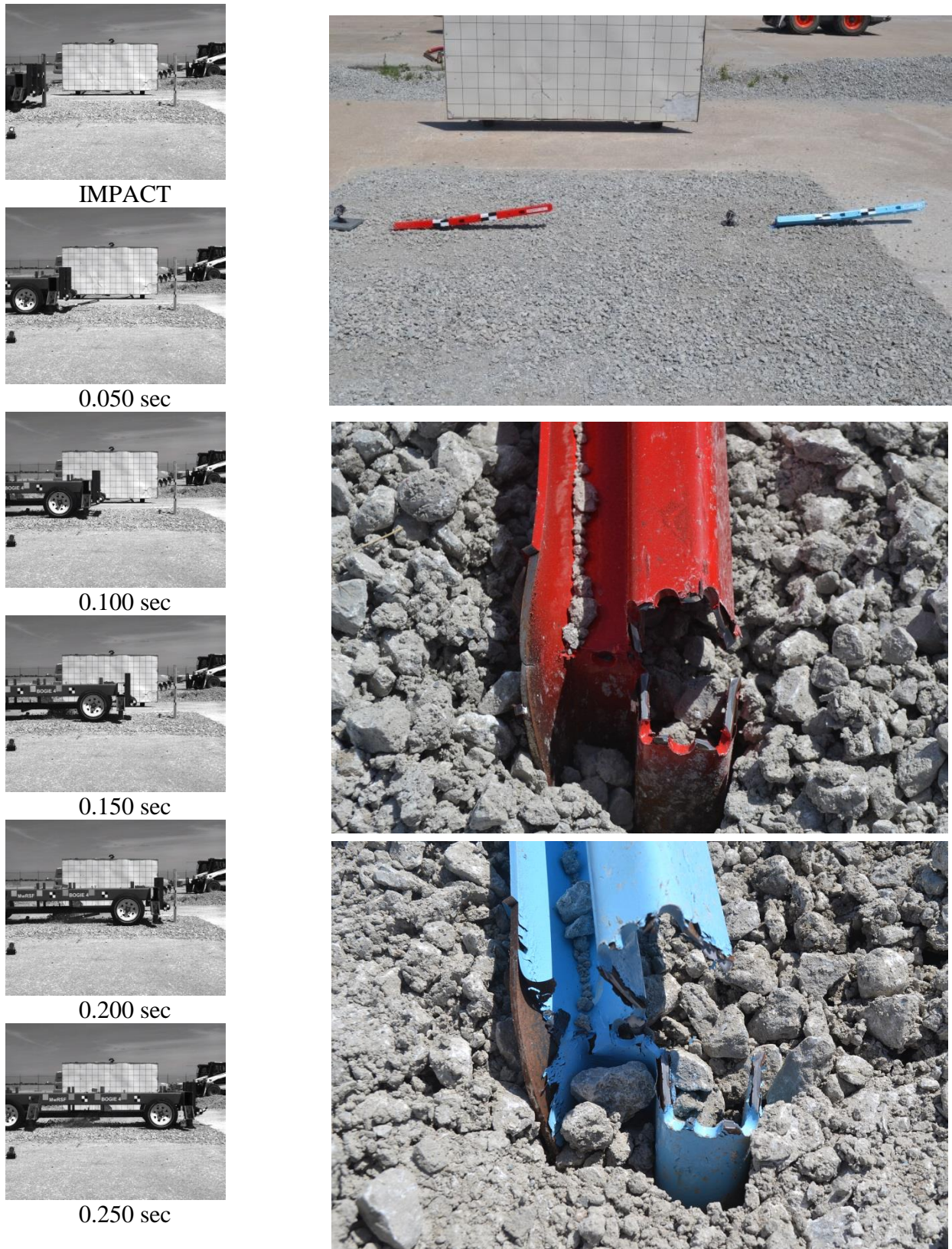


Figure 62. Time-Sequential and Post Damage Photographs, Test No. MWFPF-14

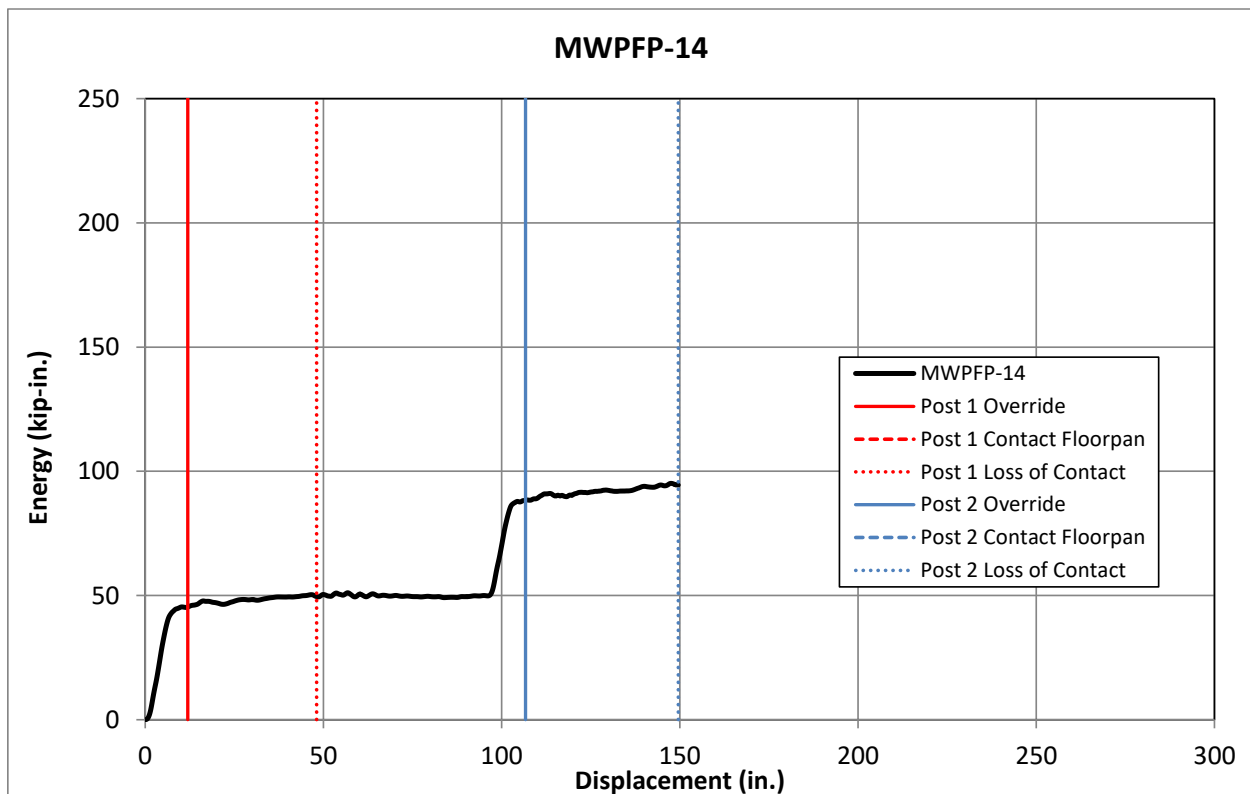
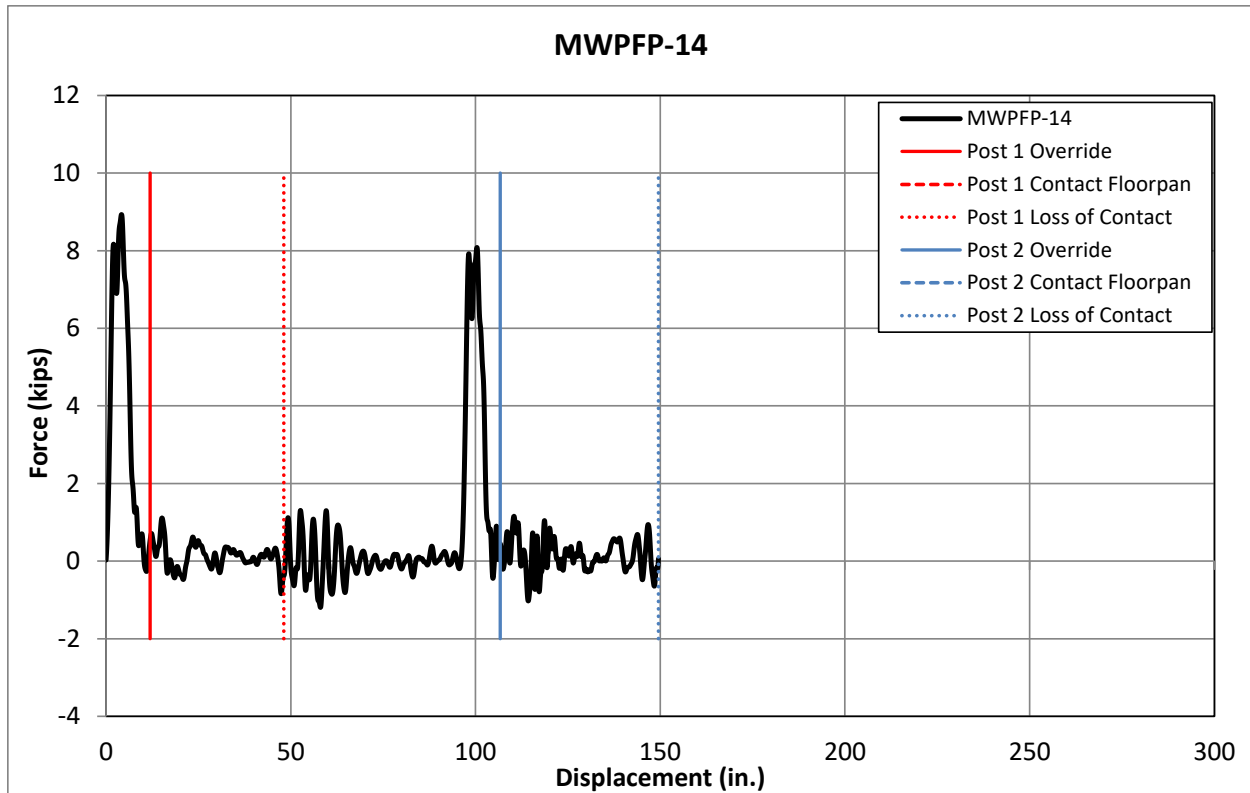


Figure 63. Force vs. Deflection and Energy vs. Deflection, Test No. MWPFP-14

5.1.13 Test No. MWFPF-15

Test no. MWFPF-15 was conducted on the MWP with $\frac{3}{8}$ -in. x $1\frac{1}{8}$ -in. (10-mm x 29-mm) weakening slots in the weak-axis flanges at the groundline. The posts were installed in strong soil with a 25-degree orientation angle matching the impact angle of full-scale MASH testing for median barriers. During the test, the bogie impacted the first post at a speed of 26.1 mph (42.0 km/h). Upon impact, the post began to bend and tear near groundline, and the post bent over until the bogie overrode it. Due to the severity of the tearing, the post bent completely to the ground and did not spring back upward. Thus, the post never contacted the simulated floorpan. The bogie impacted the second post at 0.209 seconds and caused similar behavior as observed in the first post.

The posts were completely bent over, and tearing was present in both posts, as shown in Figure 64. The tears initiated from the weakening slots on the impact side of the posts and extended through the adjacent flanges and the webs. Only the opposite-side flanges of the posts were still intact and held the posts together. The posts displaced approximately $\frac{1}{2}$ in. (13 mm) through the soil at groundline. The simulated floorpan was undamaged as the posts never contacted the undercarriage of the bogie vehicle.

Force vs. deflection and energy vs. deflection curves were created from the accelerometer data. Additionally, the high-speed video was analyzed to determine the times in which the bogie overrode each post and the posts lost contact with the bogie vehicle. Results from the data and video analysis are shown in Figure 65. The peak impact loads and absorbed energies were relatively constant between the two posts.

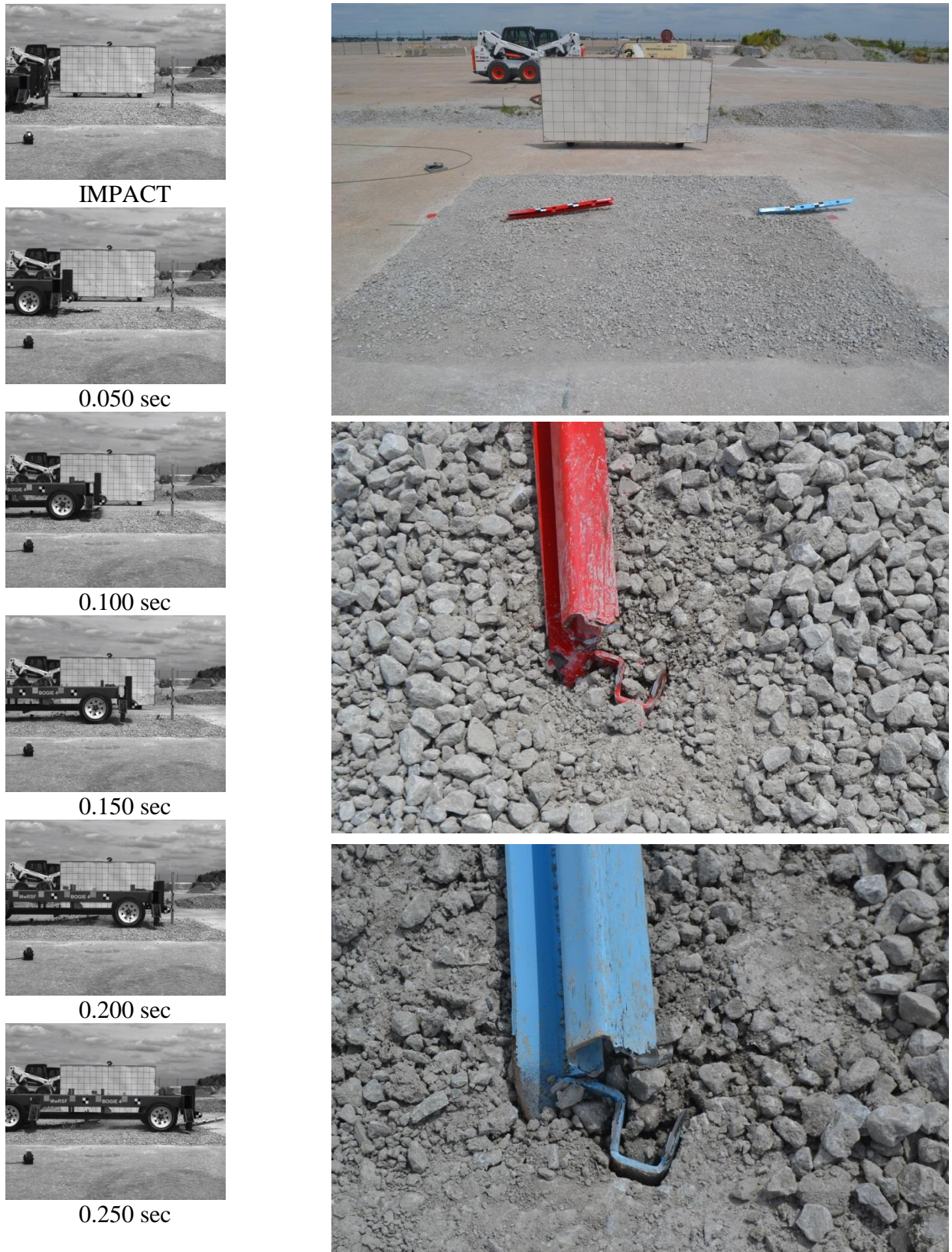


Figure 64. Time-Sequential and Post Damage Photographs, Test No. MWFPF-15

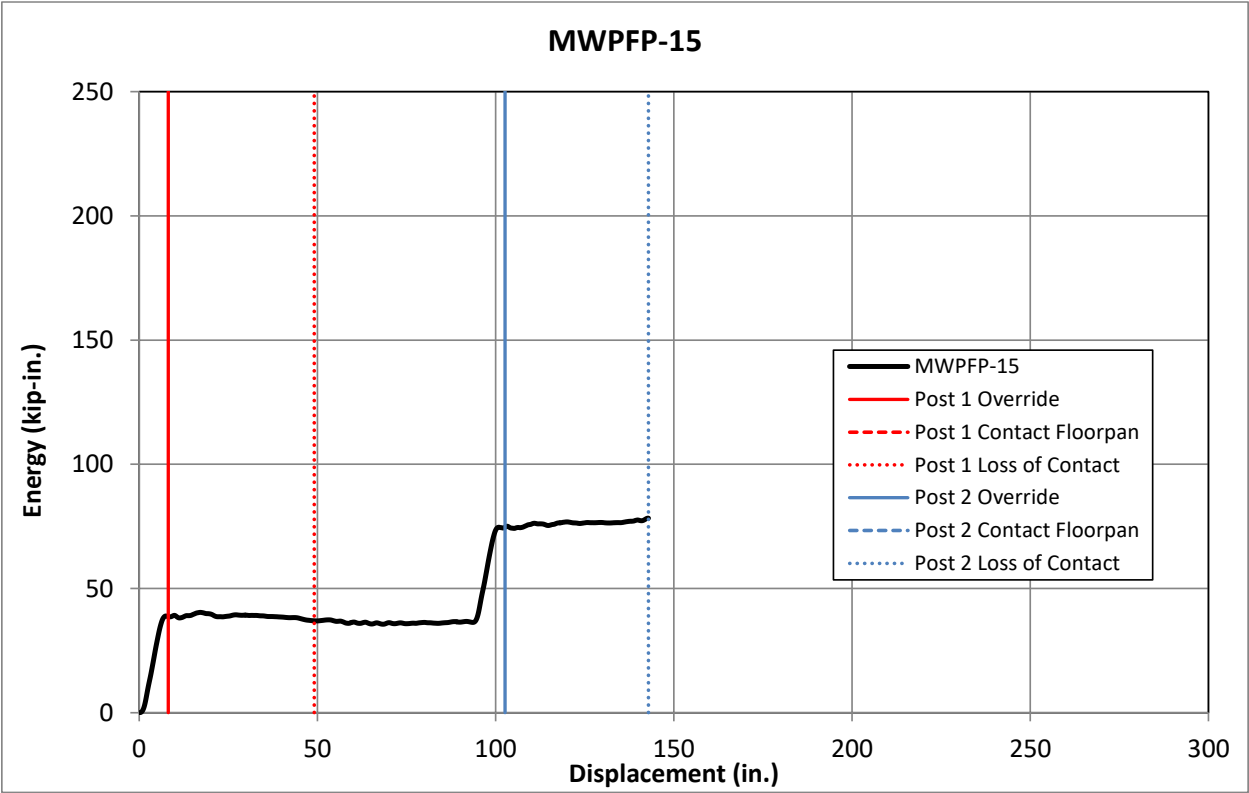
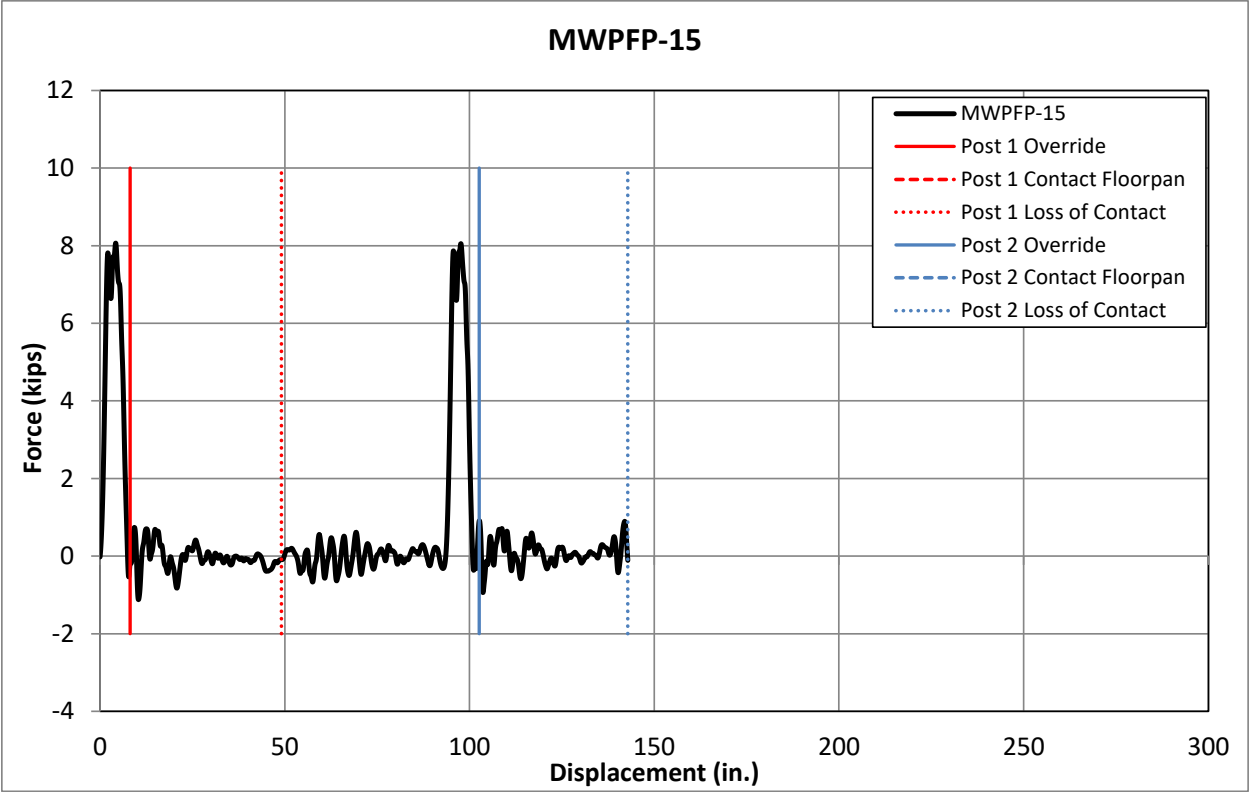


Figure 65. Force vs. Deflection and Energy vs. Deflection, Test No. MWPFP-15

5.1.14 Test No. MWFPF-18

Test no. MWFPF-18 was conducted on the MWP with $\frac{3}{4}$ -in. (19-mm) diameter weakening holes in the weak-axis flanges at the groundline. The posts were installed in strong soil with a 25-degree orientation angle matching the impact angle of full-scale MASH testing for median barriers. During the test, the bogie impacted the first post at a speed of 25.7 mph (41.4 km/h). Upon impact, the post began to bend and tear at the groundline, and the post bent over until the bogie overrode it. The severity of the tearing prevented the post from rebounding upward and contacting the floorpan. The bogie impacted the second post at 0.216 seconds, and the post began to bend and tear near the groundline. As the crossbeams passed over the post, elastic restoration caused the top of the second post to rebound upward and impact the simulated floorpan. The second post impacted the front and rear bays of the simulated floorpans at 0.390 seconds and 0.528 seconds, respectively.

The posts were bent plastically near the groundline, and tearing was present in both posts, as shown in Figure 66. The tears initiated from the weakening holes on the impact side of the posts and extended into the webs and adjacent flanges. Additional tearing was found on the opposite side flange of the first post. The posts displaced approximately $1\frac{1}{2}$ in. (38 mm) through the soil at the groundline. Damage to the simulated floorpan included scrapes and creases, but no tearing. Two creases were found in both the front and rear bays of the simulated floorpan, as shown in Figure 67. Only one of the creases extended past the region of initial contact. All creases observed on the simulated floorpan were measured and are summarized in Table 13.

Force vs. deflection and energy vs. deflection curves were created from the accelerometer data. Additionally, the high-speed video was analyzed to determine the times in which the bogie overrode each post, the posts contacted the simulated floorpan, and the posts lost contact with the bogie vehicle. Results from the data and video analysis are shown in Figure 68. The peak impact loads and absorbed energies were relatively constant between the two posts.

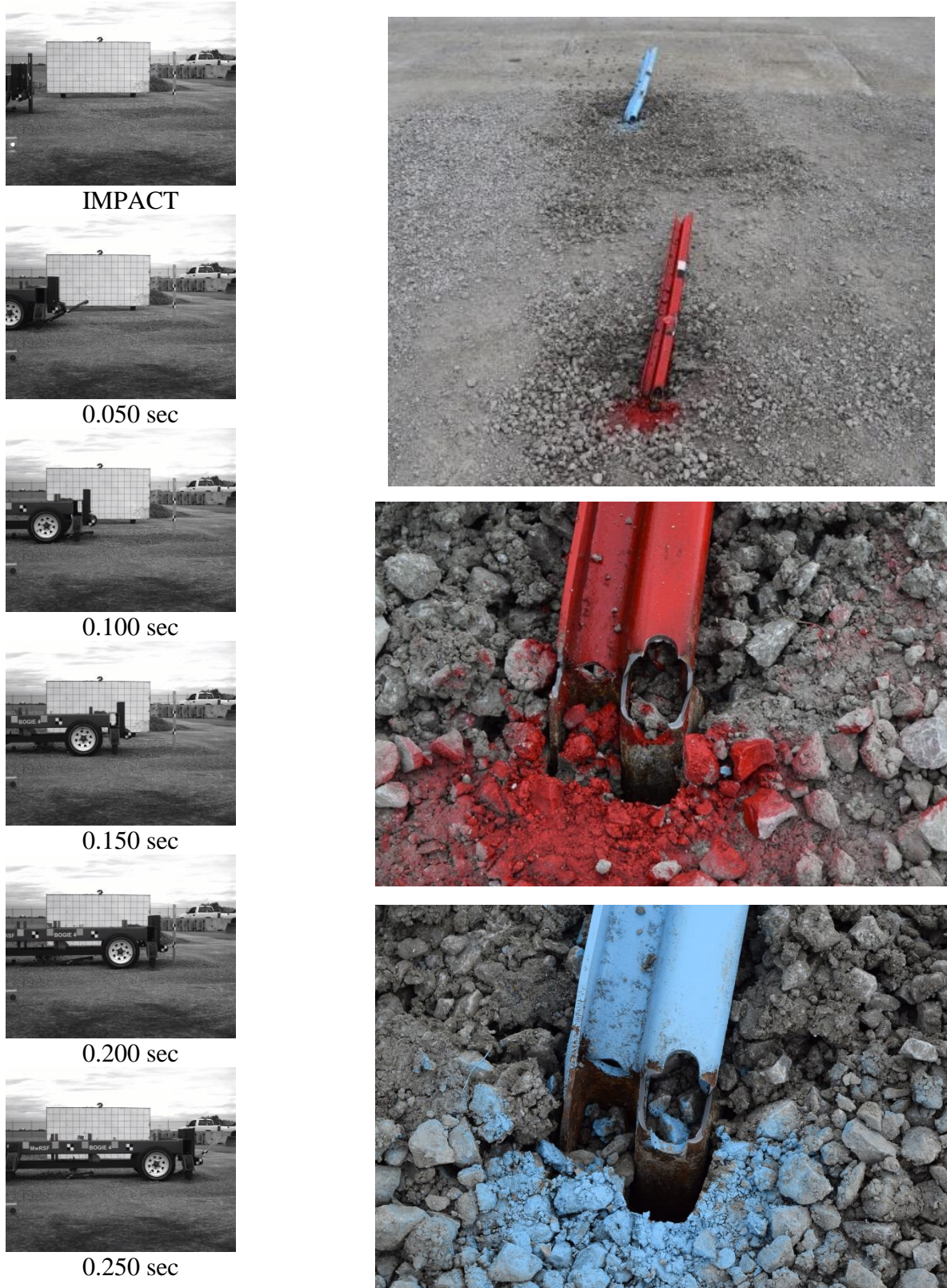
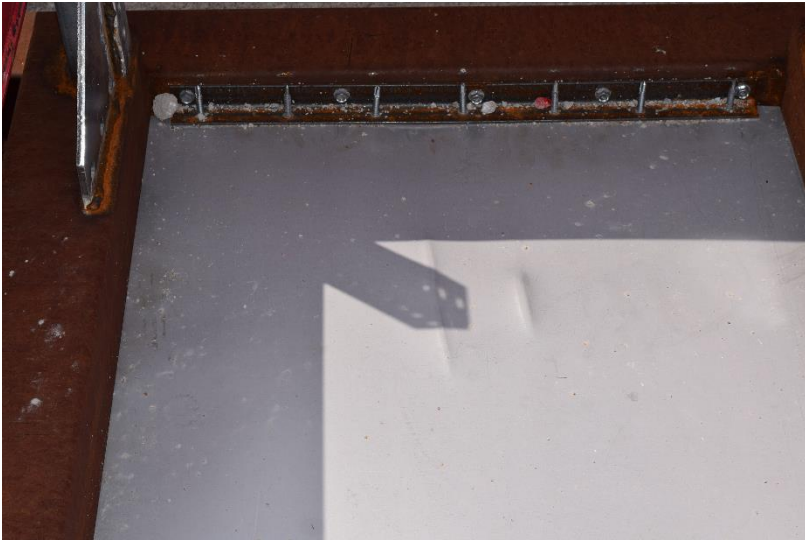
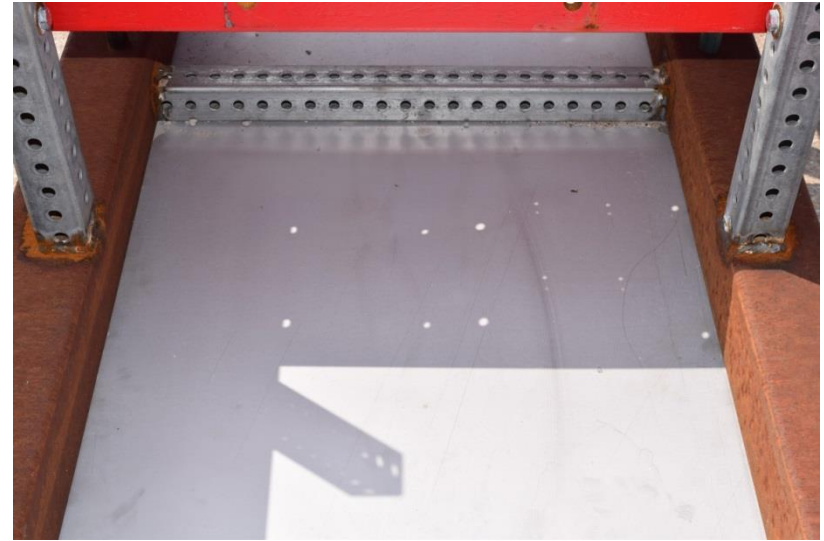


Figure 66. Time-Sequential and Post Damage Photographs, Test No. MWFPF-18



Front Bay

Rear Bay

Figure 67. Simulated Floorpan Damage, Test No. MWPFP-18

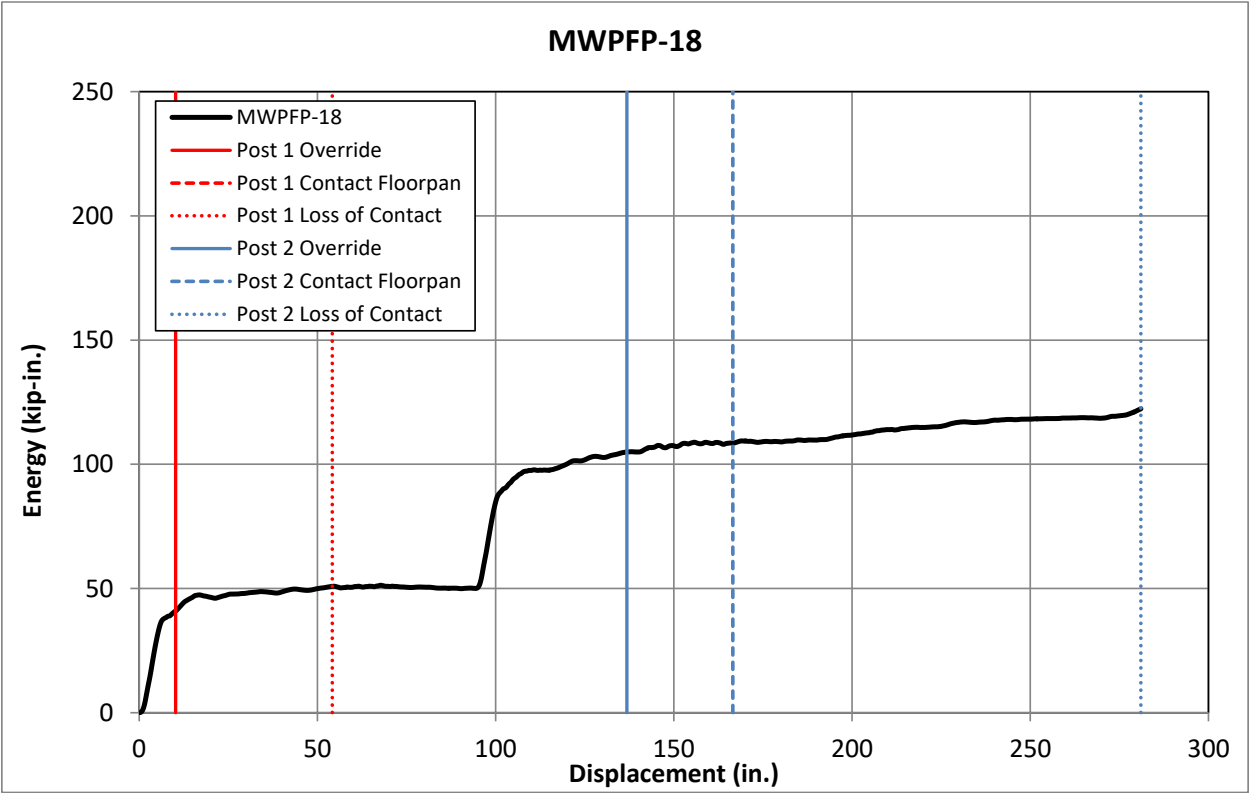
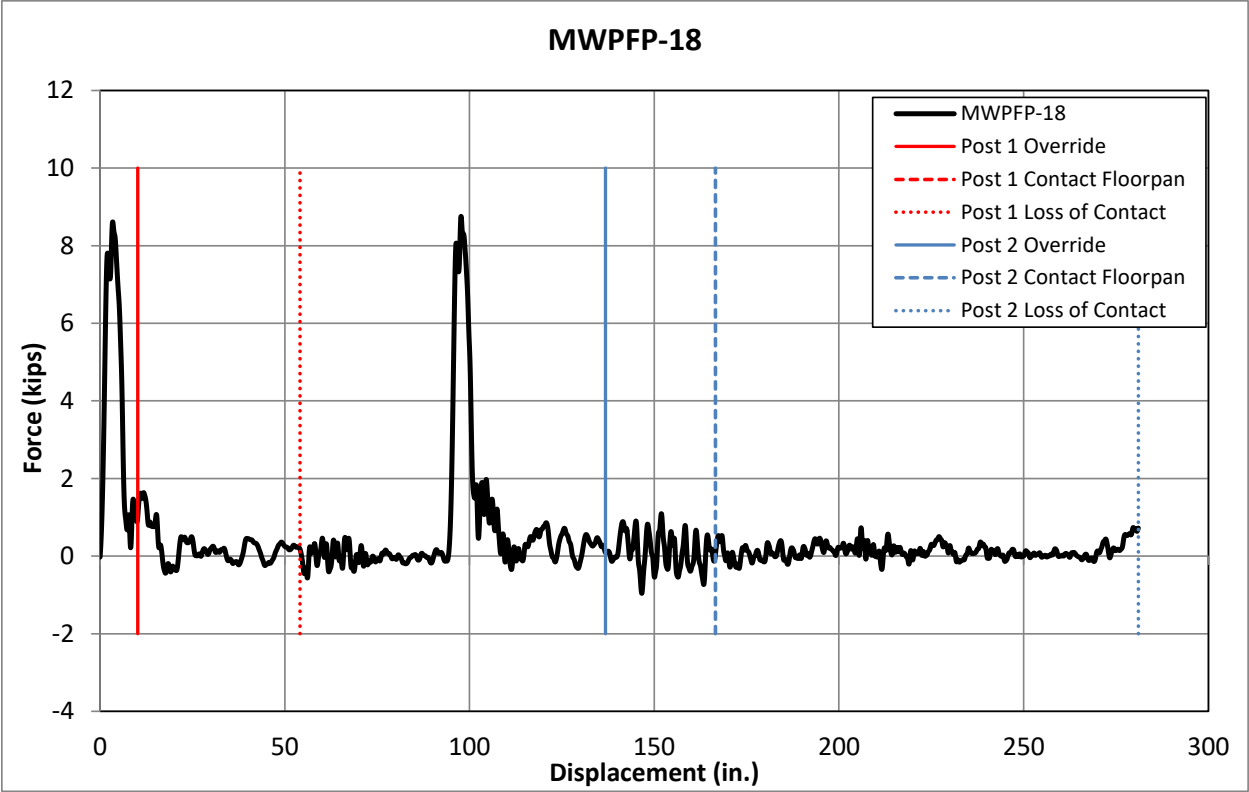


Figure 68. Force vs. Deflection and Energy vs. Deflection, Test No. MWPFP-18

Table 13. Floorpan Damage Measurements, Test No. MWPFP-18

MWPFP-18 Floorpan Damage					
Location	Description	1st Post		2nd Post	
		Free Edge in. (mm)	Continuous Edge in. (mm)	Free Edge in. (mm)	Continuous Edge in. (mm)
Front Bay	Tear Length	-	-	-	-
	Max. Tear Width	-	-	-	-
	Crease Length	-	-	33 (838)	5 (127)
Rear Bay	Tear Length	-	-	-	-
	Max. Tear Width	-	-	-	-
	Crease Length	-	-	5 (127)	5 (127)

5.1.15 Test No. MWPFP-21

Test no. MWPFP-21 was conducted on the MWP with ¾-in. (19-mm) diameter weakening holes in the weak-axis flanges at the groundline. The posts were installed in strong soil with a -25 degree orientation angle matching the impact angle of MASH if the cable barrier system was installed on the roadside as opposed to the median. During the test, the bogie impacted the first post at a speed of 25.7 mph (41.4 km/h). Upon impact, the post began to bend and tear at the groundline, and the post bent over until the bogie overrode it. As the crossbeams passed over the post, elastic restoration caused the top of the post to rebound upward and impact the simulated floorpan. The first post impacted the front and rear bays of the simulated floorpan 0.166 seconds and 0.304 seconds after impact, respectively. The bogie impacted the second post at 0.218 seconds and caused similar deformation and spring-back characteristics as observed in the first post. The second post impacted the front and rear bays of the simulated floorpan at 0.392 seconds and 0.538 seconds, respectively.

The posts were bent plastically near the groundline, and tearing was present in both posts, as shown in Figure 69. The tears initiated from the weakening holes on the impact side of the posts and extended into the webs and adjacent flanges. The posts displaced approximately 1½ in. (38 mm) through the soil at the groundline. Damage to the simulated floorpan included scrapes and creases, but no tearing. Three creases were found in both the front and rear bays of the simulated floorpan, as shown in Figure 70. Creases resulting from contact with free edges extended along the length of the simulated floorpan. Creases formed from contact with continuous edges were limited to only the area of initial contact. All creases observed on the simulated floorpan were measured and are summarized in Table 14.

Force vs. deflection and energy vs. deflection curves were created from the accelerometer data. Additionally, the high-speed video was analyzed to determine the times in which the bogie overrode each post, the posts contacted the simulated floorpan, and the posts lost contact with the bogie vehicle. Results from the data and video analysis are shown in Figure 71. The peak impact loads and absorbed energies were relatively constant between the two posts.

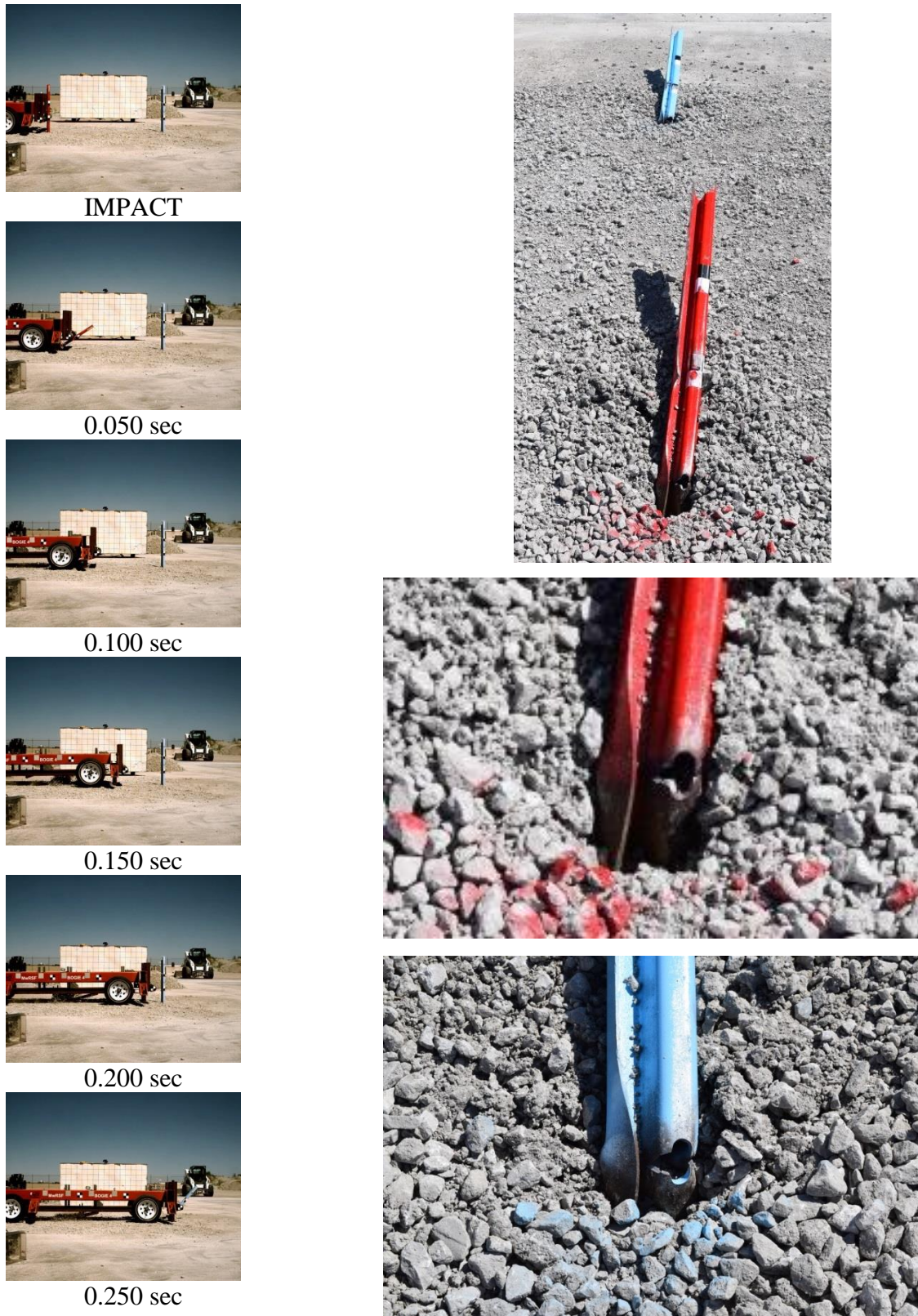
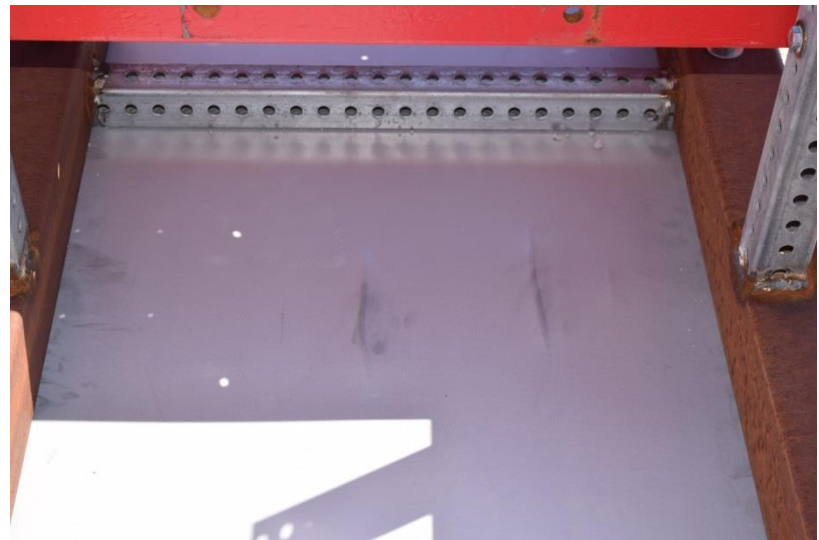


Figure 69. Time-Sequential and Post Damage Photographs, Test No. MWFPF-21



Front Bay

Rear Bay

Figure 70. Simulated Floorpan Damage, Test No. MWPFPP-21

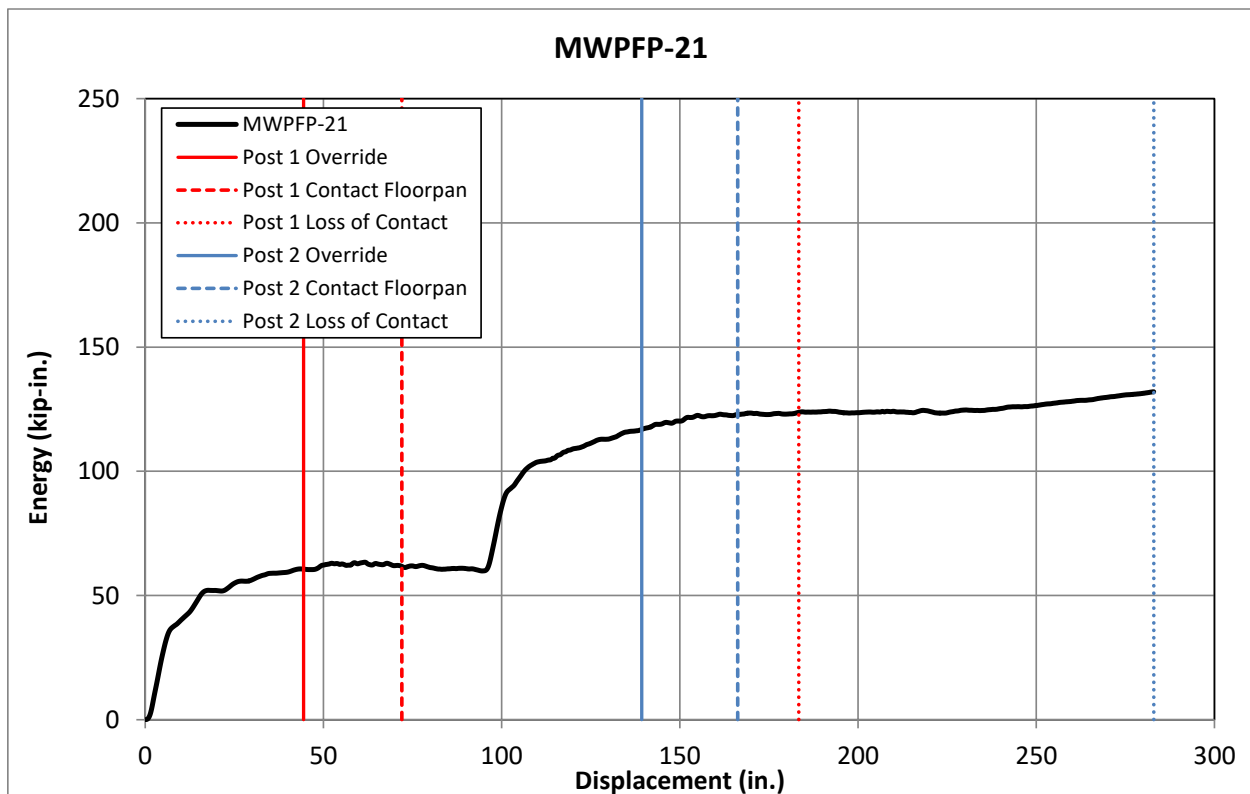
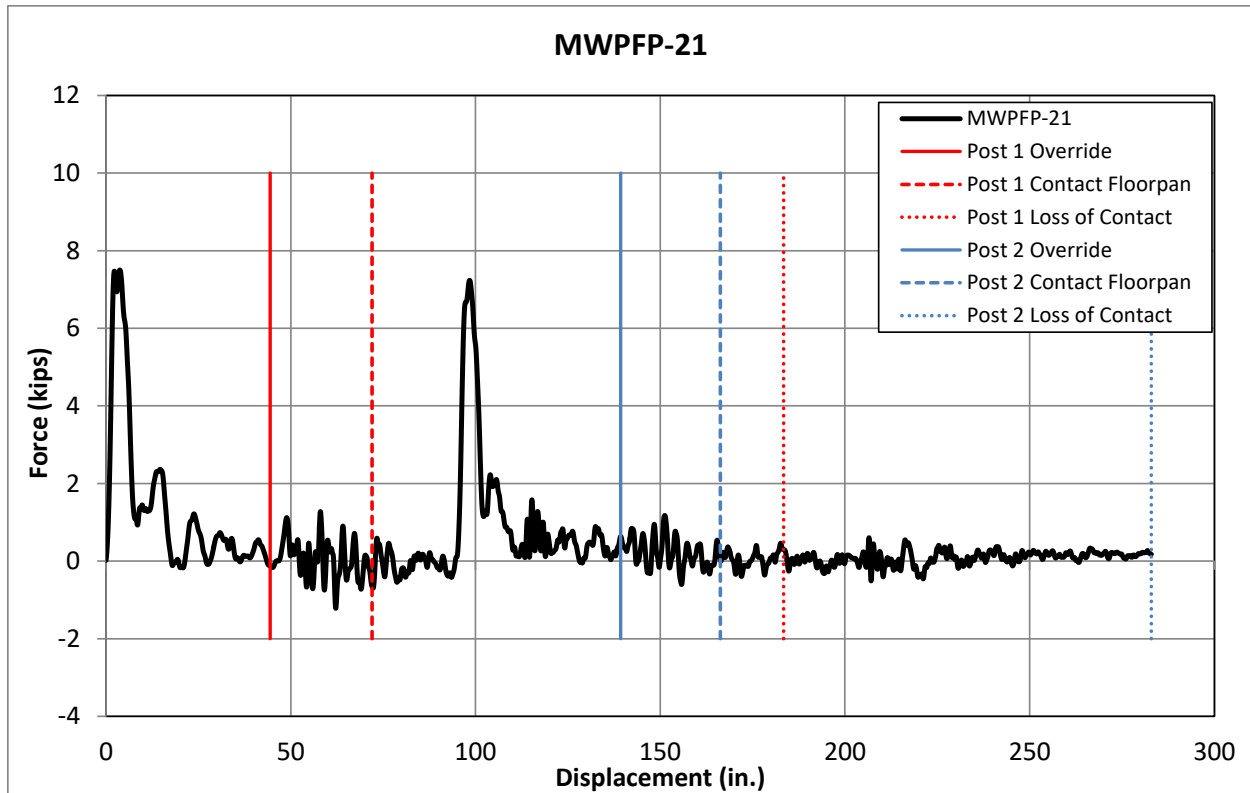


Figure 71. Force vs. Deflection and Energy vs. Deflection, Test No. MWPFP-21

Table 14. Floorpan Damage Measurements, Test No. MWFPF-21

MWFPF-21 Floorpan Damage					
Location	Description	1st Post		2nd Post	
		Free Edge in. (mm)	Continuous Edge in. (mm)	Free Edge in. (mm)	Continuous Edge in. (mm)
Front Bay	Tear Length	-	-	-	-
	Max. Tear Width	-	-	-	-
	Crease Length	37 (940)	2½ (64)	31 (787)	-
Rear Bay	Tear Length	-	-	-	-
	Max. Tear Width	-	-	-	-
	Crease Length	49 (1,245)	2½ (64)	40 (1,016)	-

5.2 Discussion

A total of fifteen dynamic component tests were conducted utilizing a bogie vehicle with a simulated floorpan. The first two tests were conducted to verify the test setup could replicate the floorpan tearing and creasing observed during the previous full-scale crash tests. In test no. MWFPF-2, the free edges of both posts caused tears to form in both the front and rear bays of the simulated floorpan. Additionally, contact with both corners of the posts caused creases to form along the length of the simulated floorpan. This tearing and creasing behavior was very similar to that observed in the full-scale tests. The following thirteen tests were conducted to evaluate the floorpan damage associated with various posts and post modifications designed to prevent floorpan tearing.

Test nos. MWFPF-4 and MWFPF-5 were conducted on S3x5.7 (S76x8.5) posts oriented at 0 degrees, or about the post's weak-axis of bending. During the tests, both of the free edges on each S3x5.7 (S76x8.5) post caused tears to both bays of the simulated floorpan. Not only did the S3x5.7 (S76x8.5) posts cause twice as many tears as the MWP, but the tears tended to be larger than those observed from testing with the MWP. Test no. MWFPF-5 evaluated a 31-in. (787-mm) tall post matching the height of the non-proprietary, low-tension, cable median barrier. The shorter height seemed to result in higher vertical loads being imparted to the simulated floorpan as the post elastically restored. Subsequently, sharp creases and secondary tears were found within the first bay of the floorpan. Testing with S3x5.7 (S76x8.5) posts indicated that floorpan tearing was not specific to the MWP. Rather, any post with free/exposed edges may be at risk to cause floorpan tearing.

One test was conducted on the MWP with simulated no. 1 edge rounding. The edge rounding did not appear to have much of an effect as the free edges still caused tearing to the simulated floorpan during test no. MWFPF-6. Thus, edge rounding was not recommended for further evaluation as a method to mitigate tearing.

Test no. MWFPF-13 featured the MWP with $\frac{3}{16}$ -in (5-mm) thick steel plate edge protectors. The edge protectors successfully mitigated floorpan tearing as the free-edge side of the posts only created creases in the simulated floorpan. The tears that occurred in the floorpan

during test no. MWFPF-13 were the result of contact with the continuous edges of the posts. A fabrication error resulted in a sharp corner in the continuous edge of the MWP being exposed to contact. If the proper radius had been applied to the cut pattern for the posts, it is unlikely that any tearing would have occurred. Therefore, these tears were not considered a result of the edge protectors, and the use of edge protectors was deemed an effective tearing mitigation method.

Five tests were conducted on the MWP with $\frac{3}{4}$ -in. (19-mm) diameter weakening holes. Testing of these posts with orientation angles of 0, 25, and -25 degrees all produced similar results. The holes weakened the cross section of the posts and led to tearing of the posts at the weakening holes. These tears reduced the elastic restoration forces of the posts and limited the magnitude of the contact forces between the posts and the vehicle undercarriage. Subsequently, tearing to the simulated floorpan was averted, and damage was limited to contact marks and creases. One test, test no. MWFPF-8, was accidentally conducted with the weakened posts oriented at 65 degrees and resulted in tearing in both the front and rear bays of the simulated floorpan. However, a vehicle impact at 65 degrees is extremely severe and likely beyond the capture and/or redirection capabilities of the cable barrier system. Thus, the results of test no. MWFPF-8 were not considered relevant, and the utilization of $\frac{3}{4}$ -in. (19-mm) diameter weakening holes was deemed a viable option to mitigate tearing in actual vehicle floorpans.

Two other post weakening techniques were evaluated: (1) three $\frac{3}{8}$ -in. (10-mm) diameter holes and (2) a $\frac{3}{8}$ -in. x $1\frac{1}{8}$ -in (10-mm x 29-mm) slot. When tested at both 0- and 25-degree orientation angles, both of these weakening methods caused extensive tearing of the MWPs and eliminated the ability of the posts to spring-back upward to contact the vehicle undercarriage. The weakening slots actually resulted in complete rupture of the post at the groundline during the 0-degree orientation test, test no. MWFPF-12. All four tests resulted in no contact between the post and the simulated floorpan. Therefore, both the three $\frac{3}{8}$ -in. (10-mm) diameter holes and the $\frac{3}{8}$ -in. x $1\frac{1}{8}$ -in (10-mm x 29-mm) slot were also deemed viable options to prevent vehicle floorpan tearing.

Dynamic component testing results illustrated that both edges protectors and post weakening were effective methods to mitigate floorpan tearing. However, weakening of the MWP seemed easier and less costly to implement. Weakening holes or slots could be added to the keyway punch pattern for the posts at minimal cost and would require no additional fabrication time. Using edge protectors would require additional parts and labor to apply them to the posts. Therefore, it was recommended that weakening holes/slots be implemented in the MWP to prevent floorpan tearing in future testing and development of the prototype cable median barrier system.

To better understand the effect of the various weakening mechanisms, the accelerometer data from each test was analyzed to obtain peak forces and absorbed energies for each post. Table 16 provides a comparison of these values organized by post section and impact conditions. Test nos. MWFPF-8 and MWFPF-21 were not included because they had unique impact angles and could not be directly compared to any other tests. MWFPF-7 was also excluded as it was the only 0-degree test to be conducted in soil. As expected, the S3x5.7 (S76x8.5) posts provided the highest peak forces. The standard MWP provided the second highest forces, and the weakening holes and slots followed in order of the amount of section removed. This pattern remained the same when looking at absorbed energy per post and was consistent for both the 0-degree and 25-degree impact conditions. Interestingly, a comparison of the level of floorpan damage caused by

each post section would result in the same pattern. The S3x5.7 (S3x5.7) posts caused the most tearing, the standard MWP's caused tearing and creasing, the 3/4-in. (19-mm) diameter weakening holes caused creasing only, and the three 3/8-in. (10-mm) diameter holes and the 3/8-in. x 1 1/8-in (10-mm x 29-mm) slot caused no damage at all. These results support the theory that post strength and the restoration force of deformed posts directly relates to the potential for floorpan damage.

The average peak force did not change dramatically between the various standard and weakened configurations of the MWP. This finding may be a result of post inertia accounting for a large portion of the initial forces during an impact event. The average absorbed energy values provided a better metric for which to compare the MWP configurations. For 0-degree impacts, the 3/4-in. (19-mm) diameter holes resulted in a 28 percent reduction in absorbed energy, the three 3/8-in. (10-mm) diameter holes resulted in a 34 percent reduction, and the 3/8-in. x 1 1/8-in (10-mm x 29-mm) slot resulted in a 43 percent reduction compared to the standard MWP section. These energy reductions have already been shown to reduce the propensity for floorpan damage, but they may also result in reducing small car instabilities during impact events – another benefit of weakened posts that the other tearing mitigation methods could not provide.

Unfortunately, the addition of weakening holes/slots to the system posts may also affect the stiffness and behavior of the cable barrier system. The post strength comparison was only relevant to impacts through the longitudinal, or weak axis of the posts. Prior to the selection of a specific weakening mechanism, the effect of these holes and slots on the post's strong-axis of bending needed to be quantified as lateral post strength can greatly affect system deflections and working widths. Thus, dynamic component testing was required to evaluate the strong-axis bending strengths of the various weakened MWP configurations.

Table 15. Component Testing Summary, Floorpan Tearing Evaluation

Test No.	Post				Tarmac or Soil	Impact Speed mph (km/h)	Impact Angle (deg.)	Post Damage	Floorpan Damage			
	Type	Height in. (mm)	Modifications						Front Bay		Rear Bay	
			Top	Groundline					Tears	Creases	Tears	Creases
MWPFP-1	MWP	39¼ (997)	R⅝"	N/A	Tarmac	25.0 (40.2)	0	Bending	2	4	0	0
MWPFP-2	MWP	39¼ (997)	R⅝"	N/A	Tarmac	25.8 (41.5)	0	Bending	2	4	2	4
MWPFP-3	MWP	39¼ (997)	R⅝"	Ø¾" Holes	Tarmac	26.8 (43.1)	0	Bending & Tearing	0	4	0	4
MWPFP-4	S3x5.7	39¼ (997)	N/A	N/A	Tarmac	27.9 (44.9)	0	Bending	4	4	4	4
MWPFP-5	S3x5.7	31 (787)	N/A	N/A	Tarmac	30.5 (49.0)	0	Bending	6*	2	4*	4
MWPFP-6	MWP	39¼ (997)	R⅝" #1 Edge	N/A	Tarmac	28.1 (45.2)	0	Bending	2	4	2	4
MWPFP-7	MWP	39¼ (997)	R⅝"	Ø¾" Holes	Soil	29.7 (47.8)	0	Bending & Tearing	0	4	0	4
MWPFP-8	MWP	39¼ (997)	R⅝"	Ø¾" Holes	Soil	26.6 (42.8)	65	Bending	2*	3	2*	3
MWPFP-11	MWP	39¼ (997)	R⅝"	(3) Ø⅜" Holes	Tarmac	25.9 (41.7)	0	Bending & Tearing	0	0	0	0
MWPFP-12	MWP	39¼ (997)	R⅝"	Ø⅜"x 1⅛" Slots	Tarmac	24.4 (39.3)	0	Rupture	0	0	0	0
MWPFP-13	MWP	39¼ (997)	Flange Extension	N/A	Tarmac	24.2 (38.9)	0	Bending	2	3	2	4
MWPFP-14	MWP	39¼ (997)	R⅝"	(3) Ø⅜" Holes	Soil	26.7 (43.0)	25	Bending & Tearing	0	0	0	0
MWPFP-15	MWP	39¼ (997)	R⅝"	Ø⅜"x 1⅛" Slots	Soil	26.1 (42.0)	25	Bending & Tearing	0	0	0	0
MWPFP-18	MWP	39¼ (997)	R⅝"	Ø¾" Holes	Soil	25.7 (41.4)	25	Bending & Tearing	0	2	0	2
MWPFP-21	MWP	39¼ (997)	R⅝"	Ø¾" Holes	Soil	25.7 (41.4)	-25	Bending & Tearing	0	3	0	3

*Additional tears formed beyond initial contact with simulated floorpan

N/A – Not Applicable

Table 16. Component Testing Summary of Forces and Energies

Test No.	Post Type	Weakening	Installed in	Impact Angle (deg.)	Post 1		Post 2		Average	
					Peak Force kips (kN)	Absorbed Energy kip-in. (kJ)	Peak Force kips (kN)	Absorbed Energy (kip-in.)	Peak Force kips (kN)	Absorbed Energy (kip-in.)
MWPFP-4	S3x5.7	N/A	Tarmac	0	12.35 (54.9)	110.89 (12.5)	9.90 (44.0)	89.00 (10.1)	11.13 (49.5)	99.94 (11.3)
MWPFP-5	S3x5.7	N/A	Tarmac	0	12.40 (55.2)	101.85 (11.5)	10.17 (45.2)	65.17 (7.4)	11.28 (50.2)	83.51 (9.4)
Average S3x5.7			Tarmac	0	12.38 (55.1)	106.37 (12.0)	10.04 (44.7)	77.08 (8.7)	11.21 (49.9)	91.73 (10.4)
MWPFP-1	MWP	N/A	Tarmac	0	10.35 (46.0)	78.07 (8.8)	9.30 (41.4)	70.83 (8.0)	9.82 (43.7)	74.45 (8.4)
MWPFP-2	MWP	N/A	Tarmac	0	9.98 (44.4)	79.74 (9.0)	8.58 (38.2)	74.75 (8.4)	9.28 (41.3)	77.24 (8.7)
MWPFP-13	MWP	N/A	Tarmac	0	9.30 (41.4)	80.17 (9.1)	8.25 (36.7)	79.35 (9.0)	8.77 (39.0)	79.76 (9.0)
MWPFP-6	MWP	N/A	Tarmac	0	10.60 (47.2)	92.14 (10.4)	7.95 (35.4)	68.16 (7.7)	9.27 (41.2)	80.15 (9.1)
Average MWP			Tarmac	0	10.06 (44.7)	82.53 (9.3)	8.52 (37.9)	73.27 (8.3)	9.29 (41.3)	77.90 (8.8)
MWPFP-3	MWP	Ø¾" Hole	Tarmac	0	10.02 (44.6)	55.61 (6.3)	9.91 (44.1)	57.15 (6.5)	9.97 (44.3)	56.38 (6.4)
MWPFP-11	MWP	(3) Ø¾" Holes	Tarmac	0	9.75 (43.4)	51.42 (5.8)	9.71 (43.2)	50.80 (5.7)	9.73 (43.3)	51.11 (5.8)
MWPFP-12	MWP	Ø¾"x 1½" Slot	Tarmac	0	9.02 (40.1)	39.40 (4.4)	13.36* (59.4)	49.64* (5.6)	9.02 (40.1)	44.52 (5.0)
MWPFP-18	MWP	Ø¾" Hole	Soil	25	8.61 (38.3)	40.92 (4.6)	8.75 (38.9)	54.93 (6.2)	8.68 (38.6)	47.92 (5.4)
MWPFP-14	MWP	(3) Ø¾" Holes	Soil	25	8.93 (39.7)	45.39 (5.1)	8.08 (35.9)	38.50 (4.3)	8.50 (37.8)	41.94 (4.7)
MWPFP-15	MWP	Ø¾"x 1½" Slot	Soil	25	8.06 (35.9)	38.91 (4.4)	8.05 (35.8)	38.33 (4.3)	8.06 (35.9)	38.62 (4.4)

*Top of post no. 1 impacted at same time as post no. 2 causing erroneous and high forces

Test nos. MWPFP-8 and MWPFP-21 were not included here due to unique impact angles

Test no. MWPFP-7 was not included here due to unique combination of 0 degree angle and soil

N/A – Not Applicable

6 COMPONENT TESTING CONDITIONS – POST STRENGTH

6.1 Purpose

Dynamic component testing has demonstrated that post weakening can mitigate the propensity for guardrail posts to tear, or penetrate, a vehicle's floorpan. The weakening holes and slots evaluated in Chapter 5 were placed on the upstream and downstream flanges of the MWP to maximize weakening along the longitudinal barrier axis, or about the post's weak-axis, while minimizing their effect on the strong-axis bending strength of the post. Reductions to the strong-axis bending strength of the barrier posts could affect system performance by altering initial stiffness, cable release times, cable pocketing angles, system deflections, and working widths. Therefore, prior to the selection of a specific weakening mechanism, the effect that holes and slots had on the MWP's strong-axis bending strength needed to be quantified through dynamic component testing.

6.2 Scope

A total of six dynamic bogie tests were conducted in order to evaluate the lateral, or strong-axis, bending strength of the MWP with various weakening holes or slots. Three different weakening mechanisms were evaluated along with the unmodified MWP for a total of four different post configurations. Two tests each were conducted on both the unmodified MWP and the MWP with 3/4-in. (19-mm) diameter weakening holes. One test each was conducted on both the MWP with three 3/8-in. (10-mm) diameter holes and the MWP with 3/8-in. x 1 1/8-in. (10-mm x 29-mm) slots. However, the latter two tests were conducted with two posts offset 8 ft (2.4 m) longitudinally. Thus, each post configuration was impacted a total of two times within the six dynamic component tests.

All posts were installed within an 8-in. (203-mm) diameter hole cored into the tarmac and backfilled with a compacted, coarse, crushed limestone material that met AASHTO standard soil designation M147 Grade B, as recommended by MASH. The MWPs were oriented at a 90-degree angle, thus creating an impact about the post's strong-axis of bending. The bogie vehicle impacted the posts at a height of 27 in. (686 mm) above the groundline at a targeted impact speed of 25 mph (40 km/h). The dynamic testing matrix is summarized in Table 17, while the single- and double-post test setups are shown in Figures 72 and 73, respectively. Details for each of the MWP configurations are shown in Figures 74 through 77. Material specifications, mill certifications, and certificates of conformity for the posts are shown in Appendix B.

Table 17. Dynamic Component Testing Matrix, Post Strength Evaluation

Test No.	Post		Post Installed in Tarmac/Soil	Targeted Impact Conditions		
	No. of Posts	Weakening Mechanism		Speed mph (km/h)	Height in. (mm)	Angle (deg)
MWPFP-9	1	Ø¾" holes	Tarmac	25 (40)	27 (686)	90
MWPFP-10	1	N/A	Tarmac	25 (40)	27 (686)	90
MWPFP-16	2	(3) Ø¾" holes	Tarmac	25 (40)	27 (686)	90
MWPFP-17	2	Ø¾" x 1½" slots	Tarmac	25 (40)	27 (686)	90
MWPFP-19	1	N/A	Tarmac	25 (40)	27 (686)	90
MWPFP-20	1	Ø¾" holes	Tarmac	25 (40)	27 (686)	90

90 degree orientation corresponds to lateral, or strong-axis, impacts

N/A – Not Applicable

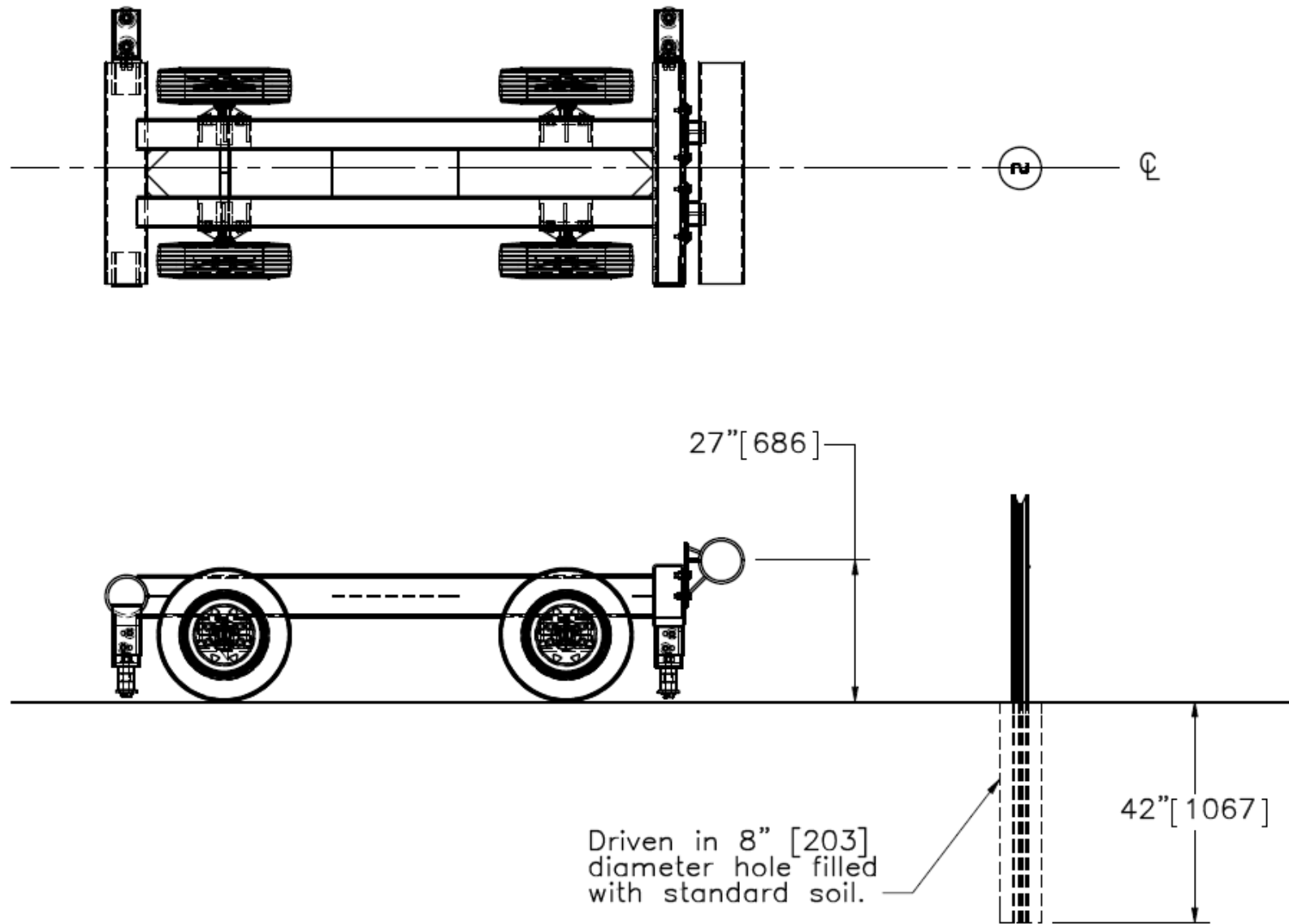


Figure 72. Single Post Dynamic Component Test Setup, Test Nos. MWPFP-9, MWPFP-10, MWPFP-19, and MWPFP-20

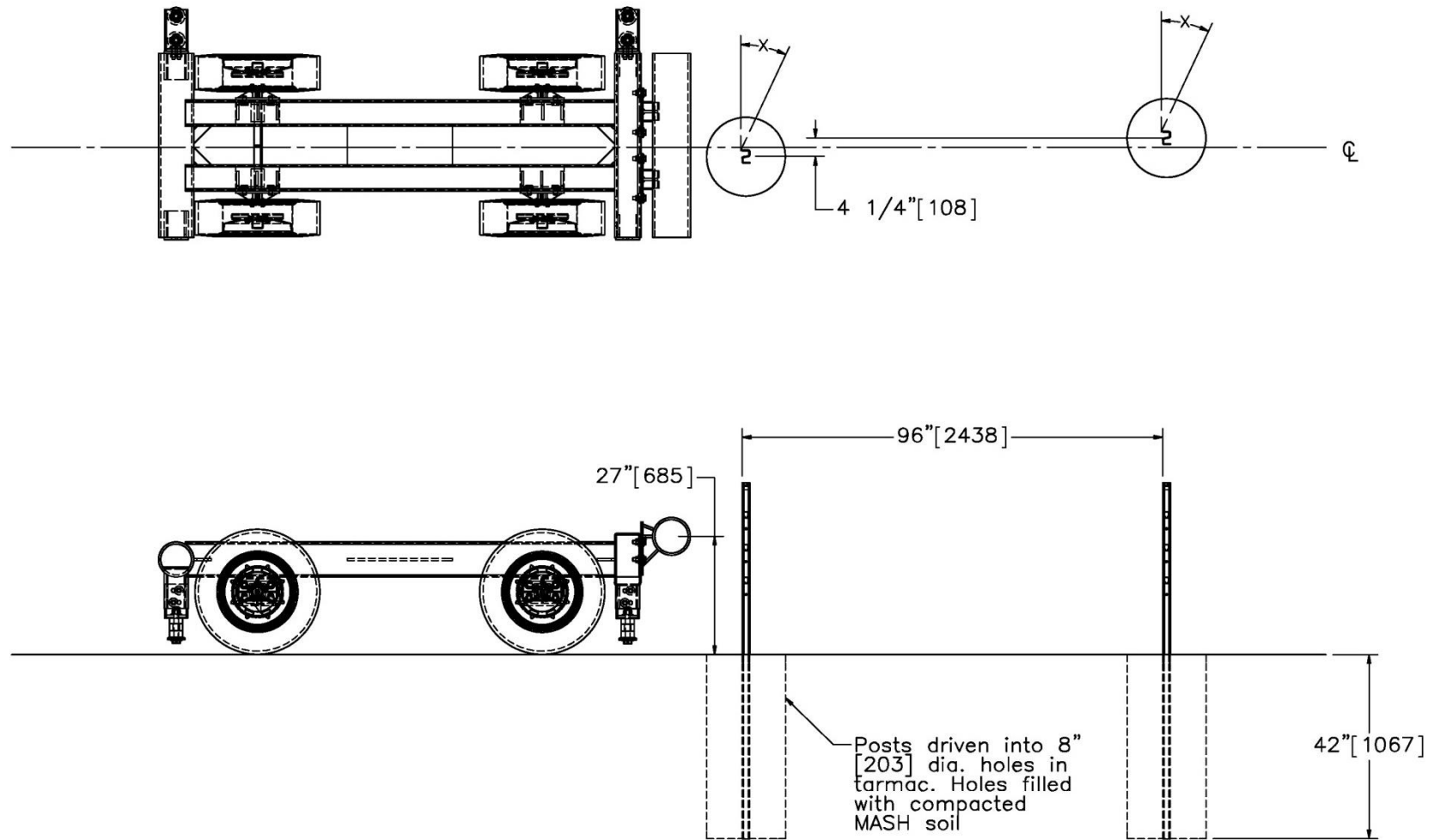


Figure 73. Double Post Dynamic Component Test Setup, Test Nos. MWPFP-16 and MWPFP-17

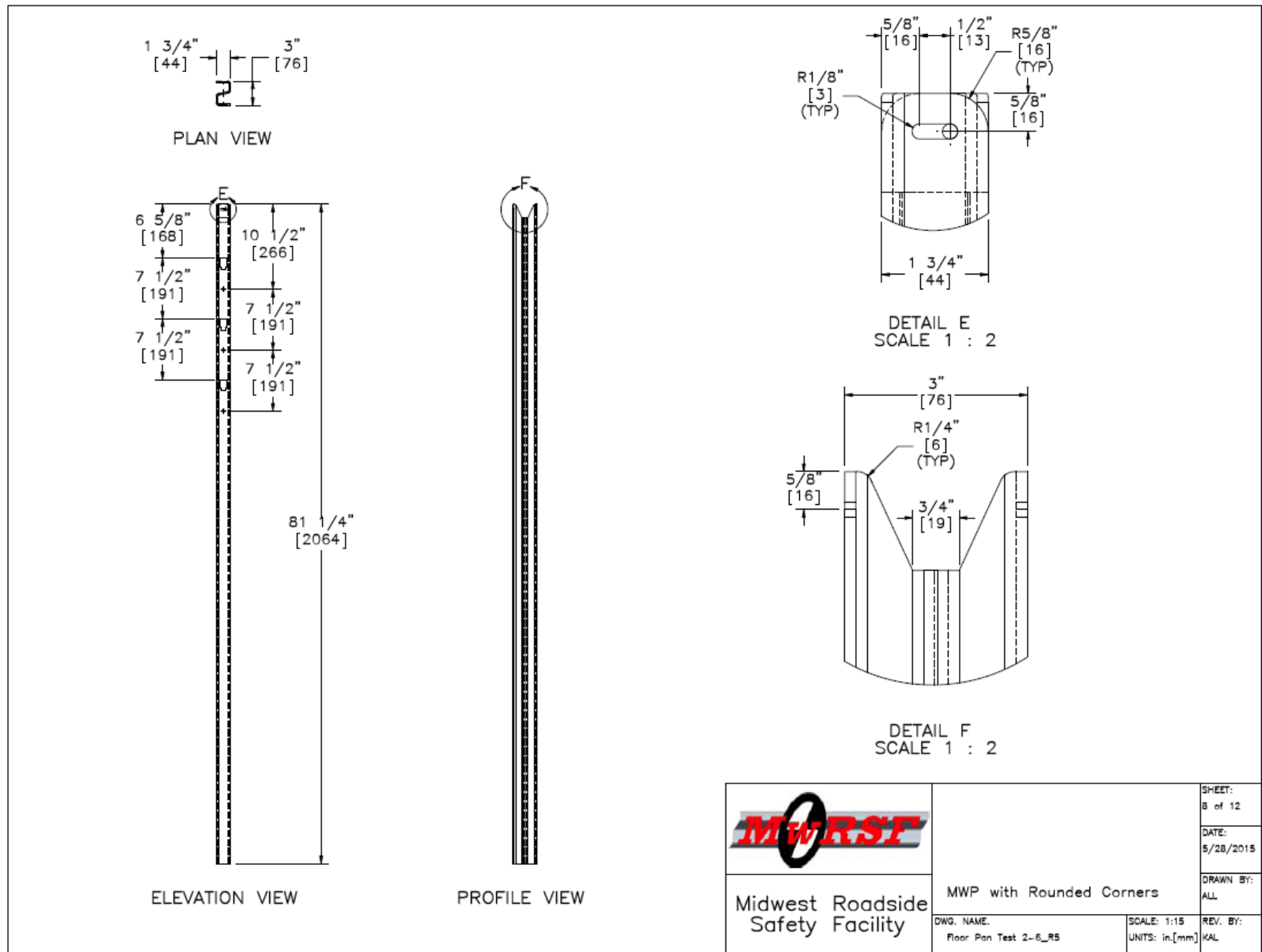


Figure 74. Unmodified MWP, Test Nos. MWFPF-10 and MWFPF-19

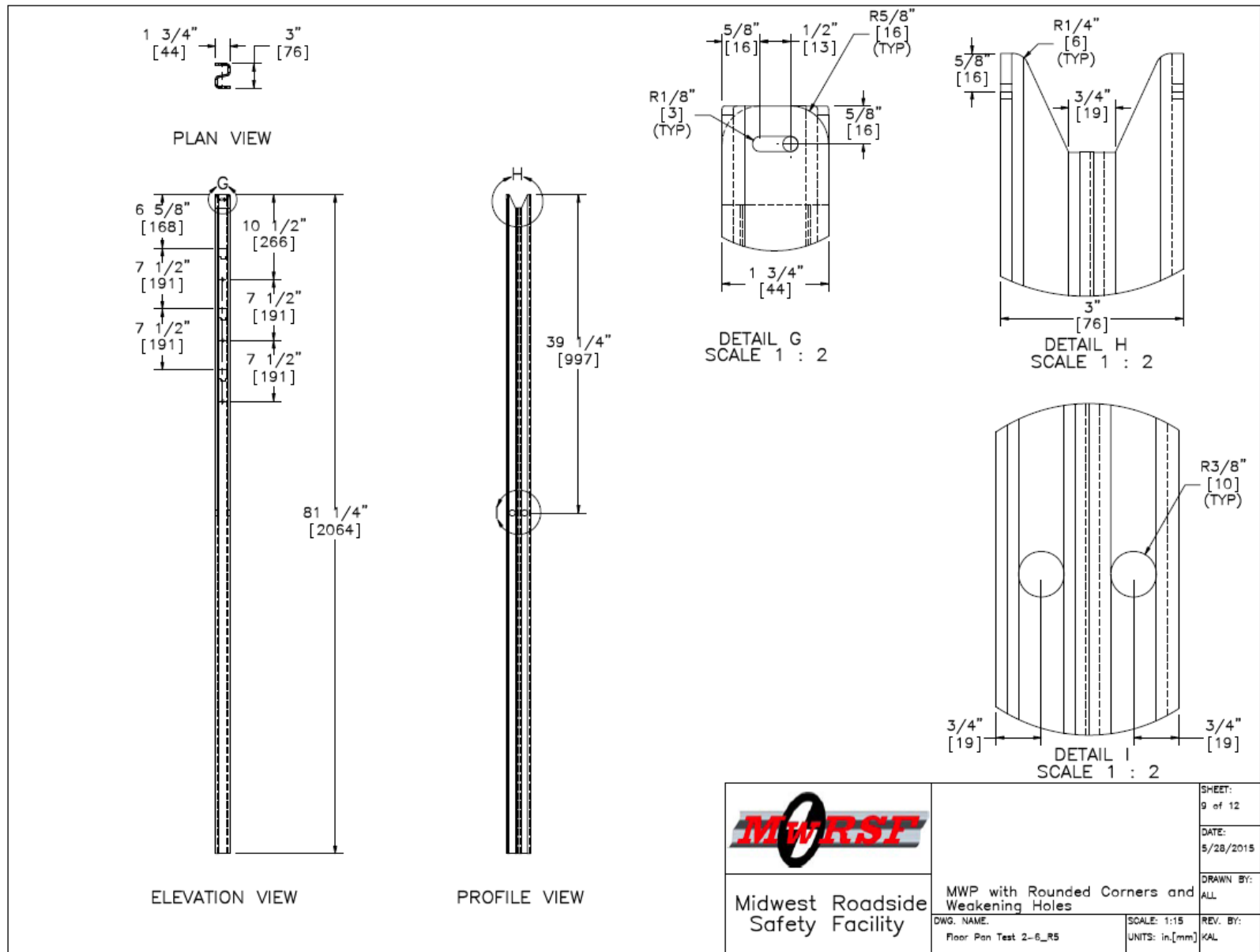


Figure 75. MWP with 3/4-in. (19-mm) Holes, Test Nos. MWPFP-9 and MWPFP-20

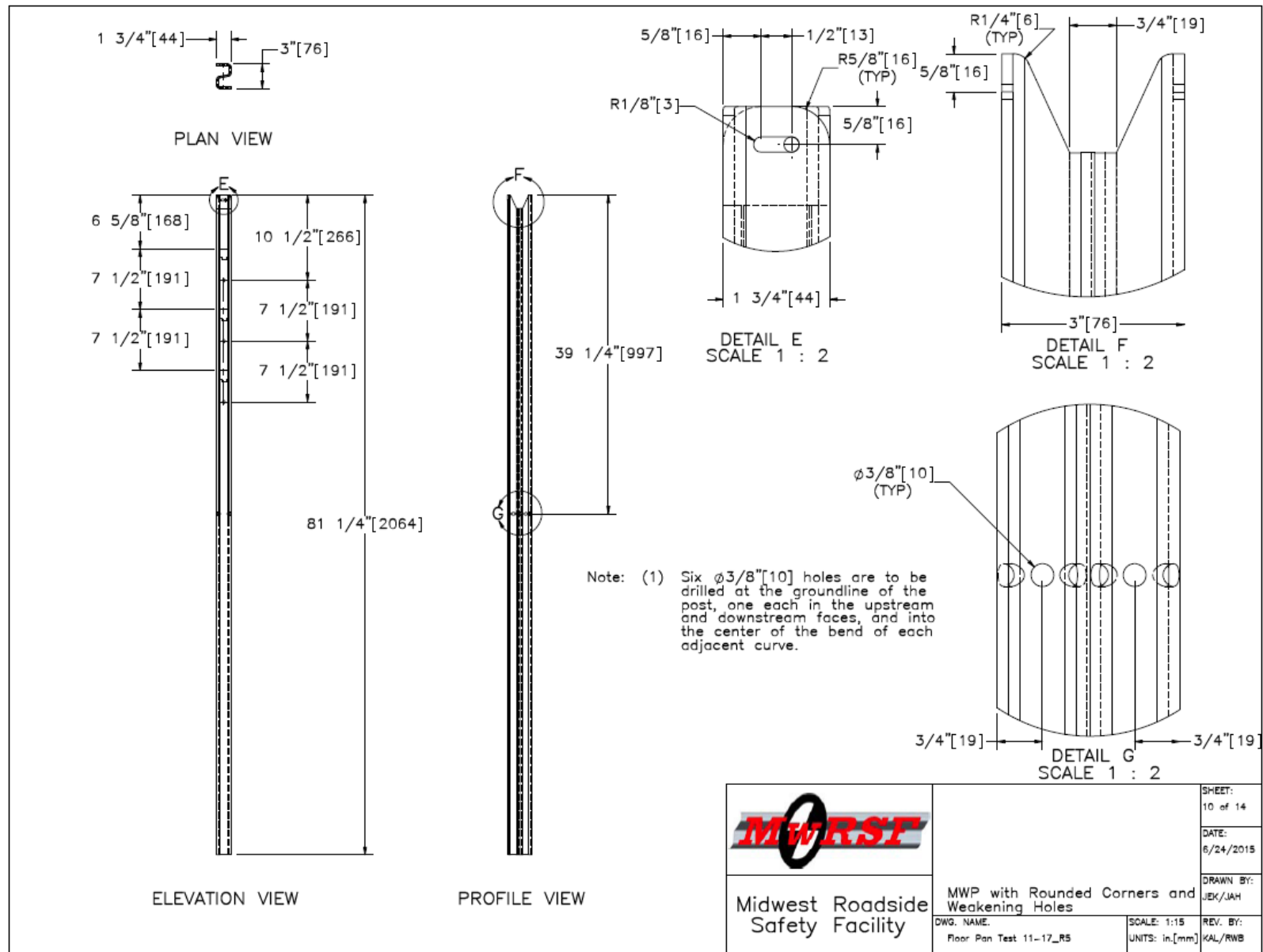


Figure 76. MWP with three 3/8-in. (10-mm) Holes, Test No. MWFP-16

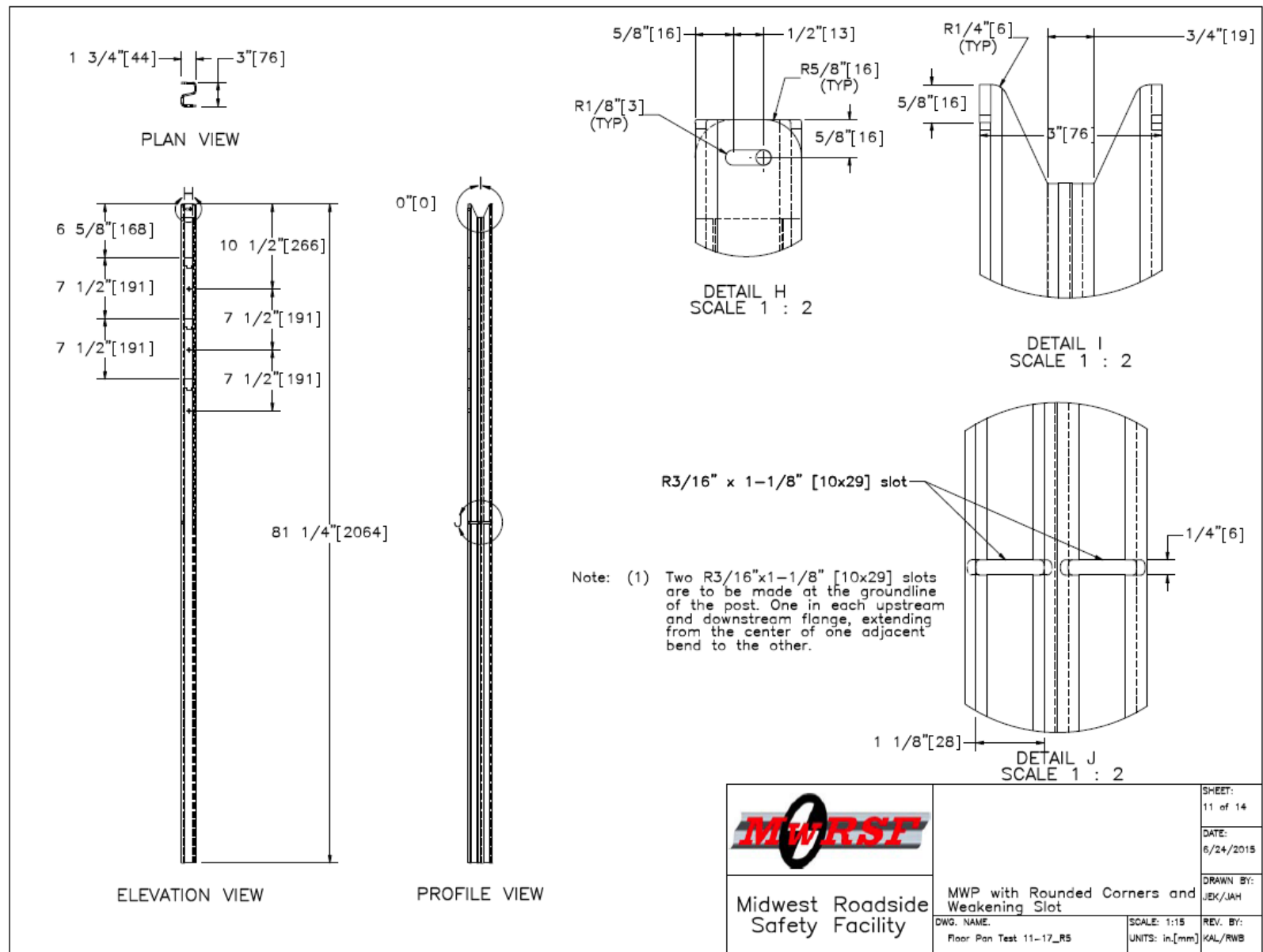


Figure 77. MWP with 3/8-in. x 1 1/8-in. (10-mm x 29-mm) Slots, Test No. MWFP-17

6.3 Equipment and Instrumentation

Equipment and instrumentation that was utilized to collect and record data during the dynamic bogie tests included: a bogie vehicle; an accelerometer; a retroreflective speed trap; high-speed and standard-speed digital video; and still cameras.

6.3.1 Bogie Vehicle

A rigid-frame bogie, equipped with a variable-height, detachable impact head, was used to impact the posts. The bogie head was constructed of 8-in. (203-mm) diameter, ½-in. (13-mm) thick standard steel pipe, with ¾-in. (19-mm) neoprene belting wrapped around the pipe to prevent local damage to the post from the impact. The impact head was bolted to the bogie vehicle, creating a rigid frame with an impact height of 27 in. (686 mm). The bogie with the impact head is shown in Figure 78. The weight of the bogie with the addition of the mountable impact head and accelerometers was 1,874 lb (850 kg).



Figure 78. Second Rigid-Frame Bogie and Guidance Track

A pickup truck with a reverse-cable tow system was used to propel the bogie to a target impact speed of 25 mph (40 km/h). When the bogie approached the end of the guidance system, it was released from the tow cable, allowing it to be free rolling when it impacted the post. A remote-controlled, braking system was installed on the bogie, allowing it to be brought safely to rest after the test.

6.3.2 Accelerometers

One environmental shock and vibration sensor/recorder system was used to measure the accelerations in the longitudinal, lateral, and vertical directions. The accelerometer was mounted near the center of gravity of the bogie vehicle. The electronic accelerometer data obtained in dynamic testing was filtered using the SAE Class 60 and the SAE Class 180 Butterworth filters conforming to the SAE J211/1 specifications [12].

The SLICE-2 accelerometer unit was a modular data acquisition system manufactured by Diversified Technical Systems of Seal Beach, California. The acceleration sensors were mounted inside the body of a custom built SLICE 6DX event data recorder and recorded data at 10,000 Hz to the onboard microprocessor. The SLICE 6DX was configured with 7 GB of non-volatile flash memory, a range of ± 500 g's, a sample rate of 10,000 Hz, and a 1,650 Hz (CFC 1000) anti-aliasing filter. The "SLICEWare" computer software program and a customized Microsoft Excel worksheet were used to analyze and plot the accelerometer data.

6.3.3 Retroreflective Optic Speed Trap

The retroreflective optic speed trap was used to determine the speed of the bogie vehicle before impact. Five retroreflective targets, spaced at approximately 18-in. (457-mm) intervals, were applied to the side of the vehicle. When the emitted beam of light was reflected by the targets and returned to the Emitter/Receiver, a signal was sent to the data acquisition computer as well as the external LED box activating the LED flashes. The speed was then calculated using the spacing between the retroreflective targets and the time between the signals. LED lights and high-speed digital video analysis are used only as a backup in the event that vehicle speeds cannot be determined from the electronic data.

6.3.4 Digital Photography

A combination of one AOS high-speed digital video camera and three GoPro digital video cameras were used to document each test. The AOS high-speed camera had a frame rate of 500 frames per second, while the GoPro video cameras had a frame rate of 120 frames per second. The cameras were typically placed laterally from the post, with a view perpendicular to the bogie's direction of travel. A Nikon D50 digital still camera was also used to document pre- and post-test conditions for all tests.

6.4 Data Processing

The electronic accelerometer data obtained in dynamic testing was filtered using the SAE Class 60 Butterworth filter conforming to the SAE J211/1 specifications [12]. The pertinent acceleration signal was extracted from the bulk of the data signals. The processed acceleration data was then multiplied by the mass of the bogie to get the impact force using Newton's Second Law. Next, the acceleration trace was integrated to find the change in velocity versus time. Initial velocity of the bogie, calculated from the retroreflective optic speed trap data, was then used to determine the bogie velocity, and the calculated velocity trace was integrated to find the bogie's displacement. This displacement is also the displacement of the post. Combining the previous results, a force vs. deflection curve was plotted for each test. Finally, integration of the force vs. deflection curve provided the energy vs. deflection curve for each test.

7 TESTING RESULTS – POST STRENGTH EVALUATION

7.1 Results

A total of six dynamic component tests were conducted to evaluate the strength of the MWPs with various weakening holes or slots. Two of these tests, test nos. MWFPF-16 and MWFPF-17, were conducted with two posts in series. Since the two posts were spaced such that the bogie vehicle would only be in contact with one post at a time, each post impact was analyzed as though it was a separate impact test. A summary of the eight independent dynamic component impact events is provided in the following sections. The accelerometer data for each test was processed in order to obtain acceleration, velocity, and deflection curves, as well as force vs. deflection and energy vs. deflection curves. Detailed accelerometer results for each test are provided in Appendix B.

7.1.1 Test No. MWFPF-9

During test no. MWFPF-9, the bogie impacted the MWP with ¾-in. (19-mm) diameter weakening holes at a speed of 25.3 mph (40.7 km/h) and at an angle of 90 degrees for a strong-axis evaluation. Upon impact, the post yielded and began to bend backward. The bogie eventually overrode the top of the post at a deflection of 38.3 in. (973 mm).

Force vs. deflection and energy vs. deflection curves created from the accelerometer data are shown in Figure 79. The forces quickly rose to a peak force of 4.93 kips (21.94 kN) over the first few inches of deflection. The forces steadily declined through the rest of the impact event. The post provided an average resistive force of 1.91 kips (8.50 kN) and absorbed 38.3 kip-in. (4.3 kJ) of energy through 20 in. (508 mm) of deflection.

Sequential and post damage photographs are shown in Figure 80. Contact marks were present along the top portion of the impact-side flange. A plastic hinge was observed around the weakening holes near groundline, and the post flanges collapsed inward toward the web. The weakening holes were deformed, but the post did not tear.

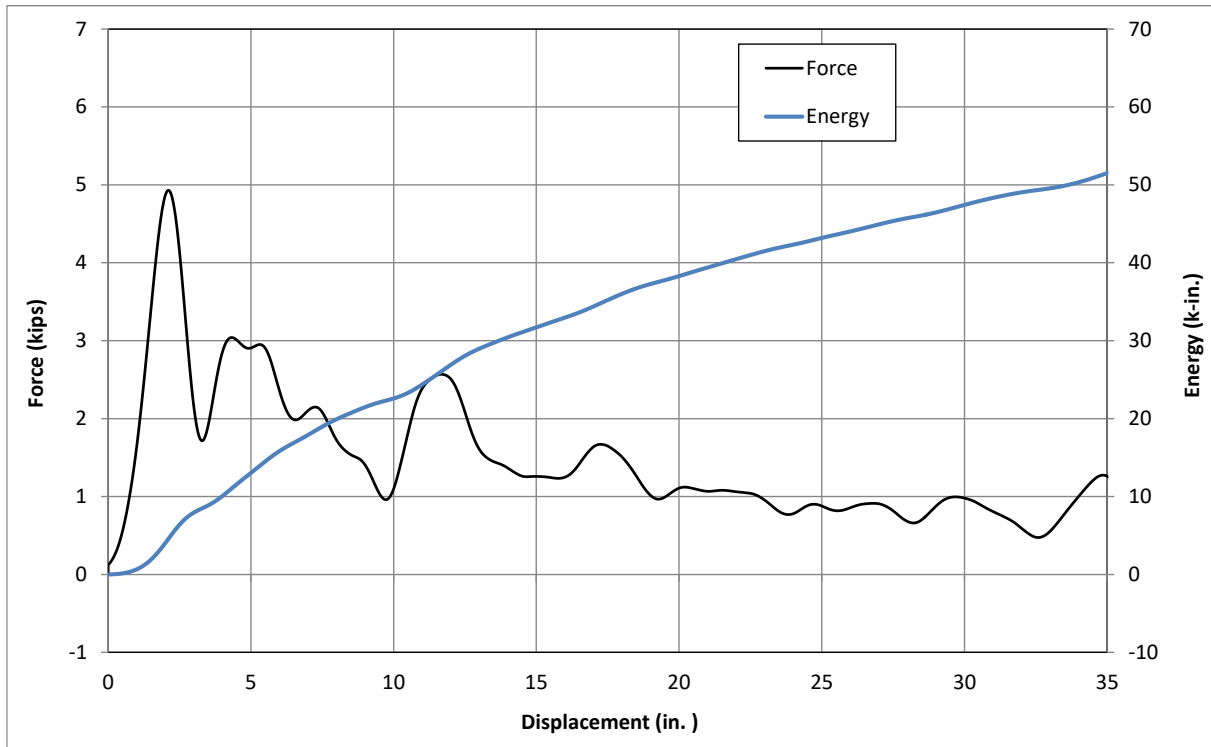


Figure 79. Force vs. Deflection and Energy vs. Deflection, Test No. MWPF9-9



Figure 80. Time-Sequential and Post-Impact Photographs, Test No. MWPFP-9

7.1.2 Test No. MWFPF-10

During test no. MWFPF-10, the bogie impacted the unmodified MWP at a speed of 26.0 mph (41.8 km/h) and at an angle of 90 degrees for a strong-axis evaluation. Upon impact, the post yielded and began to bend backward. The bogie eventually overrode the top of the post at a deflection of 38.5 in. (978 mm).

Force vs. deflection and energy vs. deflection curves created from the accelerometer data are shown in Figure 81. The forces quickly rose to a peak force of 4.88 kips (21.72 kN) over the first few inches of deflection. The forces steadily declined through the rest of the impact event. The post provided an average resistive force of 1.74 kips (7.74 kN) and absorbed 34.7 kip-in. (3.9 kJ) of energy through 20 in. (508 mm) of deflection.

Sequential and post damage photographs are shown in Figure 82. Contact marks were present along the top portion of the impact-side flange. A plastic hinge had formed in the post near the groundline, and the post flanges collapsed inward toward the web, but the post did not tear.

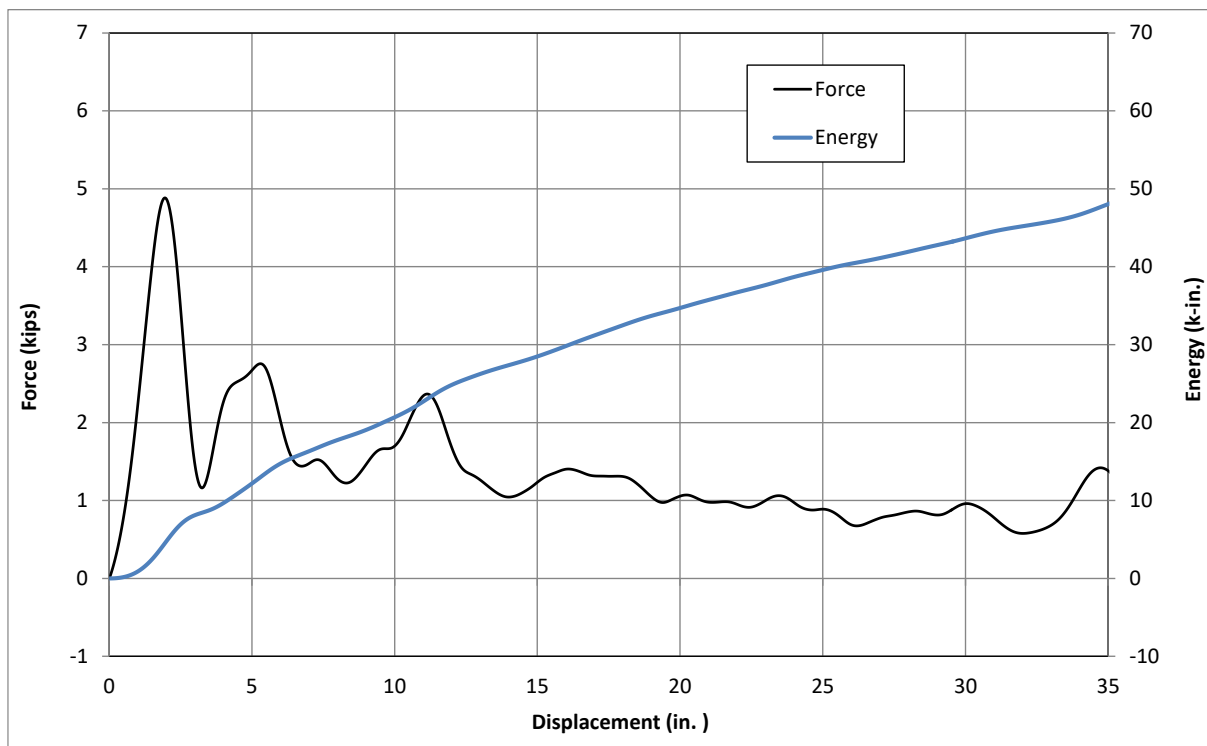


Figure 81. Force vs. Deflection and Energy vs. Deflection, Test No. MWFPF-10



Figure 82. Time-Sequential and Post-Impact Photographs, Test No. MWPFP-10

7.1.3 Test No. MWFPF-16 Post 1

During test no. MWFPF-16, the bogie impacted the first MWP with three $\frac{3}{8}$ -in. (10-mm) diameter weakening holes at a speed of 26.4 mph (42.5 km/h) and at an angle of 90 degrees for a strong-axis evaluation. Upon impact, the post yielded and began to bend backward. The bogie eventually overrode the top of the post at a deflection of 34.4 in. (874 mm).

Force vs. deflection and energy vs. deflection curves are shown in Figure 83. The forces quickly rose to a peak force of 5.74 kips (25.54 kN) over the first few inches of deflection. The forces oscillated throughout the rest of the impact event with the local peaks steadily decreasing in magnitude. The post provided an average resistive force of 1.47 kips (6.54 kN) and absorbed 29.4 kip-in. (3.3 kJ) of energy through 20 in. (508 mm) of deflection.

Sequential and post damage photographs are shown in Figure 84. Contact marks were present along the top portion of the impact-side flange. The post was bent and tore near the groundline. The front flange was completely torn, and the tear extended through the adjacent weakening holes. A second tear occurred between the weakening holes on the backside of the post.

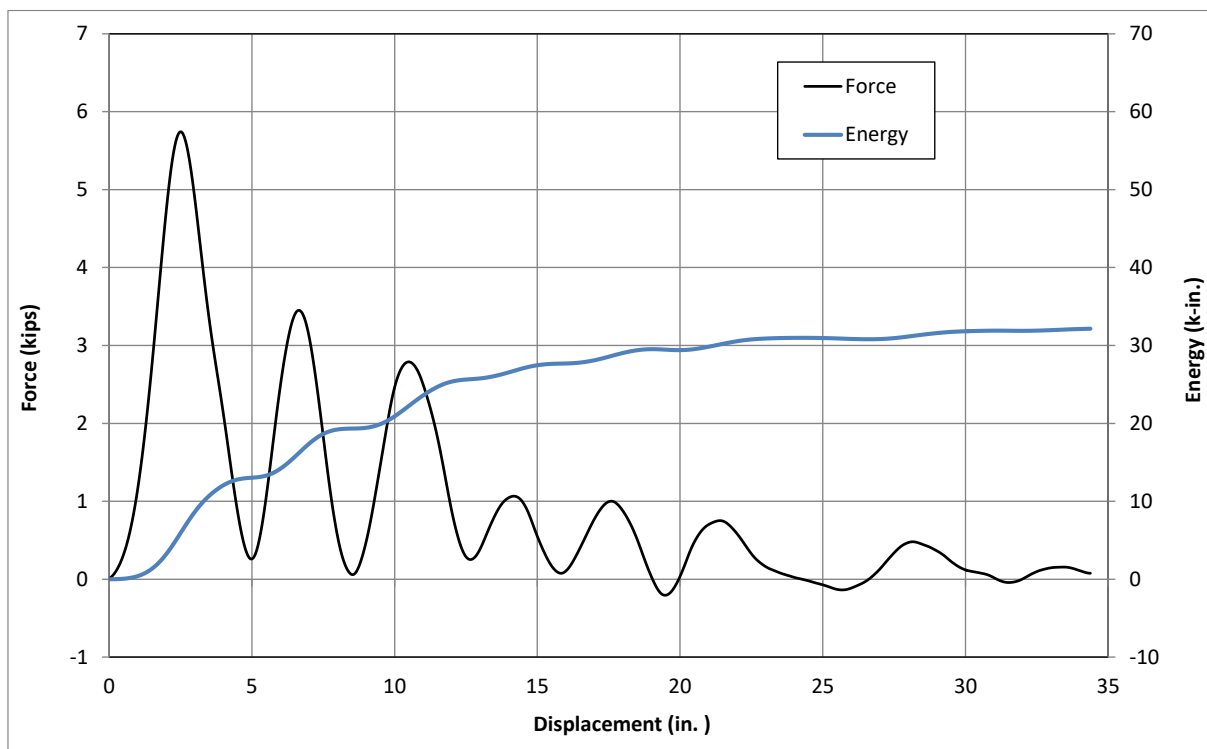


Figure 83. Force vs. Deflection and Energy vs. Deflection, Test No. MWFPF-16 Post 1

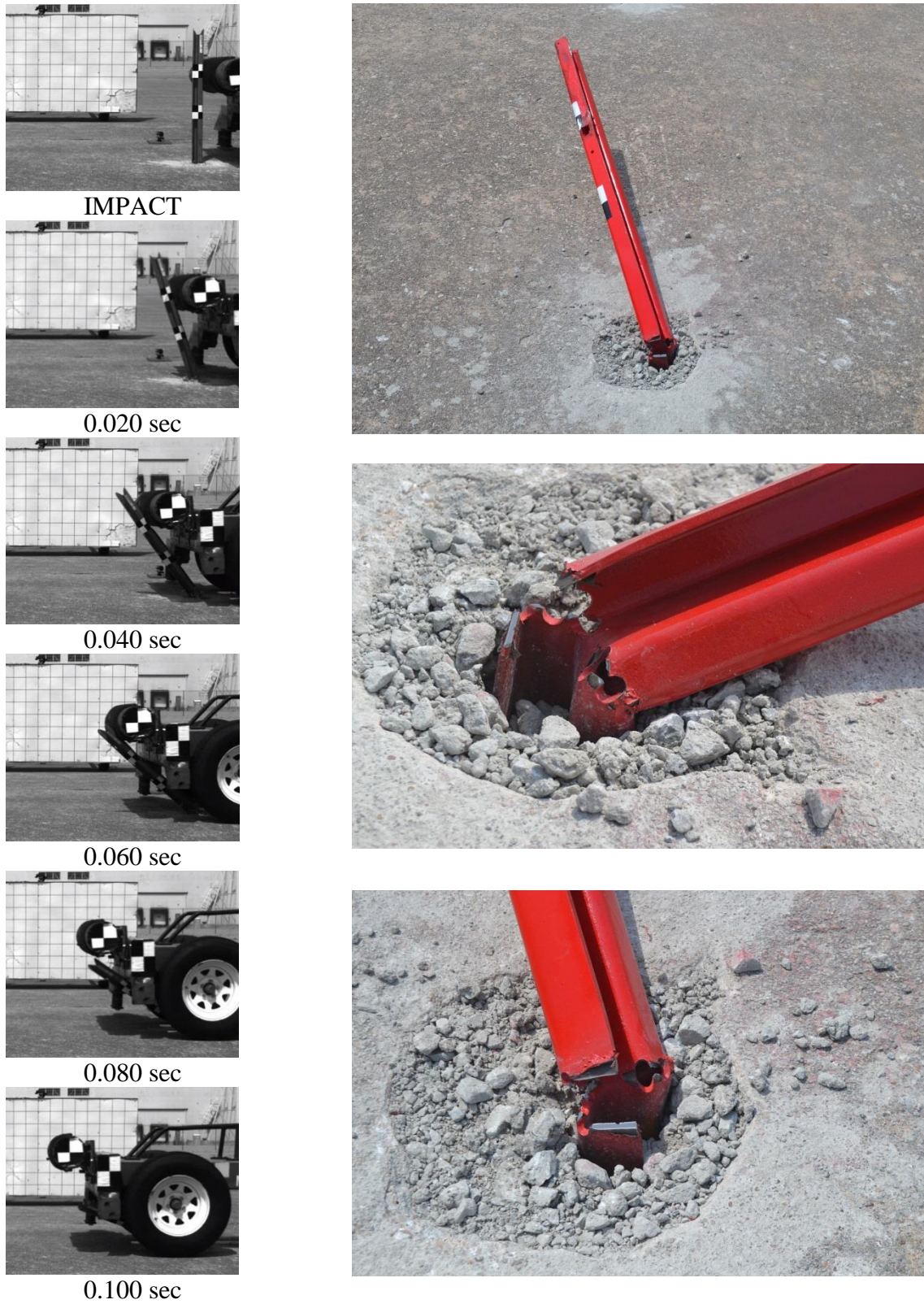


Figure 84. Time-Sequential and Post-Impact Photographs, Test No. MWPFP-16 Post 1

7.1.1 Test No. MWPFP-16 Post 2

The bogie impacted the second MWP with three $\frac{3}{8}$ -in. (10-mm) diameter weakening holes at a speed of 25.5 mph (41.0 km/h) and at an angle of 90 degrees for a strong-axis evaluation. Upon impact, the post yielded and began to bend backward. The bogie eventually overrode the top of the post at a deflection of 31.3 in. (795 mm).

Force vs. deflection and energy vs. deflection curves are shown in Figure 85. The forces quickly rose to a peak force of 5.14 kips (22.87 kN) over the first few inches of deflection. The forces oscillated throughout the rest of the impact event with the local peaks decreasing in magnitude. The post provided an average resistive force of 1.32 kips (5.87 kN) and absorbed 26.5 kip-in. (3.0 kJ) of energy through 20 in. (508 mm) of deflection.

Sequential and post damage photographs are shown in Figure 86. Contact marks were present along the top portion of the impact-side flange. The post was bent and tore near the groundline. The front flange was completely torn, and the tear extended through the adjacent weakening holes. A second tear occurred between the weakening holes on the backside of the post.

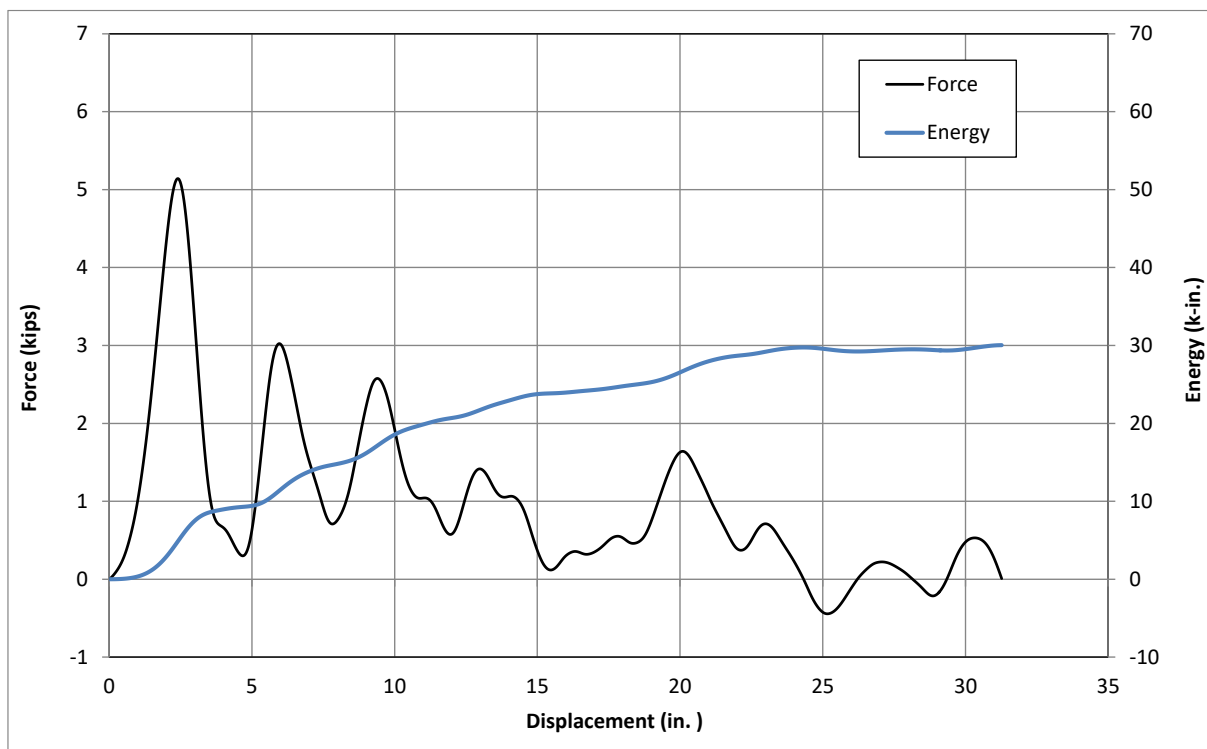


Figure 85: Force vs. Deflection and Energy vs. Deflection, Test No. MWPFP-16 Post 2

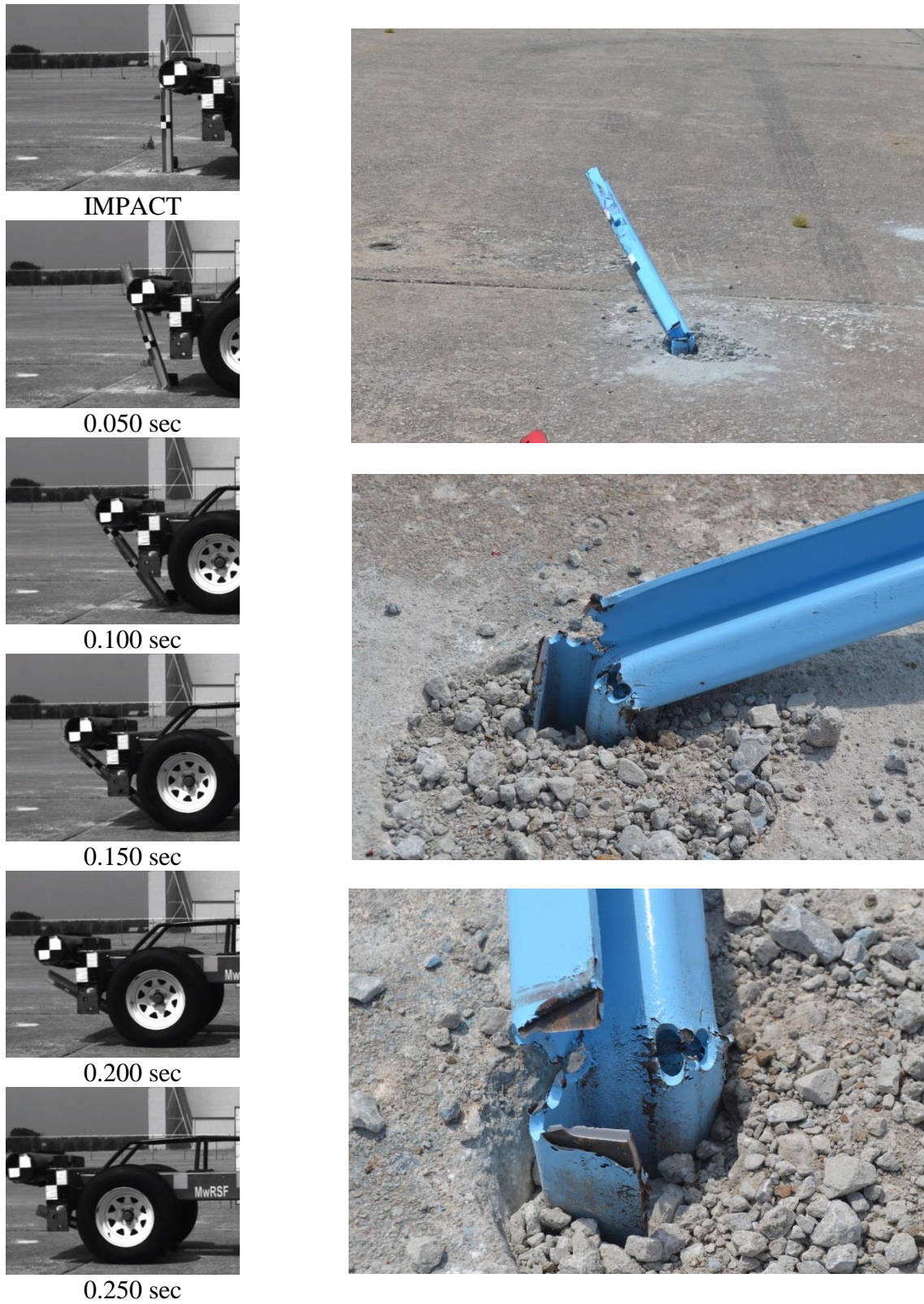


Figure 86. Time-Sequential and Post-Impact Photographs, Test No. MWPFP-16 Post 2

7.1.2 Test No. MWFPF-17 Post 1

During test no. MWFPF-17, the bogie impacted the first MWP with a $\frac{3}{8}$ -in. x $1\frac{1}{8}$ -in. (10-mm x 29-mm) slot at a speed of 25.2 mph (40.6 km/h) and at an angle of 90 degrees for a strong-axis evaluation. Upon impact, the post yielded and began to bend backward. The bogie eventually overrode the post at a deflection of 34.3 in. (871 mm).

Force vs. deflection and energy vs. deflection curves are shown in Figure 87. The forces quickly rose to a peak force of 5.30 kips (23.59 kN) over the first few inches of deflection. The forces oscillated throughout the rest of the impact event with the local peaks decreasing in magnitude. The post provided an average resistive force of 1.07 kips (4.76 kN) and absorbed 21.5 kip-in. (2.4 kJ) of energy through 20 in. (508 mm) of deflection.

Sequential and post damage photographs are shown in Figure 88. Contact marks were present along the top portion of the impact-side flange. The post was bent near the groundline, and the front flange tore completely adjacent to the slot. The back flange buckled inward at the location of the plastic hinge. The slot adjacent to the back flange was deformed, but no additional tearing was observed.

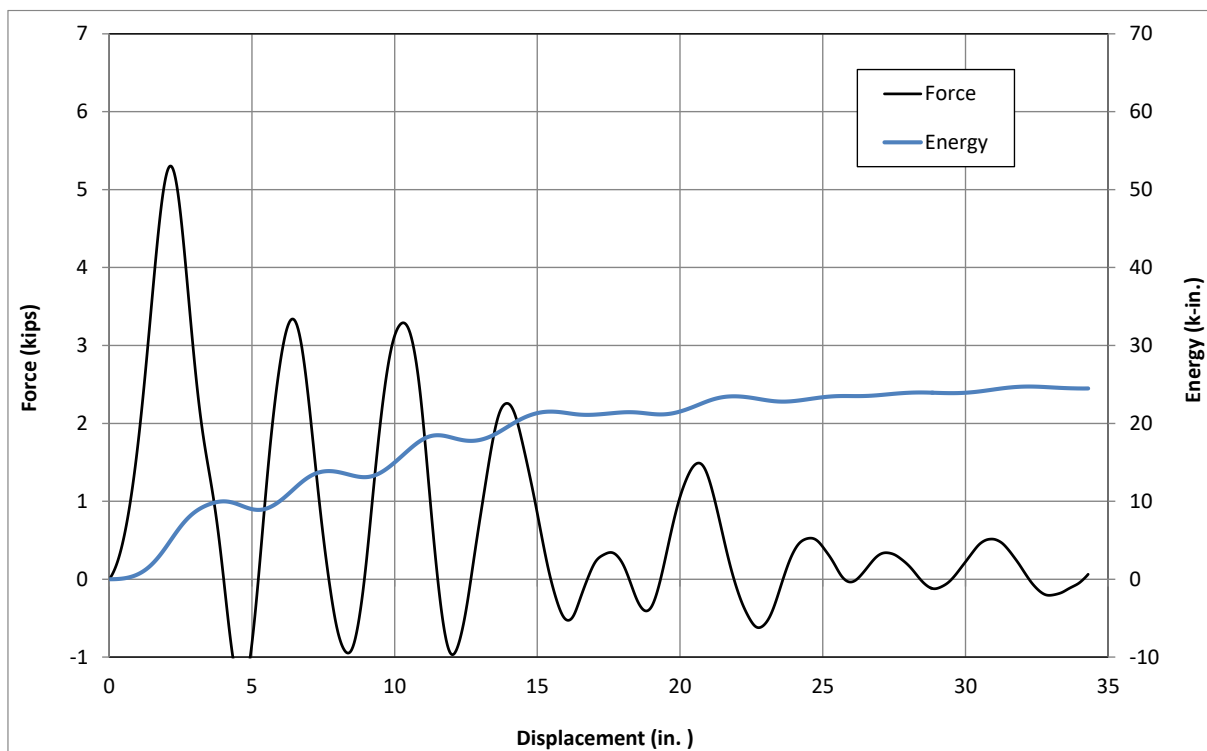


Figure 87. Force vs. Deflection and Energy vs. Deflection, Test No. MWFPF-17 Post 1



Figure 88. Time-Sequential and Post-Impact Photographs, Test No. MWPFP-17 Post 1

7.1.1 Test No. MWPFP-17 Post 2

The bogie impacted the second MWP with a $\frac{3}{8}$ -in. x $1\frac{1}{8}$ -in. (10-mm x 29-mm) slot at a speed of 24.3 mph (39.1 km/h) and at an angle of 90 degrees for a strong-axis evaluation. Upon impact, the post yielded and began to bend backward. The bogie eventually overrode the post at a deflection of 31.9 in. (810 mm).

Force vs. deflection and energy vs. deflection curves are shown in Figure 89. The forces quickly rose to a peak force of 5.11 kips (22.74 kN) over the first few inches of deflection. The forces oscillated throughout the rest of the impact event with the local peaks decreasing in magnitude. The post provided an average resistive force of 1.19 kips (5.30 kN) and absorbed 23.9 kip-in. (2.7 kJ) of energy through 20 in. (508 mm) of deflection.

Sequential and post damage photographs are shown in Figure 90. Contact marks were present along the top portion of the impact-side flange. The post was bent near the groundline, and the front flange tore completely adjacent to the slot. The back flange buckled inward at the location of the plastic hinge. The slot adjacent to the back flange was deformed, but no additional tearing was observed.

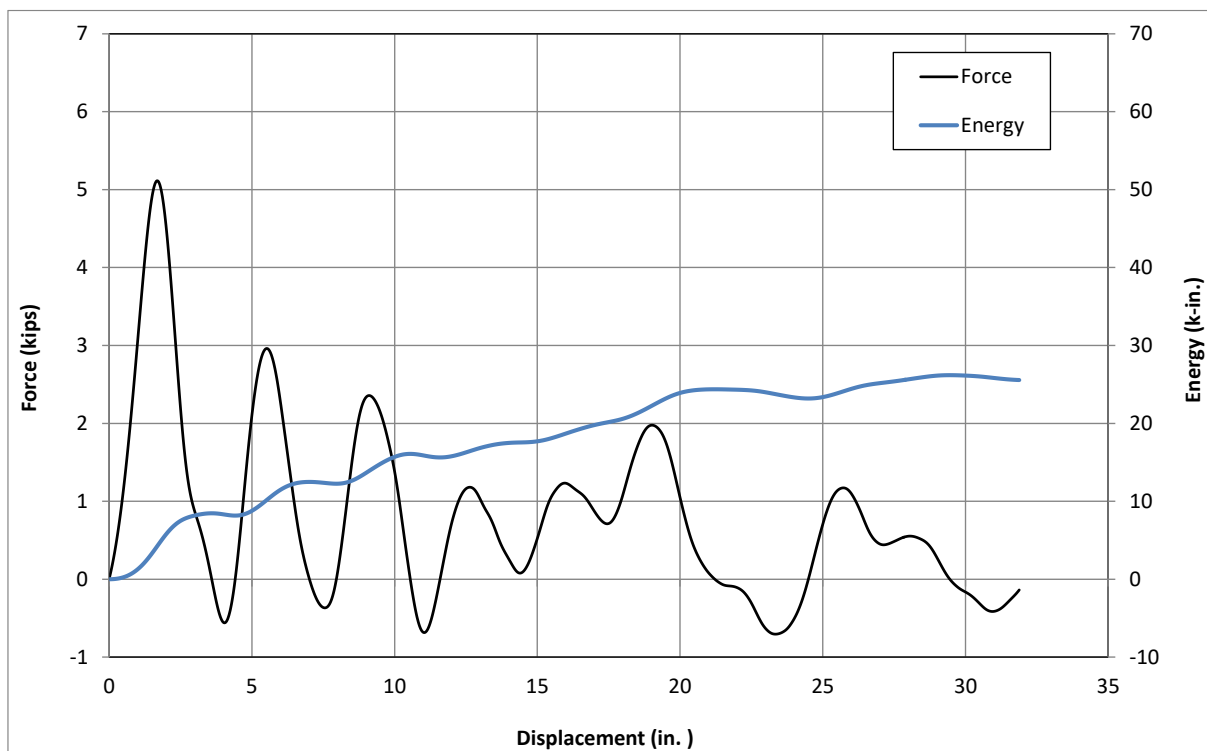


Figure 89. Force vs. Deflection and Energy vs. Deflection, Test No. MWPFP-17 Post 2

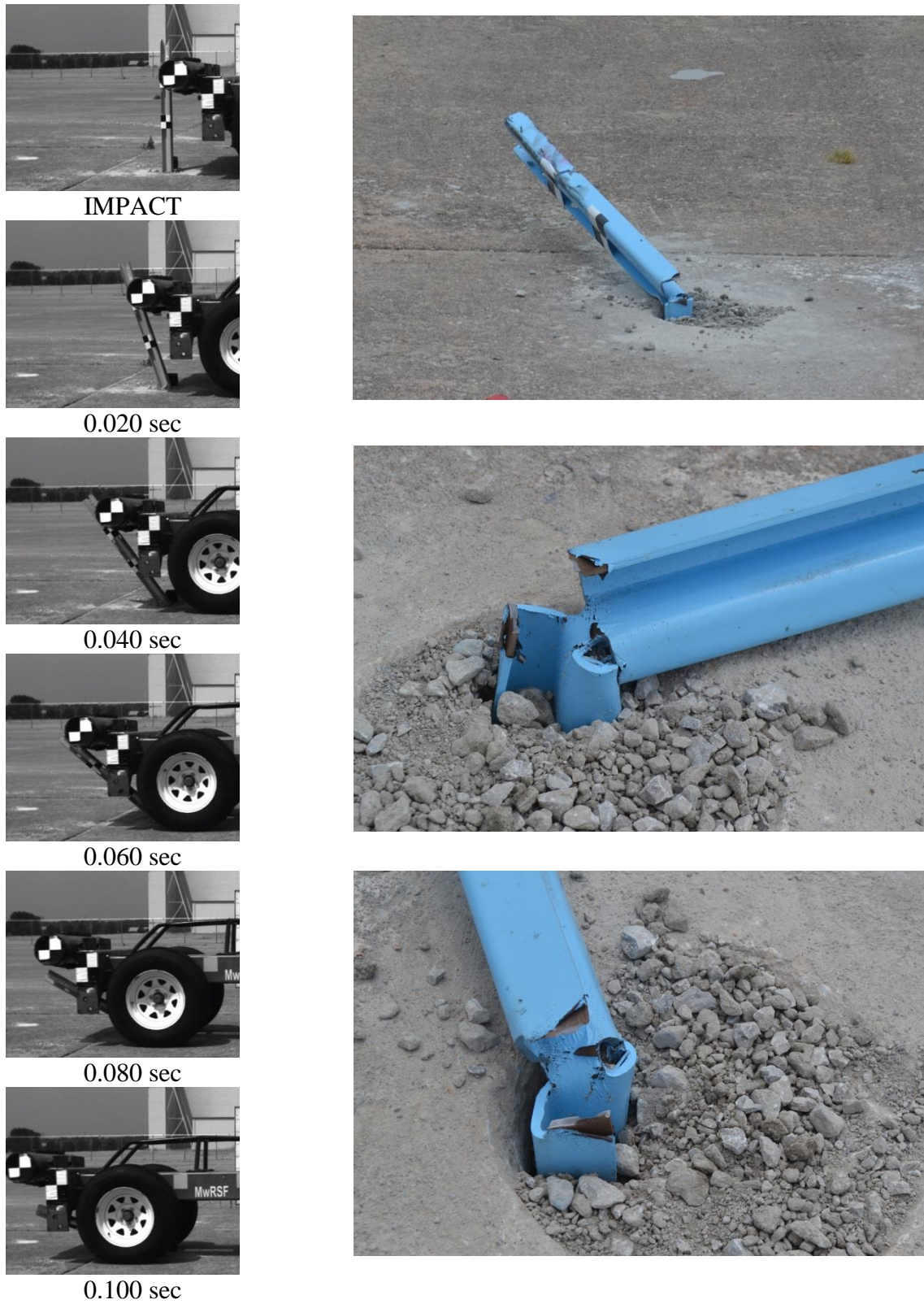


Figure 90. Time-Sequential and Post-Impact Photographs, Test No. MWPFP-17 Post 2

7.1.2 Test No. MWPF-19

During test no. MWPF-19, the bogie impacted the unmodified MWP at a speed of 26.4 mph (42.5 km/h) and at an angle of 90 degrees for a strong-axis evaluation. Upon impact, the post yielded and began to bend backward. The bogie eventually overrode the top of the post at a deflection of 33.5 in. (851 mm).

Force vs. deflection and energy vs. deflection curves created from the accelerometer data are shown in Figure 91. The forces quickly rose to a peak force of 6.07 kips (27.01 kN) over the first few inches of deflection. The forces oscillated while decreasing through the rest of the impact event. The post provided an average resistive force of 2.29 kips (10.19 kN) and absorbed 45.8 kip-in. (5.2 kJ) of energy through 20 in. (508 mm) of deflection.

Sequential and post damage photographs are shown in Figure 92. Contact marks were present along the top portion of the impact-side flange. A plastic hinge had formed in the post near the groundline, and the post flanges collapsed inward toward the web, but the post did not tear.

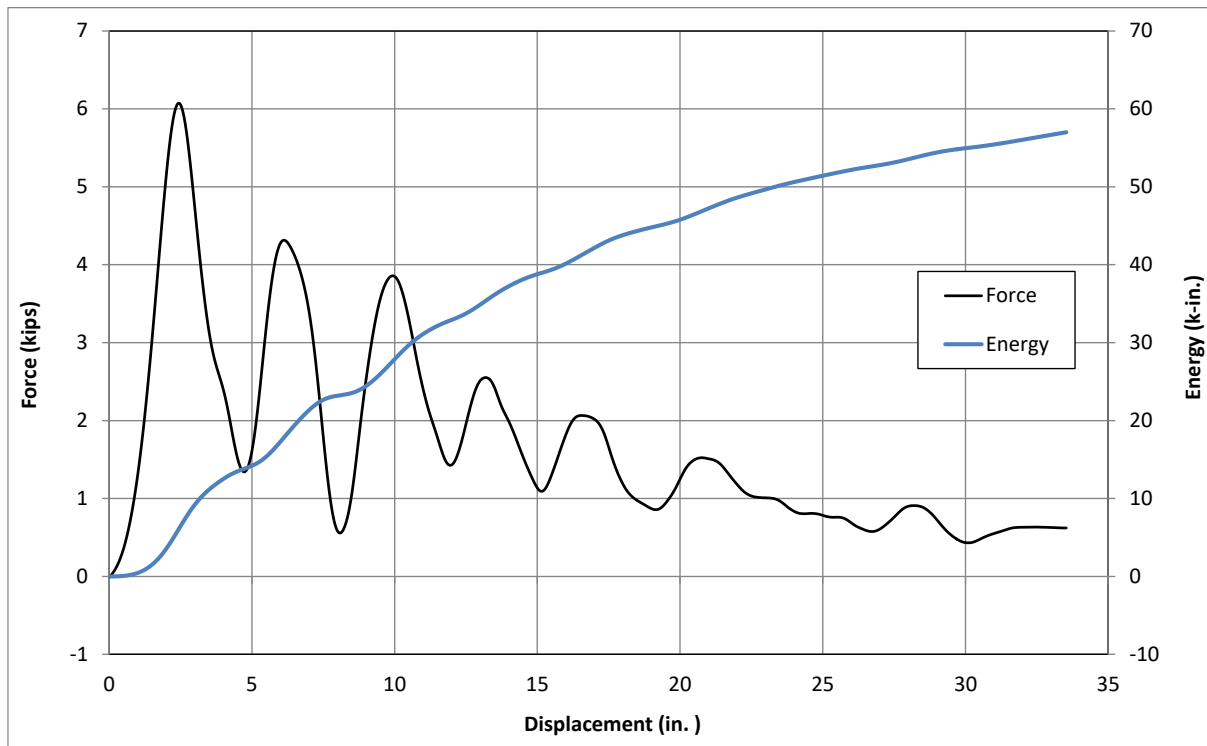


Figure 91. Force vs. Deflection and Energy vs. Deflection, Test No. MWPF-19

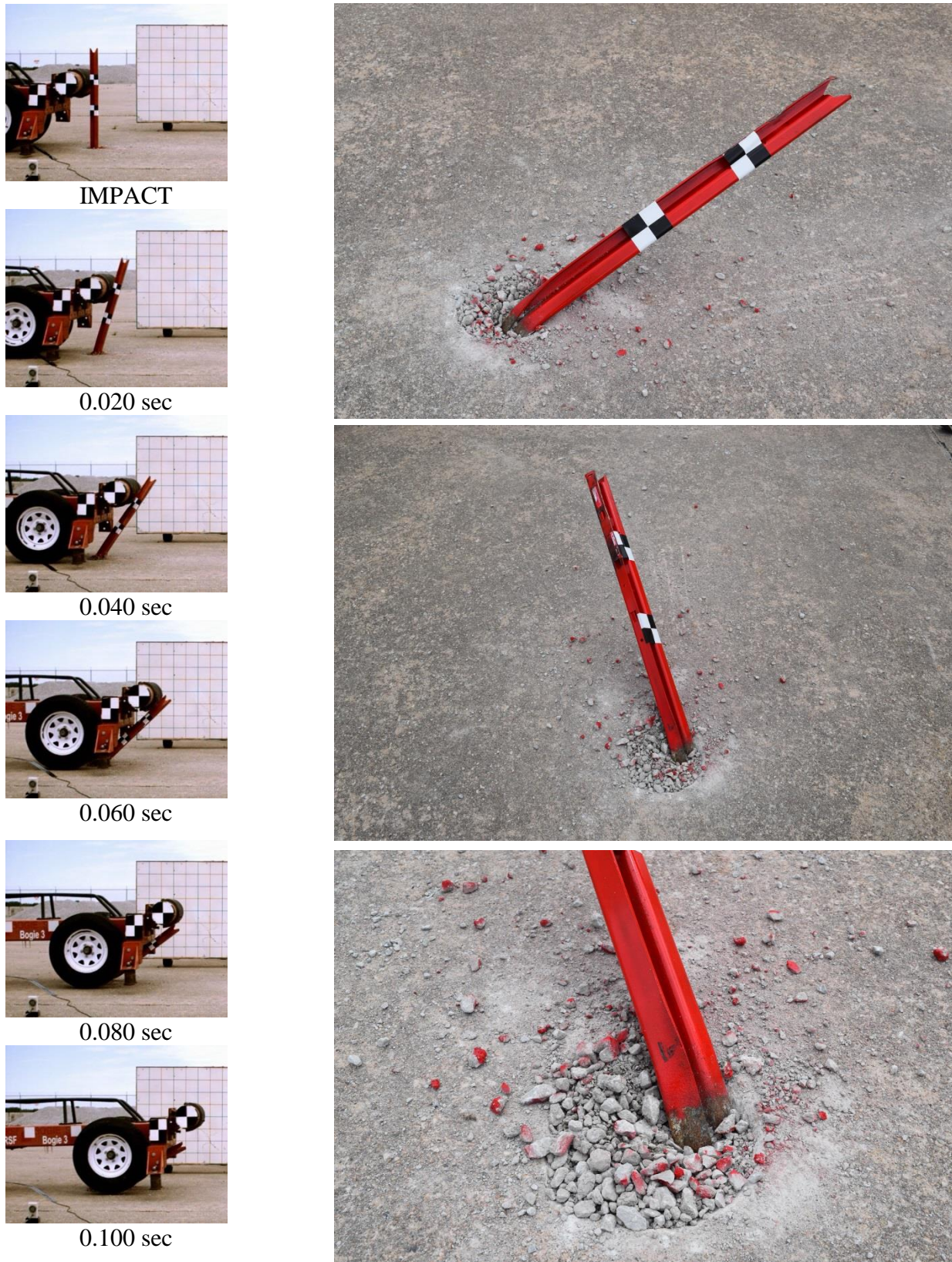


Figure 92. Time-Sequential and Post-Impact Photographs, Test No. MWPFP-19

7.1.3 Test No. MWPFP-20

During test no. MWPFP-20, the bogie impacted the MWP with $\frac{3}{4}$ -in. (19-mm) diameter weakening holes at a speed of 26.2 mph (42.2 km/h) and at an angle of 90 degrees for a strong-axis evaluation. Upon impact, the post yielded and began to bend backward. The bogie eventually overrode the post at a deflection of 33.6 in. (853 mm).

Force vs. deflection and energy vs. deflection curves created from the accelerometer data are shown in Figure 93. The forces quickly rose to a peak force of 5.33 kips (23.72 kN) over the first few inches of deflection. The forces oscillated while decreasing through the rest of the impact event. The post provided an average resistive force of 1.69 kips (7.16 kN) and absorbed 33.7 kip-in. (3.8 kJ) of energy through 20 in. (508 mm) of deflection.

Sequential and post damage photographs are shown in Figure 94. Contact marks were present along the top portion of the impact-side flange. A plastic hinge was observed around the weakening holes near the groundline, and the post flanges collapsed inward toward the web. The weakening holes were deformed, but did not tear.

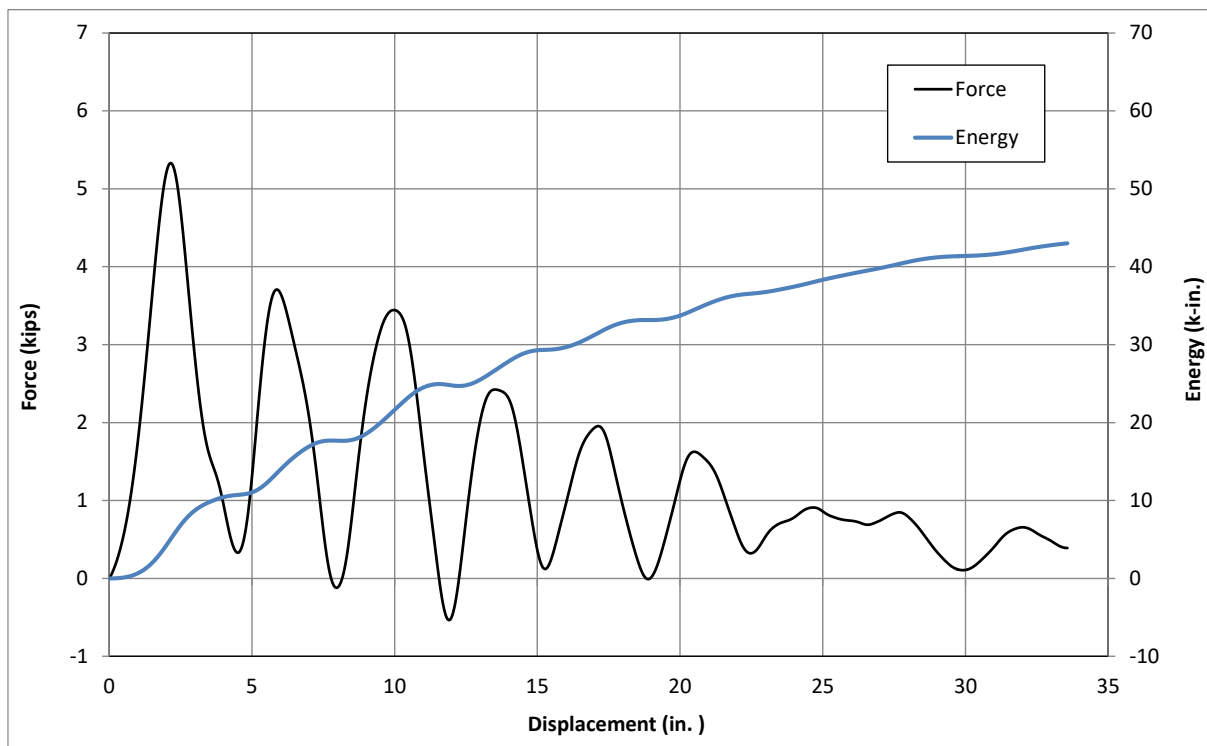


Figure 93. Force vs. Deflection and Energy vs. Deflection, Test No. MWPFP-20

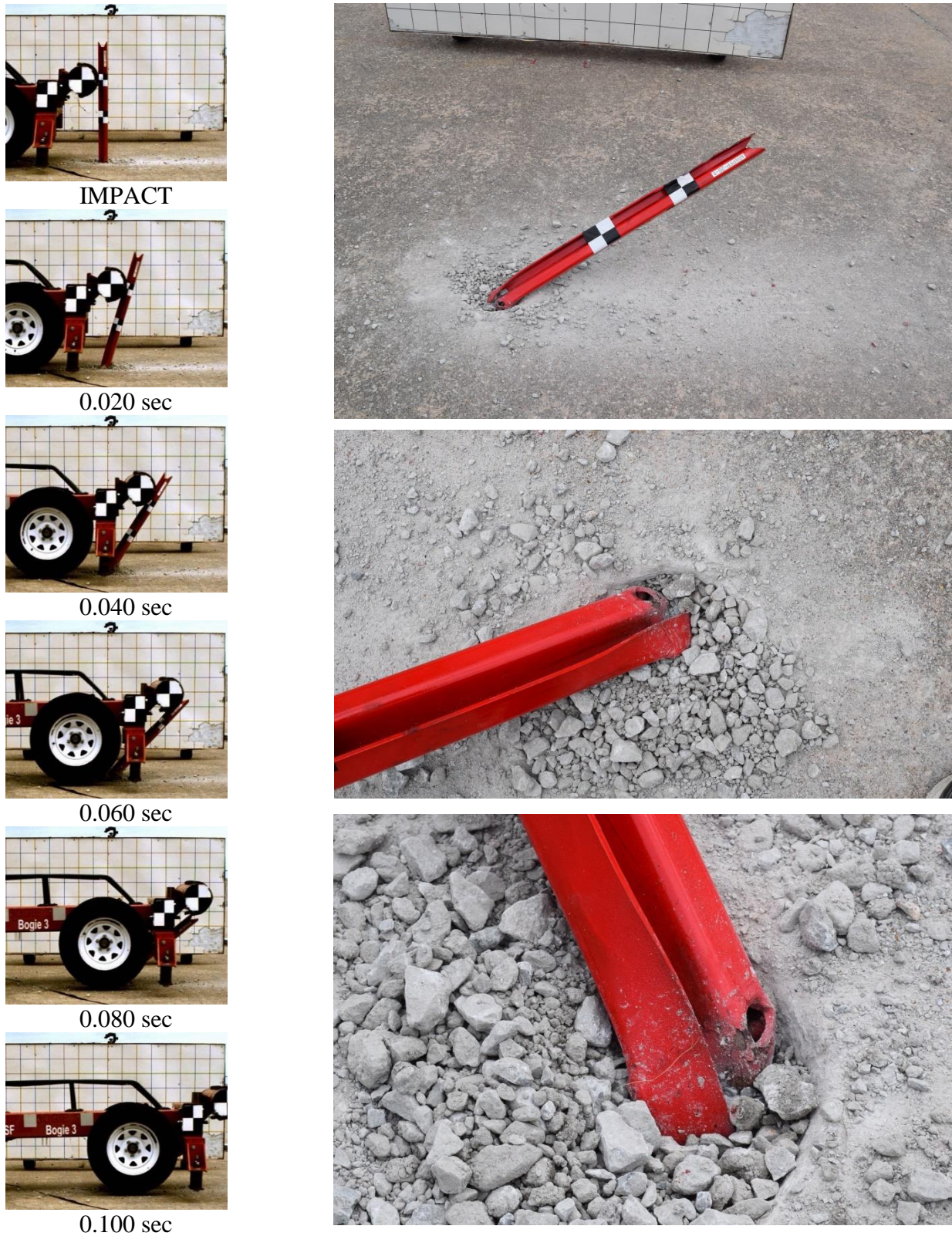


Figure 94. Time-Sequential and Post-Impact Photographs, Test No. MWPFP-20

7.2 Discussion

Six dynamic component tests were conducted to evaluate the strong-axis bending strength of the MWP with various weakening holes or slots. Due to the double-post setup utilized in two of the tests, a total of eight posts were impacted. Two impacts were conducted on each of four different MWP configurations: (1) unmodified; (2) $\frac{3}{4}$ -in. (19-mm) diameter holes; (3) three $\frac{3}{8}$ -in. (10-mm) diameter holes; and (4) $\frac{3}{8}$ -in. x $1\frac{1}{8}$ -in. (10-mm x 39-mm) slots. Each post was impacted at approximately 25 mph (40 km/h) and 90 degrees (strong-axis impact) at a height of 27 in. (686 mm) above the groundline. A summary of the test results are shown in Table 18.

All eight posts were hinged at the groundline due to the bogie vehicle impact. Both the MWPs with weakening slots and the MWPs with three $\frac{3}{8}$ -in. (10-mm) diameter holes also experienced tearing of the post's cross section as the front flange completely tore in all four posts. Additional tearing was observed between the three $\frac{3}{8}$ -in. (10-mm) diameter holes at both weakening locations. The posts with $\frac{3}{4}$ -in. (19-mm) diameter holes were deformed, but it did not experience any tearing. The unmodified MWPs also showed no signs of tearing.

The weakening mechanisms also affected the resistive forces of the MWP. The average peak forces were similar between the four configurations, but the initial peaks were largely the result of inertia. However, the unmodified MWPs provided an average force of 2.01 kips (8.94 kN) over 20 in. (508 mm) of deflection. Over the same deflection interval, the MWPs with $\frac{3}{4}$ -in. (19-mm) diameter holes provided an average force of 1.80 kips (8.01 kN), the MWPs with three $\frac{3}{8}$ -in. (10-mm) diameter holes provided an average force of 1.40 kips (6.23 kN), and the MWPs with the $\frac{3}{8}$ -in. x $1\frac{1}{8}$ -in. (10-mm x 39-mm) slot provided an average force of 1.13 kips (5.03 kN). These average forces for one $\frac{3}{4}$ -in. (19-mm) hole; three $\frac{3}{8}$ -in. (10-mm) holes, and one slot; corresponded to reductions of 10 percent, 30 percent, and 44 percent, respectively, when compared to the unmodified MWPs. Similar results were observed when comparing the absorbed energy from each configuration.

The two weakening patterns that resulted in tearing of the post's cross section caused significant reductions in the post strength. Alternatively, the $\frac{3}{4}$ -in. (19-mm) diameter weakening holes provided results similar to the unmodified MWP in terms of post damage and strength during strong-axis impacts. Therefore, a modified MWP with $\frac{3}{4}$ -in. (19-mm) diameter weakening holes was recommended for implementation into the prototype cable barrier system as a way to mitigate floorpan tearing without affecting the stiffness or deflections of the system.

Table 18. Component Testing Summary, Strong-Axis Bending Impacts

Test No.	Post Weakening	Impact Speed mph (km/h)	Post Damage	Peak Force kip (kN)	Average Force kips (kN)			Absorbed Energy kip-in. (kJ)			
					@10"	@15"	@20"	@10"	@15"	@20"	Total
MWPFP-10	N/A	26.0 (41.8)	Bending	4.88 (21.7)	2.07 (9.2)	1.90 (8.8)	1.74 (7.7)	20.7 (2.3)	28.5 (3.2)	34.7 (3.9)	51.0 (5.8)
MWPFP-19	N/A	26.4 (42.5)	Bending	6.07 (27.0)	2.78 (12.4)	2.58 (11.5)	2.29 (10.2)	27.8 (3.1)	38.7 (4.4)	45.7 (5.2)	57.0 (6.4)
Average				5.48 (24.4)	2.42 (10.8)	2.24 (10.0)	2.01 (8.9)	24.2 (2.7)	33.6 (3.8)	40.2 (4.5)	54.0 (6.1)
MWPFP-9	Ø¾" dia. Holes	25.3 (40.7)	Bending	4.93 (21.9)	2.26 (10.1)	2.11 (9.4)	1.91 (8.5)	22.6 (2.6)	31.7 (3.6)	38.3 (4.3)	54.2 (6.1)
MWPFP-20	Ø¾" dia. Holes	26.2 (42.2)	Bending	5.33 (23.7)	2.15 (9.6)	1.95 (8.7)	1.69 (7.5)	21.5 (2.4)	29.3 (3.3)	33.7 (3.8)	43.0 (4.9)
Average				5.13 (22.8)	2.20 (9.8)	2.03 (9.0)	1.80 (8.0)	22.0 (2.5)	30.5 (3.4)	36.0 (4.1)	48.6 (5.5)
MWPFP-16 P1	(3) Ø⅜" dia. Holes	26.4 (42.5)	Bending & Tearing	5.74 (25.5)	2.09 (9.3)	1.83 (8.1)	1.47 (6.5)	20.9 (2.4)	27.5 (3.1)	29.4 (3.3)	32.1 (3.6)
MWPFP-16 P2	(3) Ø⅜" dia. Holes	25.5 (41.0)	Bending & Tearing	5.14 (22.9)	1.85 (8.2)	1.58 (7.0)	1.32 (5.9)	18.5 (2.1)	23.8 (2.7)	26.5 (3.0)	30.0 (3.4)
Average				5.44 (24.2)	1.97 (8.8)	1.71 (7.6)	1.40 (6.2)	19.7 (2.2)	25.6 (2.9)	27.9 (3.2)	31.1 (3.5)
MWPFP-17 P1	⅜" x 1⅝" Slots	25.2 (40.6)	Bending & Tearing	5.30 (23.6)	1.50 (6.7)	1.42 (6.3)	1.07 (4.8)	15.0 (1.7)	21.3 (2.4)	21.5 (2.4)	24.7 (2.8)
MWPFP-17 P2	⅜" x 1⅝" Slots	24.3 (39.1)	Bending & Tearing	5.11 (22.7)	1.56 (6.9)	1.18 (5.2)	1.19 (5.3)	15.6 (1.8)	17.7 (2.0)	23.9 (2.7)	26.2 (3.0)
Average				5.21 (23.2)	1.53 (6.8)	1.30 (5.8)	1.13 (5.0)	15.3 (1.7)	19.5 (2.2)	22.7 (2.6)	25.5 (2.9)

N/A – Not Applicable

8 EVALUATION OF SPLICE HARDWARE

8.1 Purpose

All of MwRSF's full-scale crash test installations for the prototype, high-tension, cable median barrier have utilized a cable coupler manufactured by Bennett Bolt Works, Inc., model no. CGBBHT. The cable is inserted through one end of the coupler, and a malleable iron wedge is placed between the three strands of the cable to prevent it from pulling out of the coupler. A threaded rod and nut is used on the opposite side of the coupler to complete the assembly. These couplers have been used on both sides of turnbuckle splices as well as for configuring end fittings within the cable anchorage system, as shown in Figure 95.

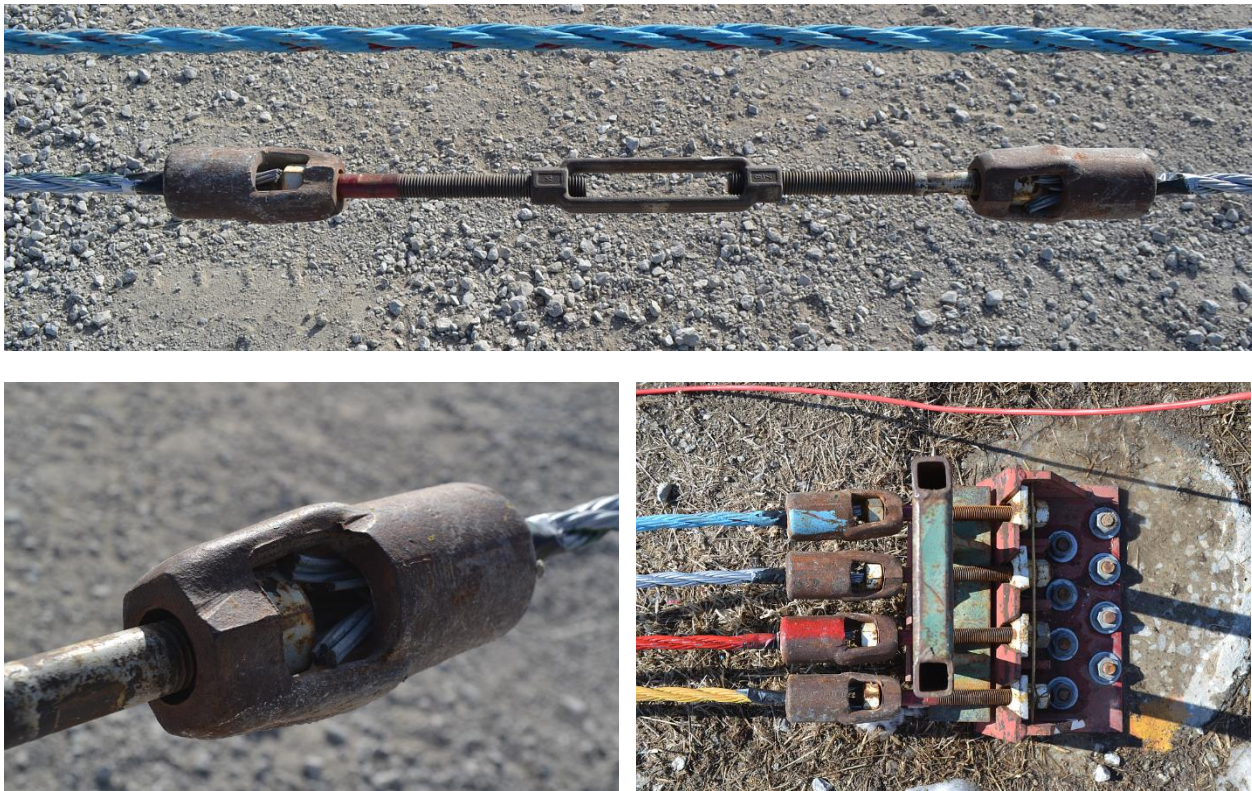


Figure 95. Bennett Bolt Works, Inc. Cable Coupler – Model No. CGBBHT

During full-scale crash testing, the cable splices located within the impact region of the barrier system have caused significant exterior sheet metal damage to the impacting vehicles. Due to the relatively large cross section of the coupler as compared to the cable, the couplers have snagged on vehicle doors and A-pillars, thus causing crushing and sheet metal tearing. Examples of this damage were observed in full-scale crash tests of small cars, sedans, and pickup trucks, as shown in Figure 96. The interaction between the vehicle and the couplers has not resulted in failure of the MASH safety performance criteria, but the undesired snagging and tearing did reveal some risk of eventual penetration into the occupant compartment. Therefore, an investigation was launched to investigate alternative cable splices that may mitigate snagging and decrease sheet metal damage.



Figure 96: Vehicle Door and A-Pillar Damage from Splice Snagging

8.2 Review of Wire Rope Coupler Options

Various wire rope couplers, including proprietary connection systems, mechanical connectors, epoxy sockets, and field swaged connections, were investigated for use in the cable barrier system. The Bennett Bolt Works, Inc. coupler currently implemented in the prototype cable barrier system, model no. CGBBHT, consists of two components: a coupler housing and a wedge, both fabricated from ASTM-A47 malleable cast iron. The cable is inserted into one side of the housing and is seated using the wedge. The other side of the housing is connected to threaded rod using a standard nut. The housing has a cross section diameter of 2½ in. (64 mm) on the cable attachment end and 2¼ in. (57 mm) on the threaded rod end, as shown in Figure 97. Previous dynamic testing of this coupler assembly resulted in a peak load of 41 kips (182 kN) prior to the cable pulling out of the coupler [13]. The ¾-in. (19 mm) diameter, 3x7 wire rope has an estimated capacity of 39 kips (174 kN), so the coupler demonstrated the ability to develop the full capacity of the cable.

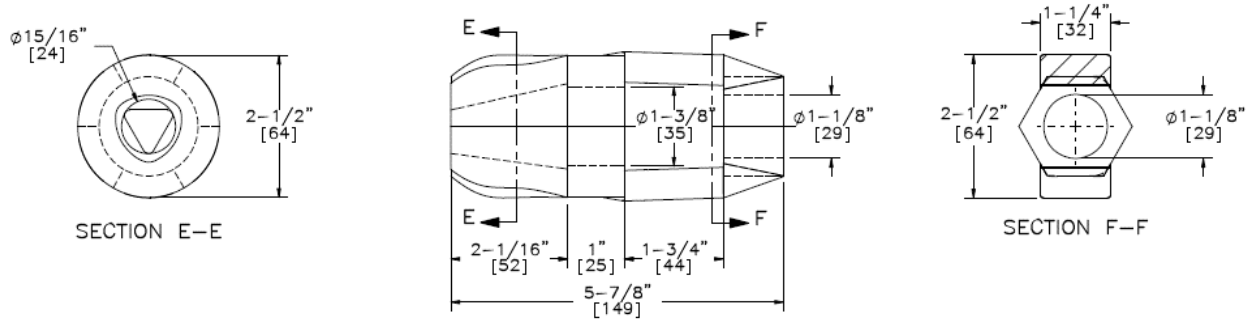


Figure 97: Bennett Bolt Coupler Dimensions, Model No. CGBBHT

The Texas A&M Transportation Institute has conducted both static and dynamic testing on four types of cable splices: (1) an epoxy socket; (2) the Field Swage Termination; (3) the Precision Sure-Lock Prototype 2; and (4) the Nucor Steel Marion termination connection [14]. The static tests used a hydraulic cylinder to pull on the 3x7 wire rope attached to the coupler assembly until failure. Dynamic testing consisted of the cable and coupler assembly attached to a rigid post at one end and a pendulum at the other end. The falling mass created an impulse load on the assembly to simulate dynamic tension loads. The wire rope for these tests was rated to 43 kips (191 kN).

Both the Precision Sure-Lock Prototype 2 and the Nucor Steel Marion Connection failed prior to reaching the full capacity of the wire rope. The Precision Sure-Lock Prototype 2 connection failed the static test at 32.20 kips (142.34 kN) and failed the dynamic tests at 34.80 and 33.58 kips (154.80 and 149.37 kN). The Nucor Steel Marion Connection failed the static tests at 31.47 and 32.03 kips (139.99 and 142.48 kN) and the dynamic tests at 35.88 and 34.73 kips (159.60 and 154.49 kN). Due to these connections failing prior to reaching the capacity of the wire rope, they were not considered viable options for use within the prototype cable median barrier system.

The epoxy socket connection failed the static tests at 38.92 and 38.43 kips (173.12 and 170.95 kN) and the dynamic tests at 37.04, 38.37, and 43.49 kips (164.76, 170.68, and 193.47 kN). Thus, the average failure strength of the epoxy socket connection was within 10% of the wire rope capacity. Unfortunately, the connection has a large socket diameter, which would promote snagging and vehicle damage, and the epoxy hardening time is temperature dependant, which could create installation issues as the epoxy can take weeks to harden during cold winter months. Therefore, the epoxy socket was also not considered a viable option for use within the prototype cable median barrier system.

Testing of the Field Swage Termination connection resulted in failure strengths of 37.94, 32.89, and 38.28 kips (168.77, 146.30, and 170.28 kN) statically and 40.77 and 46.83 kips (181.35 and 208.31 kN) dynamically. Thus, the average tensile capacities were within 10% of the wire rope. Field swages use a thinner body than the epoxy and mechanical couplers, including the Bennett Bolt Works coupler, which would reduce the risk of vehicle snagging. Thus, field swage connections showed promise as a replacement for the current Bennett Bolt Works Coupler. However, at the time of this study, the swaging machine required for this

process costs around \$25,000. Due to this high cost, field swaging was not selected for further evaluation.

The last option investigated for use in the prototype cable barrier system was a new Bennett Bolt Works mechanical coupler, model no. CGBBWTH. This new coupler was fabricated from ASTM-A536, a stronger iron casting material than the older model. This selection allowed for the end diameter of the coupler to be reduced to 1¼ in. (32 mm) compared to the 2½ in. (63.5 mm) diameter of the older model. The geometry of the opposite side of the coupler, which received the threaded rod, remained very similar between the two Bennett Bolt Works couplers. A photograph comparing the end fittings is shown in Figure 98. The new coupler model utilized the same wedge as the previous model, making the assembly process identical. The new coupler model was also rated to the same strength as the previous coupler model. Therefore, the Bennett Bolt Works coupler model no. CGBBWTH was selected for further testing and evaluation as an alternative coupler for use in the prototype cable barrier system.



Figure 98: Bennett Bolt Works Coupler Model Nos. CGBBHHT (Left) and CGBBWTH (Right)

8.3 Component Testing Scope and Instrumentation

Three dynamic component tests were conducted to evaluate the capacity of the cable couplers. Two tests were conducted on the newer Bennett Bolt Works coupler, model no. CGBBWTH, and one test was conducted on the model no. CGBBHHT coupler currently utilized within the prototype cable barrier system. For each test, the couplers were installed at both ends of a ¾-in. (19-mm) diameter, 3x7 wire rope. One end of the wire rope was attached to a cable barrier anchor bracket, and the other end was attached to a bogie vehicle. For test no. BBNC-1, two additional couplers were utilized within a turnbuckle splice located near the center of the wire rope. The bogie was accelerated to a target speed of 20 mph (32 km/h) and the wire rope was jerked to simulate dynamic tension. The test layout is shown in Figures 99 through 101, and installation photographs are shown in Figures 102 through 105. Complete drawing sets are shown in Appendix C. Material specifications and mill certifications for the couplers are shown in Appendix D.

A 50-kip (222-kN) tension load cell was used to record the forces in the wire rope during each test. For test no. BBNC-1, the load cell was placed within the turnbuckle splice assembly. For test nos. BBNC-2 and BBNC-3, the load cell was located between the end coupler and the anchor bracket. An additional 80-kip (356-kN) compression load cell was installed around the anchor rods during test nos. BBNC-2 and BBNC-3. Both load cells were operating with a sample rate of 10,000 Hz. The locations of the load cells during each test are shown in Figures 103 through 105.

A combination of AOS high-speed digital video cameras and GoPro digital video cameras were used to document each test. The AOS high-speed cameras had a frame rate of 500 frames per second, while the GoPro video cameras had a frame rate of 120 frames per second. The cameras were placed near each of the couplers utilized during a particular test. A Nikon D50 digital still camera was also used to document pre- and post-test conditions for all tests.

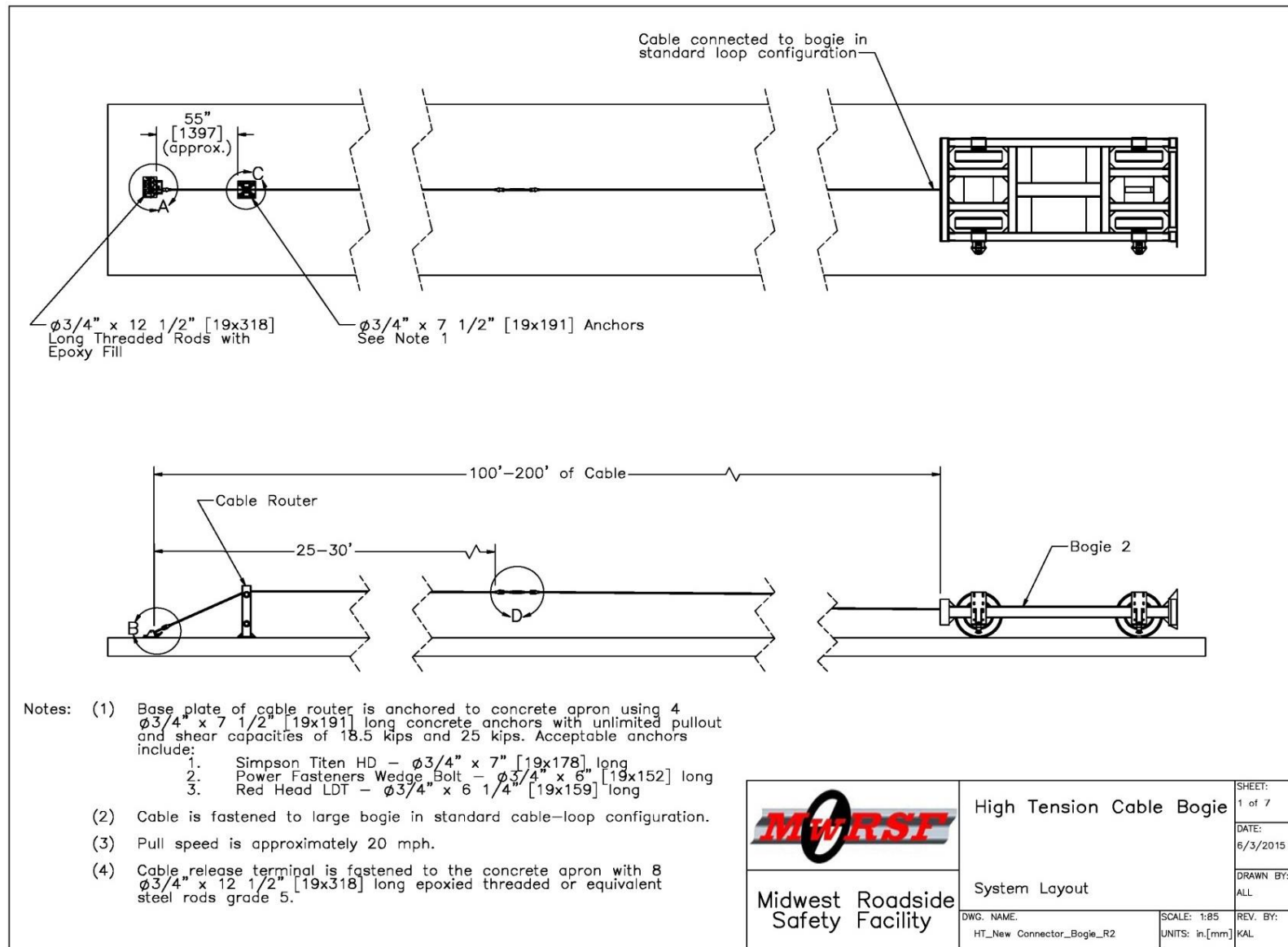


Figure 99. Coupler Testing Layout, Test Nos. BBNC-1 through BBNC-3

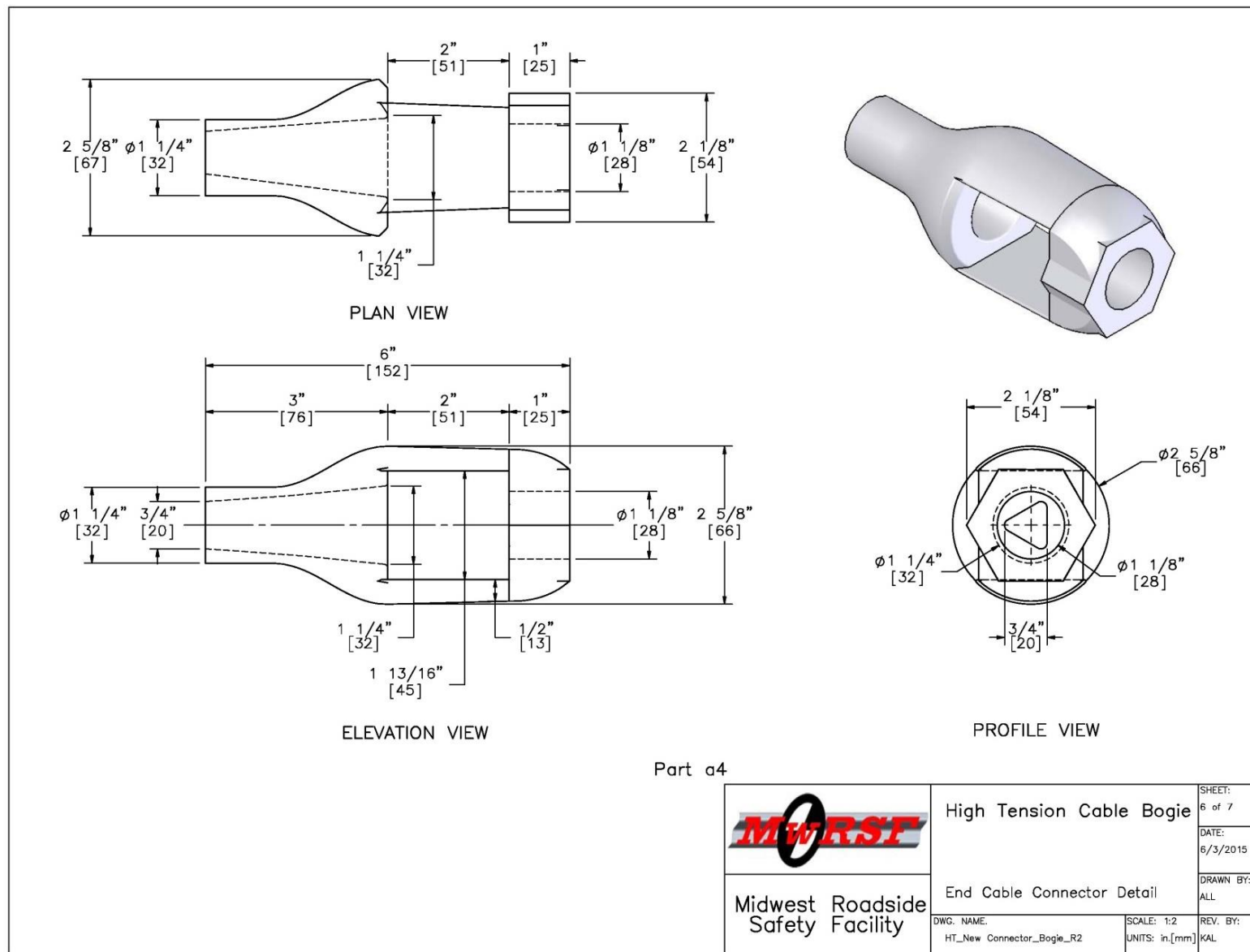


Figure 100. Bennett Bolt Works Coupler Model No. CGBBWTH, Test Nos. BBNC-1 and BBNC-2

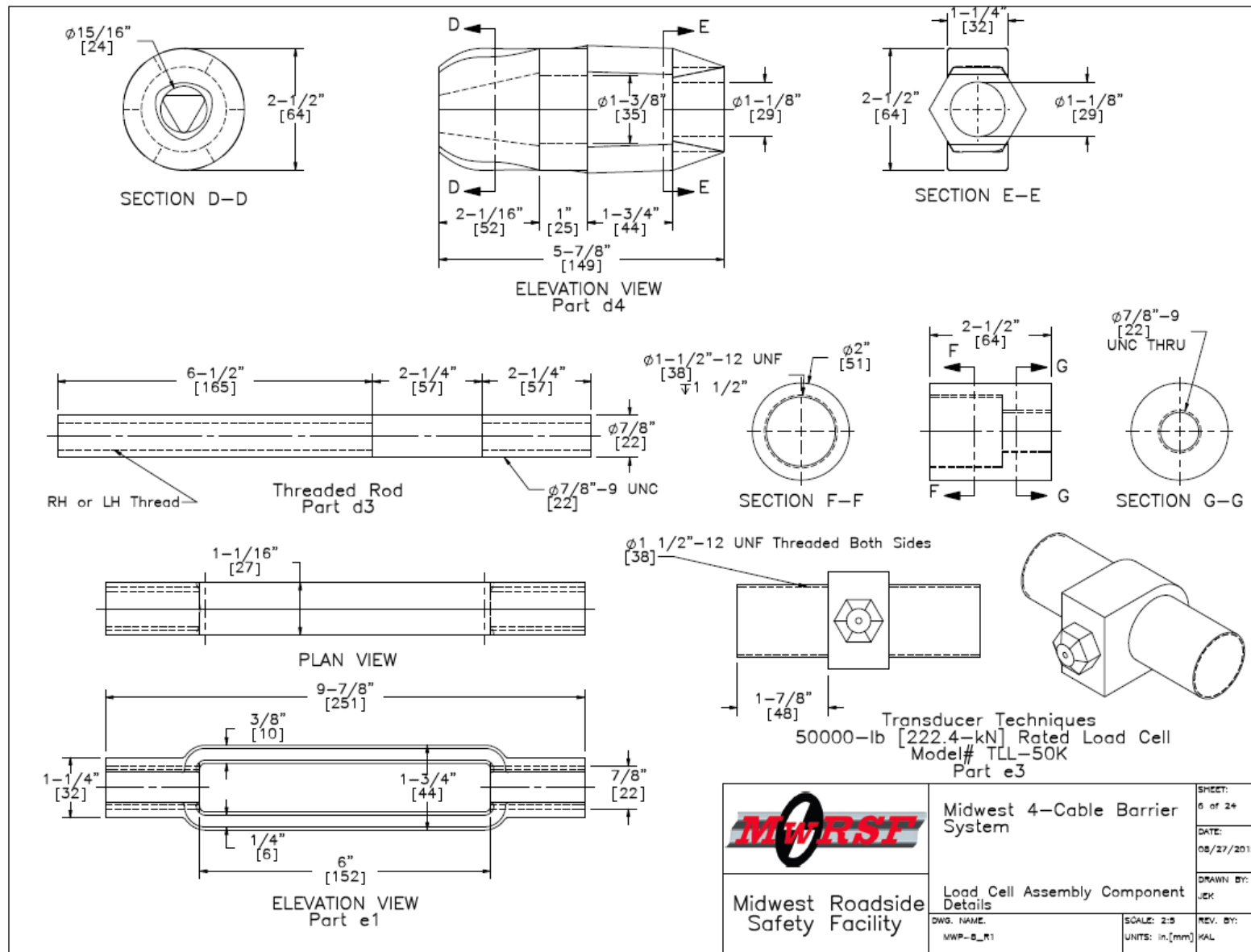


Figure 101. Coupler Model No. CGBBHT and Associated Splice Hardware, Test No. BBNC-3



Figure 102. Test Installation Photographs, Test Nos. BBNC-1 through BBNC-3

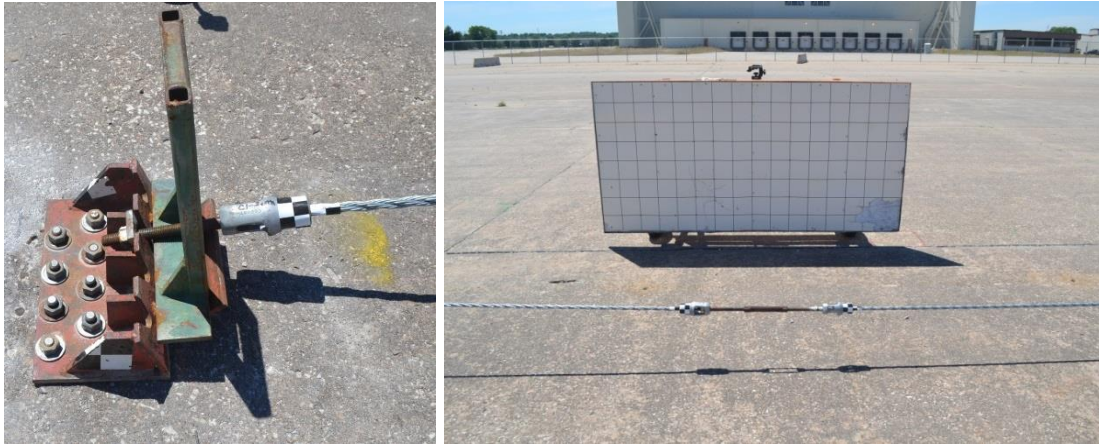


Figure 103. Test Installation Photographs, Test No. BBNC-1



Figure 104. Test Installation Photographs, Test No. BBNC-2

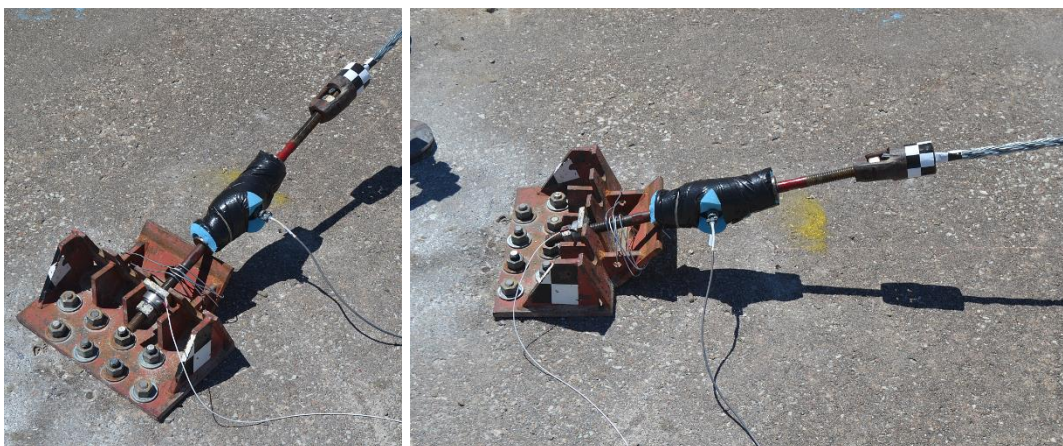


Figure 105. Test Installation Photographs, Test No. BBNC-3

8.4 Testing Results

Results from all three dynamic component tests are provided in the following sections. Although the loads recorded from the various transducers were similar, only the data recorded by the 50-kip (222-kN) load cell is described herein to establish consistency between tests. Results from all load cells can be found in Appendix E. Note, there was not a direct link between the load cell data and the recording of the digital video camera. As such, event times from individual devices may not agree with one another.

8.4.1 Test No. BBNC-1

Test no. BBNC-1 was conducted with the newer Bennett cable couplers, model no. CGBBWTH, located on both ends of the cable and on both sides of the turnbuckle splice. During the test, the cable was loaded to a maximum tension of 33.28 kips (148.10 kN), after which, the cable and wedge pulled through the coupler linking the cable to the anchor bracket. Sequential photographs and system damage photographs are shown in Figure 106.

The inside of the failed coupler contained striations, formed from the wire rope as it pulled through the opening, but the coupler was otherwise undamaged. The upstream end of the cable that pulled through the coupler was deformed and frayed, and the wedge was no longer entwined within the wire strands. The cable ends pulled $\frac{5}{8}$ in. (16 mm) out of the other three couplers.

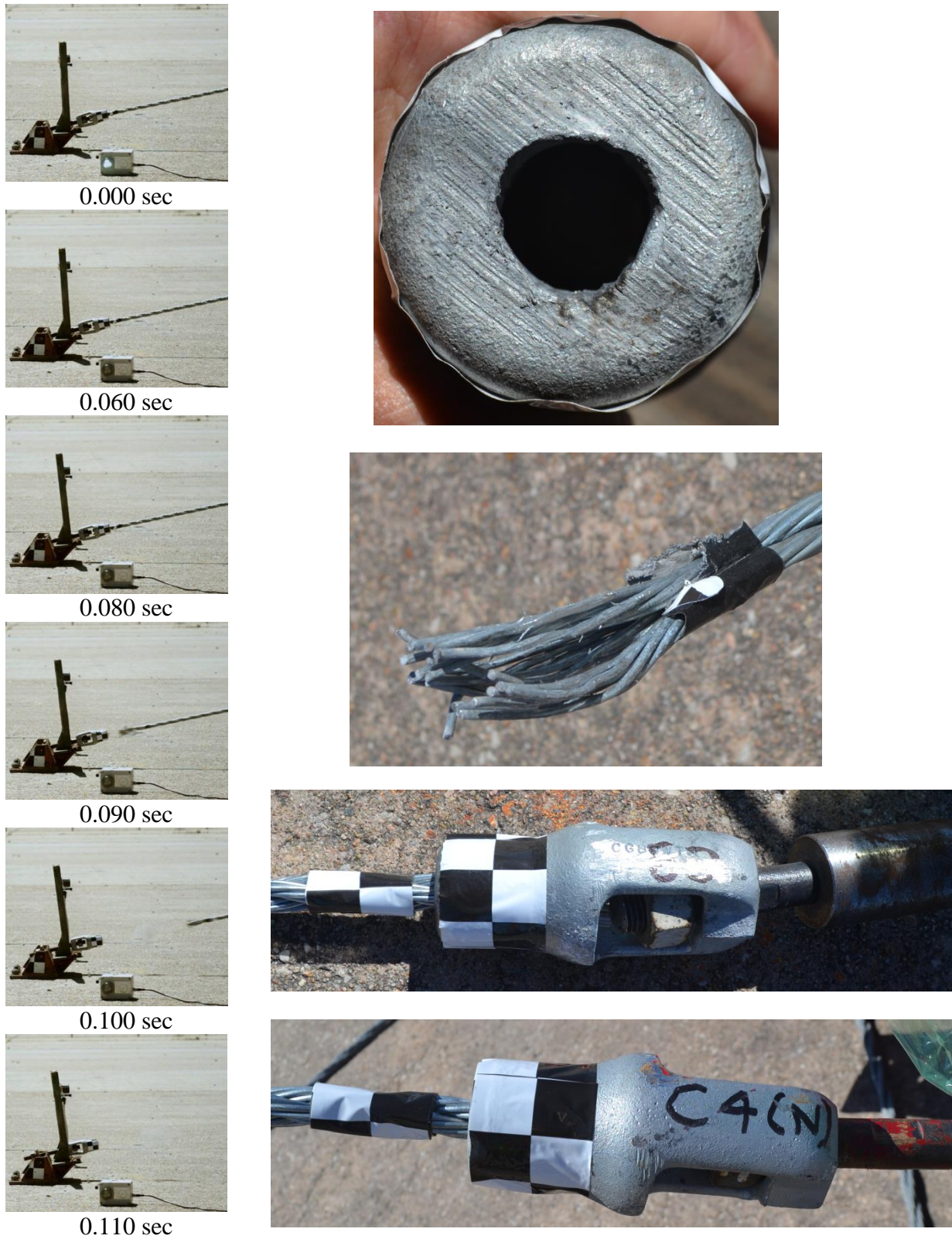


Figure 106. Time-Sequential and Post-Test Photographs, Test No. BBNC-1

8.4.1 Test No. BBNC-2

Test no. BBNC-2 was conducted with the newer Bennett cable couplers, model no. CGBBWTH, located on both ends of the cable. During the test, the cable was loaded to a maximum tension of 32.43 kips (144.26 kN), after which, the cable and wedge pulled through the coupler linking the cable to the anchor bracket. Sequential photographs and system damage photographs are shown in Figure 107.

The inside of the failed coupler had striations formed from the wire rope as it pulled through the opening, but the coupler was otherwise undamaged. The upstream end of the cable that pulled through the coupler was deformed and frayed, and the wedge was no longer entwined within the wire strands. The wedge was deformed and contained more pronounced striations than the coupler. The cable end attached to the bogie vehicle pulled $1\frac{1}{8}$ in. (29 mm) out of the coupler, and the wedge pulled $\frac{1}{4}$ in. (6 mm) out of the coupler.



Figure 107. Time-Sequential and Post-Test Photographs, Test No. BBNC-2

8.4.2 Test No. BBNC-3

Test no. BBNC-3 was conducted with the Bennett cable couplers currently utilized in full-scale crash testing of the cable barrier located on both ends of the cable, model no. CGBBHT. During the test, the cable was loaded to a maximum tension of 30.17 kips (134.20 kN), after which, the cable and wedge pulled through both couplers simultaneously. Sequential photographs and system damage photographs are shown in Figure 108.

The inside of the couplers contained striations formed from the wire rope as it pulled through the opening, but the couplers were otherwise undamaged. The cable ends were deformed and frayed, but unlike the previous tests, the wedges were still entwined within the wire strands at both ends. The wedges were crushed and plastically deformed around the individual wires of the cable.

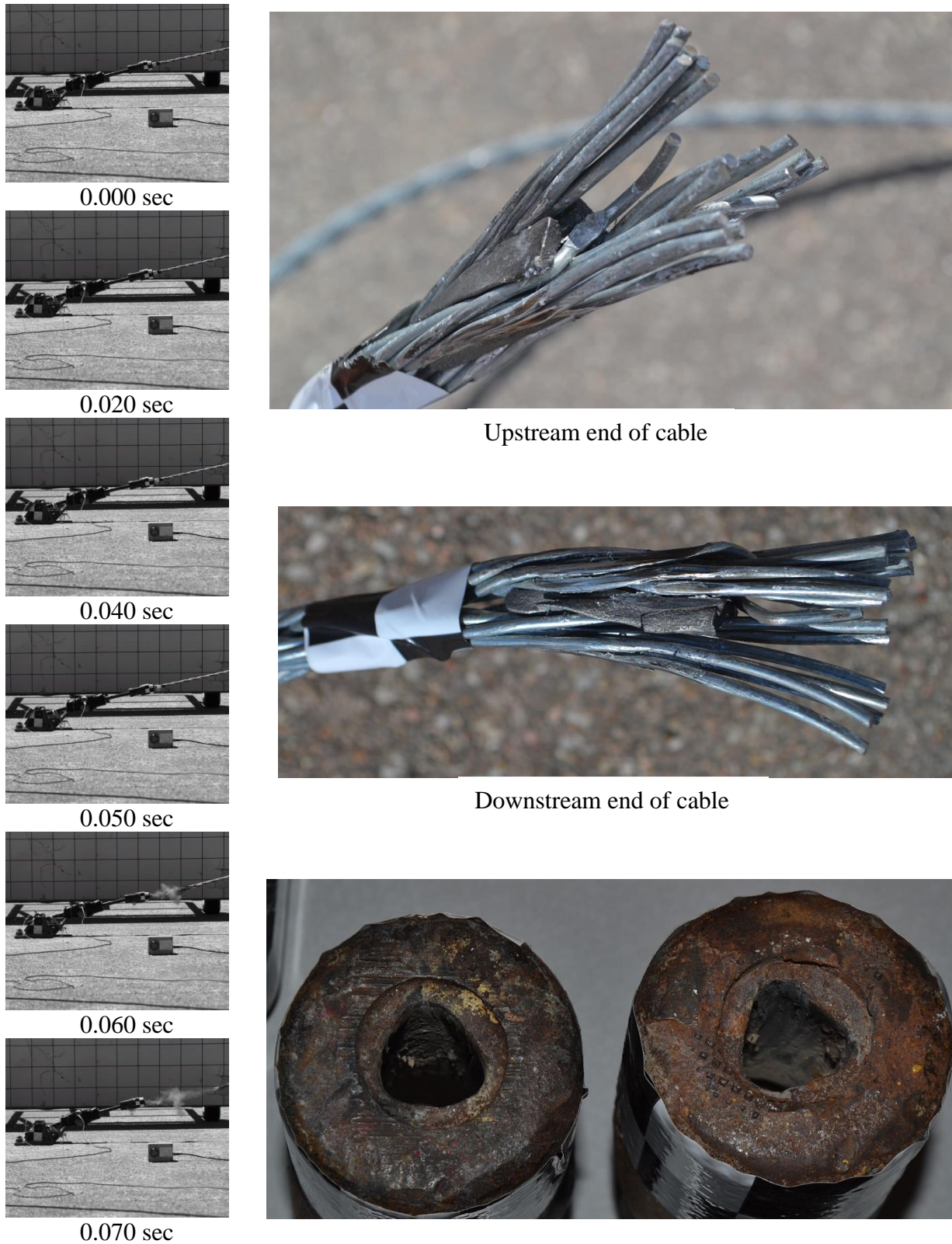


Figure 108. Time-Sequential and Post-Test Photographs, Test No. BBNC-3

8.4.3 Discussion

Three dynamic component tests were performed to evaluate the performance of two Bennett Bolt Works cable couplers. Two tests were conducted on the new cable coupler, model no. CGBBWTH, and one test was conducted on the old cable coupler, model no. CGBBHT. A summary of the coupler component testing result is shown in Table 19.

Table 19. Test Results for Test Nos. BBNC-1 through BBNC-3

Test No.	Coupler Model No.	Material Specification	Maximum Tensile Load		Failure Description
			Tension Load Cell kips (kN)	Compression Load Cell kips (kN)	
BBNC-1	CGBBWTH	ASTM-A536	33.28 (148.10)	N/A	Cable and wedge pullout from upstream coupler at anchor bracket
BBNC-2	CGBBWTH	ASTM-A536	32.43 (144.31)	37.08 (165.07)	Cable and wedge pullout from upstream coupler at anchor bracket
BBNC-3	CGBBHT	ASTM-A47	30.17 (134.26)	26.79 (119.22)	Cable and wedge pullout from upstream and downstream coupler

N/A: Not Applicable

All three tests resulted in similar failures. In test nos. BBNC-1 and BBNC-2, the cable and wedge pulled out of the coupler attached to the cable anchor bracket, while in test no. BBNC-3, the cables and wedges simultaneously pulled out of the couplers on both ends of the cable. The test components in each test sustained similar damage. The released cable ends were frayed, and the wedges were deformed and had very pronounced striations from the wires pressing into the wedge. Recall, the same wedge is utilized in both coupler models. Therefore, similar wedge damage was expected.

The couplers remained largely undamaged except for the marks and striations inside the couplers by the individual wires as the cables pulled out of the couplers. The striations appeared to be more severe in the newer coupler, model no. CGBBWTH, than in the older coupler, model no. CGBBHT. The older and newer couplers were made from ASTM A-47 malleable iron and ASTM A-536 ductile iron, respectively. Although ASTM A-536 iron has a 50 percent higher tensile strength than ASTM A-47 iron, it may also allow for greater deformations when loaded. Differences in geometry may have also played a part in the damage severity difference between the two couplers.

Both tests with the coupler model no. CGBBWTH resulted in higher load capacities than the coupler model no. CGBBHT. At first, it appeared that the newer Bennett Bolt Works coupler was stronger than the previous model and showed promise for use in the cable barrier system. However, none of the tests resulted in forces near the nominal capacity of the $\frac{3}{4}$ -in. (19-mm) diameter, 3x7 wire rope, which is 39 kips (174 kN). Utilization of a coupler that can develop the full strength of the cable was considered very important to the robustness of the cable barrier.

In previous component testing conducted under similar conditions, the coupler model no. CGBBHT had demonstrated the ability to achieve this targeted capacity prior to failure [13]. The loads from the previous study were collected via accelerometers mounted on the bogie vehicle, but the load cells utilized in this current study should have provided similar test results. There is a possibility that the couplers for test no. BBNC-3 had sustained damage prior to their component testing, which would make them susceptible to premature failure. The coupler model no. CGBBHT had been previously used in full-scale testing of the prototype cable barrier system and had not failed. Subsequently, further testing and evaluation is required of both coupler models to gain a better understanding of their strengths and durability.

9 SUMMARY, CONCLUSIONS, AND RECOMMENDATIONS

The first objective of this research study was to investigate post modifications as potential floorpan tearing mitigation techniques for the prototype cable barrier system. This effort began with the development of a new component testing apparatus to simulate a small car overriding cable barrier support posts. Through a combination of field measurements and static coupon testing, 24-gauge (0.61-mm) ASTM A653 sheet steel was found to have a similar thickness and tensile strength to the floorpan of a Kia Rio, a common test vehicle that satisfies the MASH 1100C small car requirements. Subsequently, this sheet steel was mounted to the underside of a rigid-frame bogie vehicle at 8 in. (203 mm) above the ground, which is the same height as the floorpan of the Kia Rio.

The new bogie vehicle equipped with a simulated floorpan was utilized to impact and override a series of two posts spaced 8 ft (2.4 m) apart with a targeted impact speed of 25 mph (40 km/h). Initial baseline testing conducted on the unmodified MWP resulted in tearing and creasing of the simulated floorpan which resembled the Kia Rio floorpan damage observed in actual full-scale testing of the prototype cable barrier. Thus, the component testing setup was replicating actual vehicle floorpan penetrations, and the study continued with the evaluation of various post configurations.

Two simulated floorpan tests were conducted on S3x5.7 (S76x8.5) posts, the standard low-tension cable guardrail post. Not only did the S3x5.7 (S76x8.5) posts cause twice as many tears as the MWP, but the tears tended to be larger than those observed from testing with the MWP. This finding was likely due to the increased bending strength of the S3x5.7 (S76x8.5) post. Testing of S3x5.7 (S76x8.5) posts confirmed that floorpan tearing was not specific to the MWP and can occur with any deformed post with free/exposed edges.

Additional floorpan testing was conducted to evaluate the propensity for floorpan tearing of three different MWP modification concepts. Testing of the MWP with simulated no. 1 edge rounding on the free/exposed edge resulted in tears similar to the baseline MWP configuration. Thus, edge rounding did not adequately reduce the stress concentrations that led to tearing, and edge rounding was not considered for further evaluation. Testing was also conducted on the MWP with bent steel plates covering the free edges of the posts. The steel plate edge protectors left contact marks and creases in the simulated floorpan but prevented tearing. The tears that did occur during the test were the result of a fabrication error in the post that left a sharp corner in the continuous/bent side of the post cross section. Although the edge protectors showed promise to prevent tearing, the addition of extra parts to the MWP was undesired, and the concept was not evaluated further.

Post weakening was the final MWP modification concept evaluated through a total of nine component tests with the simulated vehicle floorpan. Three different weakening patterns were investigated: (1) $\frac{3}{4}$ -in. (19-mm) diameter weakening holes; (2) three $\frac{3}{8}$ -in. (10-mm) diameter weakening holes; and (3) $\frac{3}{8}$ -in. x $1\frac{1}{8}$ -in. (10-mm x 29-mm) weakening slots. When impacted, these weakening mechanisms caused tears to form in the post cross section, subsequently reducing the section modulus and elastic spring-back of the post. Testing of the MWP retrofitted with either of the latter two weakening patterns resulted in no contact between the top of the posts and the simulated floorpan. This finding was true for impact angles of both 0 and 25 degrees.

Testing of the MWP weakened by 3/4-in. (19-mm) diameter holes resulted in less tearing of the post cross section as compared to the other two weakening patterns. Thus, the posts retained enough elastic response to spring-back upward and contact the simulated floorpan. These posts left contact marks and creases in the simulated floorpan but did not cause any tears for impact angles of 0, 25, and -25 degrees. Thus, all three of the weakened MWP designs showed a propensity to mitigate vehicle floorpan tearing.

Prior to recommending any of the weakened MWP for use in the prototype cable barrier system, it was important to study the effect these holes and slots had on the strong-axis bending strength of the MWP. Accordingly, six dynamic component tests were conducted with the bogie vehicle impacting the posts at a 90-degree angle. Two posts retrofitted with each of the weakening patterns were impacted during the strong-axis evaluation tests. All of the posts hinged at groundline, but both the MWP with weakening slots and the MWP with three 3/8-in. (10-mm) diameter holes also experienced tearing of the post cross section as the front flange completely ruptured in all four posts. Due in large part to these ruptures, the average resistance forces of these weakened MWP were reduced by 30 percent for three 3/8-in. (10-mm) holes and 44 percent for slots as compared to the unmodified MWP.

Alternatively, the MWP with 3/4-in. (19-mm) diameter holes did not experience any tearing of the post cross section around the weakening holes. These two posts provided an average resistance force similar to the unmodified MWP with only a 10 percent decrease over 20 in. (508 mm) of deflection. Therefore, the MWP with 3/4-in. (19-mm) diameter weakening holes was recommended for implementation into the prototype cable barrier system to mitigate floorpan tearing without affecting the stiffness or deflections of the system. The actual effect these weakening holes have on system performance should be evaluated through full-scale crash testing according to MASH guidelines.

The second objective of this research effort was to investigate other cable splice hardware for the use in the cable median barrier that would reduce the propensity for vehicle snag and sheet metal tearing. A review of available wire rope splicing hardware revealed three options that were rated to the full strength of the 3/4-in. (19-mm) diameter, 3x7 wire rope utilized in cable guardrails. However, the epoxy socket coupler has a large cross section that would likely result in increased snagging and deformation of an impacting vehicle. Additionally, field swaging requires the purchase of a \$25,000 specialized swaging machine, which was more than the project budget would allow. Thus, only the new Bennett Bolt Works mechanical coupler, model no. CGBBWTH, was selected for evaluation through component testing.

A total of three dynamic component tests were performed to evaluate the performance of the two Bennett Bolt Works cable couplers. Two tests were conducted on the new coupler, model no. CGBBWTH, and one test was conducted on the old coupler, model no. CGBBHT. All three of the tests resulted in similar failures. Both tests with the new coupler resulted in the cable and wedge pulling out of the coupler attached to the cable anchor bracket, while the test of the old coupler resulted in the cable ends and wedges being simultaneously pulled out of the couplers on both ends of the cable. The test components from each test sustained similar damage. The released cable ends were frayed, and the wedges were deformed and had very pronounced striations resulting from the wires pressing into the wedge. The couplers remained largely undamaged except for the marks and striations inside the couplers left by the individual wires as the cables pulled out of the couplers.

Both tests with the new coupler model no. CGBBWTH resulted in higher load capacities than the current coupler model no. CGBBHT. Since the new model is narrower than the current model, it showed promise as an alternative coupler for use in the prototype cable barrier. However, all of the tests resulted in failure loads below the full strength of the $\frac{3}{4}$ -in. (19-mm) diameter, 3x7 wire rope, and it has been considered essential for the coupler hardware to develop the full strength of the cable to ensure robustness of the cable guardrail. Previous component tests have shown that the older coupler has a capacity greater than the rated strength of the cable. Therefore, further testing and evaluation is required to further explain these unexpectedly low failure loads and to better understand the strengths and durability of each coupler type.

10 REFERENCES

1. *Manual for Assessing Safety Hardware (MASH)*, American Association of State Highway and Transportation Officials (AASHTO), Washington, D.C., 2009.
2. Bielenberg, R.W., Schmidt, T.L., Faller, R.K., Lechtenberg, K.A., Rosenbaugh, S.K., Reid, J.D., and Sicking, D.L., *Design of an Improved Post for Use in a Non-Proprietary, High-Tension, Cable Median Barrier*, Final Report to the Midwest States' Regional Pooled Fund Program, Transportation Research Report No. TRP-03-286-14, Midwest Roadside Safety Facility, University of Nebraska-Lincoln, Lincoln, NE, May 7, 2015.
3. Bielenberg, R.W., Rosenbaugh, S.K., Faller, R.K., Humphrey, B.M., Schmidt, T.L., Lechtenberg, K.A., and Reid, J.D., *MASH Test Nos. 3-17 and 3-11 on a Non-Proprietary Cable Median Barrier*, Final Report to the Midwest States' Pooled Fund Program, Transportation Research Report No. TRP-03-303-15, Midwest Roadside Safety Facility, University of Nebraska-Lincoln, Lincoln, NE, November 3, 2015.
4. Kohtz, J.E., Bielenberg, R.W., Rosenbaugh, S.K., Faller, R.K., Lechtenberg, K.A., and Reid, J.D., *MASH Test Nos. 3-11 and 3-10 on a Non-Proprietary Cable Median Barrier*, Final Report to the Midwest States' Pooled Fund Program, Transportation Research Report No. TRP-03-327-16, Midwest Roadside Safety Facility, University of Nebraska-Lincoln, Lincoln, NE, May 17, 2016.
5. Ross, H.E., Sicking, D.L., Zimmer, R.A., and Michie, J.D., *Recommended Procedures for the Safety Performance Evaluation of Highway Features, National Cooperative Research Program (NCHRP) Report No. 350*, Transportation Research Board, Washington, D.C., 1993.
6. Kampschneider, L.R., Homan, D.M., Lechtenberg, K.A., Faller, R.K., Bielenberg, R.W., Sicking, D.L., Reid, J.D., and Rosenbaugh, S.K., *Evaluation of a Non-Proprietary, High-Tension, Four-Cable, Median Barrier on Level Terrain*, Final Report to the Midwest States' Regional Pooled Fund Program, Transportation Research Report No. TRP-03-258-12, Midwest Roadside Safety Facility, University of Nebraska-Lincoln, Lincoln, NE, November 29, 2012.
7. Hitz, R.A., Molacek, K.J., Stolle, C.S., Polivka, K.A., Faller, R.K., Rhode, J.R., Sicking, D.L., Reid, J.D., and Bielenberg, R.W., *Design and Evaluation of a Low-Tension Cable Guardrail End Terminal System*, Transportation Research Report No. TRP-03-131-08, Midwest Roadside Safety Facility, University of Nebraska-Lincoln, Lincoln, NE, July 15, 2008.
8. Stolle, C.J., Zhu, L., Lechtenberg, K.A., Bielenberg, R.W., Faller, R.K., Sicking, D.L., Reid, J.D., and Rhode, J.R., *Performance Evaluation of Type II and Type IIA Box Beam End Terminals – Volume I: Research Results and Discussion*, Final Report to the Midwest States' Regional Pooled Fund Program, Transportation Research Report No. TRP-03-203-10 Revision 1, Midwest Roadside Safety Facility, University of Nebraska-Lincoln, Lincoln, NE, June 22, 2016.

9. Schmidt, J.D., Sicking, D.L., Faller, R.K., Lechtenberg, K.A., Bielenberg, R.W., Reid, J.D., and Rosenbaugh, S.K., *Phase II Development of a Non-Proprietary, Four-Cable, High Tension Median Barrier*, Final Report to the Midwest States' Regional Pooled Fund Program, Transportation Research Report No. TRP-03-253-12, Midwest Roadside Safety Facility, University of Nebraska-Lincoln, Lincoln, NE, March 21, 2012.
10. Buth, C.E., Menges, W.L., Williams, W.F., and Schoeneman, S.K., *NCHRP Report 350 Test 3-10 on the Modified PennDOT Type 2 Guide Rail – Test 4*, Report No. RF473750-4, Texas Transportation Institute, The University System of Texas A&M, College Station, TX, July 2000.
11. American Society for Testing and Materials (ASTM) Standard A370, “*Standard Testing Methods and Definitions for Mechanical Testing of Steel Products*,” ASTM International, West Conshohocken, PA, 2014.
12. Society of Automotive Engineers (SAE), *Instrumentation for Impact Test – Part 1 – Electronic Instrumentation*, SAE J211/1 MAR95, New York City, NY, July, 2007.
13. Thiele, J.C., Bielenberg, R.W., Faller, R.K., Sicking, D.L., Rohde, J.R., Reid, J.D., Polivka, K.A., and Holloway, J.C., *Design and Evaluation of High-Tension Cable Median Barrier Hardware*, Final Report to the Midwest States' Regional Pooled Fund Program, Transportation Research Report No. TRP-03-200-08, Midwest Roadside Safety Facility, University of Nebraska-Lincoln, Lincoln, NE, February 25, 2008.
14. Alberson, Dean C., Arrington, Dusty R., and Menges, Wanda L., *Development of Field Applied Fittings for Wire Rope Barrier and Conversion to High Tension*, Final Report to the Washington State Department of Transportation, Test Report No. 405160-11-1, Texas Transportation Institute, The University System of Texas A&M, College Station, TX, August 2010.

11 APPENDICES

Appendix A. Static Tension Testing Results

The recorded data results from each static coupon test are provided individually in the summary sheets found in this appendix. Summary sheets include pre- and post-test measurements, yield strength, ultimate tensile strength, elongation at fracture, force vs. displacement plots, and stress vs. displacement plots.

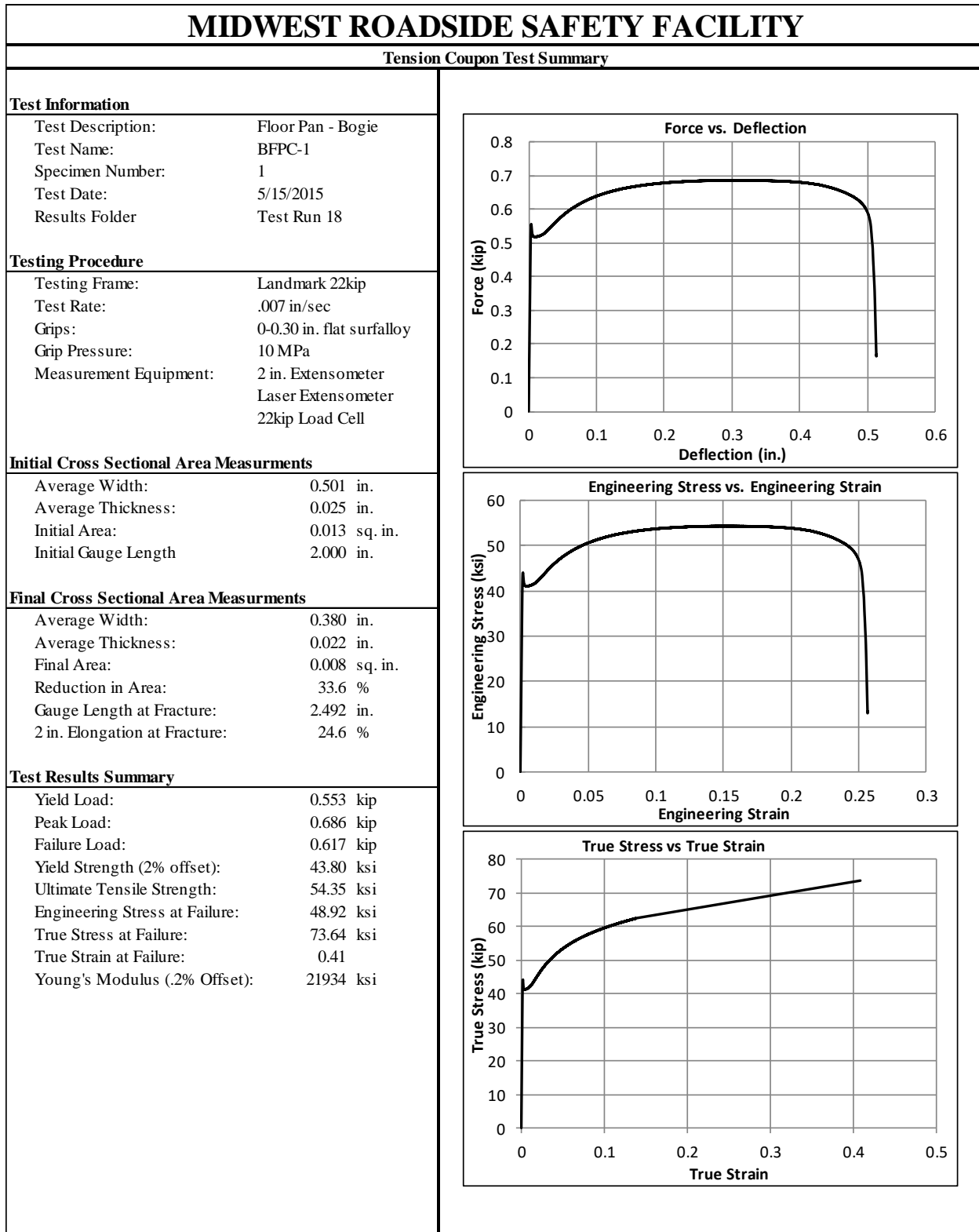


Figure A-1. Test No. BFPC-1 Results

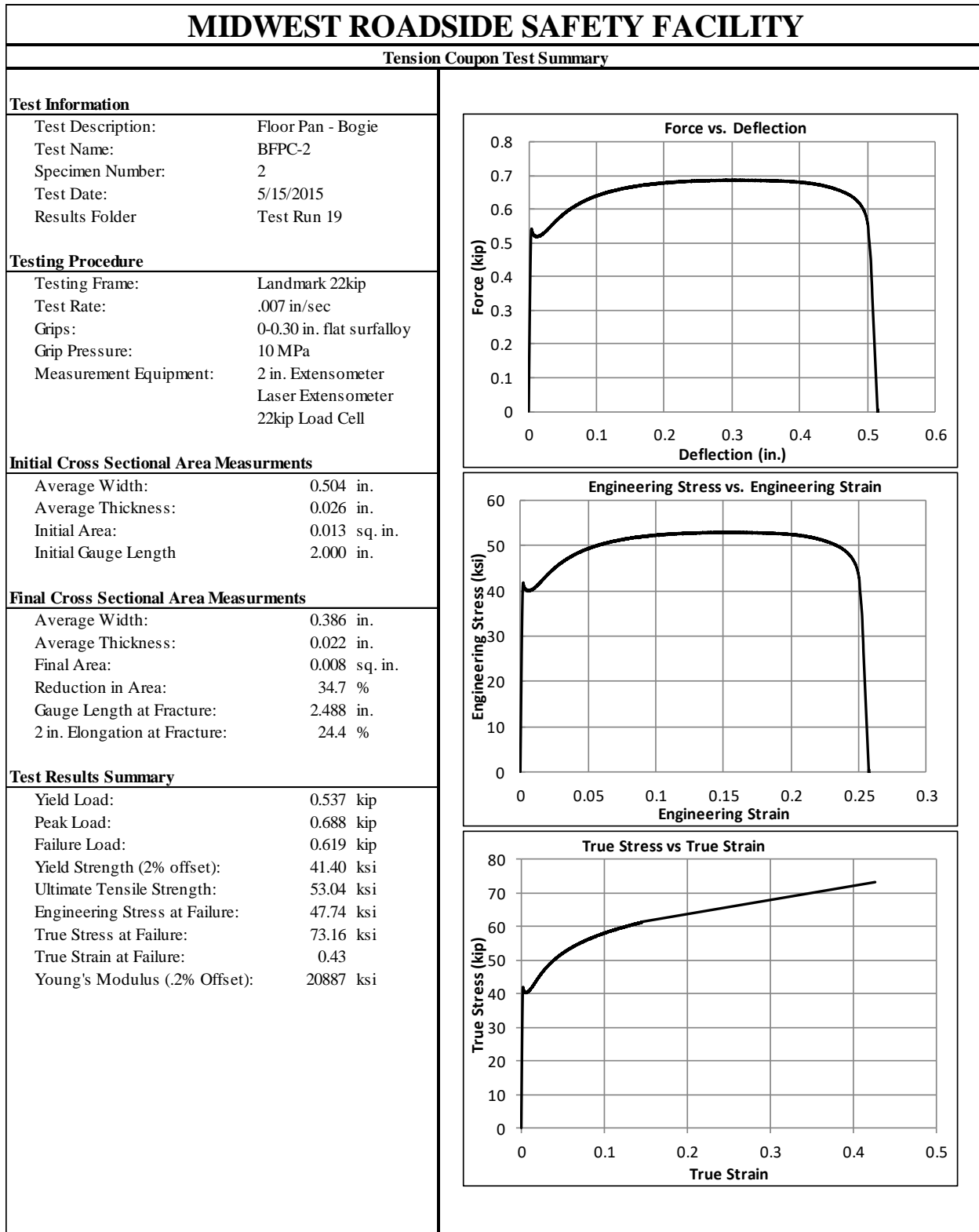


Figure A-2. Test No. BFPC-2 Results

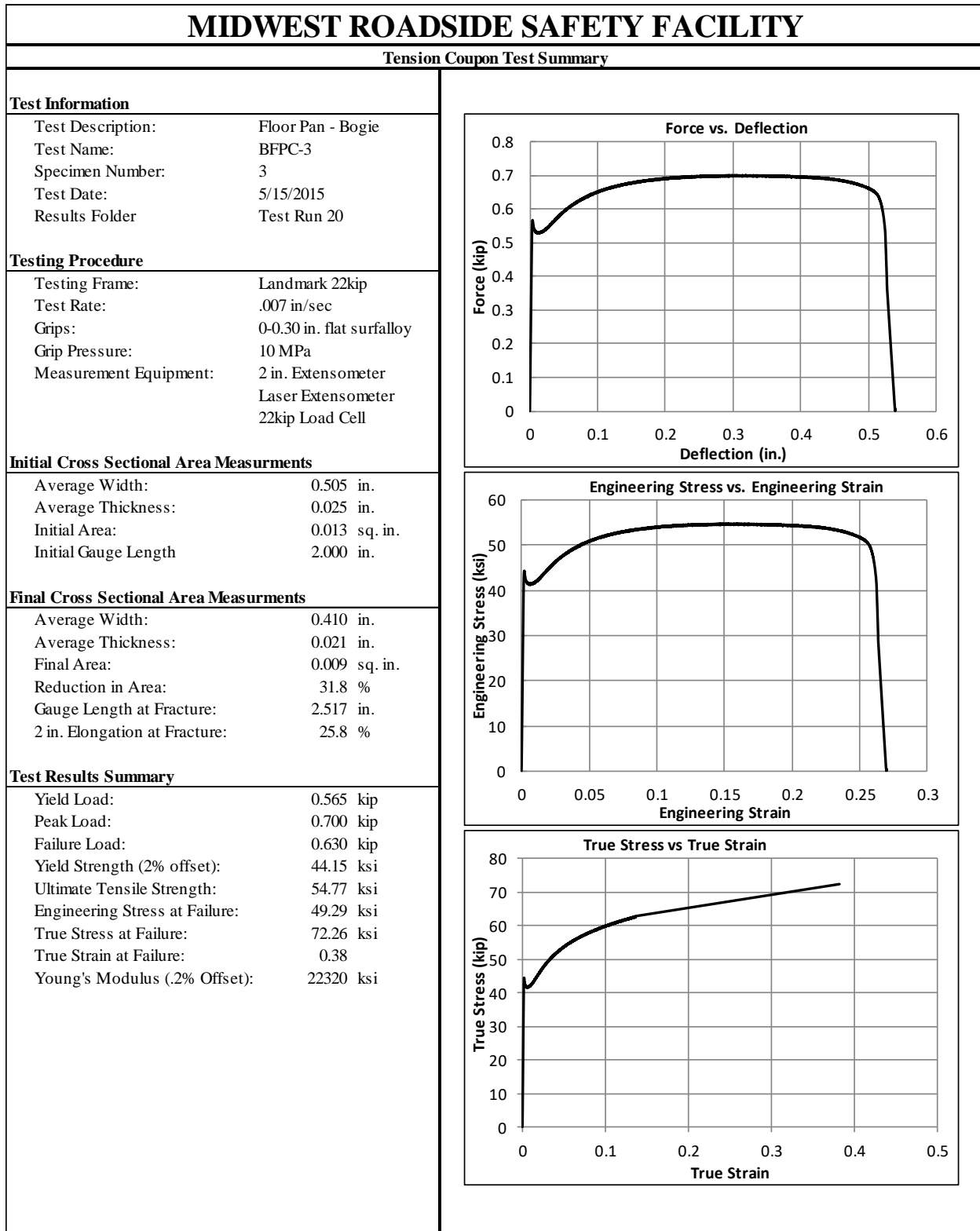


Figure A-3. Test No. BFPC-3 Results

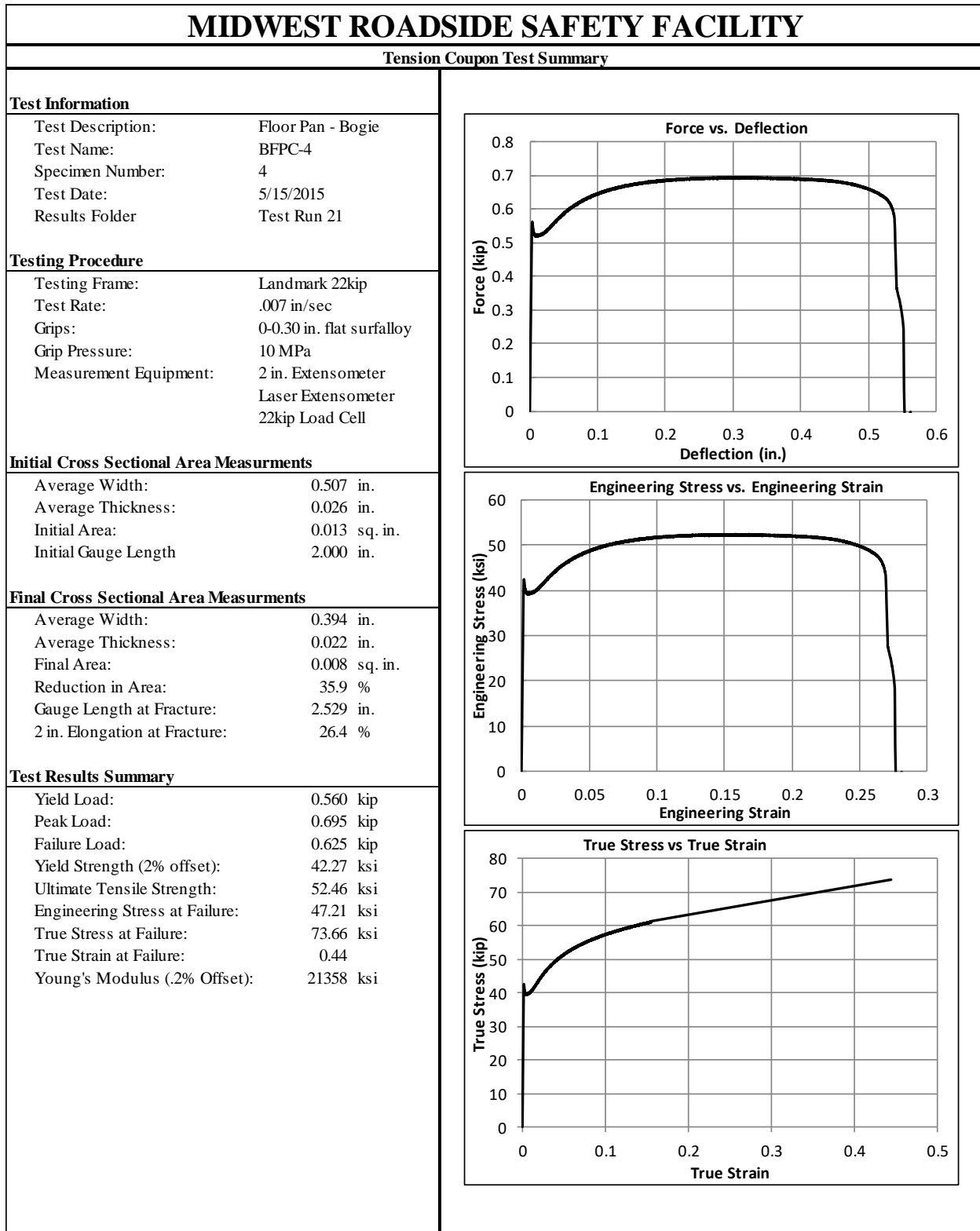


Figure A-4. Test No. BFPC-4 Results

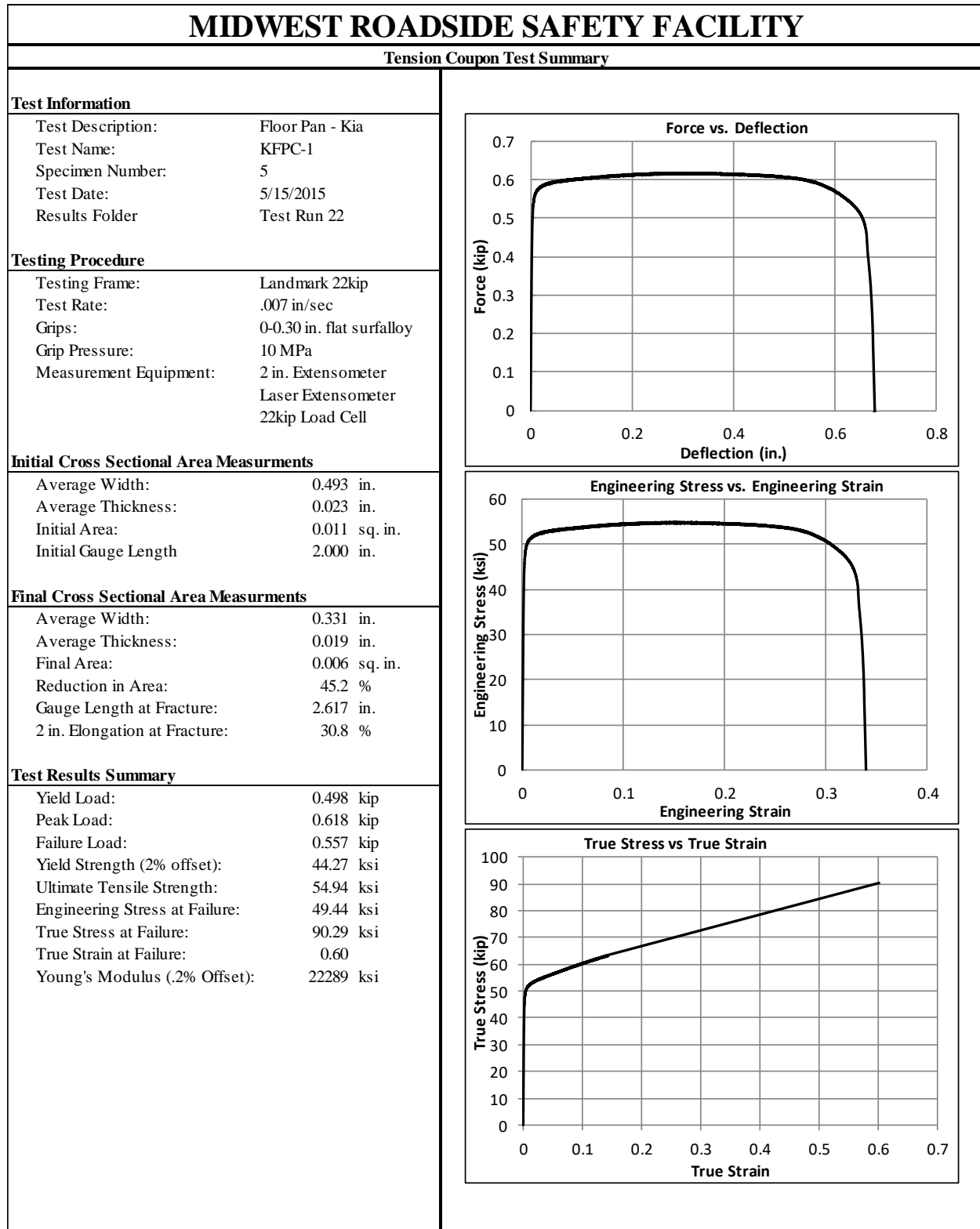


Figure A-5. Test No. KFPC-1 Results

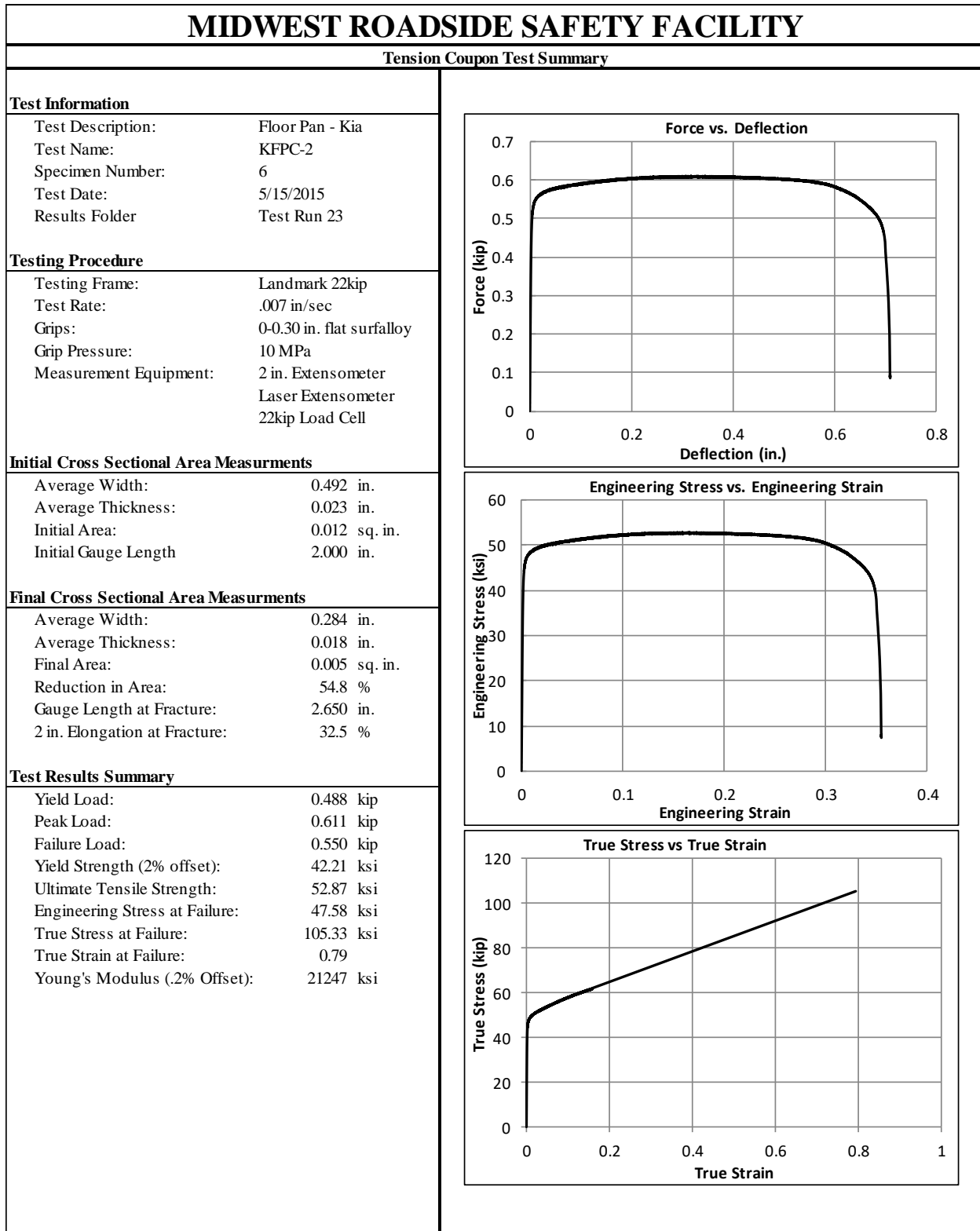


Figure A-6. Test No. KFPC-2 Results

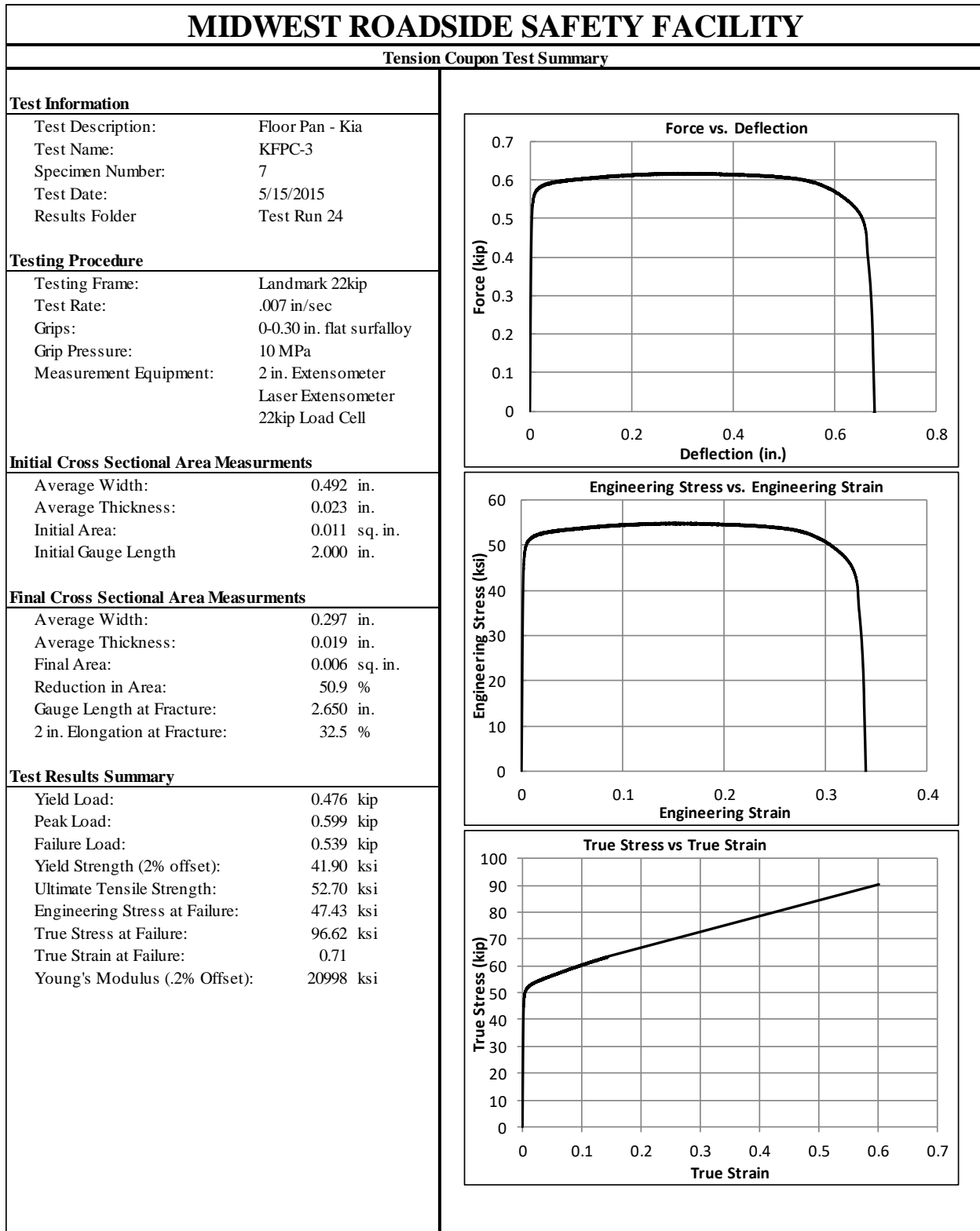


Figure A-7. Test No. KFPC-3 Results

Appendix B. Bogie Test Results

The results of the recorded data from each accelerometer for every dynamic bogie test conducted to evaluate the propensity for floorpan tearing are provided in the summary sheets found in this appendix. Summary sheets include acceleration, velocity, and deflection vs. time plots as well as force vs. deflection and energy vs. deflection plots.

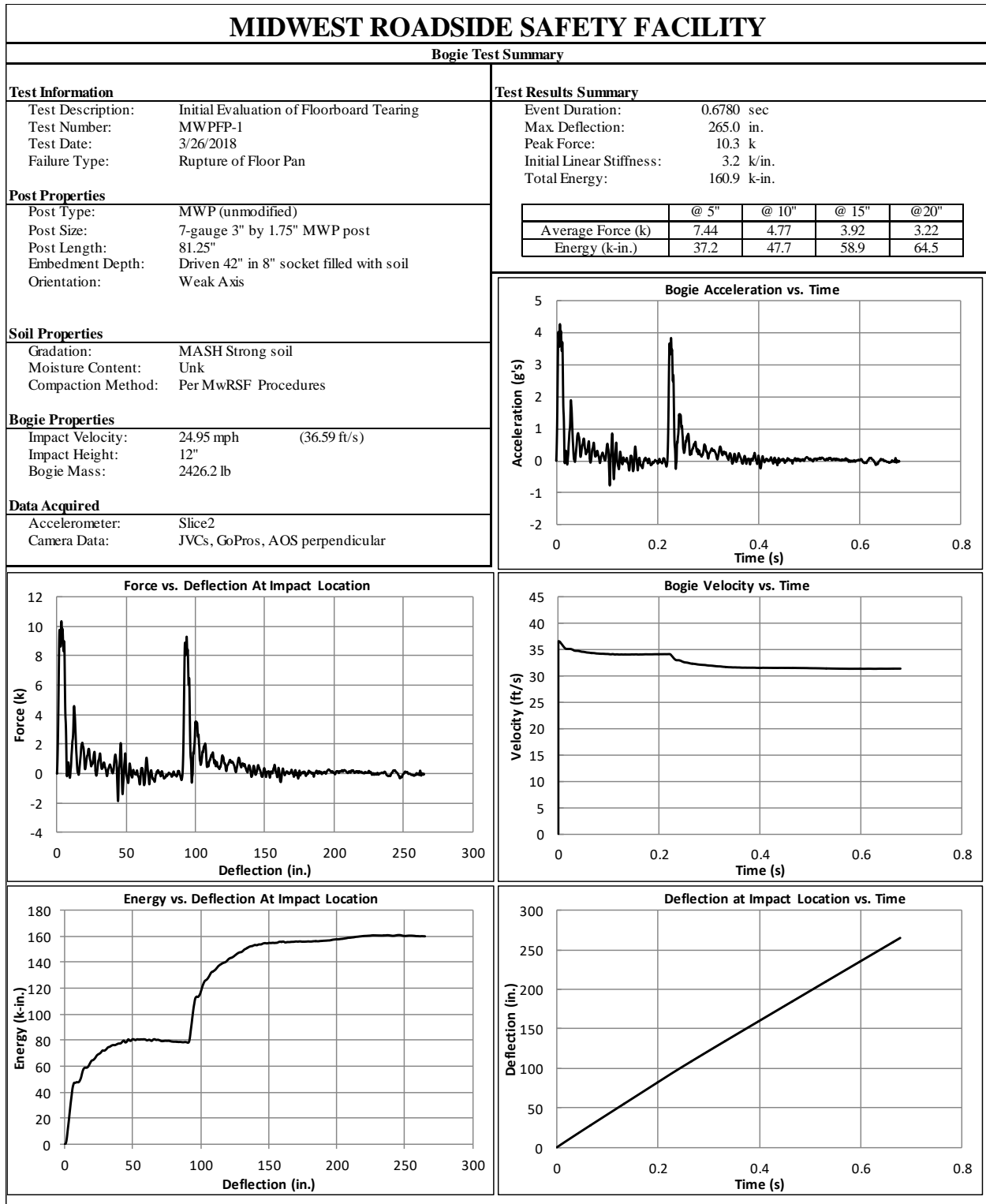


Figure B-1. Test No. MWFPF-1 Results (SLICE-2)

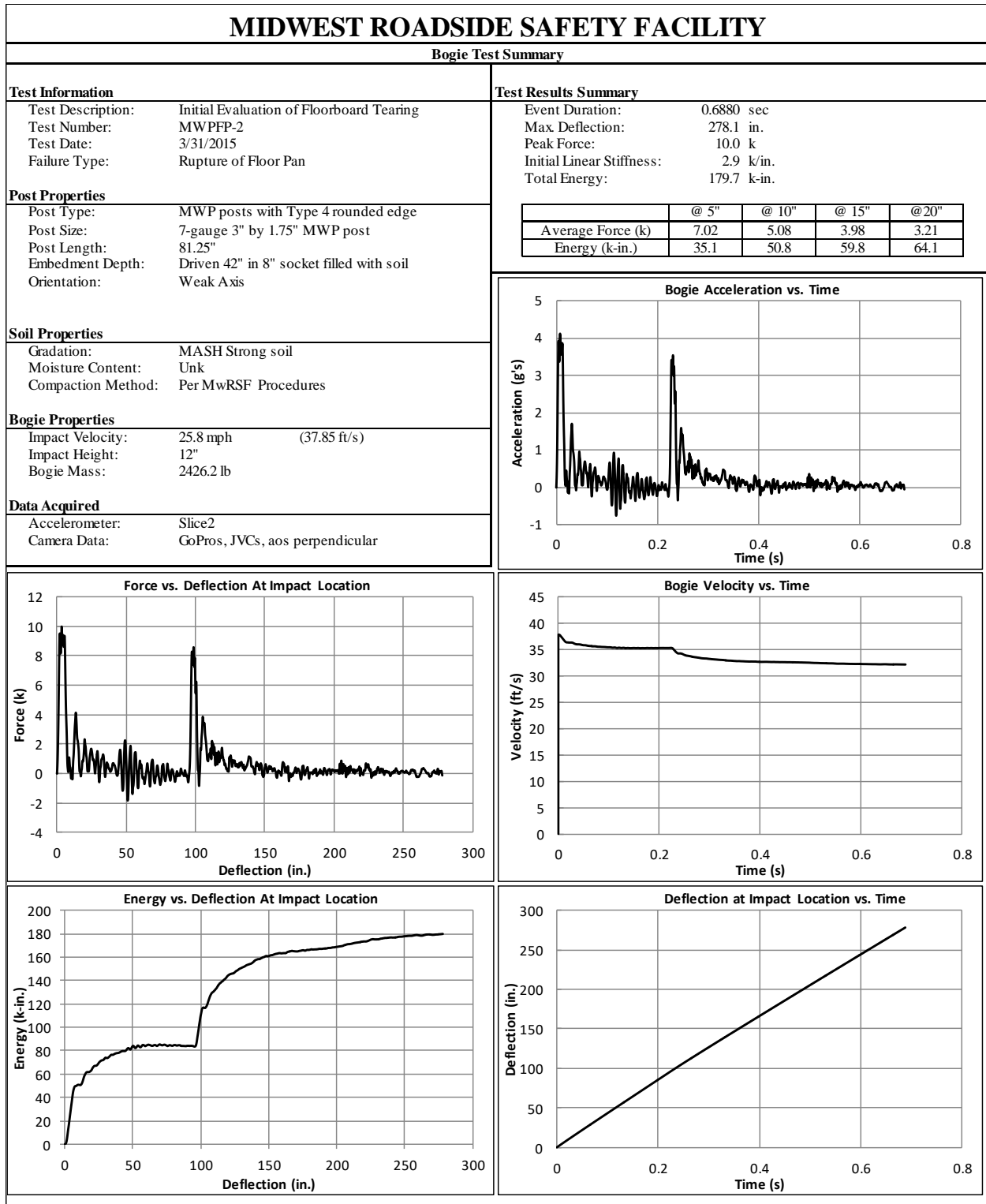


Figure B-2. Test No. MWFPF-2 Results (SLICE-2)

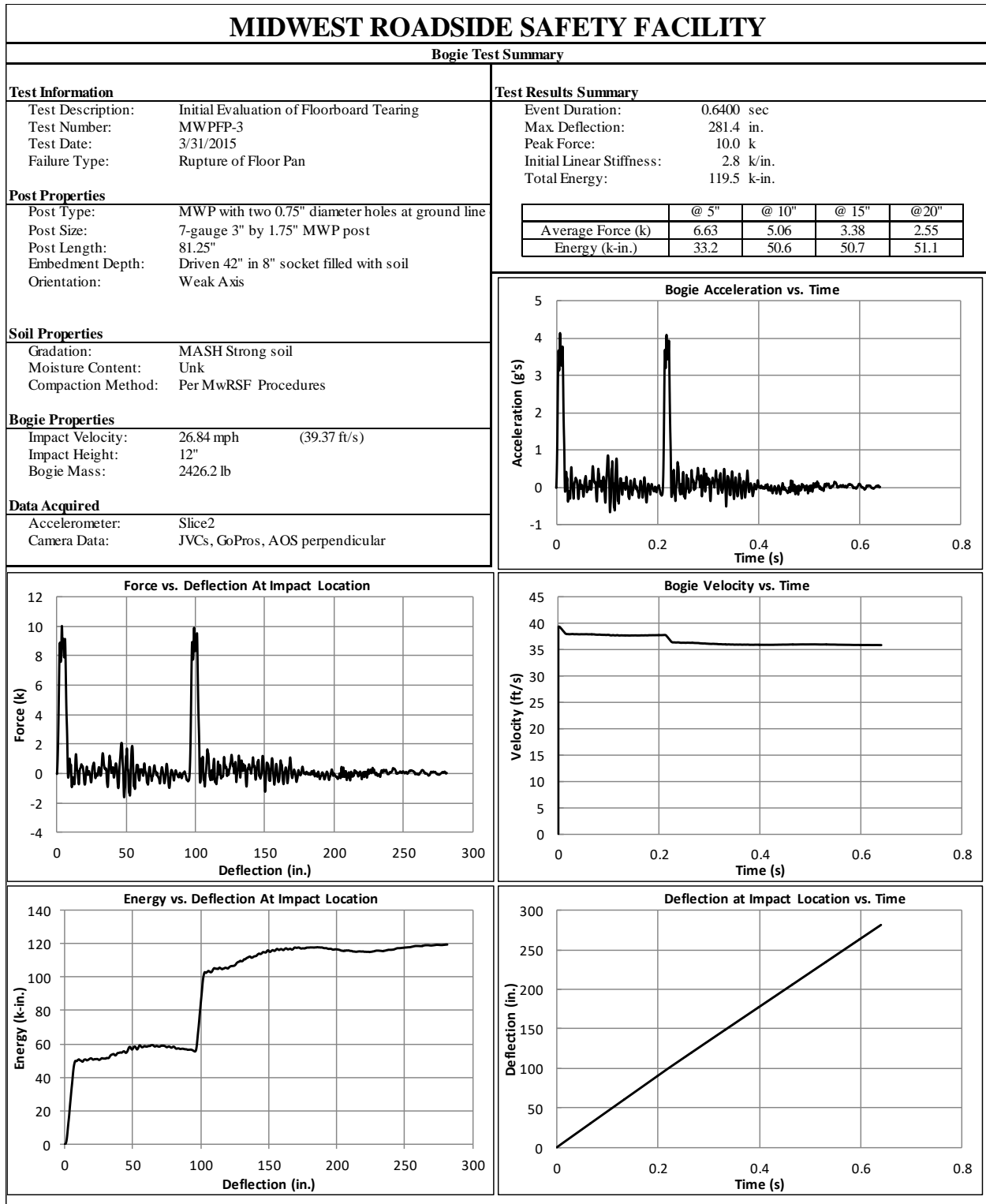


Figure B-3. Test No. MWFPF-3 Results (SLICE-2)

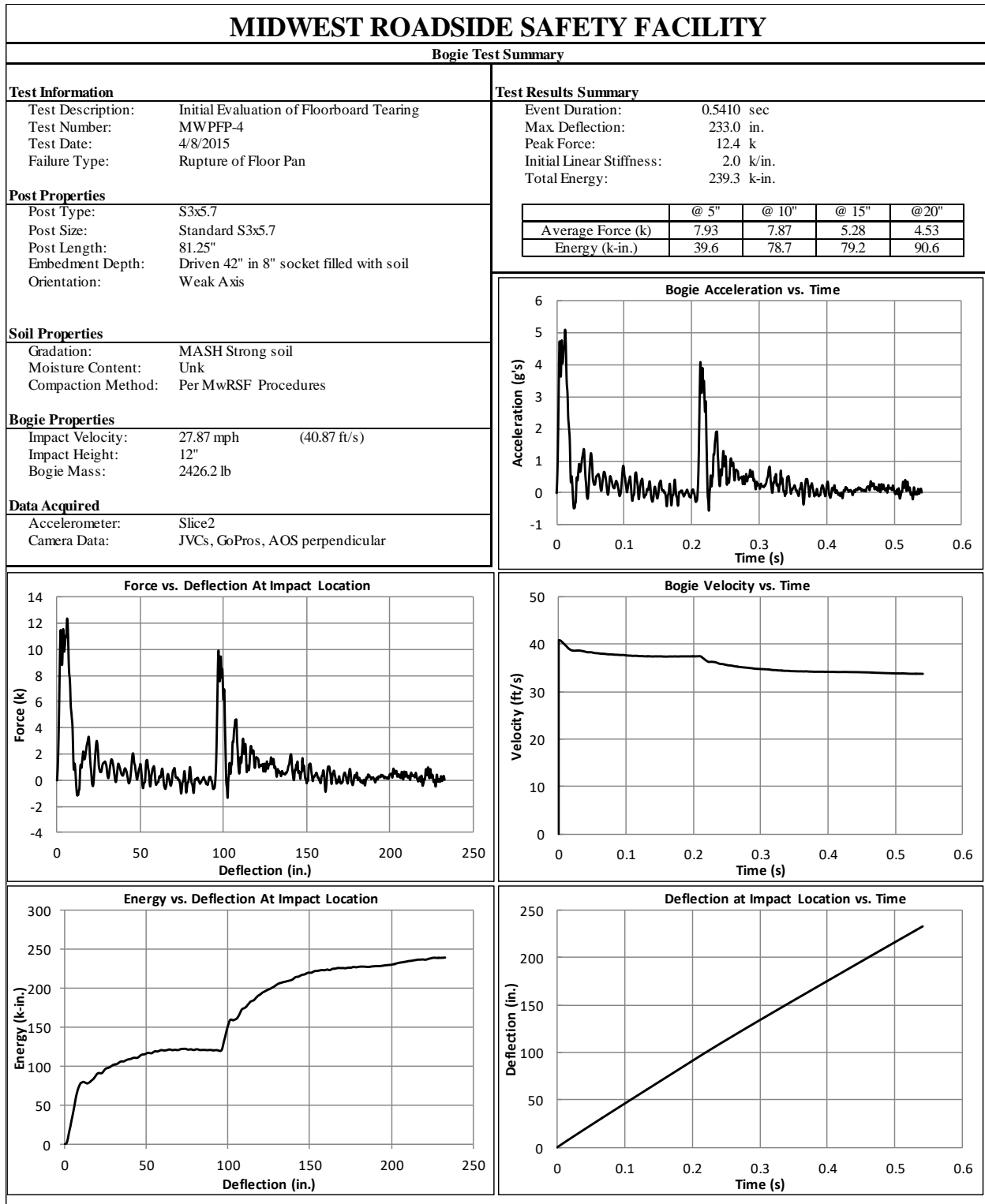


Figure B-4. Test No. MWFPF-4 Results (SLICE-2)

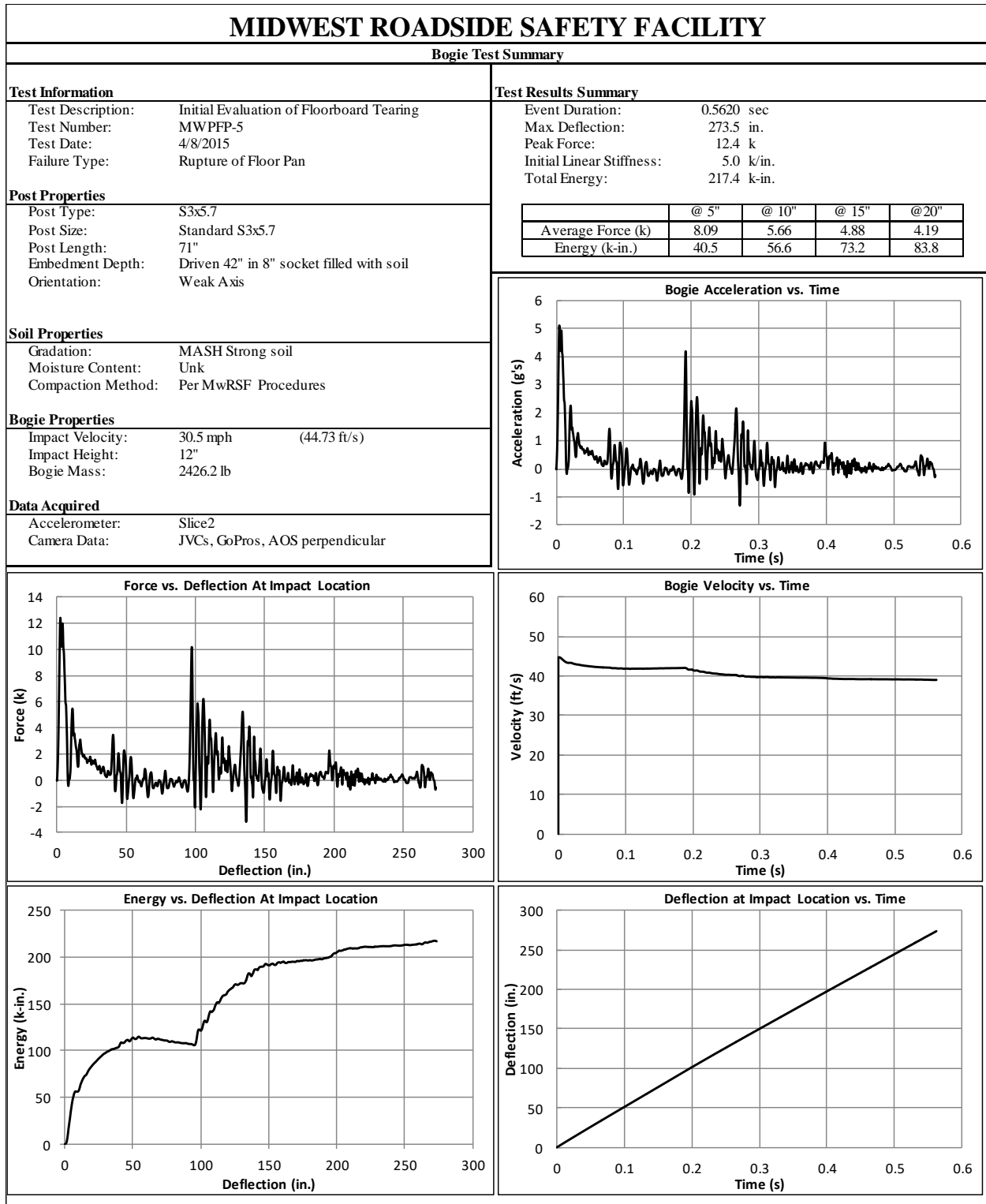


Figure B-5. Test No. MWFPF-5 Results (SLICE-2)

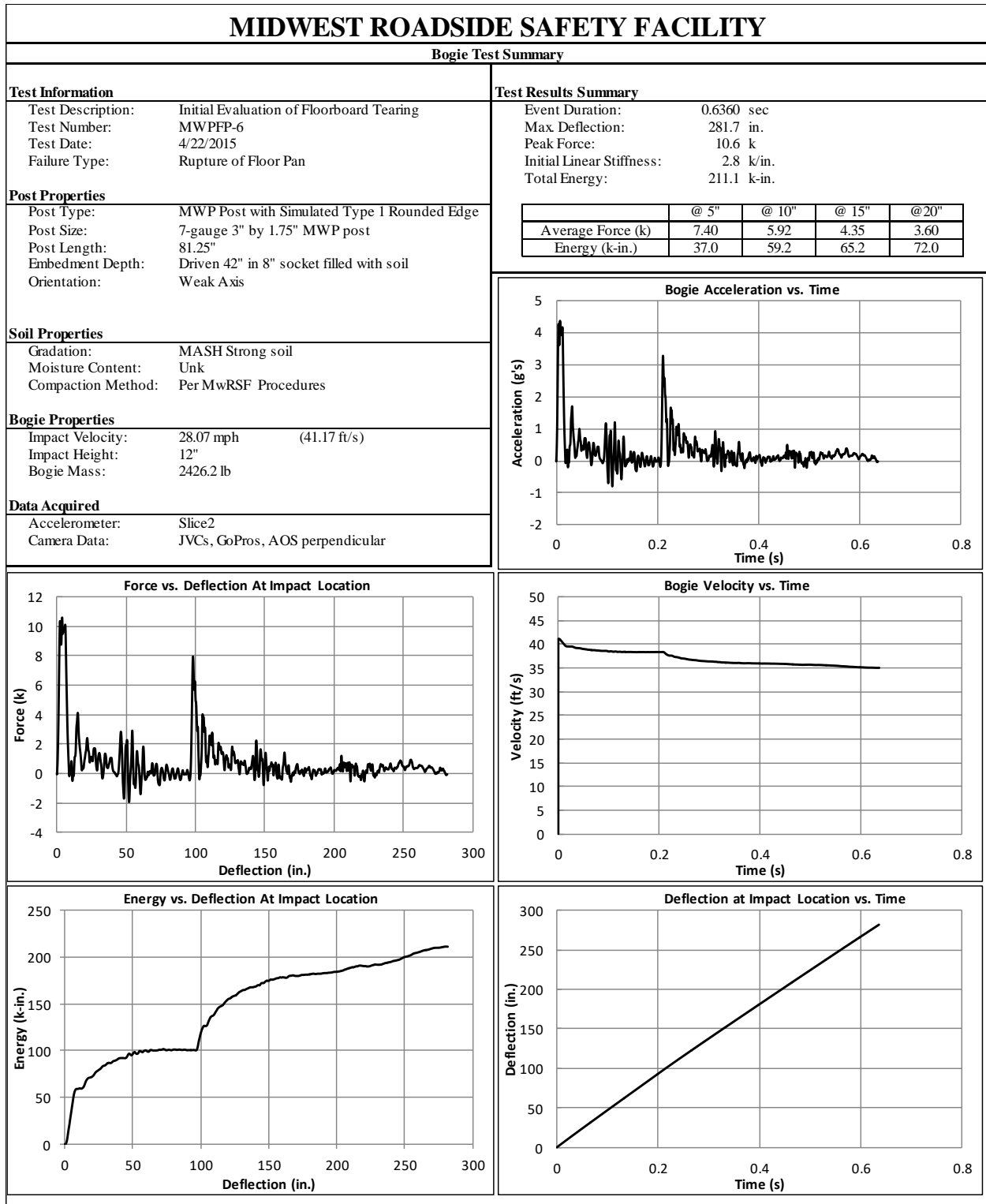


Figure B-6. Test No. MWFPF-6 Results (SLICE-2)

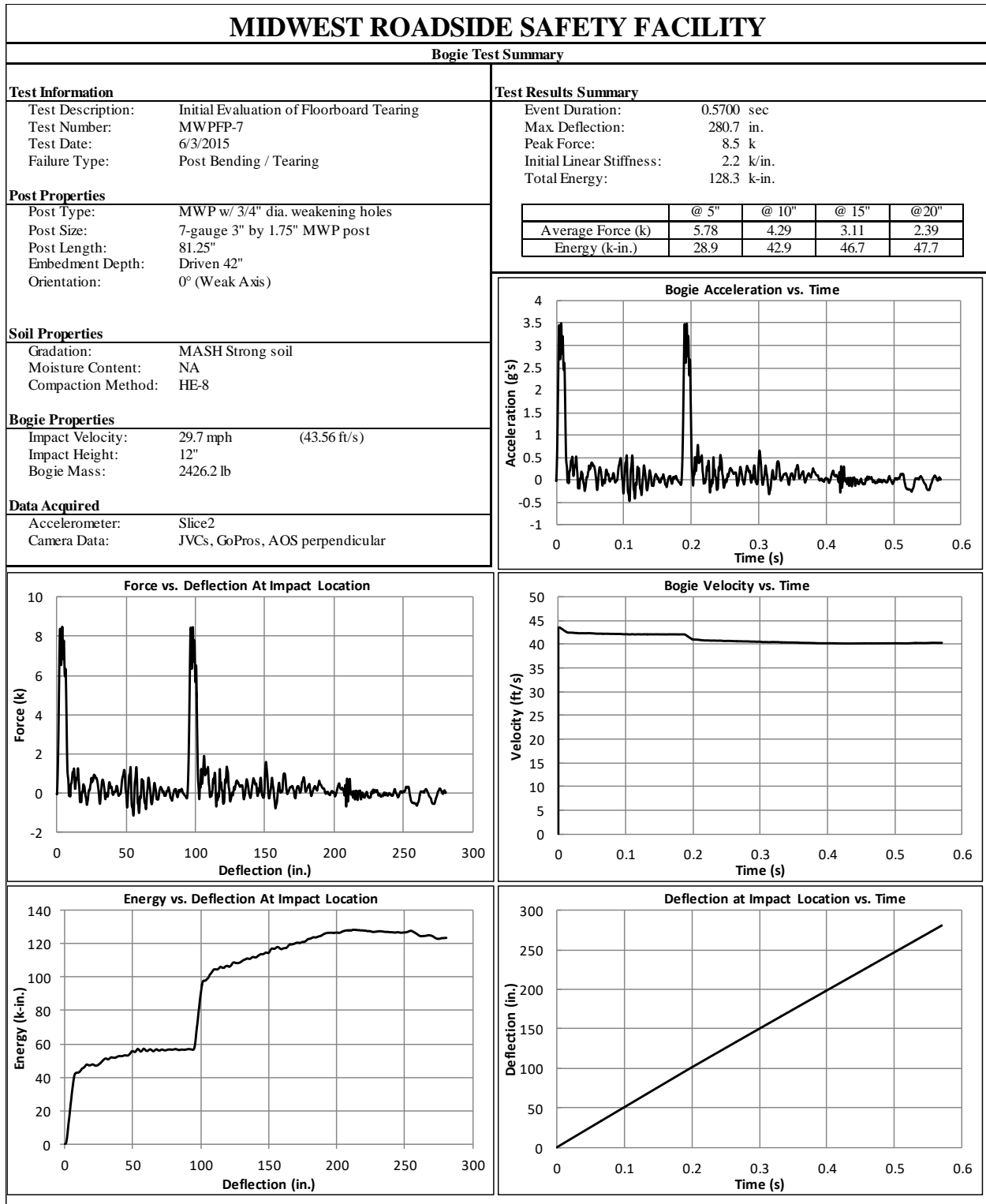


Figure B-7. Test No. MWFPF-7 Results (SLICE-2)

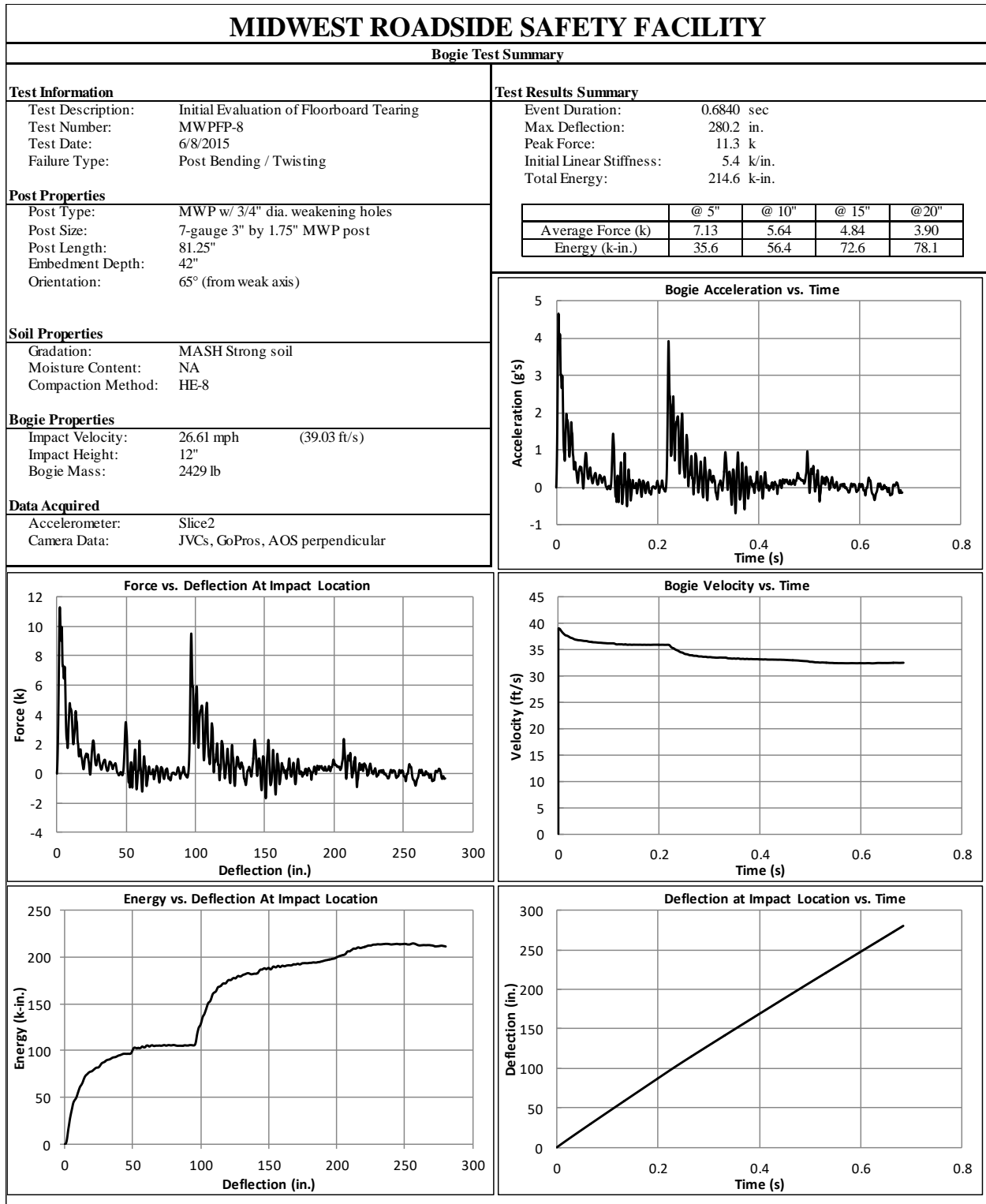


Figure B-8. Test No. MWFPF-8 Results (SLICE-2)

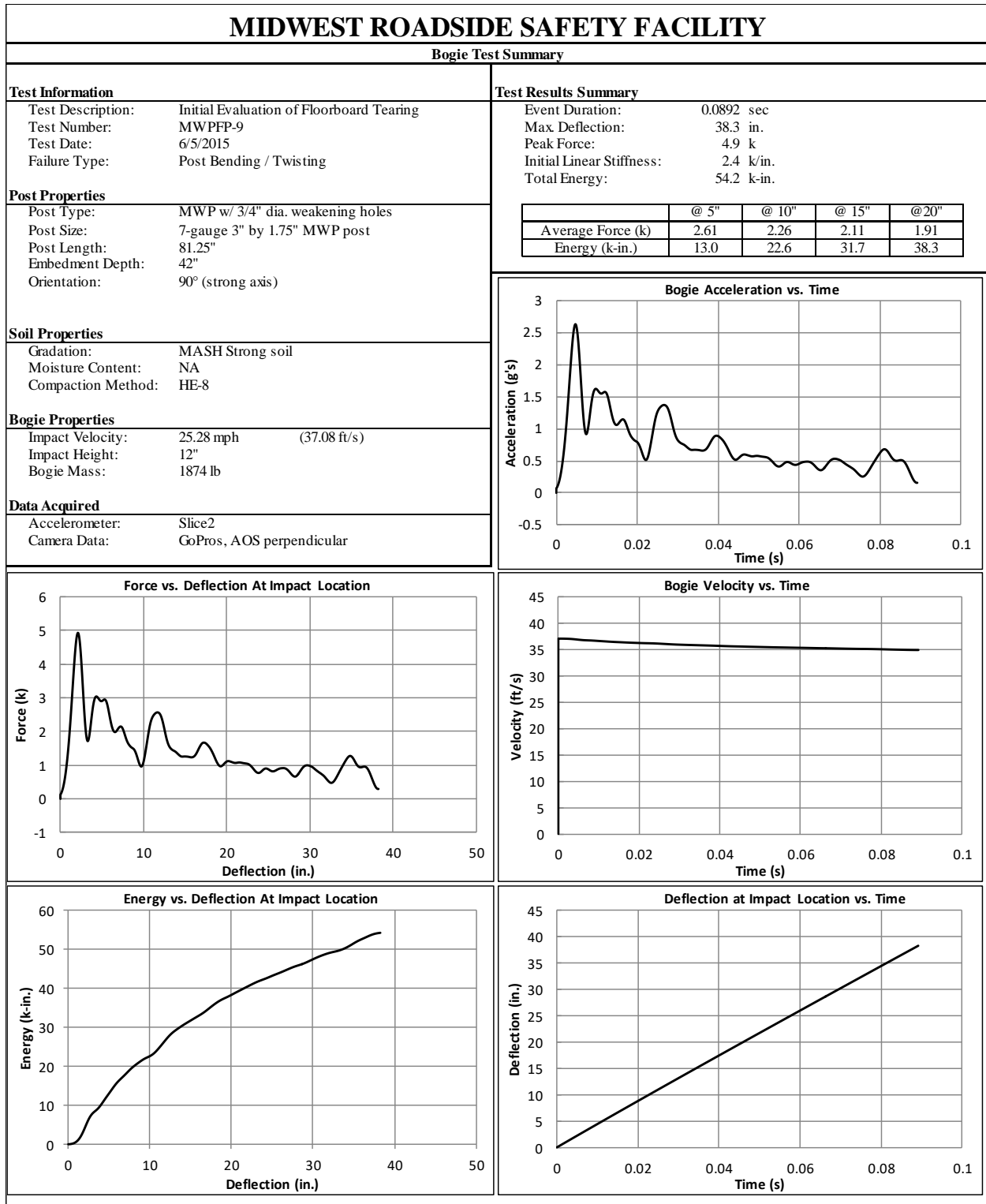


Figure B-9. Test No. MWFPF-9 Results (SLICE-2)

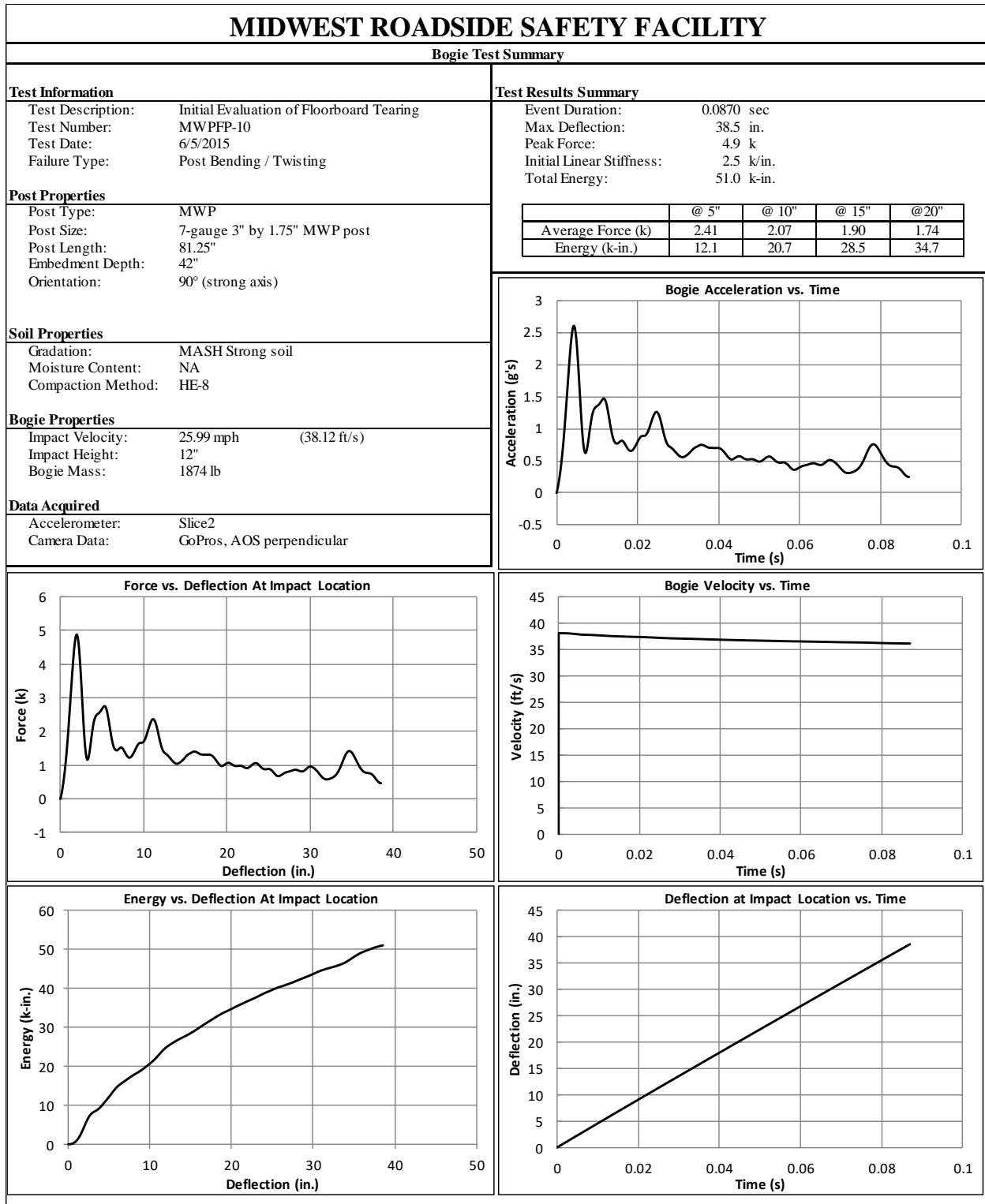


Figure B-10. Test No. MWFPF-10 Results (SLICE-2)

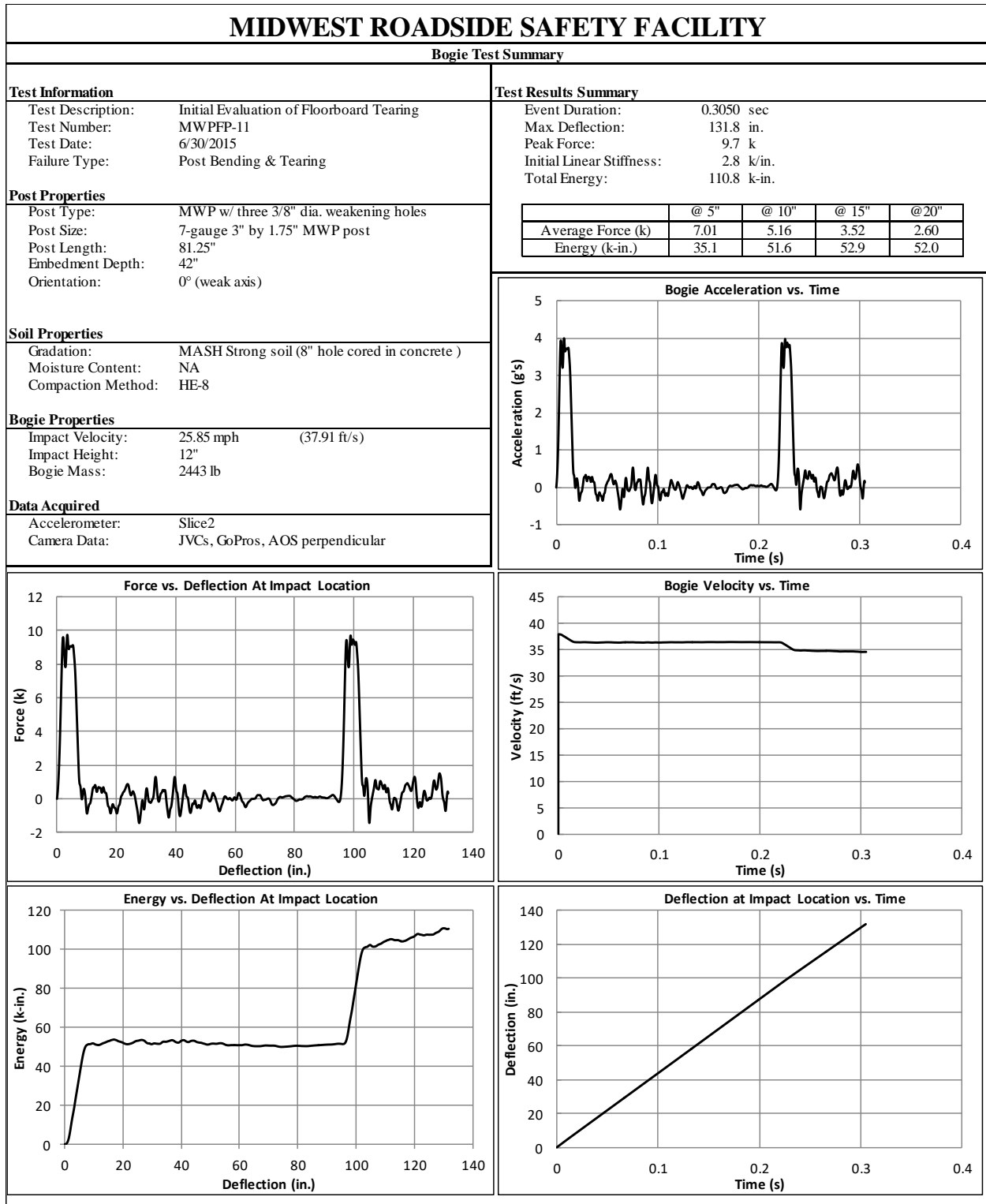


Figure B-11. Test No. MWFPF-11 Results (SLICE-2)

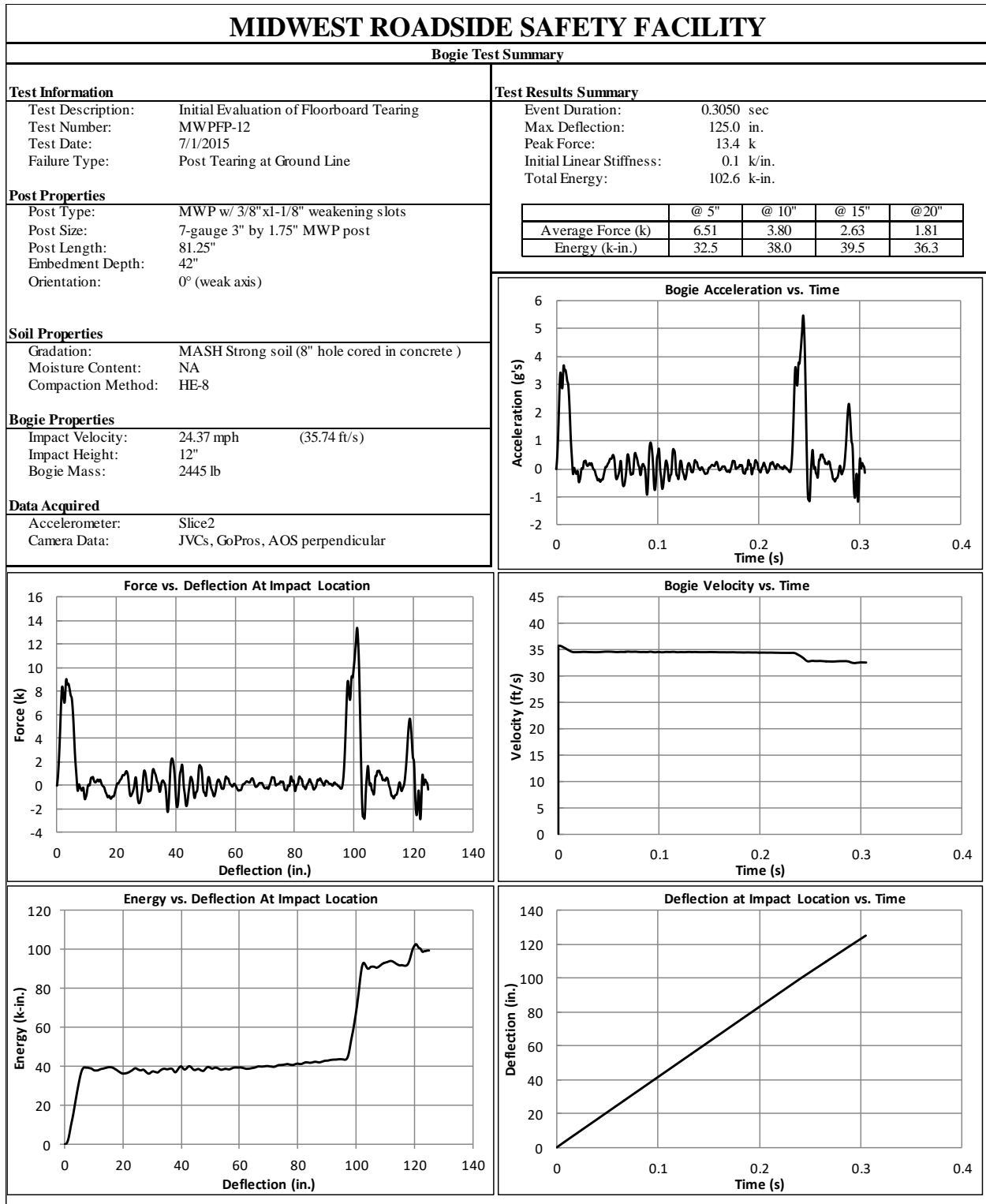


Figure B-12. Test No. MWFPF-12 Results (SLICE-2)

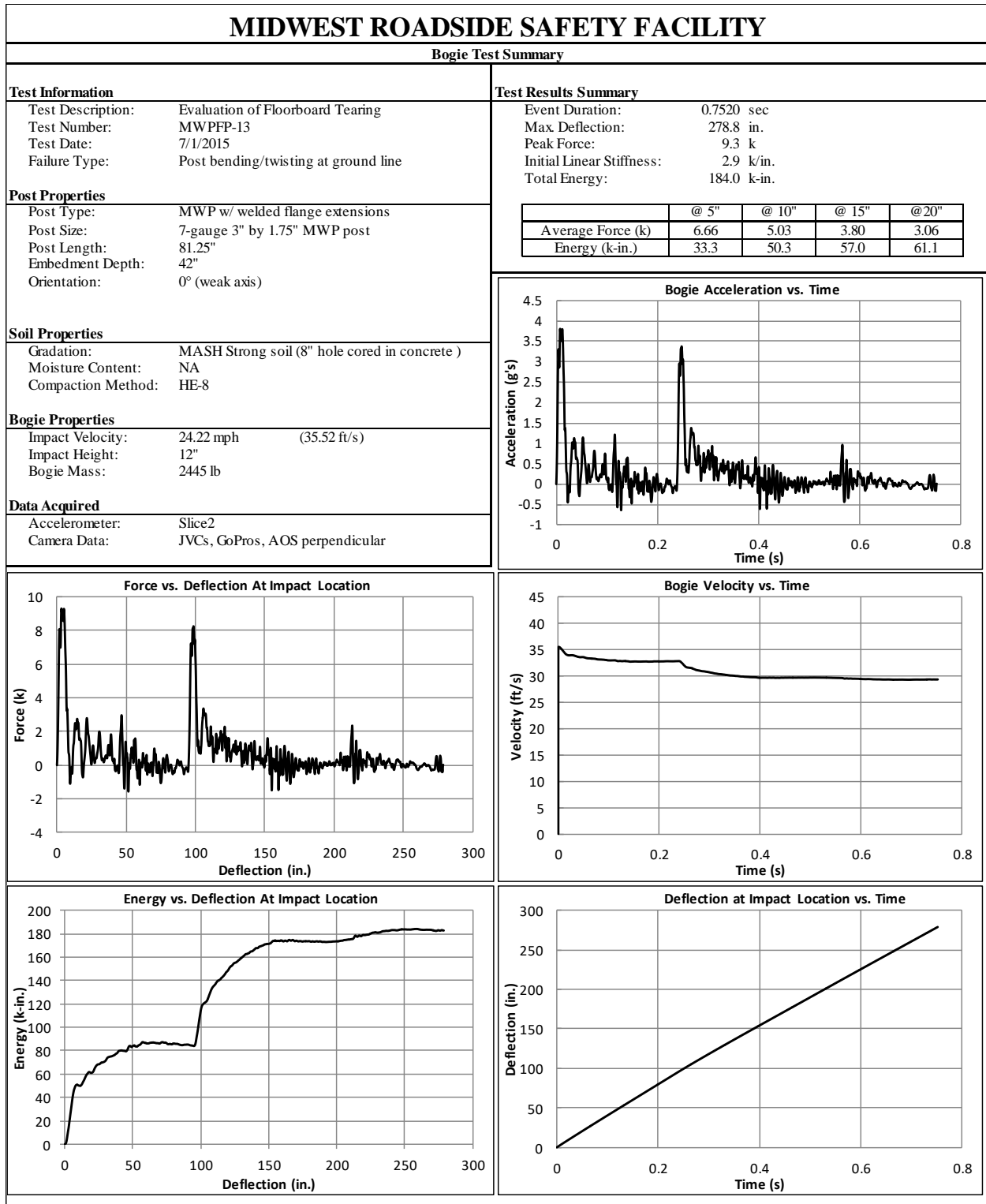


Figure B-13. Test No. MWFPF-13 Results (SLICE-2)

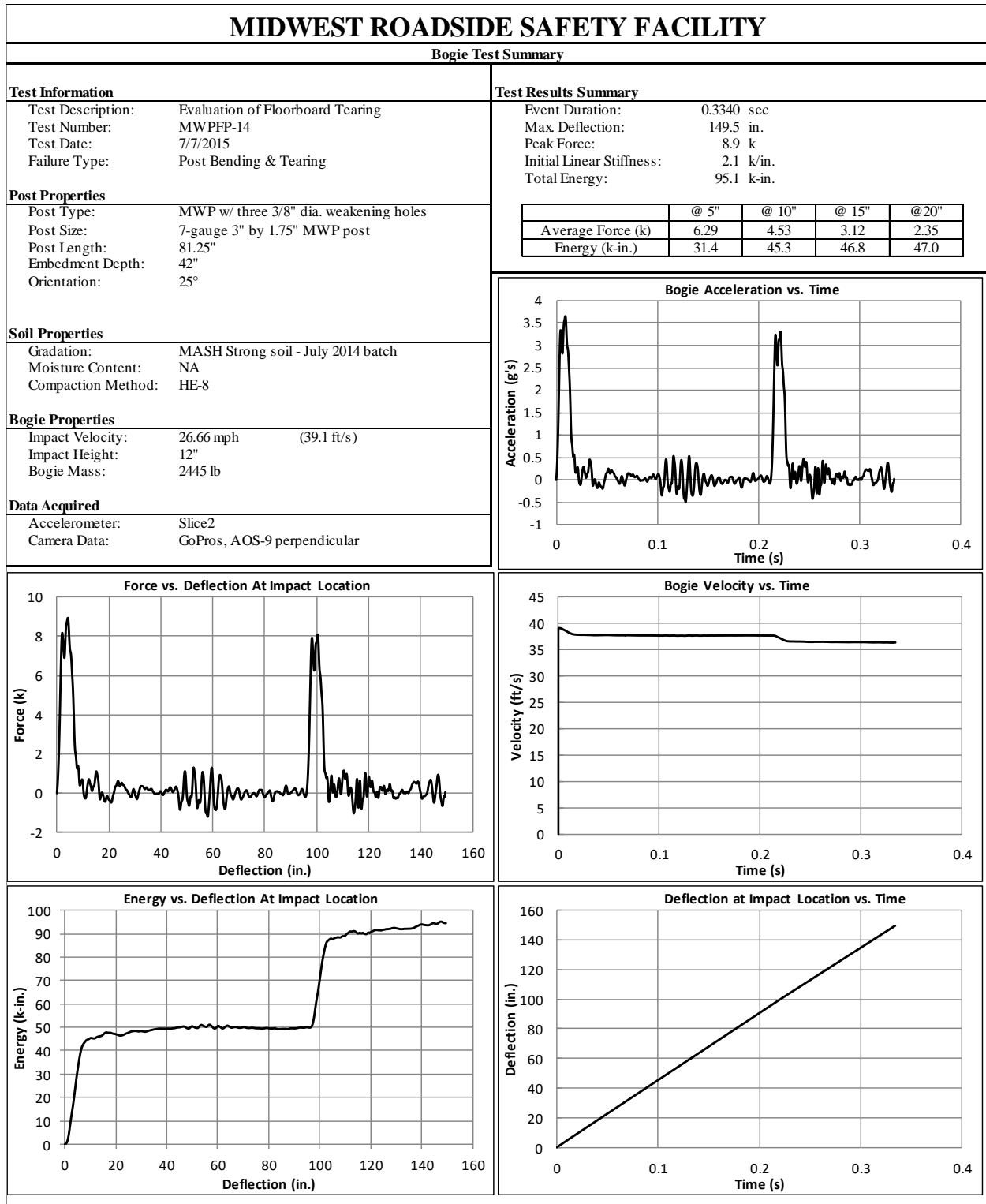


Figure B-14. Test No. MWFPF-14 Results (SLICE-2)

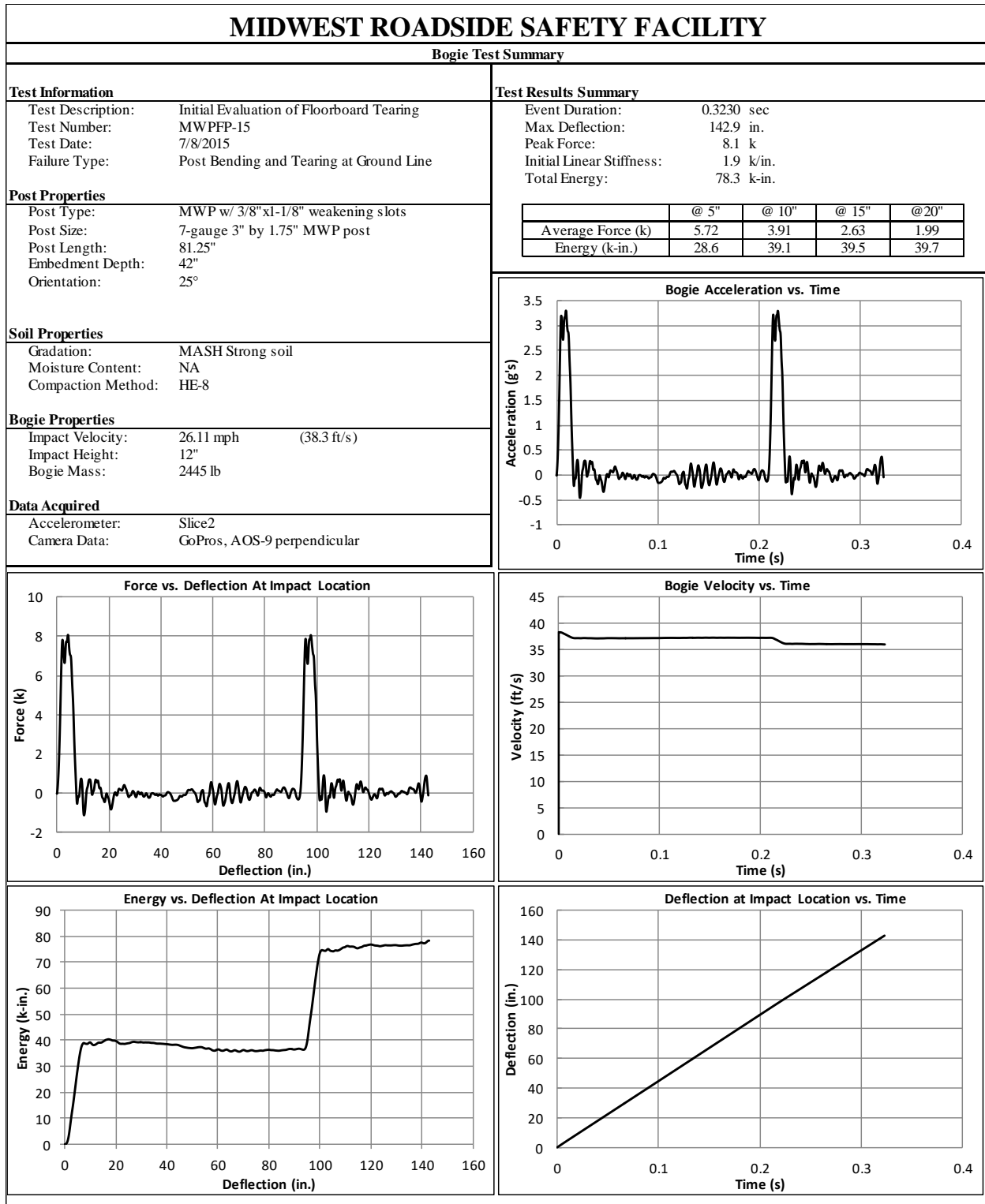


Figure B-15. Test No. MWFPF-15 Results (SLICE-2)

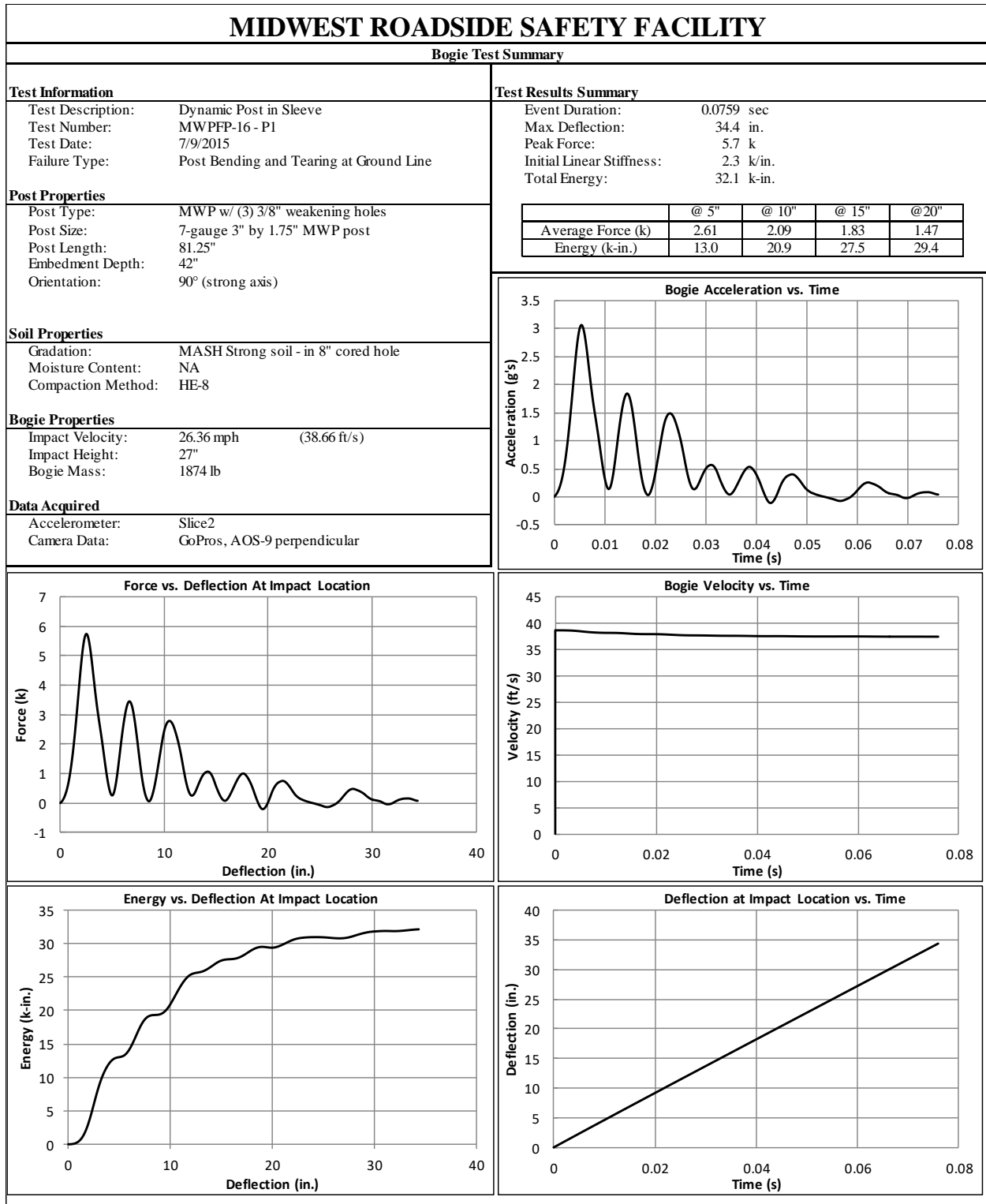


Figure B-16. Test No. MWFPF-16 P1 Results (SLICE-2)

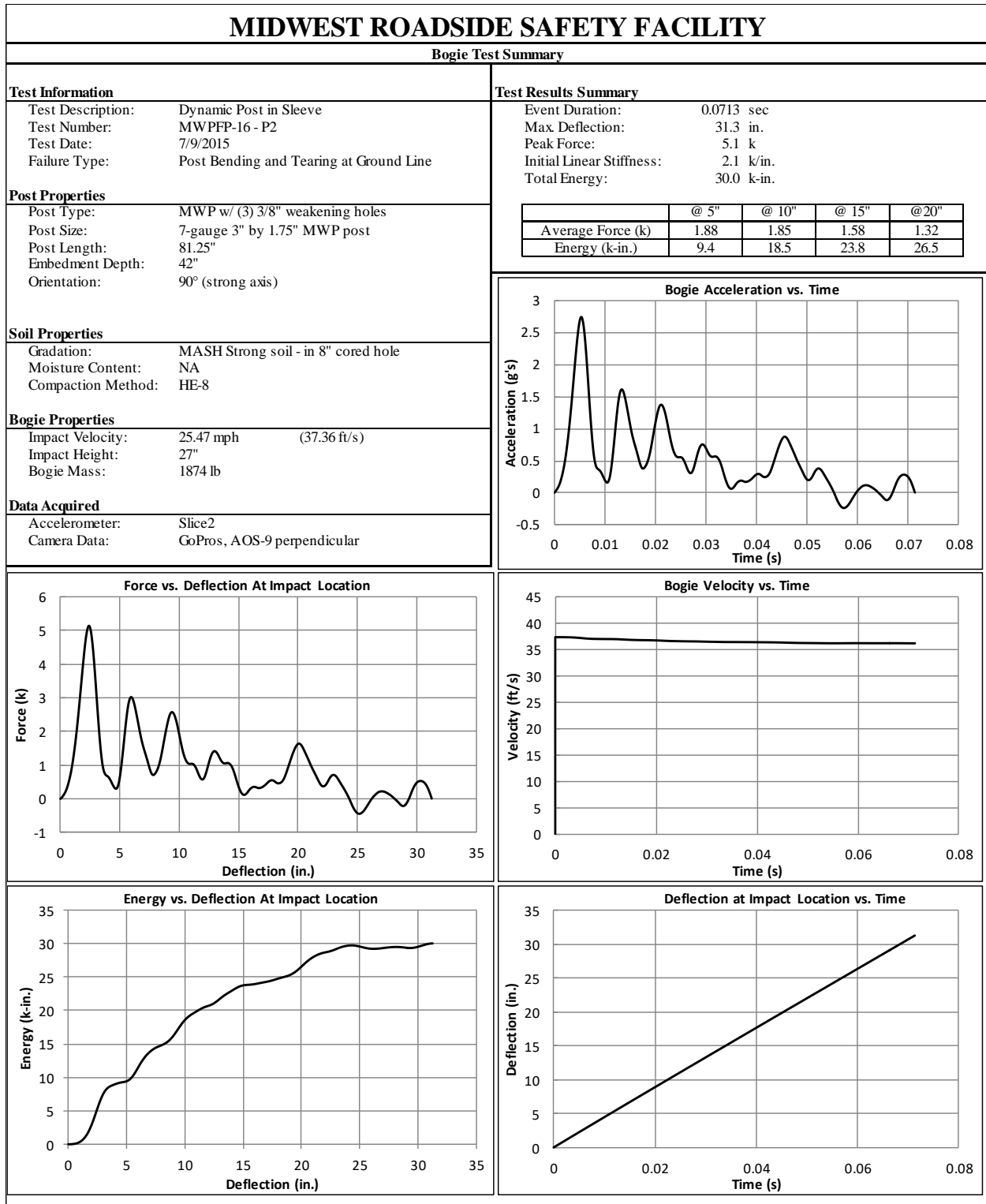


Figure B-17. Test No. MWFPF-16 P2 Results (SLICE-2)

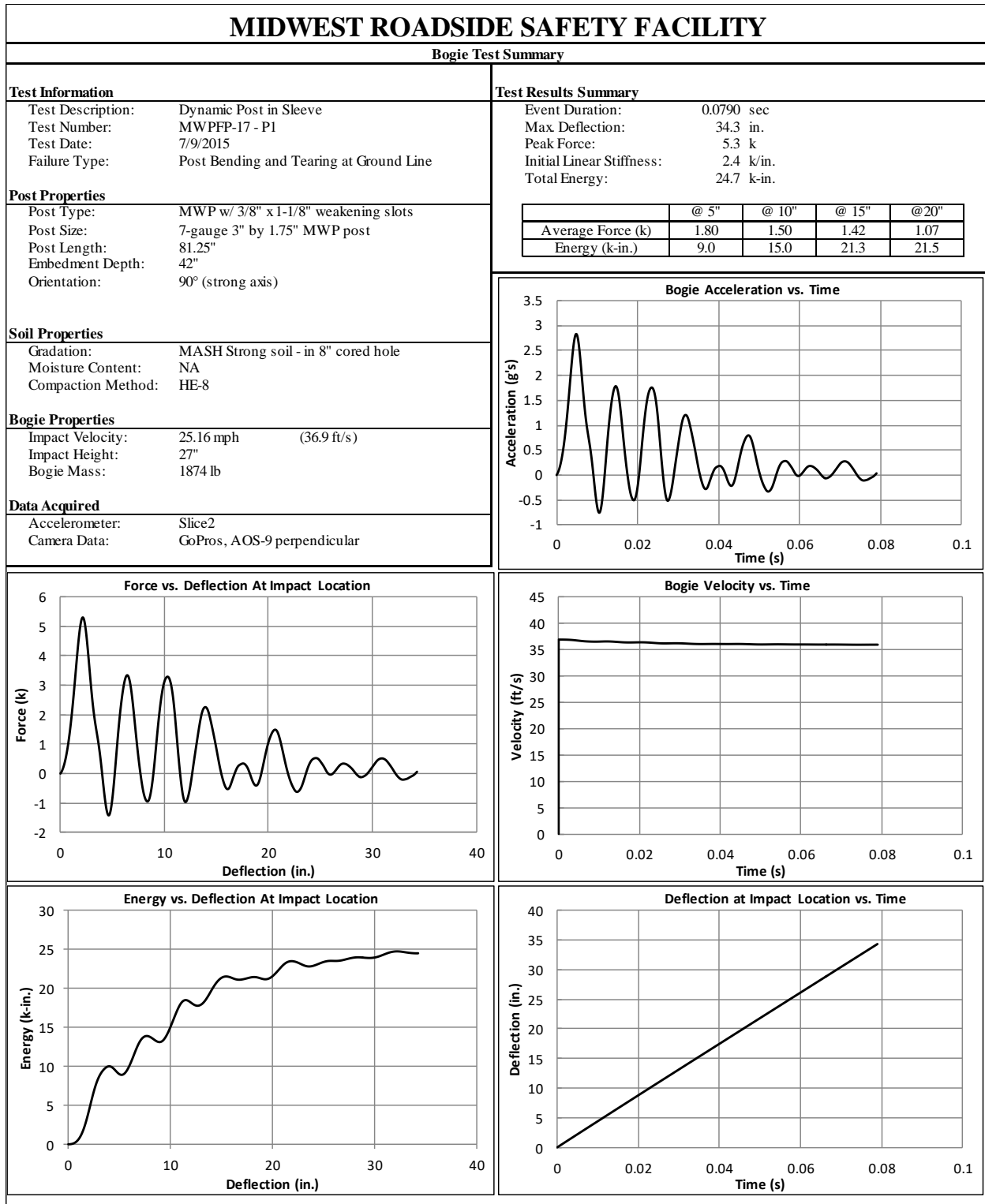


Figure B-18. Test No. MWPPF-17 P1 Results (SLICE-2)

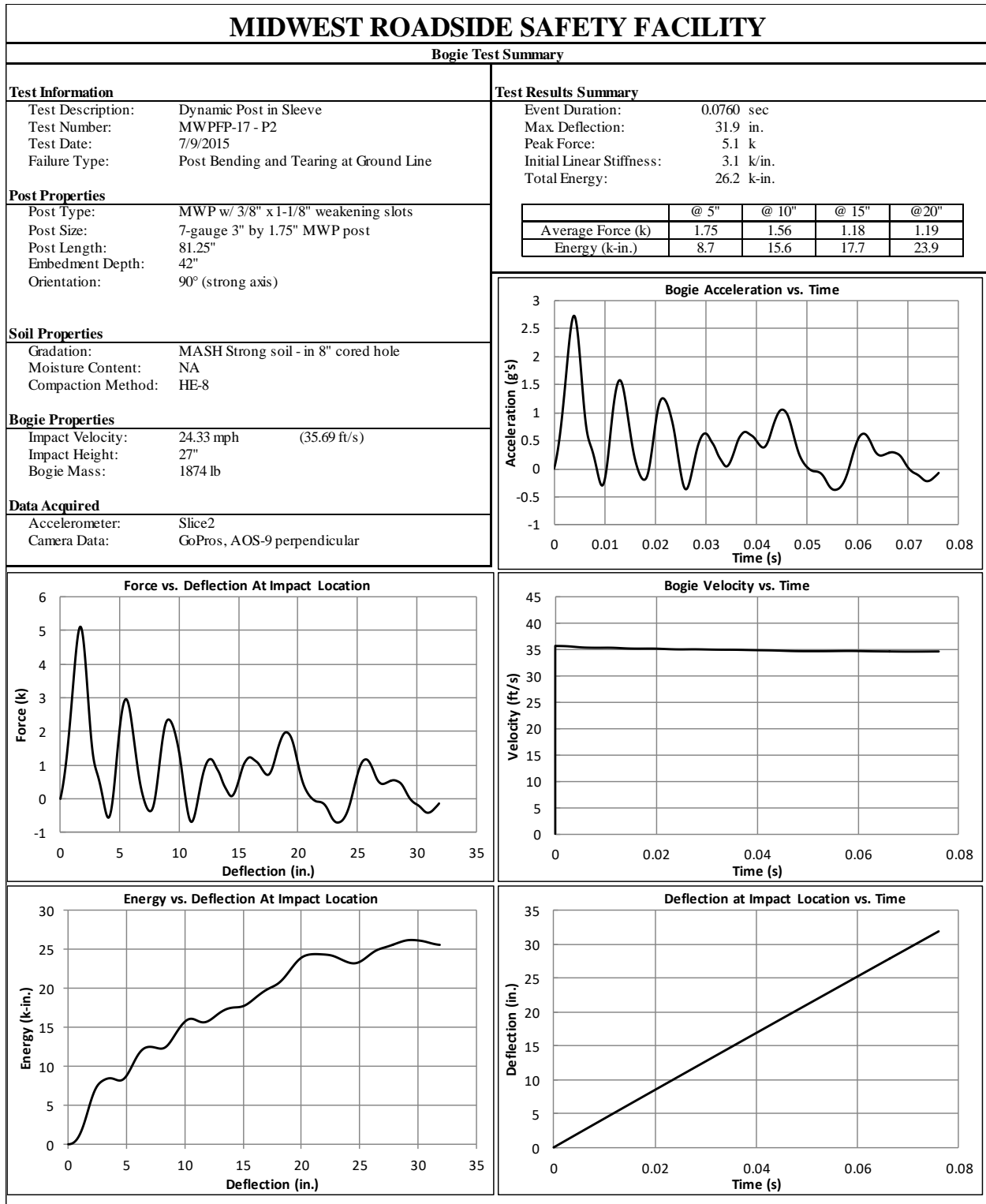


Figure B-19. Test No. MWPPF-17 P2 Results (SLICE-2)

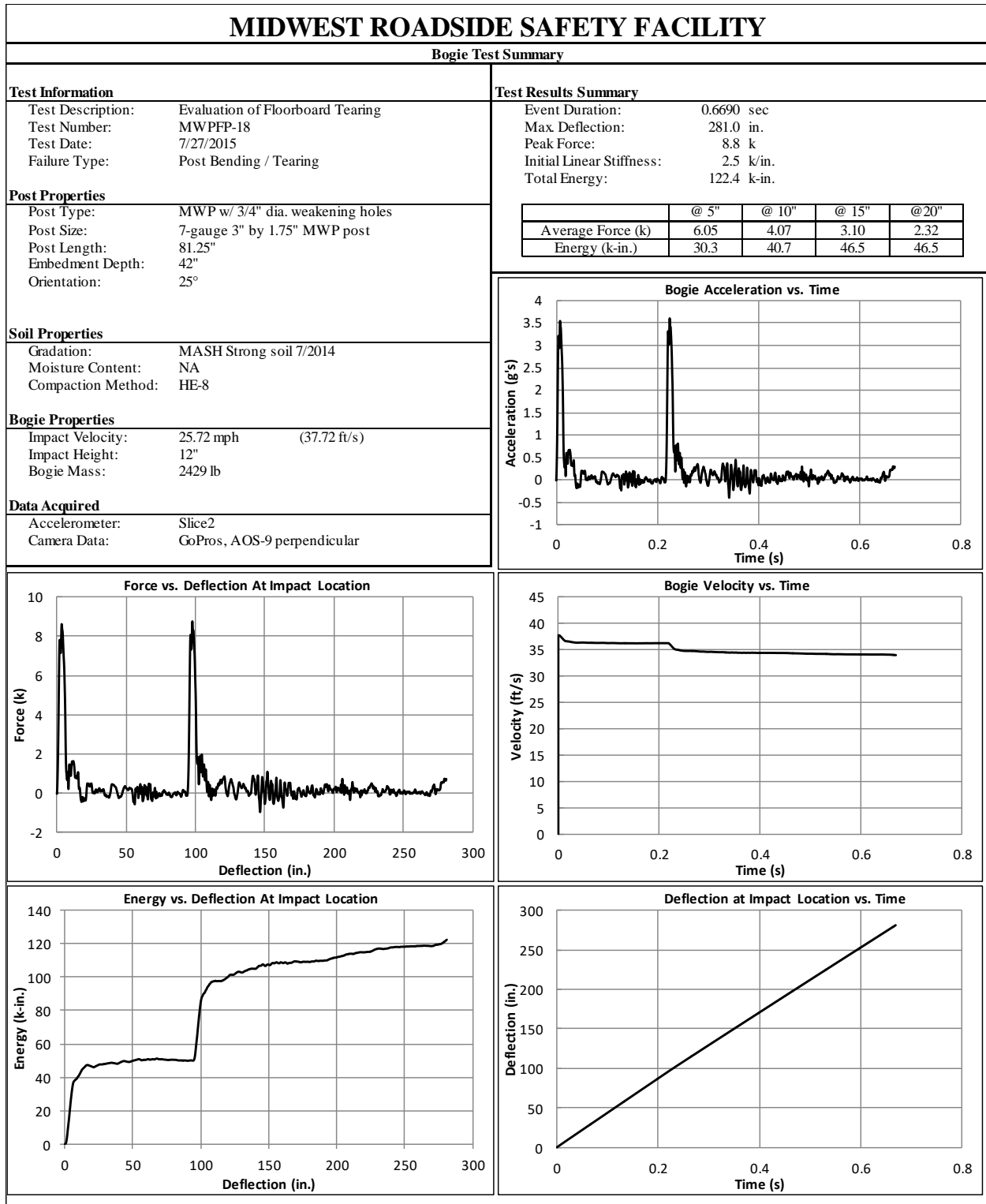


Figure B-20. Test No. MWFPF-18 Results (SLICE-2)

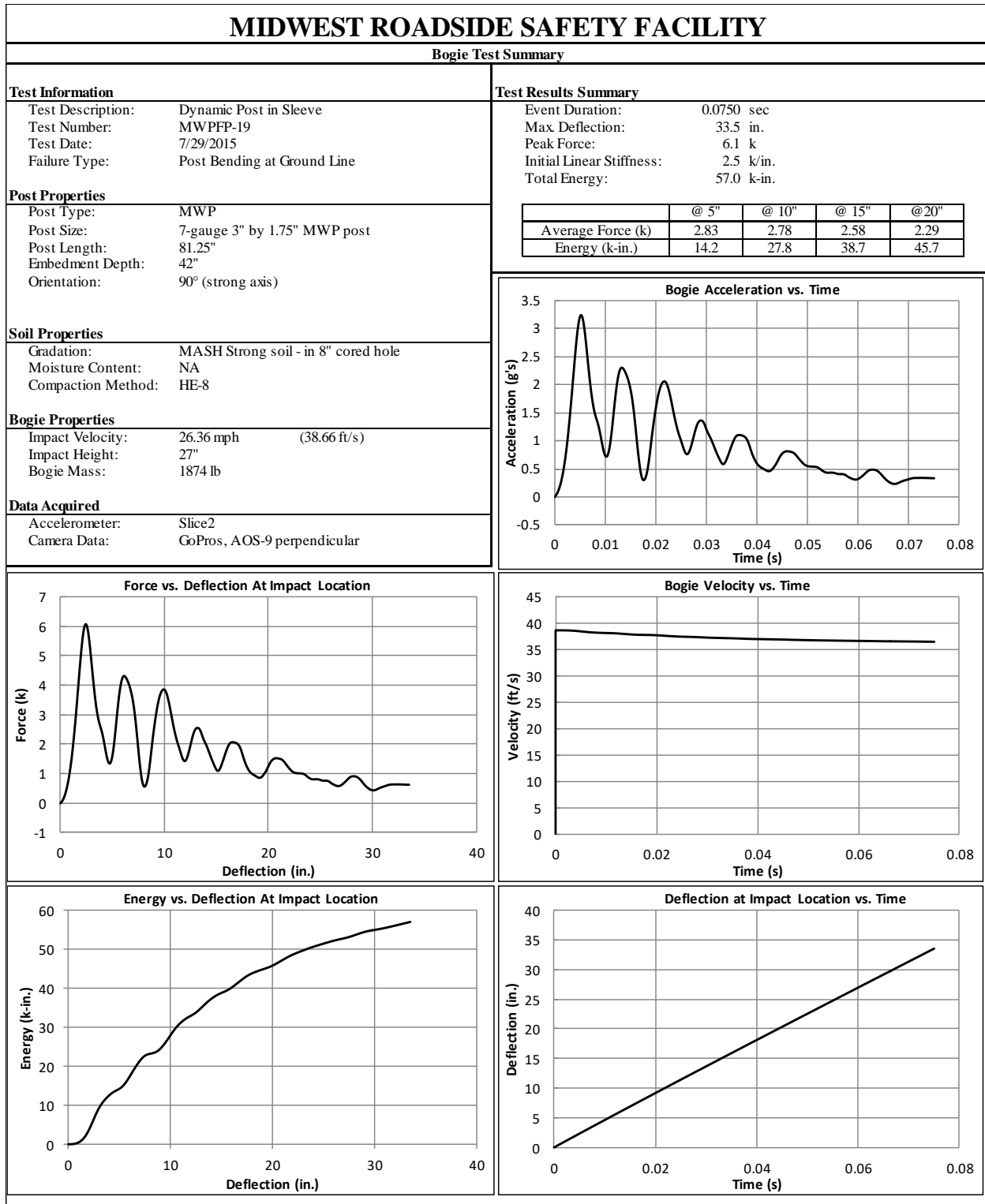


Figure B-21. Test No. MWFPF-19 Results (SLICE-2)

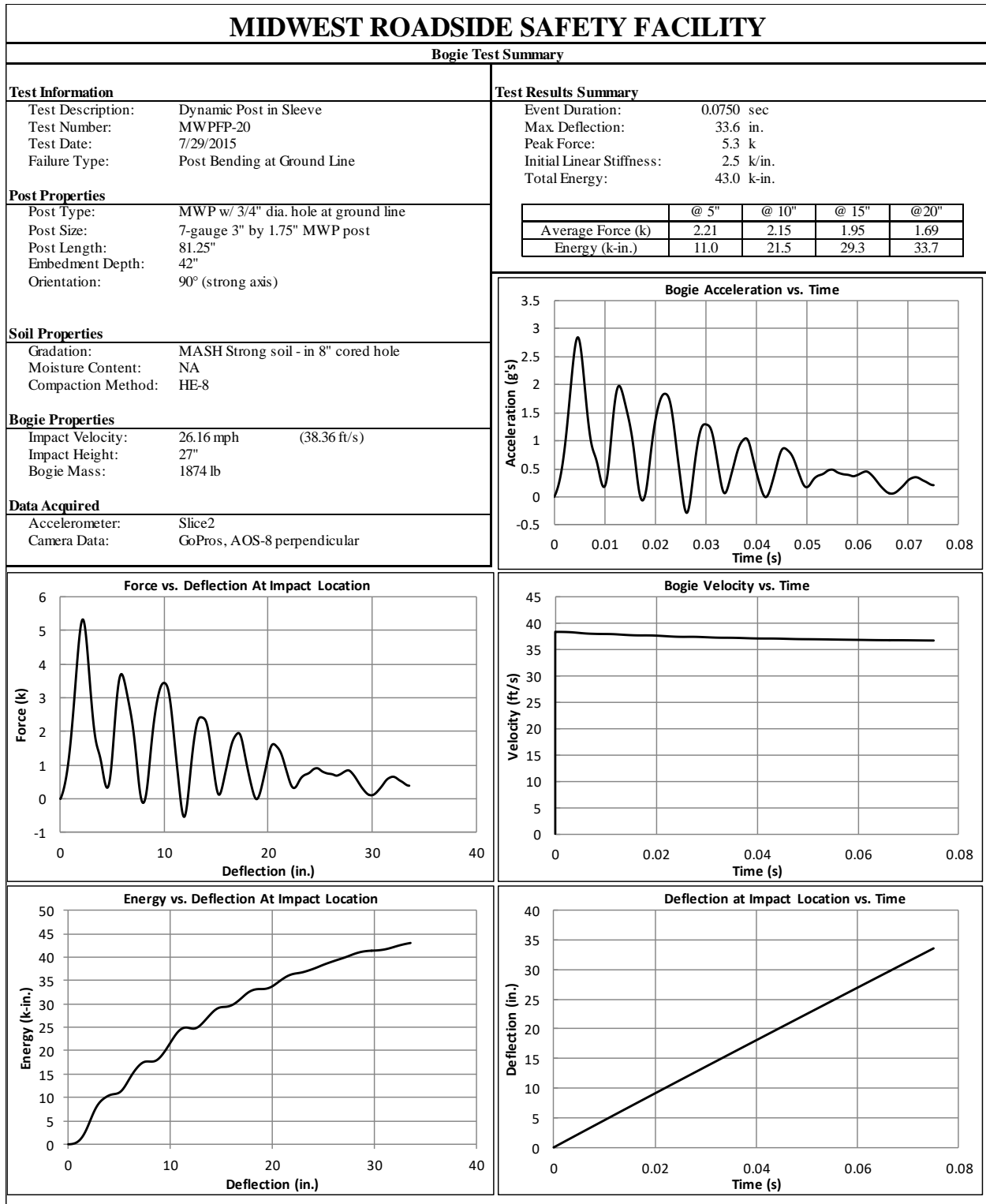


Figure B-22. Test No. MWFPF-20 Results (SLICE-2)

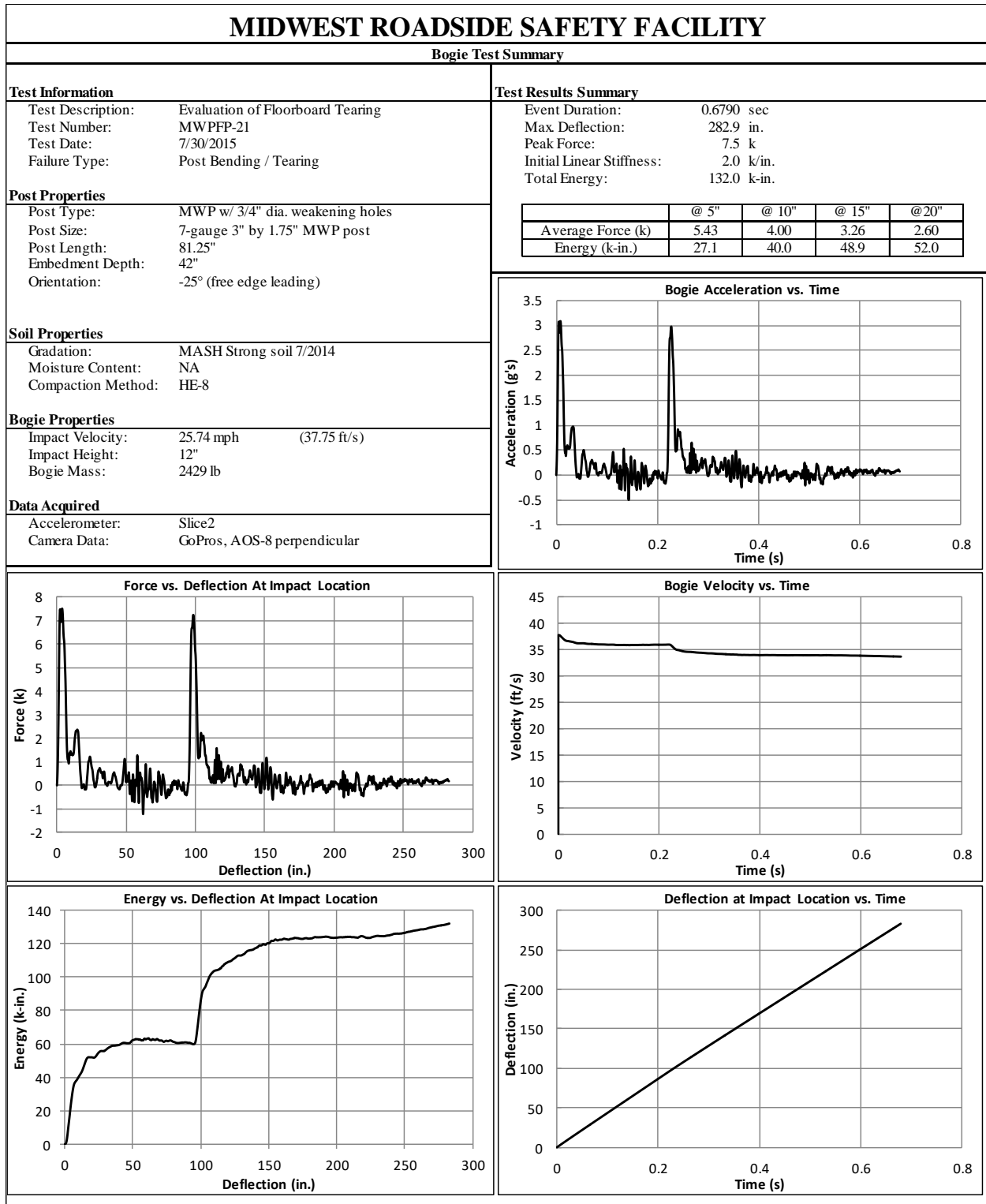


Figure B-23. Test No. MWFPF-21 Results (SLICE-2)

Appendix C. Evaluation Of Splice Hardware Drawing Set

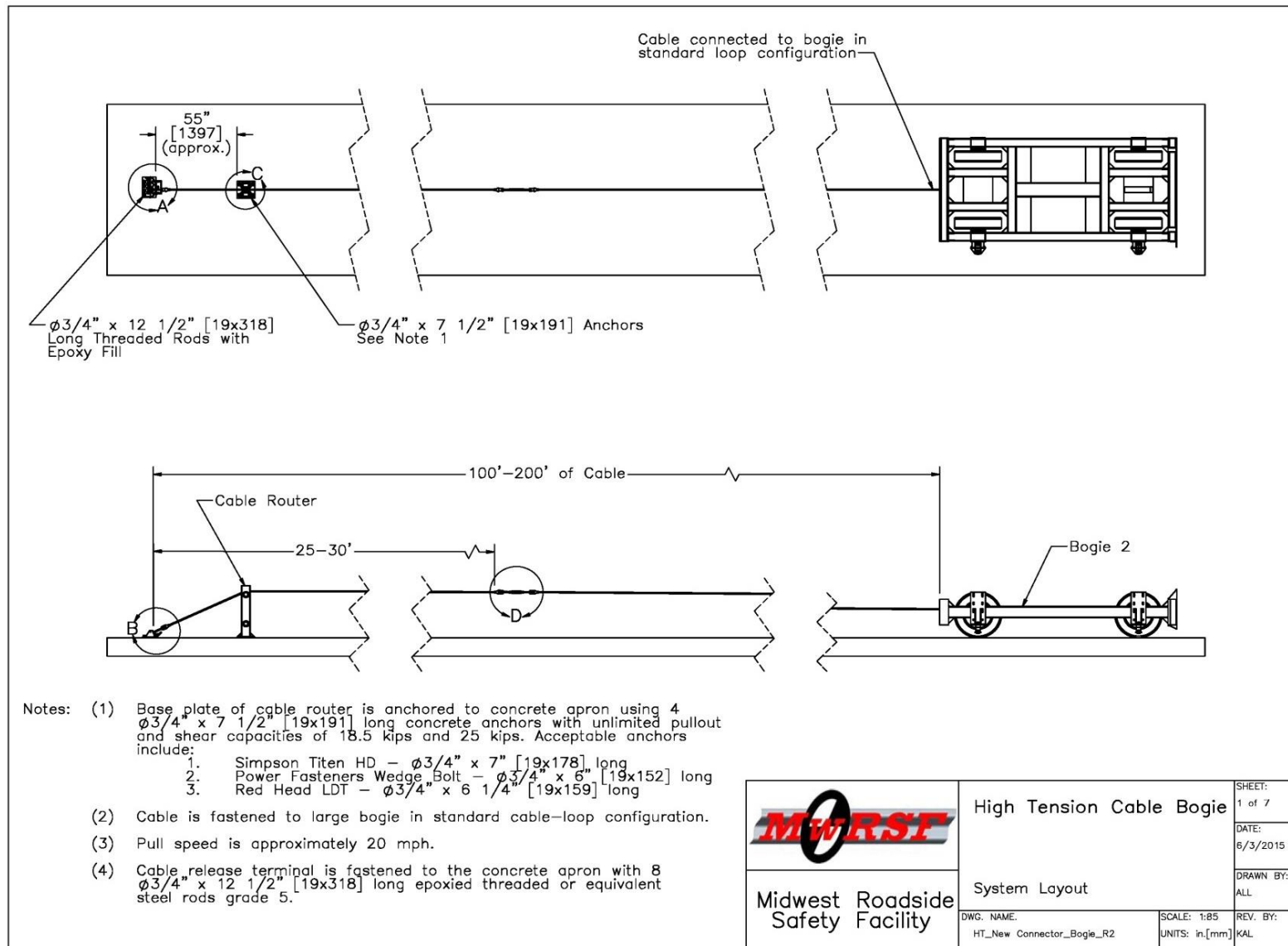


Figure C-1. System Layout, Test Nos. BBNC-1 through BBNC-3

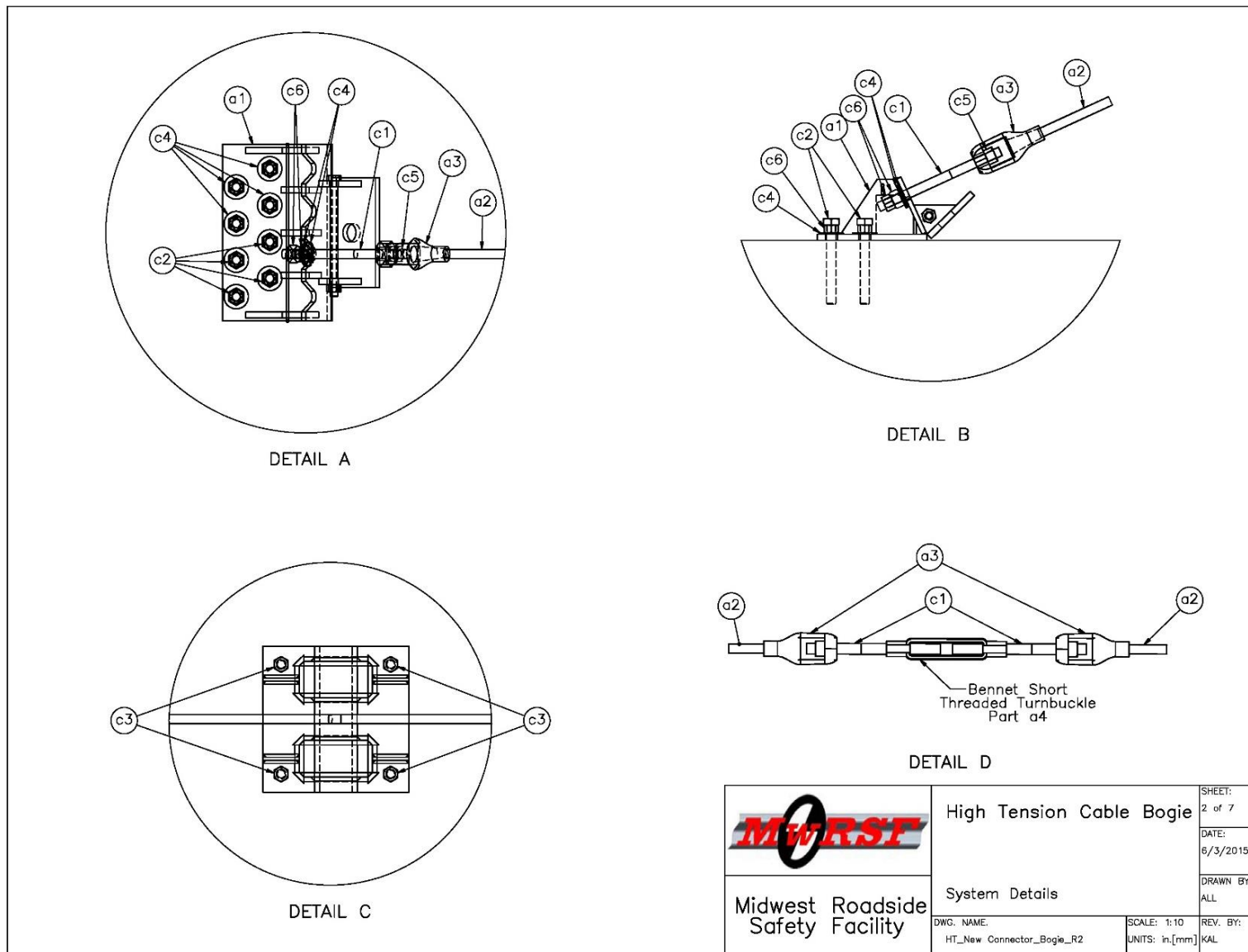


Figure C-2. System Details, Test Nos. BBNC-1 through BBNC-3

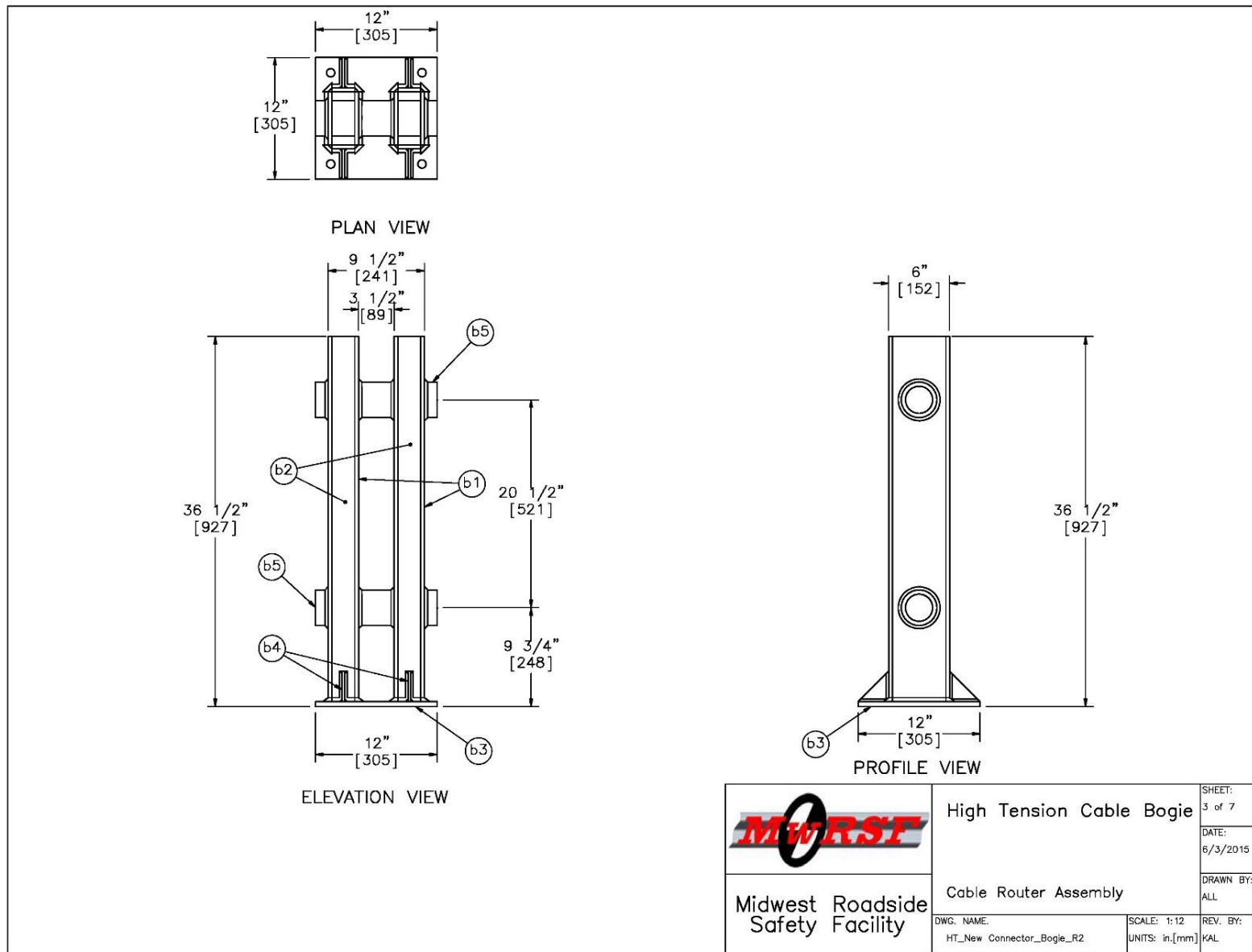


Figure C-3. Cable Router Assembly, Test Nos. BBNC-1 through BBNC-3

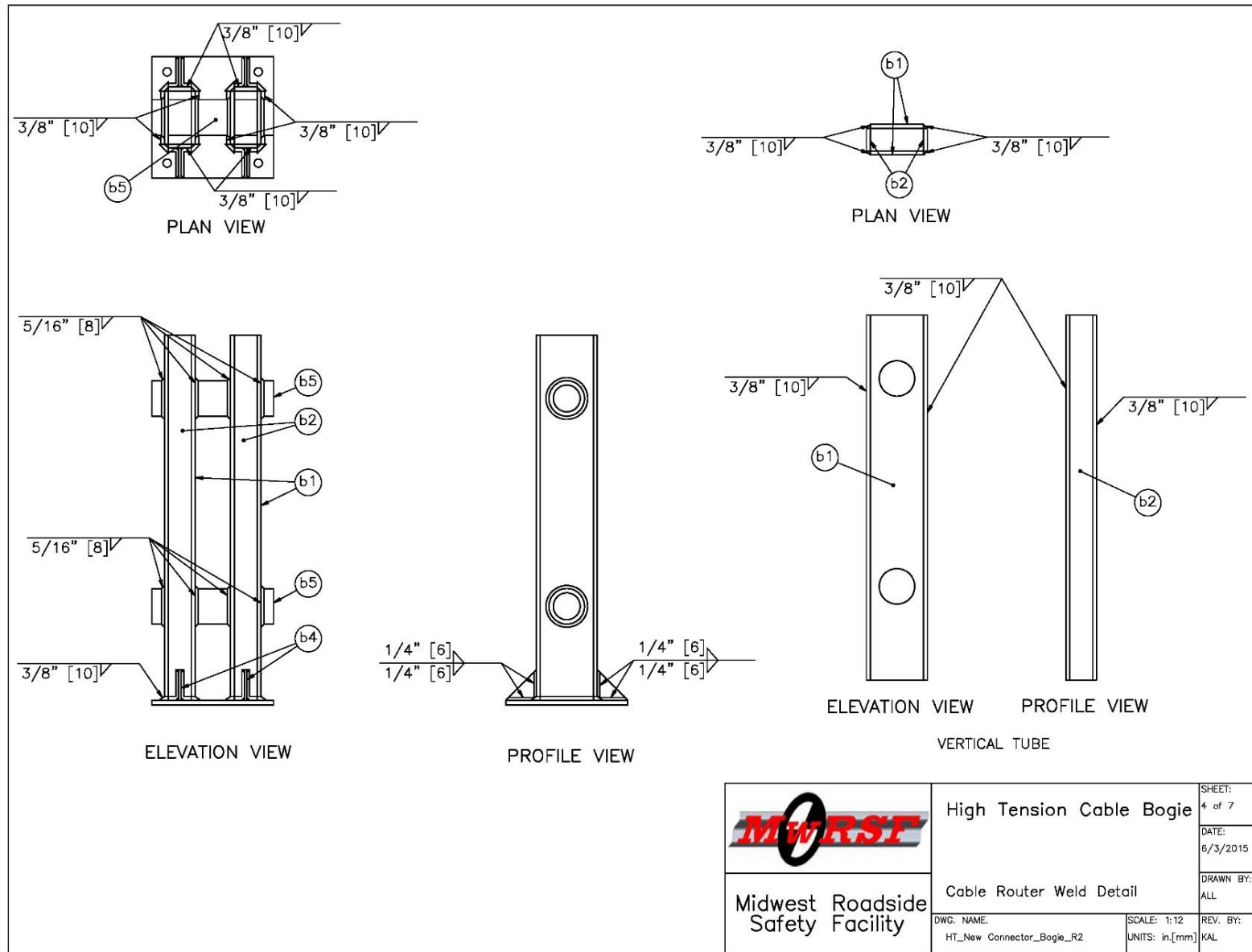


Figure C-4. Cable Router Weld Detail, Test Nos. BBNC-1 through BBNC-3

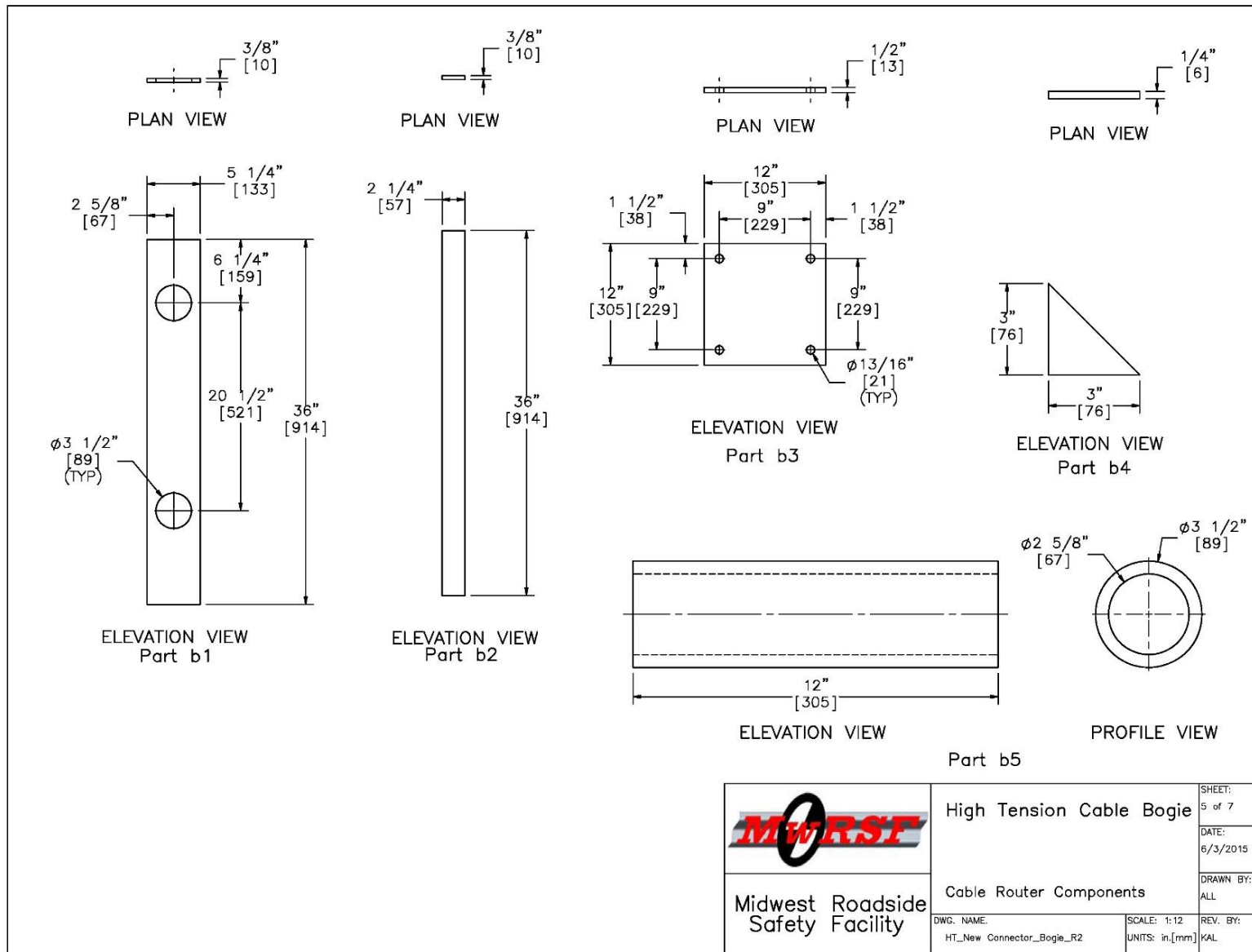


Figure C-5. Cable Router Components, Test Nos. BBNC-1 through BBNC-3

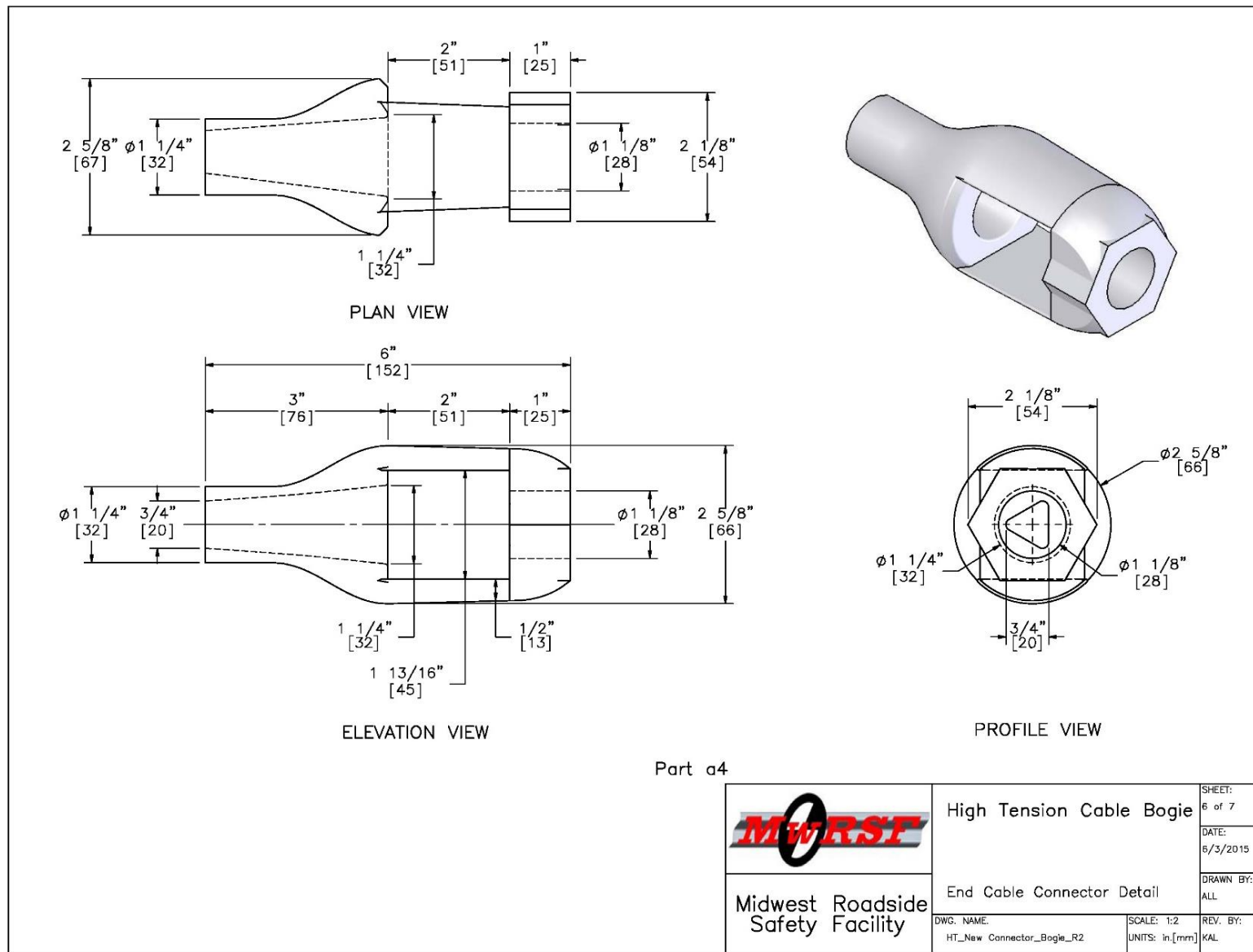


Figure C-6. End Cable Connector Detail, Test Nos. BBNC-1 through BBNC-3

Item No.	QTY.	Description	Material Spec	Hardware Guide
a1	1	Anchor Bracket	A36 Steel	—
a2	2	Cable	6x19 Wire Strand Core	—
a3	3	Cable End Coupler	ASTM A449	—
a4	1	Bennet Short Threaded Turnbuckle	Not Specified	—
b1	4	Vertical Tube Side Plate	ASTM A36 Steel	—
b2	4	Vertical Tube Front Plate	ASTM A36 Steel	—
b3	1	Cable Router Base Plate	ASTM A36 Steel	—
b4	4	Vertical Tube Gussets	ASTM A36 Steel	—
b5	2	Cable Router Guide Strap Pipe	ASTM A36 Steel	—
c1	3	3/4" x 11" [19x483] Dia. Threaded Rod	ASTM A449	—
c2	8	3/4" x 12 1/2" [19x318] Long Epoxied Threaded Rod	ASTM A449	—
c3	4	3/4" [19] Dia. UNC, 7 1/2" [191] Long Hex Bolt and Nut	Bolt SAE J429 Gr. 5, Nut ASTM A563	FBX20b
c4	10	3/4" [19] Dia. Plain Round Washer	ASTM F844	FWC20b
c5	3	3/4" Dia. UNC, Heavy Square Nut	ASTM A563M	FNS20
c6	10	3/4" [19] Dia. UNC, Heavy Hex Nut	ASTM A563 DH	FNX20b
<div> <div>  <div> <div>High Tension Cable Bogie</div> <div>Bill of Materials</div> </div> </div> <div> <div> <div> <div>DWG. NAME:</div> <div>HT_New Connector_Bogie_R2</div> </div> <div> <div>SCALE: 1:2</div> <div>UNITS: in.[mm]</div> </div> </div> <div> <div> <div>SHEET:</div> <div>1 of 1</div> </div> <div> <div>DATE:</div> <div>6/3/2015</div> </div> <div> <div>DRAWN BY:</div> <div>ALL</div> </div> <div> <div>REV. BY:</div> <div>KAL</div> </div> </div> </div> </div>				

Figure C-7. Bill of Materials, Test Nos. BBNC-1 through BBNC-3

Appendix D. Material Specifications

NUCOR

Berkeley Division of NUCOR Corporation
ISO/TS 16949 Registered

DELIVER TO: certs

phoenix metals

P.O. Box 2259
Mt. Pleasant, SC 29465

METALLURGICAL TEST REPORT
Nucor Steel - Berkeley
a division of NUCOR corporation

Phone: 843-336-6000
Sales Fax: 843-336-6150

Issuance Date 10/02/14 MTR# 1243953 MTR BER INQUIRIES@NUCOR.COM

Sold PHOENIX METALS COMPANY Ship PHOENIX METALS Ship date 10/02/14
To: PO BOX 805 To: 12420 MEANS COURT Bill of Lading # 1096908
PO BOX 7849 Vehicle # 51237
NORCROSS, GA 30091 CHARLOTTE, NC 28278

P/O # 0309281
Mill Order # 356338-1
Part # 5444 A60 023

Gauge x Width .0230 MIN X 48.0000 MIN A60
GALVANNEAL
ASTM A653 / CS TYPE B (LFQ) / 2013
Chemistry certification only

Total Wgt 44650.00 LB

MWP Floor Pan material SMT

Heat	C	Mn	P	S	Si	Cu	Ni	Cr	Mo	Sn	Al	V	Nb	N	Ti	B	Ca
2410835	.02	.16	.011	.003	.02	.08	.03	.03	.00	.005	.030	.003	.001	.005	.001	.003	.002

Coil(tag)/Heat-Bar : 149412.100 2410835-4 149412.200 2410835-4
(22400.00 LB) (22250.00 LB)

Mill Test Reports according to EN10204 3.1

All material is sold subject to the description, specifications and terms and conditions set forth on the face and reverse side of Nucor Steel - Berkeley's sales order acknowledgment.

Tensile Testing, when applicable, is performed in accordance with ASTM A-370 specifications. Specimen is machined to standard rectangular test configuration (Figure 3 of ASTM A-370) with a 2" gage length. Yield Strength is determined at 0.2% offset.

This material has been produced in compliance with the chemistry and established rolling practices of the ordered specification. If material is ordered to a chemical composition only and if physical testing is not a requirement of the customer's order, testing is not performed by the producer.

We hereby certify the above information is correct as contained in the records of the corporation.
Ann Gillespie Robert Moses ** 100% MELTED AND MANUFACTURED IN THE USA *
Cold Mill Metallurgist Chief Metallurgist

Ann M. Gillespie *Robert Moses*

Figure D-1. Simulated Floorpan Sheet Steel


CERTIFIED MATERIAL TEST REPORT												Page 1/1	
 GERDAU US-ML-MIDLOTHIAN 300 WARD ROAD MIDLOTHIAN, TX 76065 USA		CUSTOMER SHIP TO		CUSTOMER BILL TO		GRADE		SHAPE / SIZE					
		STEEL & PIPE SUPPLY CO INC		STEEL & PIPE SUPPLY CO INC		A36/A57250		Standard I-Beam / 3 X 5.7# / 75 X 8.5					
		1003 FORT GIBSON RD CATOOSA, OK 74015-3033 USA		MANHATTAN, KS 66505-1688 USA		LENGTH		WEIGHT		HEAT / BATCH			
SALES ORDER		CUSTOMER MATERIAL N°		SPECIFICATION / DATE or REVISION		40"00"		8,208 LB		59058160/03			
812105/000020		00000000035357040		A36/A36M-08 ASTM A372M-07 ASTM A36/A36M-11									
CUSTOMER PURCHASE ORDER NUMBER				BILL OF LADING		DATE							
4500221191				1327-000099969		04/02/2014							
CHEMICAL COMPOSITION													
C %	Mn %	P %	S %	Si %	Cu %	Ni %	Cr %	Mo %	Sn %	V %	Nb %	Al %	
0.09	0.79	0.014	0.026	0.20	0.36	0.11	0.06	0.027	0.009	0.001	0.011	0.003	
CHEMICAL COMPOSITION													
CEqvA6 %													
0.3													
MECHANICAL PROPERTIES													
YS KSI	UTS KSI	YS MPa	UTS MPa	G/L		G/L							
53.4	69.5	382	468	8.000		200.0							
55.3	67.9	368	479	8.000		200.0							
MECHANICAL PROPERTIES													
Elong. %	Y/T ratio												
23.20	0.786												
23.60	0.796												
COMMENTS / NOTES													
<p>MWPF - (4-7)</p> <p>BOGIE</p>													
<p>The above figures are certified chemical and physical test records as contained in the permanent records of company. This material, including the billets, was melted and manufactured in the USA. CMTR complies with EN 10204 3.1.</p> <p><i>Bhaskar</i> BHASKAR YALAMANCHILI QUALITY DIRECTOR</p> <p><i>Tom Harrington</i> TOM HARRINGTON QUALITY ASSURANCE MGR.</p>													

Figure D-2. S3x5.7 (S76x8.5) Posts, Test Nos. MWPF-4 and MWPF-5



Test Certificate

Document: 01038995

Norfolk Iron & Metal Co.

3001 North Victory Road
Norfolk, NE 68701
PH: (402) 371-1810

Sold To:
APOLLO STEEL CO
7200 AMANDA RD
LINCOLN, NE 68507

Ship To:
APOLLO STEEL CO
7200 AMANDA RD
LINCOLN, NE 68507

Sales Order: 01986281

Customer PO: PO-07608

Product Information

18452 - SHEET 7Ga GR50 COLD REDUCED

Thickness: .1800 Width: 60.0000 Length: 96.0000

Heat: 667827 Supplier: AM/NS CALVERT, LLC

Specification(s):
A1011 HSLAS-F GR50-12

7 Gauge Sheet Steel
Midwest Posts
R#14-0491 Green Paint
SMT

Chemistry Data

C	MN	P	S	SI	AL	CB	V	CU	CR
.055	.418	.013	.004	.016	.049	.018	.001	.006	.013
NI	MO	SN	TI	N	B	ZR	PB		
.011	.00	.001	.00	.006	.00	.00	.00		

Mechanical Data

	Yield (PSI)	Tensile (PSI)	Elongation	Reduction Of Area	Sample Taken From
1	54980	69271	37.85 2"	34.3600	Head
2	60541	69863	39.00 2"	30.5600	Center

Produced From Coil

Melted and Manufactured In: Not Provided

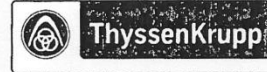
The Mechanical Data for the product described above reflect the results of tests made by us in accordance with applicable ASTM or ASME standards and our testing procedures, and we certify that the information included in this Test Certificate with respect to such Mechanical Data is accurate to the best of our knowledge.

The Chemistry Data shown above was reported to us by AM/NS CALVERT, LLC and have been included in this Test Certificate solely for your information.

Figure D-3. Midwest Weak Posts (MWP)

ThyssenKrupp Steel USA

1 ThyssenKrupp Drive
Calvert, Al. 36513



Mill Certificate

CUSTOMER ORIGINAL

Order - Item 42820-70	Certificate Number 1131814950	Delivery No 80554939-10	Ship Date 02/27/2014	Page 1 of 1						
Customer No: 10779		Cust PO: 01013159								
Customer Part No: 26576										
Customer Sold to: Norfolk Iron & Metal Company 3001 North Victory Rd. NORFOLK NE 68702 USA		Customer Ship to: Norfolk Iron & Metal Company 3001 North Victory Rd. NORFOLK NE 68702 USA		Contact - Customer Service Company ThyssenKrupp Steel USA P.O. Box 456 CALVERT AL 36513 USA Email: CS.Calvert@Thyssenkrupp.com Ph : 1-251-289-3000						
Steel Grade / Customer Specification Hot Roll Black Coil HSLAS-F GRADE 50 [340] / 0.1750 " X 60.0000 " ACCORDING TO A1011 {Light < 0.230"(6.0 mm)}										
Type of Product/Surface Hot Roll Black Coil Semi exposed										
TEST METHOD ASTM										
MATERIAL DESCRIPTION										
	ORDERED	Heat No.	Coil No.	Weight Net LB	Weight Gross LB					
(mm)	4.445	667827	1131814950	47,818	47,818					
(in)	0.1750									
CHEMICAL COMPOSITION OF THE LADLE *										
Heat No.	C	Si	Mn	P	S	Al	Cr	Cu	Mo	N
667827	0.0550	0.02	0.42	0.013	0.004	0.049	0.01	0.01	0.00	0.0058
	Ni	Nb	Ti	B	V	Ca				
	0.011	0.018	0.000	0.0001	0.001	0.0032				
TENSILE TEST										
Test Direction	Yield Strength	Tensile Strength	% Total Elong.							
L	60.7 ksi	67.1 ksi	33.0							

ThyssenKrupp Steel USA, LLC certify that the material herein described has been manufactured, sampled, tested and inspected in accordance with the contract requirements and is fully in compliance.

Bertram Ehrhardt

Bertram Ehrhardt
Director, Quality Assurance and Development

Rev.

Figure D-4. Midwest Weak Posts (MWP), Continued



BUCK COMPANY, INC.

897 Lancaster Pike, Quarryville, PA 17566-9738

Phone (717) 284-4114 Fax (717) 284-4321

www.buckcompany.com

greatcastings@buckcompany.com

MATERIAL CERTIFICATION

Date 5/7/13

Form# CERT-7A Rev C 4-21-06

CUSTOMER Bennett Bolt

ORDER NUMBER 6010480

PATTERN NUMBER CGBBWTH

REV. -

This is to certify that the castings listed conform to the following specifications and comply in all respects with the drawing or ordered requirements. All Quality Assurance provisions and / or Quality Assurance requirements and / or supplementary Quality Assurance provisions have been completed and accepted. SPC data is on file and available upon request.

Type Material: Ductile Iron

Specifications: ASTM A536

Grade or Class: 80-55-06

Heat Number: CE4

MECHANICAL PROPERTIES

Tensile Str. PSI 97,900

Yield Str. PSI 57,250

Elongation 8

PHYSICAL PROPERTIES

Brinell Hardness 217

PCS SHIPPED 2,396

1 of B

CHEMICAL ANALYSIS

Total Carbon 3.72

Silicon 2.64

Manganese .37

Sulfur .015

Phosphorus .022

Chrome .028

Magnesium .035

Copper .78

DATE SHIPPED 5/7/13

Quita Lopez
Quality Assurance Representative

Quality Castings

ISO 9001:2008 CERTIFIED

Ferritic and Pearlitic Malleable Iron, Gray and Ductile Iron, Brass, Aluminum

Figure D-5. New Bennett Bolt Works Coupler, Model No. CGBBWTH



BUCK COMPANY, INC.

897 Lancaster Pike, Quarryville, PA 17566-9738

Phone (717) 284-4114 Fax (717) 284-4321

www.buckcompany.com

greatcastings@buckcompany.com

MATERIAL CERTIFICATION

Date 12/29/14

Form# CERT-7C Rev A 4/21/06

CUSTOMER: Bennett Bolt

ORDER NUMBER 6012802

PATTERN NUMBER W1 Wedge

This is to certify that the castings listed conform to the following specifications and comply in all respects with the drawing or ordered requirements. All Quality Assurance provisions and / or Quality Assurance requirements and / or supplementary Quality Assurance provisions have been completed and accepted. SPC data is on file and available upon request. Melted & Manufactured in the USA.

Type Material: Malleable Iron

Specifications: ASTM- A47

Grade or Class: 32510

Heat Number: DR2

MECHANICAL PROPERTIES

Tensile Str. PSI 54,100

Yield Str. PSI 34,500

Elongation 19.5

PHYSICAL PROPERTIES

Brinell Hardness 137

PCS SHIPPED 8,862

1 OF 1

CHEMICAL ANALYSIS

Total Carbon 2.53

Silicon 1.54

Manganese .33

Sulfur .101

Phosphorus .015

Chrome .032

Magnesium .001

Copper .405

DATE SHIPPED 12/29/14

Louita Lopez
Quality Assurance Representative

Quality Castings
ISO 9001: 2008 CERTIFIED
Ferritic and Pearlitic Malleable Iron, Gray and Ductile Iron, Brass, Aluminum

Figure D-6. Malleable Iron Wedge for Bennett Couplers

09/27/2007 10:02 3156893999
SEP-26-2007 10:18AM FROM-Buck Co. HR

BENNETT BOLT WORKS
717-284-4321

PAGE 05

T-131 P.003/004 F-840



BUCK COMPANY, INC.

897 Lancaster Pike, Quarryville, PA 17566-9738

Phone (717) 284-4114 Fax (717) 284-4321

www.buckcompany.com

greatcastings@buckcompany.com

MATERIAL CERTIFICATION

Date 11/14/06 Form Number CERT-7C REV. A

CUSTOMER: Bennett Bolt Works

ORDER NUMBER 75410

PATTERN NUMBER CGBBHT REV. —

This is to certify that the castings listed conform to the following specifications and comply in all respects with the drawing or ordered requirements. All Quality Assurance provisions and / or Quality Assurance requirements and / or supplementary Quality Assurance provisions have been completed and accepted. SPC data is on file and available upon request. Melted & Manufactured in the USA.

Type Material: malleable Iron

Specifications: ASTM-A47

Grade or Class: 32510

Heat Number: 0P5

MECHANICAL PROPERTIES

Tensile Str. PSI 57112

Yield Str. PSI 35584

Elongation 15

PHYSICAL PROPERTIES

Brinell Hardness 121

PCS SHIPPED 105

1 of 1

CHEMICAL ANALYSIS

Total Carbon 2.53

Silicon 1.51

Manganese .33

Sulfur .030

Phosphorus .015

Chrome .030

Magnesium .001

Copper .115

DATE SHIPPED 11/14/06

Jim Bidwell
Quality Assurance Representative

Quality Castings

ISO 9002 CERTIFIED

Ferrous and Nonferrous Malleable Iron, Gray and Ductile Iron • Brass • Aluminum

Figure D-7. Current Bennett Bolt Works Coupler, Model No. CGBBHT

Appendix E. Coupler Testing – Load Cell Results

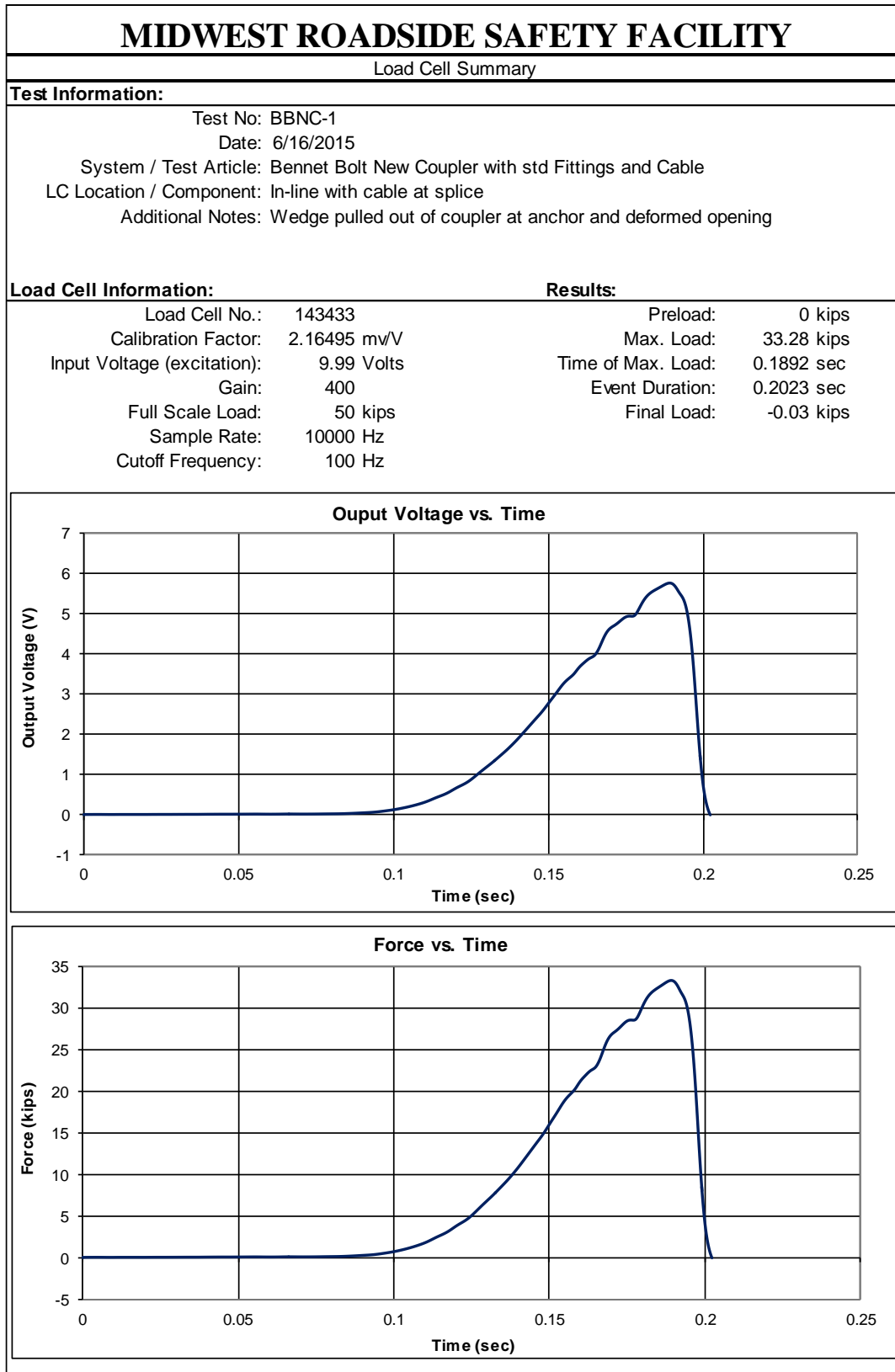


Figure E-1. Test No. BBNC-1 Results, Tension Load Cell

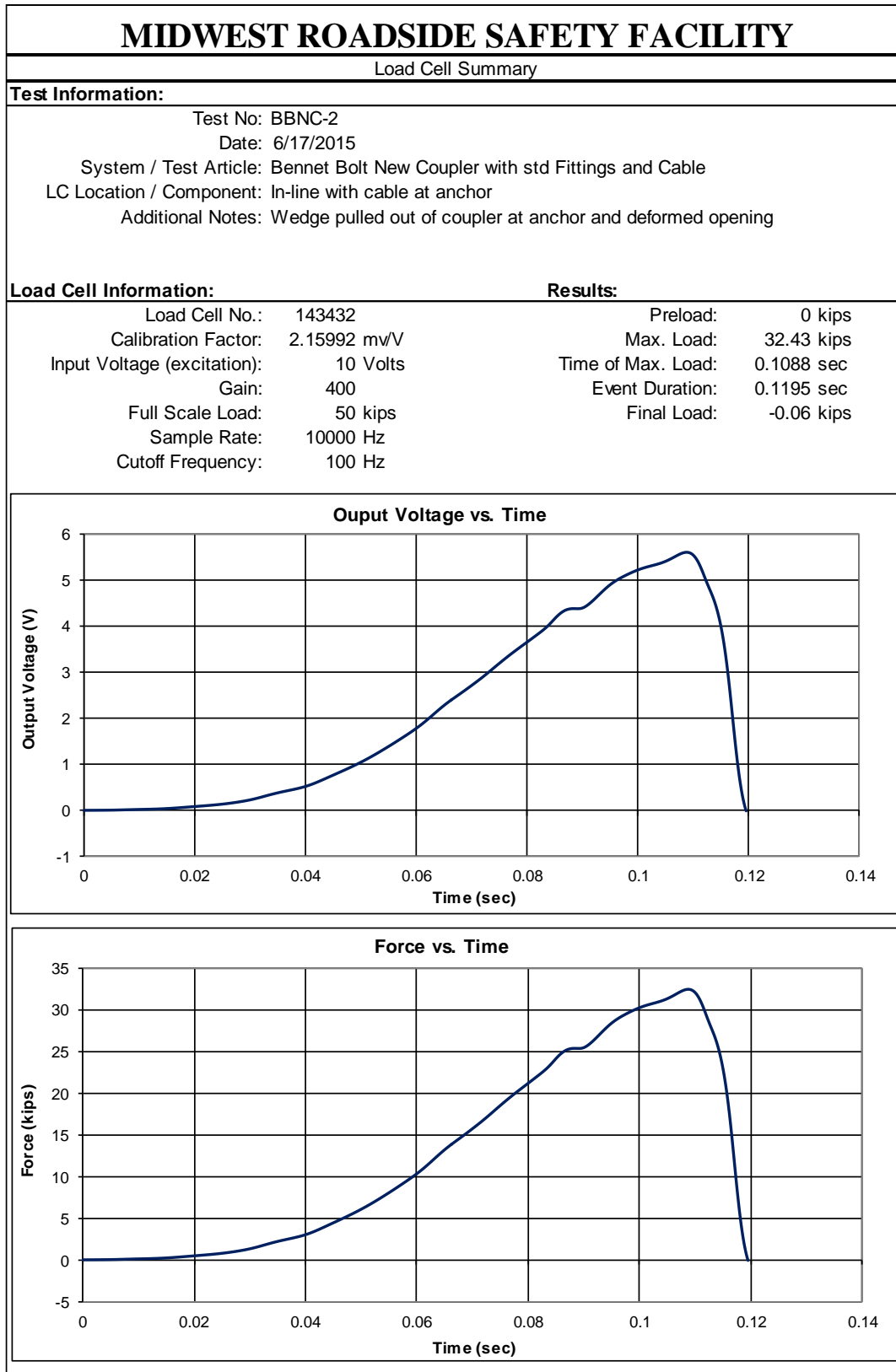


Figure E-2. Test No. BBNC-2 Results, Tension Load Cell

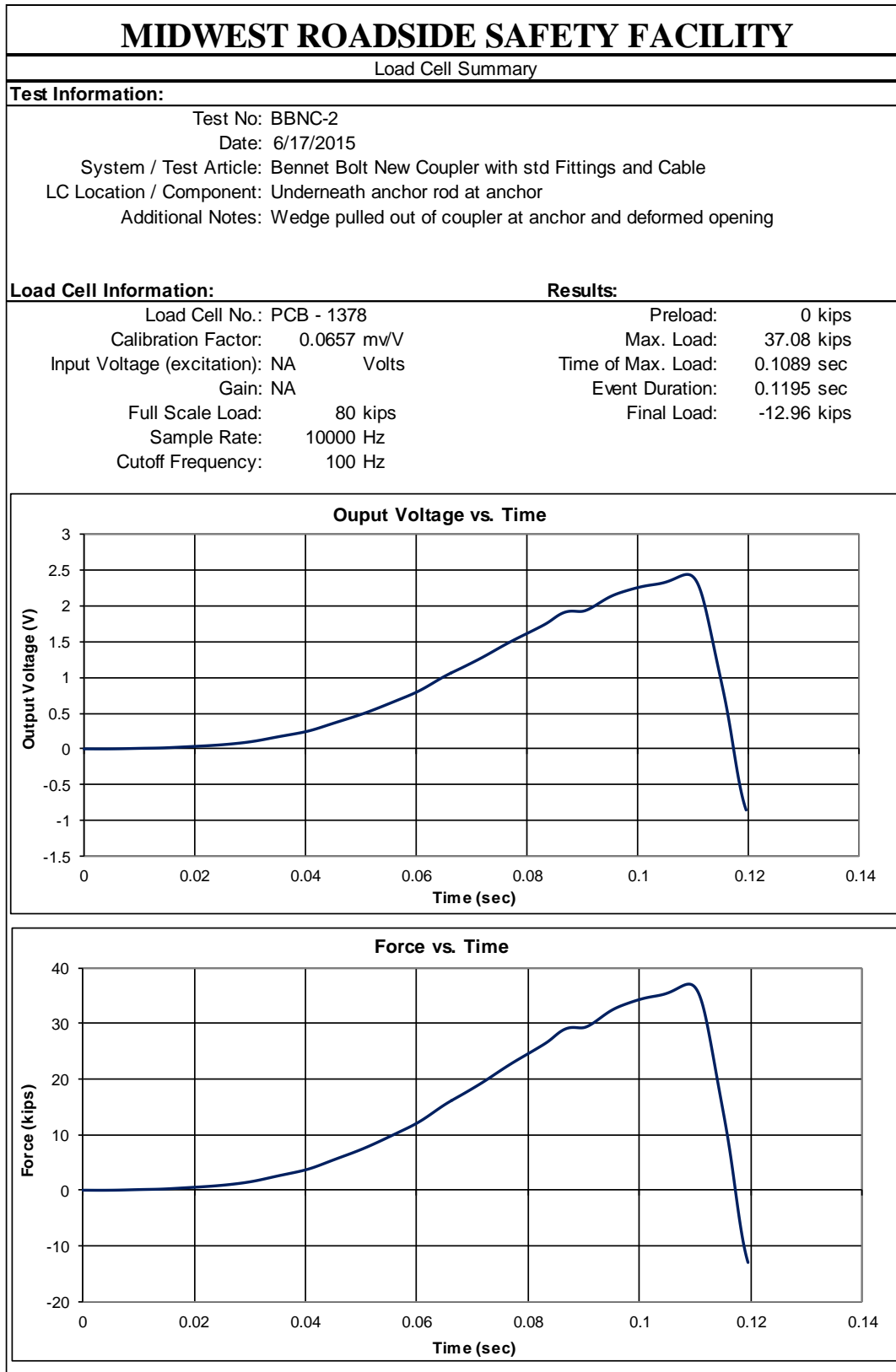


Figure E-3. Test No. BBNC-2 Results, Compression Load Cell

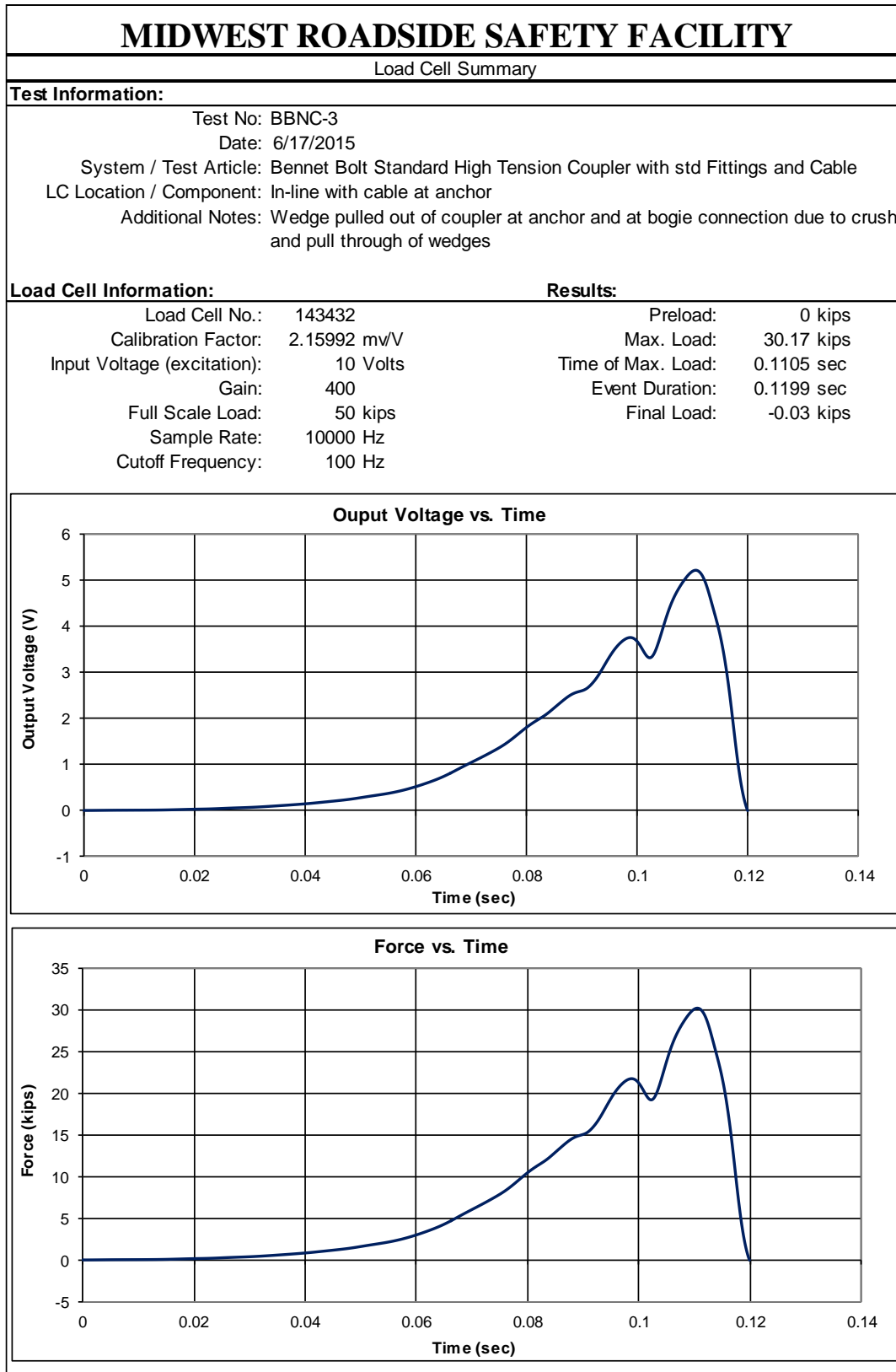


Figure E-4. Test No. BBNC-3 Results, Tension Load Cell

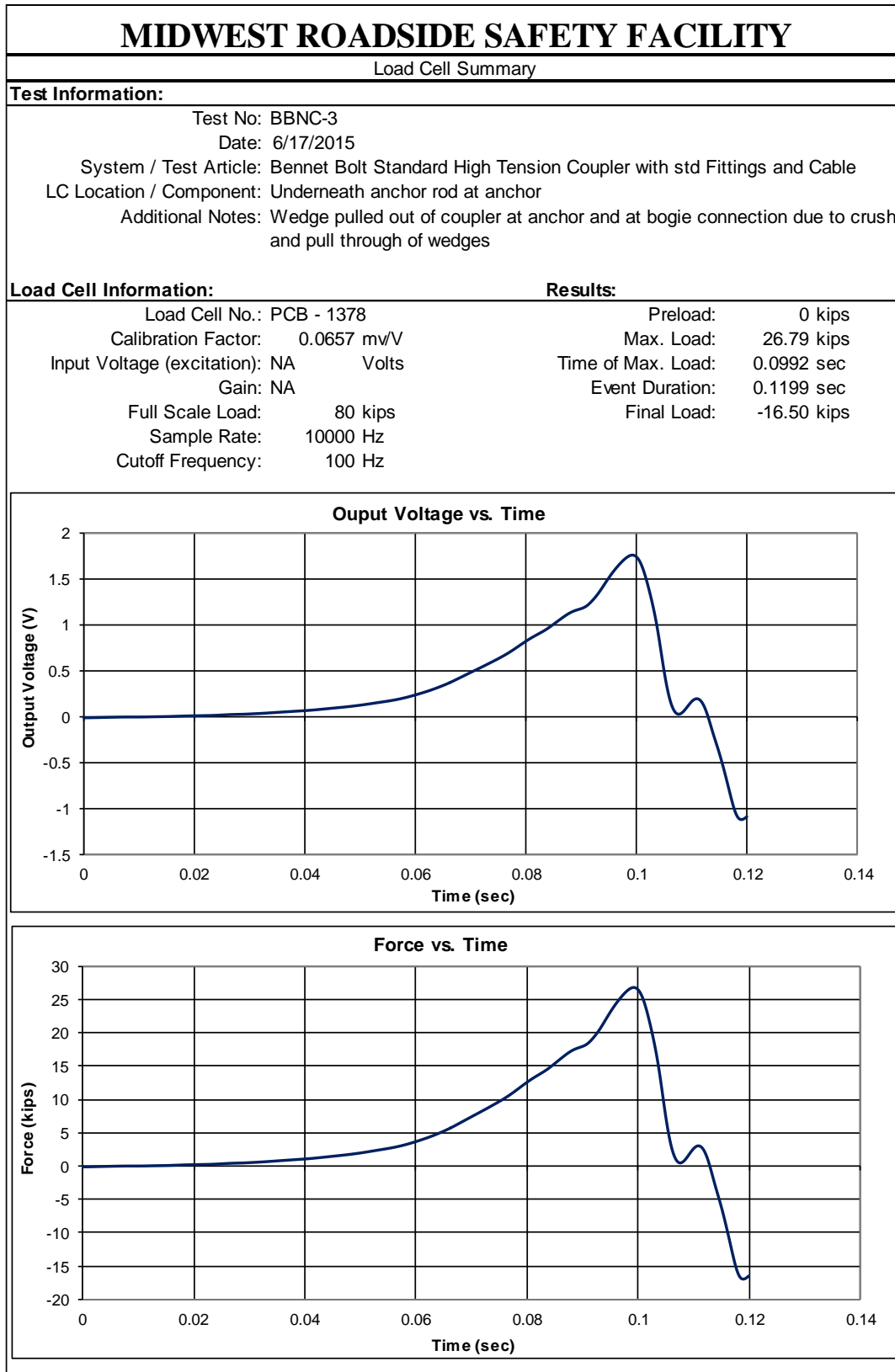


Figure E-5. Test No. BBNC-3 Results, Compression Load Cell

END OF DOCUMENT